Viscous damping in adaptive structures

dynamic analysis for vibration and deflection control of a lightweight footbridge design

Notermans, W.T.G.J.

Award date:
2018

GRADUATION THESIS

Viscous Damping in Adaptive Structures

Technische Universiteit Eindhoven University of Technology
Where innovation starts

W.T.G.J. Notermans

Viscous Damping in Adaptive Structures

Dynamic analysis for vibration and deflection control of a lightweight footbridge design.

by

W.T.G.J. (Pim) Notermans

A Thesis submitted in partial fulfillment of the requirements for the degree of

Master of Science

in Structural Design

at the EINDHOVEN UNIVERSITY OF TECHNOLOGY

Graduation Thesis	7K45M0
Author:	W.T.G.J. (Pim) Notermans
Student nr.:	0797600
E-mail:	w.t.g.j.notermans@student.tue.nl
Graduation committee:	prof.dr.ir. A.S.J. (Akke) Suiker
	ir. A.P.H.W. (Arjan) Habraken
	F.A.M. (Frits) Rooyackers MSc.
	Eindhoven University of Technology
Master:	Architecture, Building and Planning
Master track:	Structural Design
Chair:	Innovative Structural Design / Applied Mechanics
	September 2017 – October 2018
	Eindhoven, 12 October 2018

TU/e Technische Universiteit Eindhoven University of Technology

Where innovation starts

Preface

This report is the third and final part of the graduation project “Viscous Damping in Adaptive Structures”. The overall process of the project is described and where necessary supported by calculations and dynamic analysis to a large extent. The study plan is considered the first part of this graduation project. The second part consists of the literature study, which is elaborated in a separate document. As for this graduation project, a large part consists of dynamic analysis, which is not considered in conventional structural design for buildings. Hence, background information on dynamic analysis, numerical approximation methods to differential equations and control theory is briefly described in the literature study. A number of examples here supports basic theory on these topics. This theory on dynamic behavior is then applied on the described problem in this report. This master thesis continues on the work done by Frits Rooyackers, whose topic also included dynamics and control theory. In his study, an experimental model was made in the Pieter van Musschenbroek laboratory at the University of Eindhoven. This model is used as a basis for numerical analysis and in the experimental part of this master study, experimental tests have been performed on this model as well. This master thesis is part of the unit innovative structural design (ISD) and is specialized into the unit adaptive structures at the University of Eindhoven. The unit adaptive structures focusses on a very wide range of different design solutions where material optimization and adaptivity to loading configurations are main concepts.

Abstract

Dynamic actions on structures could be considered a relatively unfamiliar field of expertise within the field of structural engineering. Although more and more lightweight structures are being built, the effect of dynamics often is simplified by using static equivalent load factors or does not seem to be included in structural engineering at all, sometimes leading to unexpected (expensive) design adjustments or even catastrophic failure. Hence, more knowledge on dynamic loads in structural applications could might lead to a better structural design, especially for the case of building lightweight.

The purpose of this study is to investigate the effect of both viscous dampers and software-controlled actuators on the dynamic response of such a lightweight structure. An experimental model of a lightweight, small-scale pedestrian footbridge has been used as a basis for this study. In the first part, the approach to a numerical analysis is described, where the model of the bridge has been discretized to a multiple degree of freedom mass spring system. This mass spring system is then discretized in the time domain by means of a numerical approximation method. A number of numerical tests has been performed regarding different loading configurations for cases where the footbridge includes viscous dampers, actuators, both or none of these additional features.

Results from numerical simulations are compared for a number of different models and were taken as a basis for experimental research. As a second part of this thesis, experimental tests were set up, using comparable parameters for geometry and material properties. Here, both physical shock-absorbers and actuators are applied to the experimental model of the footbridge. Results are compared to the numerical simulations and (remarkable) differences and similarities are discussed.

For both numerical simulations and experimental research it is found that the actuators perform fairly well on deformation control, whereas uncomfortable vibrations are damped out very difficult, sometimes even introducing more vibrations than the same bridge without actuators. On the other hand, it is obtained that viscous damping is an effective method for vibration control, whereas relatively large deformations must be allowed in this case. A combination of both methods is tested as well, resulting in a compromise between deformation and vibration control. As a result, a lightweight structure, sensitive to vibrations, is stabilized by means of additional features including viscous dampers and a control system.

Table of contents

1 List of symbols

Symbol	unit	description
A	-	matrix of constants in numerical approximation
A	m^2	area
A_n	-	integration constant
$a(t)$	$\frac{m}{s^2}$	acceleration
$\mathbf{C}$	$\frac{Ns}{m}$	damping matrix of a multiple DOF system
c	$\frac{Ns}{m}$	damping coefficient
det	-	determinant of a matrix
$\frac{dx}{dt}$	-	derivative of x
E	Pa	Young's modulus
$E(s)$	-	error function in the Laplace domain
e^x	-	exponent function (may also be written as $Exp(x)$)
F	N	force
$F(t)$	N	force as a function of time
$\mathbf{F}(t)$	N	force in matrix notation
G_c	-	function of the controller in the Laplace domain
G_m	-	function of the model in the Laplace domain
$G(x(t_n))$	-	function for a numerical approximation
$h(t)$	-	response function to an impulse load
I	-	identity matrix
I	m^4	moment of inertia
i	-	complex number ($\sqrt{-1}$)
$\mathbf{K}$	$\frac{N}{m}$	spring stiffness matrix of a multiple DOF system
K_D	-	derivative gain in a PID control system
K_I	-	integral gain in a PID control system
K_P	-	proportional gain in a PID control system
k	$\frac{N}{m}$	spring stiffness
$L(f(x))$	-	Laplace transform function of the function $f(x)$
l	m	length
M	Nm	moment
$\mathbf{M}$	kg	mass matrix of a multiple DOF system
m	kg	mass
$N(s)$	-	noise function in a control system in the Laplace domain
n	-	integer indicating a certain time increment
Q	N	shear force
p	Ns	pulse
q_x	Pa	internal axial beam force
$q(x)$	Pa	load along the span of a beam
$S(s)$	-	sensitivity function in a control system
s	m	distance
T	s	one period of a system
$T(t)$	-	temporal function
t	s	time in seconds
t_n	s	time at certain time increment
v	$\frac{m}{s}$	velocity
$v(t)$	$\frac{m}{s}$	velocity as a function of time
v_0	$\frac{m}{s}$	initial velocity
w	m	displacement
$X(s)$	-	function in the Laplace domain
$X(x)$	-	spatial function

x	m	displacement
$x(t)$	m	displacement as a function of time
x_0	m	initial displacement
$\dot{x}(t)$	$\frac{m}{s}$	velocity as a function of time
$\ddot{x}(t)$	$\frac{m}{s^2}$	acceleration as a function of time
$\mathbf{x}(t)$	m	displacement matrix as a function of time
α	-	alpha damping in proportional damping
β	-	beta damping in proportional damping
ε	$\frac{mm}{m}$	strain
Δt	s	time increment
$\delta(x)$	-	Dirac delta function
ζ	-	damping ratio
κ	-	curvature
ρ	$\frac{kg}{m^3}$	density
σ	Pa	stress
τ	s	impact time
Φ	-	Heaviside step function
φ	rad	shift in phase
φ	rad	angular displacement
ω	$\frac{rad}{s}$	natural frequency
ϵ	s	time of an impulse load

2 Introduction

In the field of architectural design and engineering, there are multiple fields of expertise. One could think of for instance the urban designer, who investigates large-scale city plans. Then there is the architect, who has a job in which creativeness and ever-increasing innovative designs are pushing boundary conditions with respect to practical and economical beneficial solutions to their limits. MAD architects' design for the Harbin Opera House (Figure 2.1a), for instance, is far from a conventional multistory building design and this definitely has led to many questions and uncertainties with respect to structural aspects. Finally, the structural engineer is required to solve structural problems that were found in these very creative, but also very complex building designs. One could say that the engineer is thus responsible for a practical and proper design of the architects dream. Innovative structural design, material optimization and computer technology are often pushed to their limits in order to find the right solutions for buildings and this has led to a tremendous development of the built environment in the last centuries in both architectural and structural aspects. For instance, the largest free span worldwide is currently almost two kilometers and is found in the Akashi Kaikyo Bridge in Japan (Figure 2.1b).

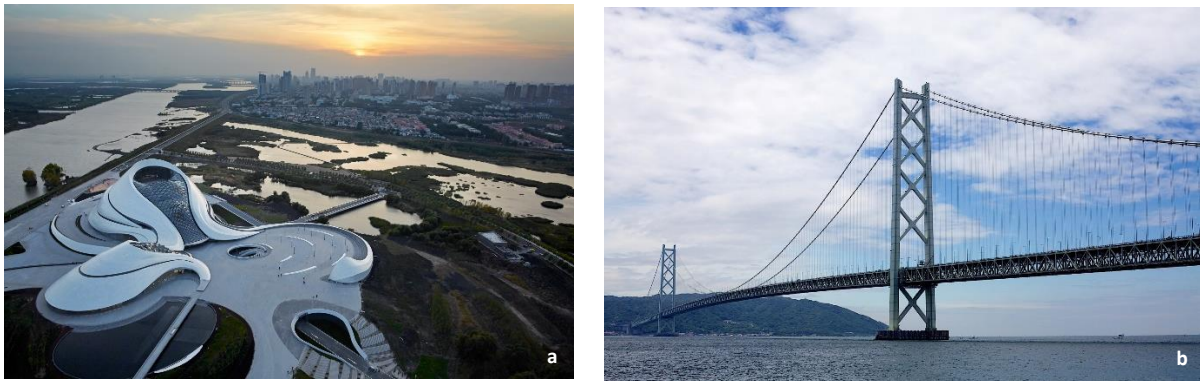

Figure 2.1: MAD Architects, Harbin Opera House (a), Akashi Kaikyo Bridge with a remarkably free span of 1991 meters (b)

Besides the growth of design freedom within structural boundaries, a number of trends can be observed within the built environment in the past few decades. Environment is a growing concept in the industry, which has become even more important in the last few decades, where the built environment is even proven to be the largest contributor to the CO_2 footprint on a global scale (Mah et al, 2011). Either reducing the material usage or the energy demand for manufacturing these materials, such as concrete or steel, can lead to large improvements regarding environmental aspects. Due to increasing standards on environmental aspects, it is necessary for these concepts to develop continuously. In the field of structural engineering, these optimization processes have led to a completely new design field: lightweight structures. Here, the main aim is to create a structure that is (generally) lighter than the variable load it is designed for. As a matter of fact, these lightweight structures are nowadays found in many examples. Many structures include design on tension forces through steel cables and minimization of moment development in structural parts.

2.1 Dynamic actions

It is seen throughout history that the concept of lightweight structures comes with new challenges in the field of structural engineering. The development of new (stronger) materials is continuously evolving and smart optimization with regard to shape or structural efficiency has led to structures that are much lighter than the external loads that they are designed for. Consequently, the total mass of lightweight structures is often much smaller than the variable ultimate load applied on these structures. Although strength and deformation can be dealt with already in these kinds of structures, the concept of vibrations in lightweight structures is a relatively new, unknown type of response to external loading that is often not considered in conservative structural engineering. Conservatively, structures are much heavier and the difference in additional variable weight is much smaller, like for instance buildings erected out of stone and concrete. That dynamic loads can lead to unforeseen structural behavior can be seen already in multiple examples. The best-known example, however, is the collapse of the Tacoma Narrows Bridge in 1940. A critical wind load gave rise to a self-excited vibration that

forced the whole bridge to vibrate until complete failure (Figure 2.2) of the bridge (Billah & Scanlan, 1990). The collapse happened already four months after the opening, as this particular design had almost no damping to resist dynamic response to wind loading due to its relative low mass compared to external loading.

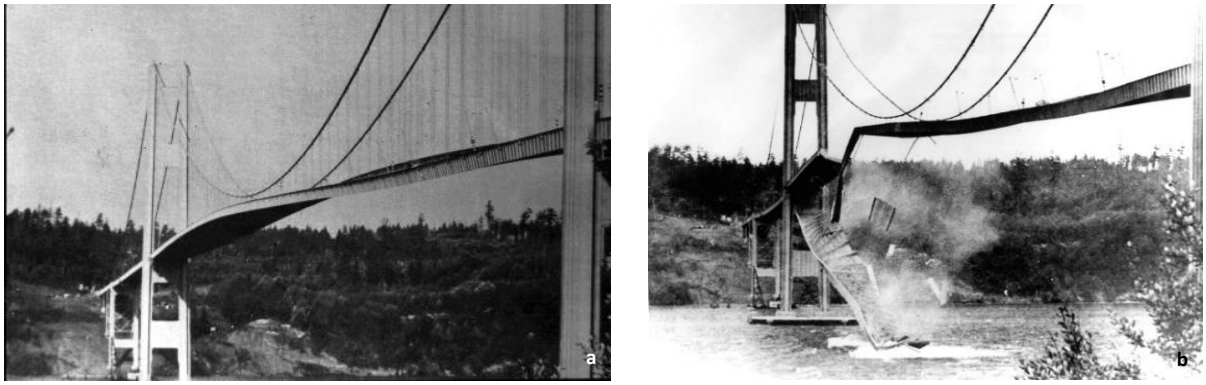

Figure 2.2: Tacoma Narrows Bridge in vibration (a) and after collapse (b)

More examples of vibration and resonance problems can be found in lightweight structures, albeit with less severe consequences. The Millennium Bridge in London, for example, was considered very uncomfortable to walk over due to vibration issues caused by the variable loading of people crossing the bridge (Taylor, 2006) (Dallard et al., 2001) (Figure 2.3a). An example in another type of structure is found in the rollercoaster Lost Gravity, recently built in Biddinghuizen in the Netherlands (Figure 2.3b). A part of the track started vibrating heavily after the train has passed a certain point and started causing resonance in the track (Walibi heeft oplossing voor, 2016). Besides, much more examples can be found trough history proving that dynamic behavior often is very important and that a conventional static structural analysis does not suffice in a lightweight design in many cases. As a result, it could be concluded that research is necessary to gather more knowledge on dynamic responses to external loading configurations like wind or frequency loads on structures that have a much smaller self-weight.

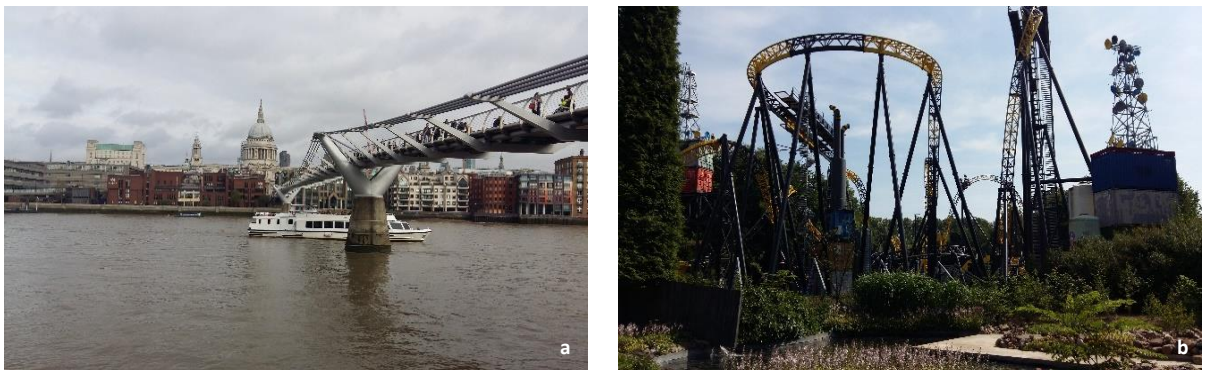

Figure 2.3: Millennium Bridge London (a), Lost Gravity Coaster Biddinghuizen (b)

2.2 Adaptivity

Conservative structures are designed on an ultimate load case. A certain load case, however, occurs only very occasionally and thus the structure is only utilized for a small part most of the time. Secondly, structures are often designed based on deflection limits in lightweight design. Deflection is governing over strength and therefore the structural properties are not fully utilized. Adaptivity comes with the concept that a structure should adapt to its loading configuration, and therefore could be designed on strength rather than deflection or strength could even be added to the structure at those very scarce moments of ultimate loading. This concept of adaptive structures is relatively new in the built environment, being very close related to designing lightweight. In addition, an adaptive system could even increase the variable to dead load ratio in a structural application. Hence, it can also be stated that adaptive structures will probably be very sensitive to the influence

of dynamic loads. On the other hand, an adaptive system always includes a certain control system to satisfy structural requirements to the constantly changing external conditions. Thus, responding on dynamic loading could also be included in this theory of adaptivity.

Within the field of control theory, many developments have been done in the past few decades, where control theory is then often stated to be the use of computer technology to maintain or regulate a certain process (Ogata, 1970). Although control systems are applied in the built environment rarely, a few examples exist. For instance, climatic air systems in buildings in which temperature and air refreshment is regulated can be categorized as control systems within the field of architectural engineering. Control systems are much more seen in robotics and in the airplane and car industry, for instance (Dorf & Bishop, 2011), whereas they are not, or very limited used in structural applications. As stated before, this is because most calculations are nowadays still designed using static calculations and structures are mainly unchangeable in time after erection. Using control systems can, however, be very beneficial for structural design as a design could then adapt to its external conditions and can therefore be designed requiring much less material. One very recent example can be found in the 'Adaptive Truss Prototype' (Figure 2.4). The truss here responds to a certain deflection due to external loading and the result is a deformation almost equal to zero for every loading configuration (Senatore, 2015). Without applying the control system, the deformation would become far above the allowable limits, even for small external loads.

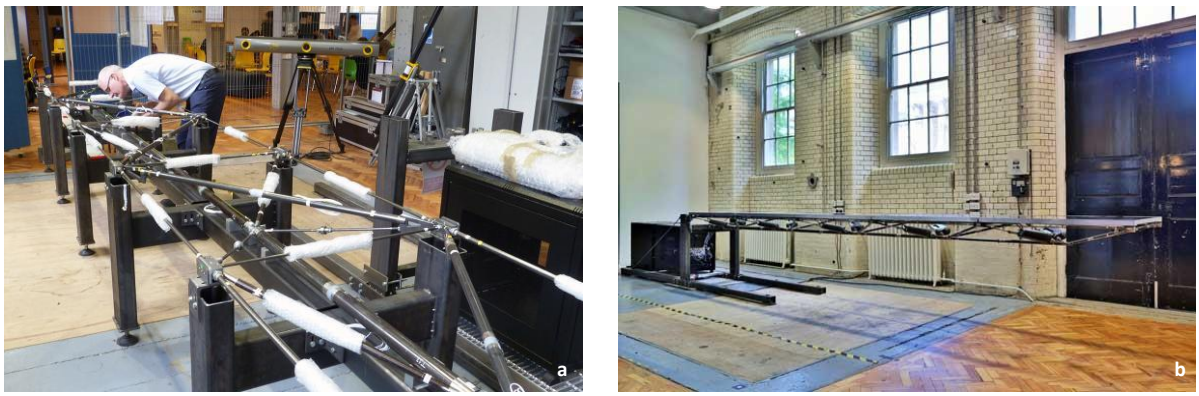

Figure 2.4: Adaptive Truss Prototype under construction (a) and finished (b)

Adaptive structural design and dynamics are two topics that are related to each other within the field of lightweight structures, where a number of uncertainties still need to be investigated in order to get more insight in the behavior of these optimized, material reduced structures. Very few examples can be found, where a structure can adapt to its external loading configuration and additionally, dynamic influences are never taken into account in this short list of adaptive systems.

3 Problem description

Producing lightweight structural elements does not only include benefits. One could conclude that lighter structures will inevitably result in larger deformations (Figure 3.1), which can be reduced by using adaptive structural elements such as control systems. Secondly, dynamic effects will occur faster and sometimes have even severe consequences, as was already seen in for instance the Millennium Bridge in London. Vibrations can be measured in every structure in the built environment, as each variable load on a structural element is in fact a load in time, which induces vibrations. However, in most cases these vibrations are so small that they are considered negligible. The span to thickness ratio in ordinary housing and offices does normally not exceed the limit for comfort criteria and vibrations are not noticed at all. In other words, the difference in the so called 'maximum overshoot' and the steady state error remains very small and as a result, a static calculation is considered sufficient. This research, however, is in the topic of lightweight structures, where variable load is always larger than dead load of the structure itself and where span to thickness ratios are typically large. Solving dynamic problems in these structures is the main topic in this master study.

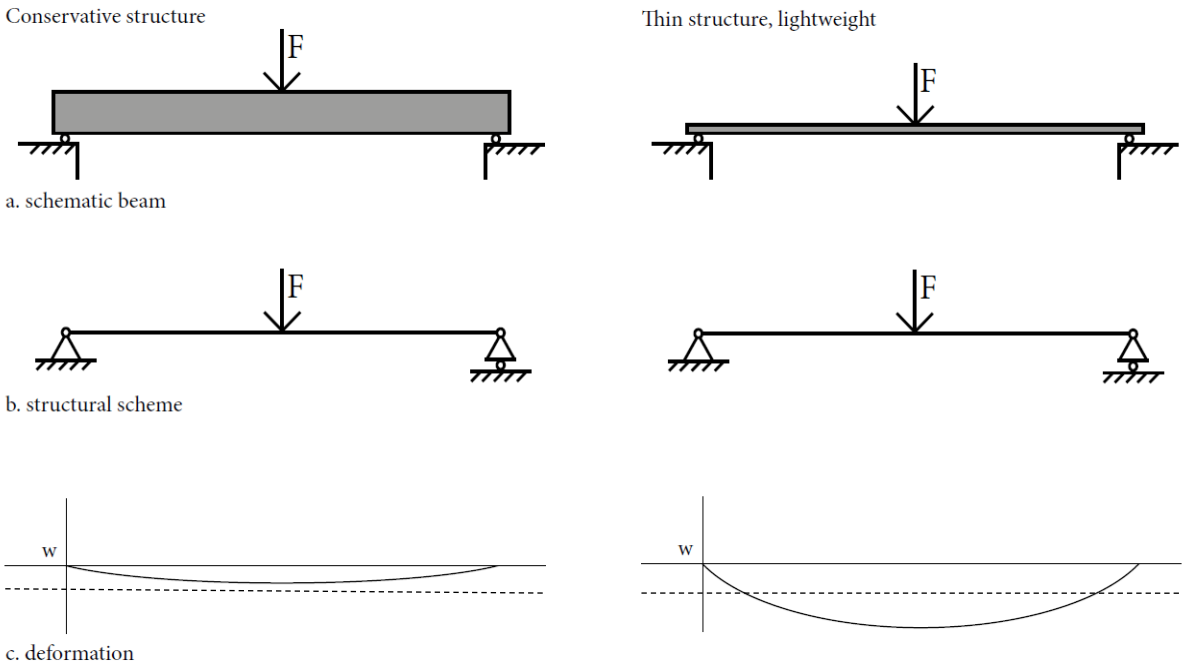

Figure 3.1: Deformation of conservative and lightweight beam

This master project continues on a previous project, where a control system was the main topic on reducing permanent deformation in a very lightweight footbridge design (Rooyackers, 2017). Hence, a slender structure was able to carry as much load as a conservative structure while having a much lower self-weight. A case study had been made for a bridge with an active cable system (Figure 3.2). The bridge consists out of two thin steel structural tubular profiles. Wooden elements are placed on top of the steel tubes to provide a walking deck (Figure 3.3). At mid span, the bridge is supported by steel wire ropes, which are connected to an external steel structure. In between the wires and the deck an actuator was placed in order to respond on deformations and vibrations. Although an actuator could theoretically damp out any vibration immediately by choosing the right control values, it was found that in practice this system did not perform as good as in a numerical simulation. Mainly the derivative gain factor (responsible for reducing overshoot and thus the actual vibration) in the chosen PID-control system appeared to be not as reliable as simulated and although the actuator performed really well on reducing deformations, small vibrations were measured continuously as a result from the actuator generated forces. A pedestrian crossing the bridge would notice these vibrations and would maybe consider the design uncomfortable to walk over, even if average deflection remained zero during this period. In this particular example, it might be concluded that the total deformation at mid span was reduced perfectly to zero using the actuators, whereas vibrations were still noticed. A reduction in these vibrations would probably lead to a more

comfortable design and therefore, structural (viscous) damping was applied as a method to reduce vibrations in the footbridge design.

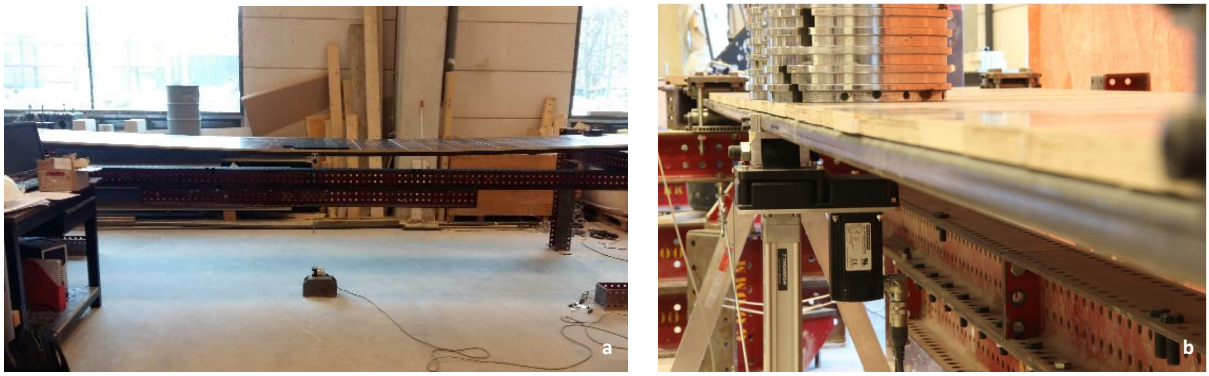

Figure 3.2: Pedestrian bridge in laboratory: without structural wires (a), loaded with active actuator and structural wires (b)

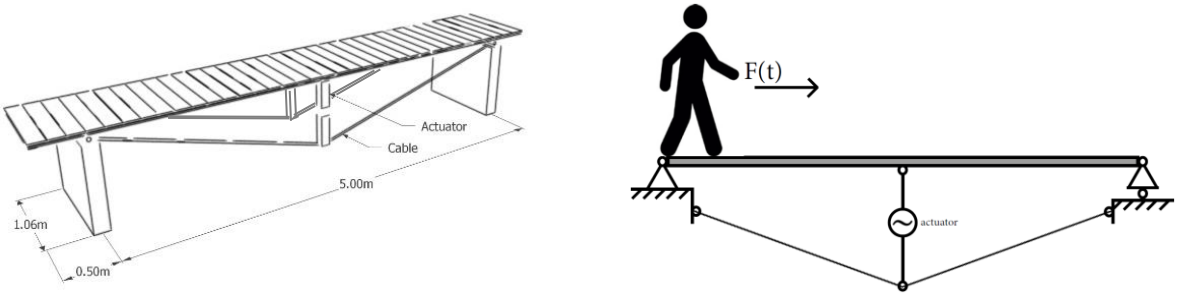

Figure 3.3: Schematic model of the small-scale pedestrian bridge with structural steel wire ropes

3.1 Structural damping

Implementing damping into a structural system is a topic that is currently becoming more and more important when it comes to the built environment. Viscous damping has proven its benefits with regard to impulse loads in particular. Besides lightweight (foot)bridges, where loads will in practice be a number of impulses exited by crossing traffic, impulse loading is seen in for instance earthquake design or bomb blast resisting façades. In this particular case study, an actuator is considered necessary, as external loads can also consist out of long term loads if for example one decides to stop walking and enjoy the view for a while. Using only damping would theoretically result in a continuously increasing deformation of the bridge deck, until the damper would be fully suppressed. Earthquakes or bomb blasts, however, are not continuous loads and structural damping would probably be sufficient in these cases.

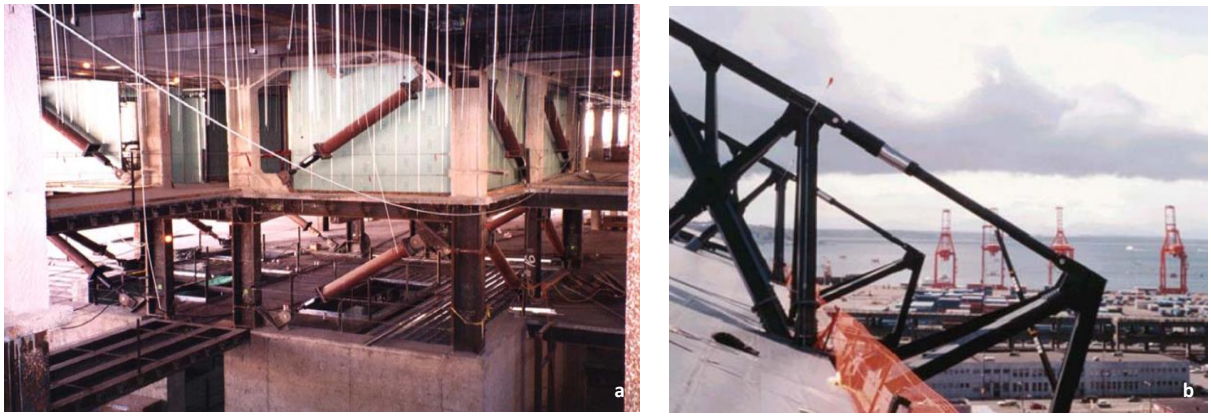

Figure 3.4: Seismic dampers in the San Francisco Civic Centre (a) and damping in the Pacific Northwest Baseball Stadium in Oregon (b)

Seismic structural damping has already been applied in many examples, such as the San Francisco Civic Centre in San Francisco (Figure 3.4a). Another example is found in Oregon (USA), where dampers were applied to the Pacific Northwest Baseball Stadium in order to reduce vibrations as a result of wind loading (Figure 3.4b) (Taylor, 1999). To that extent, structural viscous damping is important in the current development of structural engineering.

3.2 Project goal

Several examples have been described where structural damping was used in order to reduce vibrations in bridges. Hence, viscous damping seems to be a solution to vibration issues in structures. To that extent, a damper might could lead to better results in the above described case study of the footbridge design when it comes to certain uncomfortable vibrations resulting from the actuator forces. Besides adding damping, the PID control system could be enhanced to get better results in comfort criteria. The used PID controller consists roughly out of three parameters which can control the given force of the actuator. This system may be considered a very elementary control algorithm in control theory and enhancement of the control system would probably lead to better results for the actuator as well. Although it is probably possible to damp out vibrations much better by using a more sophisticated algorithm than the PID control theory, this solution methodology requires much more skills on control theory and does not fit very well in the master study structural design. Structural aspects would then become a very minor part of this graduation project. Going more into detail in control theory would be a very interesting research topic, however, would fit better in the field of mechanical engineering, for instance. Accordingly, the addition of damping to an instable (adaptive) structure is chosen as the main topic in this master study and enhancement of the control system is not part of this study at all. The viscous damper is then mainly used for damping out vibrations by means of energy dissipation, which is a direct result of impulse loading on the footbridge. The actuator should account for long-term deformations, which are a result of long-term (static) loads. Hence, the structure should allow deformation at first, in order to activate the damper and after a certain time this deformation should be reduced by the actuator. Both numerical simulations and an experimental test setup are parts of this research topic and are mainly based on the case study of the small pedestrian bridge supported by steel wires.

Using both viscous damping to control vibrations and a control system to control deflection, this would ideally result in a lightweight (dynamic sensitive) bridge that is fully stabilized and that does not have any noticeable deformations and is not sensitive to dynamic loads anymore. In other words, a footbridge where material usage is drastically reduced and where each person would consider the bridge very comfortable to walk over (Figure 3.5). Of course, these results probably will not be realized as ideal as illustrated, as theoretically many assumptions, approximations and simplifications are made whereas reality is much more complex. However, performance should be as close as possible to the described ideal behavior, proving the concept of using additional features to stabilize (highly) unstable structures.

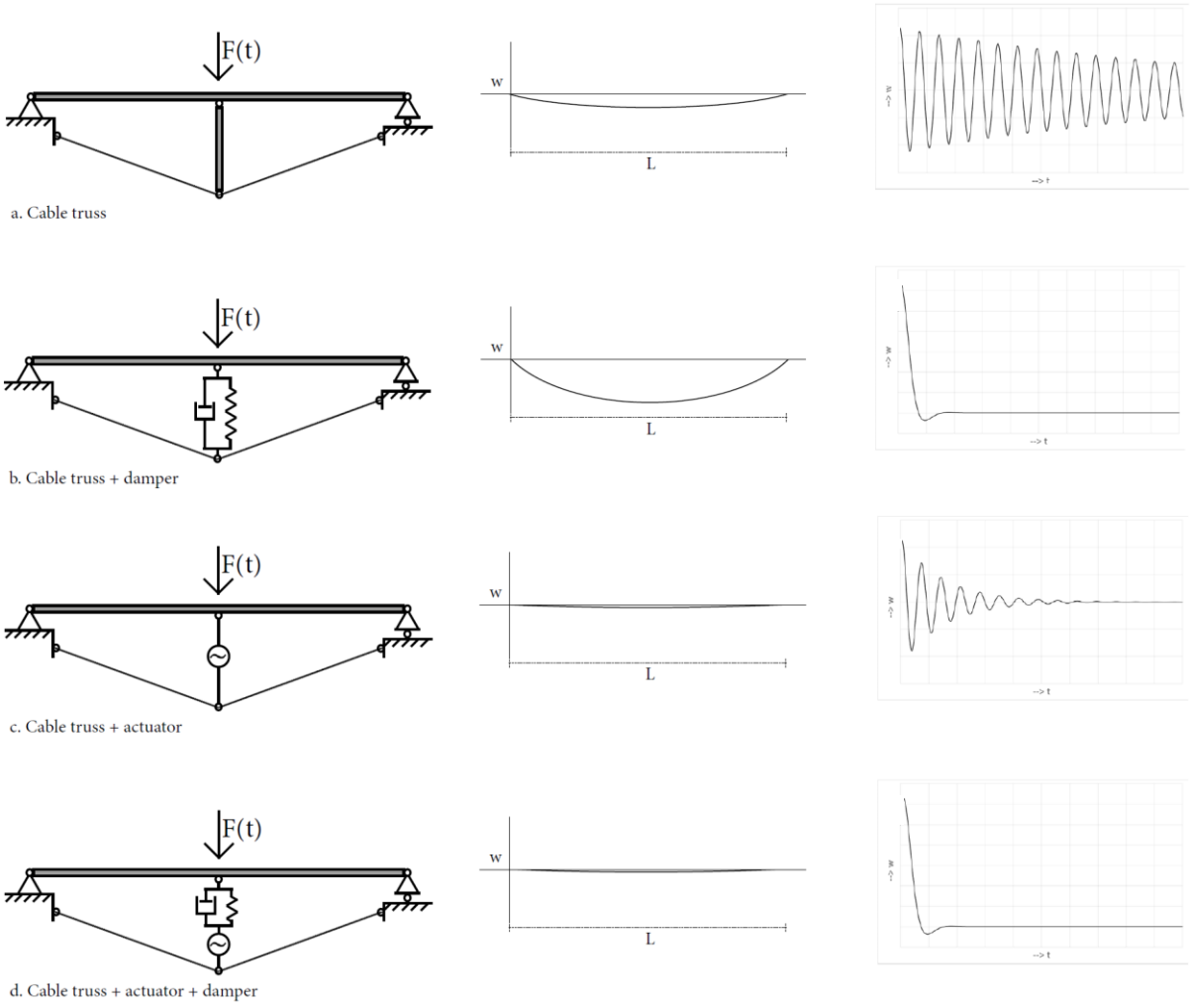

Figure 3.5: Schematic overview of expected results for damping and actuator

4 Approach to the numerical model

Generally, structures are considered static and almost all calculations are based on values, which do not change over time. Many derivations in the spatial domain are already found in structural analysis, for instance the derivation of buckling modes of a continuous beam or derivations of deflection formulas over a beam length. In this project, all derivations are based on dynamic analysis, where all values do change over time. A thorough approach is discussed towards the dynamic model, which in this case represents a small, but lightweight pedestrian bridge design. In order to give a little more insight in the complexity of dynamics, the general solution to a continuous system is discussed. It was already shown in the literature study that dynamic analysis is often quite complex to solve algebraically and that numerical approximations are very powerful to approximate the exact solution. As the full dynamic analysis involves many derivations and simplifications, a summary is given of the most important steps in finding a solution regarding modelling dynamic behavior. For more background information or examples is here referred to the literature study and secondly, many examples can be found in literature on the basics of structural dynamics like for instance Engineering Vibrations (Inman, 2001).

4.1 The analytical equation for a continuous system

Structural elements like beams and columns are continuous structures, which are not divided into a finite number of elements like for instance a multiple degree of freedom mass spring system. As a result, a beam or column also includes a theoretical infinite number of eigenvalues, which are more commonly known in structural analysis as mode shapes. A simply supported beam for instance deforms in a half sine shape in its first mode shape. When it comes to dynamic analysis, the deformation is described in both space and time, rendering two independent variables time (t) and space (x).

Multiple approaches to continuous systems have been discovered through history. However, the Euler-Bernoulli classical beam theory is generally applied in mechanical and structural engineering. The classical beam theory is based on the linear theory of elasticity, providing solutions for calculating deflection and load carrying capacity of beams and columns. The method may be used in many cases in structural engineer, although it is a simplified version of the Timoshenko beam theory, discovered by Stephen Timoshenko in the early 20th century. The Timoshenko beam theory takes into account rotational bending effects and shear deformation, whereas the classical beam theory does not (Nicholson & Simmunds, 1977). In practice, this implies that the Euler-Bernoulli beam theory may only be used if it is used for calculating small deflections and if forces are only applied perpendicular to the beam axis, resulting in negligible axial forces. Secondly, a beam must consist out of an isotropic material. The beam must be slender so that shear deformations may be neglected (Figure 4.1). As in study, the beam model suffices to all conditions for the Euler-Bernoulli beam theory and as a result, it may be assumed that this theory is sufficient to use in this master study.

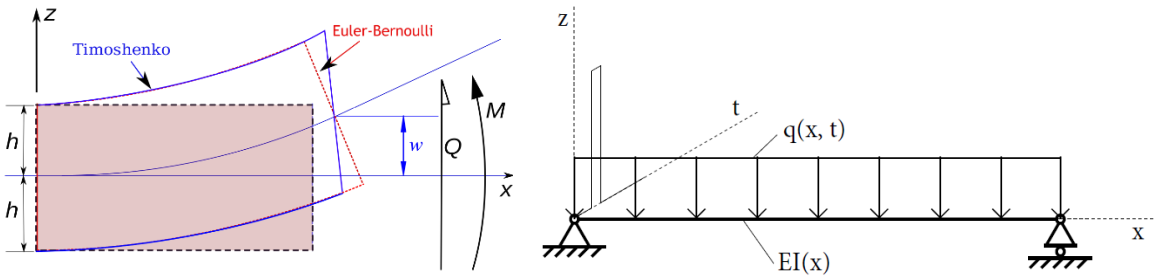

Figure 4.1: Difference in Euler-Bernoulli and Timoshenko beam theory (a) and continuous beam model (b)

From the classical beam theory, it can be found that moment is directly related to the curvature times the beam stiffness. Furthermore, curvature is equal to the derivative of the angular rotation of a beam, resulting in

$$M(x,t) = EI(x)\frac{\partial^2 w(x,t)}{\partial x^2} \tag{4.1}$$

The stiffness of the beam does not change in time and therefore only depends on the spatial location (x) over the beam. If now an infinitesimal element from the continuous beam is considered (Figure 4.2), moment equilibrium and force equilibrium in vertical direction may be derived, resulting in

$$\sum M_y = 0 \rightarrow (M + \Delta M)(x,t) - M(x,t) + f(x,t)\Delta x * \frac{\Delta x}{2} + (V + \Delta V)(x,t)\Delta x = 0$$

$$\sum F_z = 0 \rightarrow (V + \Delta V)(x,t) - V(x,t) + f(x,t)\Delta x - \rho A(x)\Delta x \, \frac{\partial^2 w(x,t)}{\partial t^2} = 0 \qquad (4.2)$$

In these equations, the increment is considered really small (i.e. $\Delta x \rightarrow 0$) and is therefore neglected. Secondly, the second derivative ∂^2 is neglected, as the derivative is already small. Solving moment equilibrium, this results in

$$V(x,t) = -\frac{\partial M(x,t)}{\partial x} \qquad (4.3)$$

Substituting this equation back into the force equilibrium condition results in a fourth order partial differential equation, describing the beam in both the spatial and the temporal domain.

$$\frac{\partial^2 w(x,t)}{\partial t^2} + c^2 \frac{\partial^4 w(x,t)}{\partial x^4} = 0 \;\; where \; c = \sqrt{\frac{EI}{\rho A}} \qquad (4.4)$$

In this equation, the geometrical properties do not change over time and no external force is acting on the system.

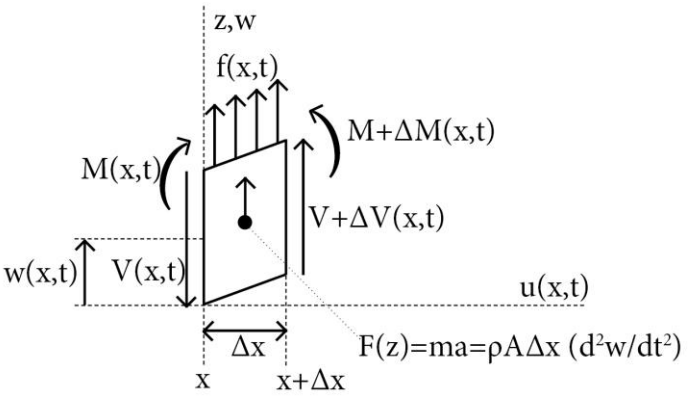

Figure 4.2: Infinitesimal beam element from a continuous, slender beam

4.2 The solution to the differential equation of a continuous system

A partial differential equation in both the spatial and the temporal domain has been found by using the Euler-Bernoulli beam theory and solving this for force equilibrium. The solution methodology to the dynamic beam equation is similar to the general solution of an initial value problem. Firstly, the boundary conditions in space and the initial conditions in time are formulated. In order to solve this system, four boundary conditions in space are needed, as the partial derivative in space is of the fourth order (∂x^4). Secondly, two initial conditions need to be known since the temporal part is of the second order (∂t^2). The boundary conditions in the spatial domain are similar to a static problem. In this case, the beam is considered simply supported and thus, the displacement and momentum at support locations will be equal to zero at every time. It is assumed that there is a certain initial displacement and velocity at $t = 0$. In mathematical terms, this renders

$$\begin{aligned}
&\text{At } x = 0, w = 0 \rightarrow w(0,t) = 0 \\
&\text{At } x = l, w = 0 \rightarrow w(l,t) = 0 \\
&\text{At } x = 0, M = 0 \rightarrow M(0) = \ddot{w}(0,t)EI = 0 \\
&\text{At } x = l, M = 0 \rightarrow M(l) = \ddot{w}(l,t)EI = 0 \\
&\text{At } t = 0, w = w_0 \rightarrow w(x,0) = w_0(x) \\
&\text{At } t = 0, v = v_0 = \dot{w}_0 \rightarrow \dot{w}(x,0) = \dot{w}_0(x)
\end{aligned} \qquad (4.5)$$

In order to solve the differential equation, a separation of variables approach is used. In this case, that indicates that the partial differential equation is a product of one function depending on only the spatial location and one function only depending on time. The separated variables can then be substituted back into the fourth order partial differential equation that was found for a simple beam.

$$w(x,t) = X(x)T(t) \tag{4.6}$$

$$X(x)T''(t) + c^2X''''(x)T(t) = 0 \tag{4.7}$$

The derivatives here become total derivatives instead of partial derivatives, as they only depend on one variable. Rearranging of variables then gives

$$c^2 \frac{X''''(t)}{X(t)} = -\frac{T''(t)}{T(t)} \tag{4.8}$$

Here, the part that depends on x is the spatial equation and the part that depends on t is the temporal equation. To solve the two differential equations separately, a separation constant must be used. This separation constant follows from a mathematical point of view that both fractions should be equal to a certain constant, as the left part (spatial) must be equal to the right part (temporal) for all x and t. The temporal equation of this part is solved for the two initial conditions that were given and follows the same solution procedure as for a mass spring system.

$$m\ddot{x}(t) + kx(t) = 0 \rightarrow mT''(t) + kT(t) = 0$$

$$T''(t) + \omega^2 T(t) = 0 \text{ where } \omega = \sqrt{\frac{k}{m}} \tag{4.9}$$

Rearranging of variables gives the solution for the temporal equation. Where the right-hand term is the separation constant.

$$\frac{T''(t)}{T(t)} = -\omega^2$$

$$X''''(x) - \left(\frac{\omega}{c}\right)^2 X(x) = 0 \tag{4.10}$$

4.2.1 The spatial equation

A fourth order differential equation is now derived where the derivative only depends on the spatial location x. This equation is called the spatial equation, where the term $\frac{\omega}{c}$ is recalled to β^2. The solution procedure to this equation is similar to the derivation of the general beam equation in static structural engineering. Each derivative term can be reformulated by using an exponential function $e^{\lambda x}$ and the equation can then be solved for arbitrary values of this exponential function. The fourth order differential equation results in four solutions, where it is stated that for linear problems an addition of all solutions is also a solution. It can then be found that

$$X(x) = C_1 e^{\beta x} + C_2 e^{-\beta x} + C_3 e^{i\beta x} + C_4 e^{-i\beta x} \tag{4.11}$$

The real part of the solution is extracted by using trigonometric identities and the formula of Euler. After reformulating, the solution must then be in the form of

$$X(x) = A_1 \sin(\beta x) + A_2 \cos(\beta x) + A_3 \sinh(\beta x) + A_4 \cosh(\beta x) \tag{4.12}$$

Clearly, it is seen that there are four unknown variables, which are also known as constants if integration. These variables all can be expressed in terms of βl, since four boundary conditions were formulated for the spatial part of the solution. The four boundary conditions can then be combined into one equation in matrix format, where each integration constant is multiplied by a certain factor in each equation. All equations need to be equal to zero. For the simply supported beam, one finds that

1) $X(0) = 0 \rightarrow A_1 \sin(0) + A_2 \cos(0) + A_3 \sinh(0) + A_4 \cosh(0) = 0$
2) $X(l) = 0 \rightarrow A_1 \sin(\beta l) + A_2 \cos(\beta l) + A_3 \sinh(\beta l) + A_4 \cosh(\beta l) = 0$
3) $M(0) = EIX''(0) = 0 \rightarrow EI\beta^2 \left(-A_1 \sin(0) - A_2 \cos(0) + A_3 \sinh(0) + A_4 \cosh(0)\right) = 0$
4) $M(l) = EIX''(l) = 0 \rightarrow EI\beta^2 \left(-A_1 \sin(\beta l) - A_2 \cos(\beta l) + A_3 \sinh(\beta l) + A_4 \cosh(\beta l)\right) = 0$

$$\begin{bmatrix} 0 & 1 & 0 & 1 \\ \sin(\beta l) & \cos(\beta l) & \sinh(\beta l) & \cosh(\beta l) \\ 0 & -EI\cdot\beta^2 & 0 & EI\cdot\beta^2 \\ -EI\cdot\beta^2\cdot\sin(\beta l) & -EI\cdot\beta^2\cdot\cos(\beta l) & EI\cdot\beta^2\cdot\sinh(\beta l) & EI\cdot\beta^2\cdot\cosh(\beta l) \end{bmatrix} \begin{bmatrix} A_1 \\ A_2 \\ A_3 \\ A_4 \end{bmatrix} = \begin{bmatrix} 0 \\ 0 \\ 0 \\ 0 \end{bmatrix} \quad (4.13)$$

Obviously, a solution can be found by simply make all integration constants equal to zero. However, the solution to the spatial equation is found for arbitrary values for the integration constants. The left hand matrix should then be equal to zero. This results in

$$\sin(\beta l) = 0 \rightarrow \beta = \frac{n\pi}{l} \; V \; \beta = 0 \quad (4.14)$$

Obviously, the only satisfactory solution is when $\beta \neq 0$, as otherwise the solution would always be equal to zero. Three constants can now be solved as well, resulting in the solution to the spatial part of the partial differential equation.

$$X(x) = C_n \sin(\frac{n\pi}{l}x) \quad (4.15)$$

4.2.2 The temporal equation

In the temporal domain, there is always a certain form of energy dissipation as a result of movement of air or material deformation, for instance. Hence, a result without damping is not a good resemblance to reality, as a certain beam will not vibrate infinitely. Therefore, damping is included in the temporal domain. For inserting a certain amount of damping, the spatial equation will not change, as it is not dependent on any time variable. The temporal equation that was previously found is expanded with a damping term. This is similar to a mass spring damper system, where the damping term was chosen from mathematical convenience rather than a number with any physical meaning. The temporal equation is equal to

$$T_n''(t) + 2\zeta\omega_n T_n'(t) + \omega_n{}^2 T_n(t) = 0 \quad (4.16)$$

The solution procedure for this equation is similar to that of a single degree of freedom mass spring system, which was elaborately described in the literature study. For the underdamped case, it can be shown that

$$T_n(t) = A_n e^{-\zeta_n\omega_n t}\sin(\omega_{d,n}t) + B_n e^{-\zeta_n\omega_n t}\cos(\omega_{d,n}t) \quad \text{where} \quad \omega_d = \omega\sqrt{\zeta^2 - 1} \quad (4.17)$$

4.2.3 The total solution

The two solutions for both the spatial and the temporal domain are found and thus, these two solutions can be substituted back into the equation where the separation of variables technique was used. As a result of an infinite number of mode shapes, an infinite number of solutions is found for the analytical solution. Again, it is stated that the sum of all solutions is also a solution in linear problems. That finally renders the total solution for an underdamped beam.

$$w(x,t) = \sum_{n=1}^{\infty} A_n e^{-\zeta_n\omega_n t}\sin(\omega_n t)\sin(\frac{n\pi}{l}x) + B_n e^{-\zeta_n\omega_n t}\cos(\omega_n t)\sin(\frac{n\pi}{l}x) \quad (4.18)$$

$$\frac{dw(x,t)}{dt} = \sum_{n=1}^{\infty} A_n\omega_n \sin(\frac{n\pi}{l}x)\left(e^{-\zeta_n\omega_n t}\cos(\omega_n t) - \zeta_n e^{-\zeta_n\omega_n t}\sin(\omega_n t)\right) - B_n\omega_n \sin(\frac{n\pi}{l}x)\left(\zeta_n e^{-\zeta_n\omega_n t}\cos(\omega_n t) + \sin(\omega_n t)\right) \quad (4.19)$$

This solution can now be solved for initial conditions, consisting out of a certain initial displacement $w_0(x)$ and a certain initial velocity $\dot{w}_0(x)$. This implies that the solution that was found is equal to initial conditions at every location, so that

$$w(x,0) = \sum_{n=1}^{\infty} B_n \sin(\frac{n\pi}{l}x) \tag{4.20}$$

$$\dot{w}(x,0) = \sum_{n=1}^{\infty} A_n\omega_n \sin(\frac{n\pi}{l}x) - B_n\omega_n \sin(\frac{n\pi}{l}x) \tag{4.21}$$

In order to solve the constant in terms of initial conditions, both sides are multiplied by $\int_0^l \sin(\frac{m\pi}{l}x)$.

$$\int_0^l \sin(\frac{m\pi}{l}x)\, w(x,0)dx = \sum_{n=1}^{\infty} B_n \int_0^l \sin(\frac{m\pi}{l}x)\sin(\frac{n\pi}{l}x)dx$$

$$\int_0^l \sin(\frac{m\pi}{l}x)\, \dot{w}(x,0)dx = \sum_{n=1}^{\infty} A_n\omega_n \int_0^l \sin(\frac{m\pi}{l}x)\sin(\frac{n\pi}{l}x)dx - B_n\omega_n \int_0^l \sin(\frac{m\pi}{l}x)\sin(\frac{n\pi}{l}x) \tag{4.22}$$

Using the fact that mode shapes are orthogonal, this leads to

$$\int_0^l \sin(\frac{m\pi}{l}x)\, w(x,0)dx = \sum_{n=1}^{\infty} B_n \left(0 + 0 + \cdots + \frac{l}{2}\right) = \frac{D_n l}{2} \tag{4.23}$$

$$\int_0^l \sin(\frac{m\pi}{l}x)\, \dot{w}(x,0)dx = \sum_{n=1}^{\infty} A_n\omega_n \left(0 + 0 + \cdots + \frac{l}{2}\right) - B_n\omega_n \left(0 + 0 + \cdots + \frac{l}{2}\right) = \frac{(C_n - D_n)\omega_n l}{2} \tag{4.24}$$

The constant B_n can be directly expressed in terms of initial conditions. As for the other term, the derivation is slightly more elaborate.

$$B_n = \frac{2}{l}\int_0^l \sin(\frac{n\pi}{l}x)\, w(x,0)dx$$

$$A_n - B_n = \frac{2}{\omega_n l}\int_0^l \sin(\frac{n\pi}{l}x)\, \dot{w}(x,0)dx$$

$$A_n = \frac{2}{\omega_n l}\int_0^l \sin(\frac{n\pi}{l}x)\, \dot{w}(x,0)dx + \frac{2}{l}\int_0^l \sin(\frac{n\pi}{l}x)\, w(x,0)dx \tag{4.25}$$

Substituting these values back into the total solution, this yields the result expressed in terms of boundary conditions and initial conditions. As this beam was given an initial deformation, only the first mode shape affects the deformation if a certain initial displacement is given to the beam at exactly mid span (Figure 4.3).

$$w(x,t) = x_0 e^{-\zeta\omega t} \sin(\frac{\pi}{l}x)(\sin(\omega t) + \cos(\omega t)) \tag{4.26}$$

Similar to linear one-dimensional dynamics, a difference is made in an underdamped, an overdamped and a critically damped situation. The spatial equation will not change for the overdamped solution, however, the temporal equation is now solved for the overdamped case, similar to a one-dimensional problem. For the overdamped situation, the solution to the temporal equation then becomes

$$T_n(x) = A_n e^{-\zeta_n\omega_n t + \omega_{d,n}* t} + B_n e^{-\zeta_n\omega_n t - \omega_{d,n}* t} \quad \text{where} \quad \omega_{d,n} = \omega_n\sqrt{{\zeta_n}^2 - 1} \tag{4.27}$$

Again, these terms can be expressed in terms of initial conditions in the temporal domain and boundary conditions in the spatial domain, resulting in the analytical solution for the overdamped case.

4.3 Discretization of the continuous beam model

Even a simply supported beam subjected to only an initial deformation results already in a complex solution, as one could conclude from the previous section in this part of the report. Furthermore, including the cable truss would render an even more complex analytical solution. Hence, the continuous beam system is approximated by discretizing it in the spatial domain. In contrast to the continuous beam, this approximation only has a limited number of degrees of freedom and although these approximations perform really well, the analytical solution can never be obtained exactly. There are multiple approximation methods available current such as the finite difference method, the finite element method or the discrete element method. Although the finite element method is the most popular one in structural engineering by far, in this case a so called lumped mass model is

used, where the beam is subdivided into three masses, resulting in three degrees of freedom and three natural frequencies for the bridge deck.

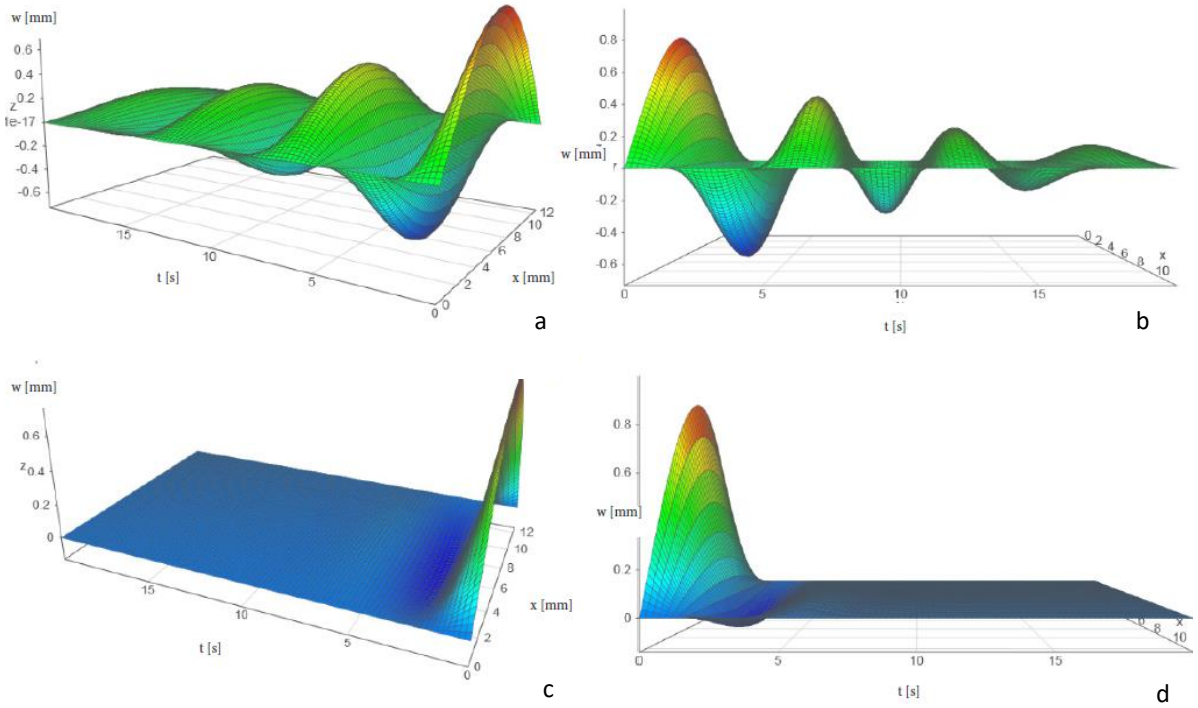

Figure 4.3: Plot of the analytical solution to a continuous beam, underdamped (a and b: ζ=0.1, c and d: ζ=0.7)

The discretized equation is now similar to one-dimensional linear dynamics, where the general solution is found by solving the second order differential equation in time. Each degree of freedom can have its own initial conditions, generally expressed in terms of an initial displacement x_0 and an initial velocity $v_0 = \dot{x}_0$. Initial conditions are in most situations equal to zero, as excitation of a dynamic system is often a result of external loading rather than initial conditions in mechanical engineering. As for this report, the external force acting on the system can be any arbitrary force, for instance an impulse load or a step load. The initial conditions are always taken equal to zero, indicating that the system is not in movement at $t = 0$. Consequently, the differential equation is expanded with a force matrix. In matrix notation, the initial value problem is then equal to

$$\mathbf{M}\ddot{\mathbf{x}}(t) + \mathbf{C}\dot{\mathbf{x}}(t) + \mathbf{K}\mathbf{x}(t) = \mathbf{F}(t)$$

$$\mathbf{x}_0 = 0, \mathbf{v}_0 = 0 \qquad (4.28)$$

4.3.1 The mass matrix

In this report, the beam model was discretized to five masses, where two masses are located directly above the restraints. It should be noted that rotational degrees of freedom are not included in this model, as this model only allows for vertical movement. As a result, these masses simply cannot move over time and a three degree of freedom model remains (Figure 4.4). Each mass should now be taken equal to one quarter of the mass of the total bridge, resulting in

$$m_i = \frac{1}{4}\rho A l \qquad (4.29)$$

It should be noted that discretizing in more degrees of freedom obviously results in a better approximation to the exact solution. In this study, however, it can be shown that a discretization to five nodes already performs fairly accurate.

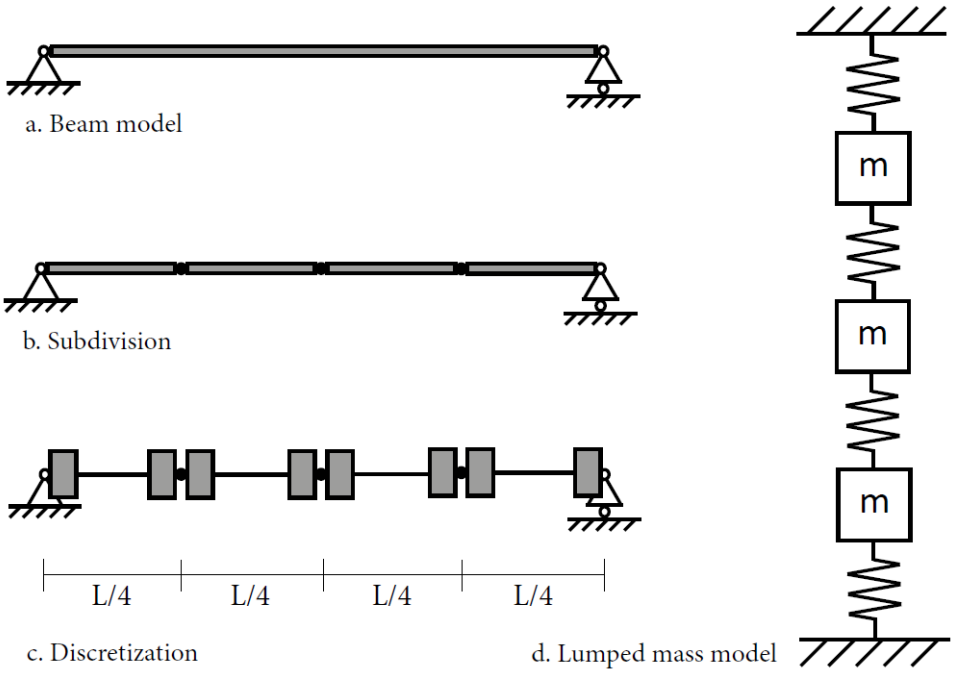

Figure 4.4: Discretization of a continuous system in the spatial domain

4.3.2 The stiffness matrix

Most load cases considered in conservative structural engineering are static loads, independent on time. When considering a pedestrian footbridge in this case, a static load cannot suffice and a moving point load is considered instead. This implies that a certain impulse load, generated by a walking pedestrian, will change over the span of the bridge in time. Again, the Euler-Bernoulli beam theory is used, as it was previously stated that the case study in this report suffices to the conditions of an Euler beam. A relation exists between the external force $q(x)$, which can be any force, and the beam deflection. Here, the constitutive relation between moment (M) and curvature (κ) must be considered as well. As a result, the beam deflection can be described by a fourth order differential equation (Figure 4.5).

$$V(x) = \int q(x)dx \qquad \text{shear force}$$

$$M(x) = \int V(x)dx = \iint q(x)dx \qquad \text{moment distribution}$$

$$\varphi(x) = \int \frac{1}{EI} M(x)\,dx = \frac{1}{EI} \iiint q(x)dx \qquad \text{angular rotation}$$

$$w(x) = \int \varphi(x)dx = \frac{1}{EI} \iint \iint q(x)dx \qquad \text{beam deflection}$$

$$q(x) = EI \frac{d^4 w(x)}{dx^4} \qquad (4.30)$$

In the case of a moving point load, the external force is taken equal to $q(x) = \delta(x - y)$. Here, a unit point load is located somewhere along the beam length at location y. For a simply supported beam, four boundary conditions can be described equal to the boundary conditions in the spatial domain stated previously (eq. 4.5).

$$q(x) = \delta(x - y)$$

$$V(x) = \int \delta(x - y)dx = \Phi(x - y) + c_1$$

$$M(x) = \int \Phi(x - y) + c_1 dx = (x - y)\Phi(x - y) + c_1 x + c_2$$

$$EI\varphi(x) = \int (x - y)\Phi(x - y) + c_1 x + c_2\,dx = \frac{1}{2}(x - y)^2 \Phi(x - y) + \frac{1}{2} c_1 x^2 + c_2 x + c_3$$

$$EIw(x) = \int \frac{1}{2}(x-y)^2\Phi(x-y) + \frac{1}{2}c_1x^2 + c_2x + c_3 = \frac{1}{6}(x-y)^3\Phi(x-y) + \frac{1}{6}c_1x^3 + \frac{1}{2}c_2x^2 + c_3x + c_4 \quad (4.31)$$

Solving for initial conditions, an equation can be found for the deflection of the beam at any location for a point load at a location over the span of the beam. This equation is known as Green's equation, named after the British mathematician George Green (Cabada et al., 2004).

$$w(x,y) = \left(\left(\frac{x-y}{l}\right)^3 \Phi(x-y) + \frac{l-y}{l}\cdot\frac{x}{l}\cdot\left(1-\left(\frac{l-y}{l}\right)^2 - \left(\frac{x}{l}\right)^2\right)\right)\cdot\frac{1}{6}\frac{l^3}{EI} \quad (4.32)$$

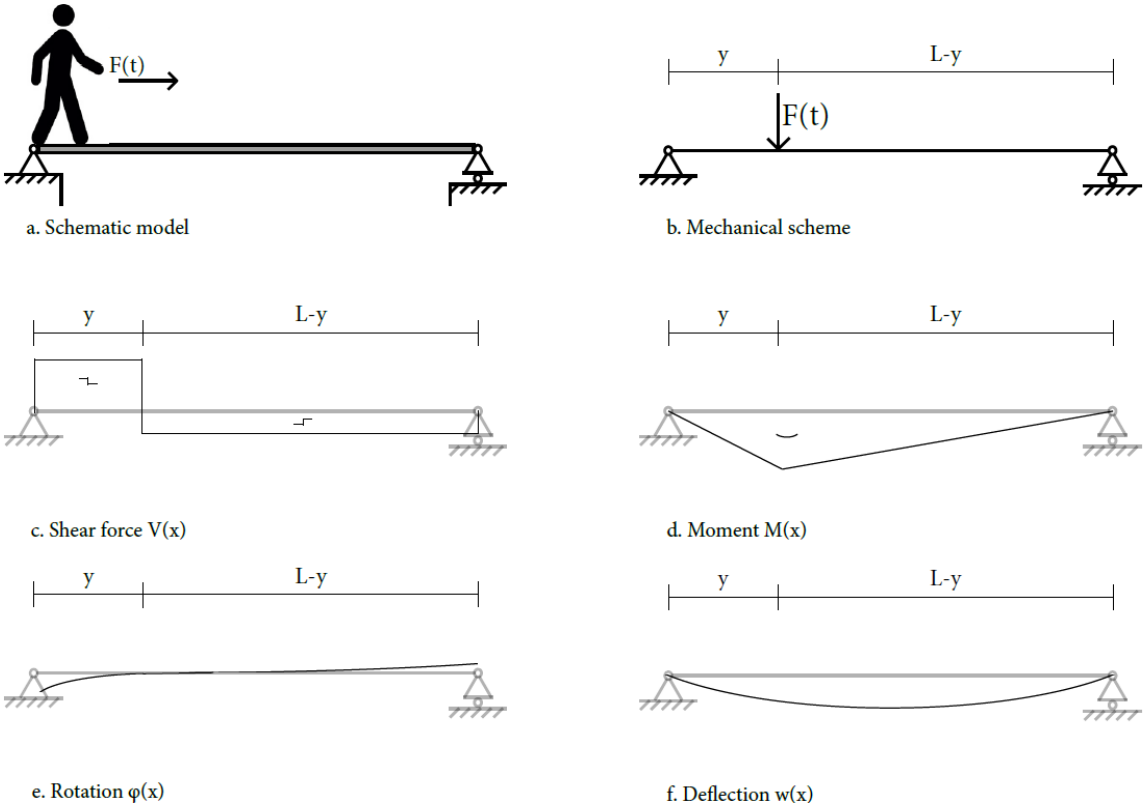

Figure 4.5: Euler-Bernoulli beam theory for a simply supported beam

In this case the beam was discretized into five nodal elements, rendering a three degree of freedom system. That implies that the external force can be applied at three locations over the span of the bridge and that for each applied force three deformations can be measured at the three discretized locations with respect to this applied force. This yields the flexibility matrix of the beam, which is in this case equal to

$$w(x,y) = \mathbf{F} = \begin{bmatrix} w\left(\frac{l}{4},\frac{l}{4}\right) & w\left(\frac{l}{2},\frac{l}{4}\right) & w\left(\frac{3l}{4},\frac{l}{4}\right) \\ w\left(\frac{l}{4},\frac{l}{2}\right) & w\left(\frac{l}{2},\frac{l}{2}\right) & w\left(\frac{3l}{4},\frac{l}{2}\right) \\ w\left(\frac{l}{4},\frac{3l}{4}\right) & w\left(\frac{l}{2},\frac{3l}{4}\right) & w\left(\frac{3l}{4},\frac{3l}{4}\right) \end{bmatrix} = \frac{l^3}{EI}\begin{bmatrix} \frac{3}{256} & \frac{11}{768} & \frac{7}{768} \\ \frac{11}{768} & \frac{1}{48} & \frac{11}{768} \\ \frac{7}{768} & \frac{11}{768} & \frac{3}{256} \end{bmatrix} \quad (4.33)$$

The stiffness matrix is then equal to the inverse of the flexibility matrix of the beam.

$$\mathbf{K} = \mathbf{F}^{-1} = \frac{EI}{l^3}\begin{bmatrix} \frac{4416}{7} & -\frac{4224}{7} & \frac{1728}{7} \\ -\frac{4224}{7} & \frac{6144}{7} & -\frac{4224}{7} \\ \frac{1728}{7} & -\frac{4224}{7} & \frac{4416}{7} \end{bmatrix} \quad (4.34)$$

4.3.3 The damping matrix

As for now, an undamped discretized model is found that represents a continuous system, which is a beam in this case. In practice, there is always some kind of energy dissipation present in a structure. Hence, an undamped system would not be a realistic representation of reality. Damping in discretized models differs from that of a continuous system and there are many models that can describe damping is such systems. The most common form of damping is viscous damping, which was also described extensively in one-dimensional linear dynamics in the literature study. Although it is known that viscous damping is based on mathematical convenience rather that physical meaning, this form of damping performs very well and is widely the most applied form of damping in problems that involve dynamic responses. Many other forms of damping like for instance Coulomb damping do have more physical meaning, however do often include non-linear terms. As for this problem, these forms of damping are not included, as damping is already considered a complex part in the dynamic problem. In the discretized dynamical model in this project, proportional damping is used, which is a special form of viscous damping. In proportional damping, also known as Rayleigh damping, the damping matrix is a linear combination of the mass and stiffness matrix, where two constants α and β are to be determined and can be related to the material property, for instance. The damping matrix is then equal to

$$\mathbf{C} = \alpha\mathbf{M} + \beta\mathbf{K} \tag{4.35}$$

As there are two coefficients, only two damping ratios can be chosen directly, although there is in fact a different damping ratio for each natural frequency. It seems rather straightforward to choose these factors for the first and second natural frequency, as these are the main contributors to the total behavior of the system. From one-dimensional dynamics it was found that the damping coefficient can expressed in terms of the natural frequency as $c = 2\zeta m\omega$ and that the natural frequency is equal to $\omega = \sqrt{k/m}$. Using proportional damping, it can thus be shown that

$$2\zeta_i\omega_i = \alpha + \beta\omega_i^2 \tag{4.36}$$

This expression can be solved for the first two natural frequencies to find proper values for α and β (Figure 4.6). Values for ζ have been determined in a number of experimental studies. Structural steel, for instance, has values for ζ around $0.01 - 0.1$ (Bachmann, 1995).

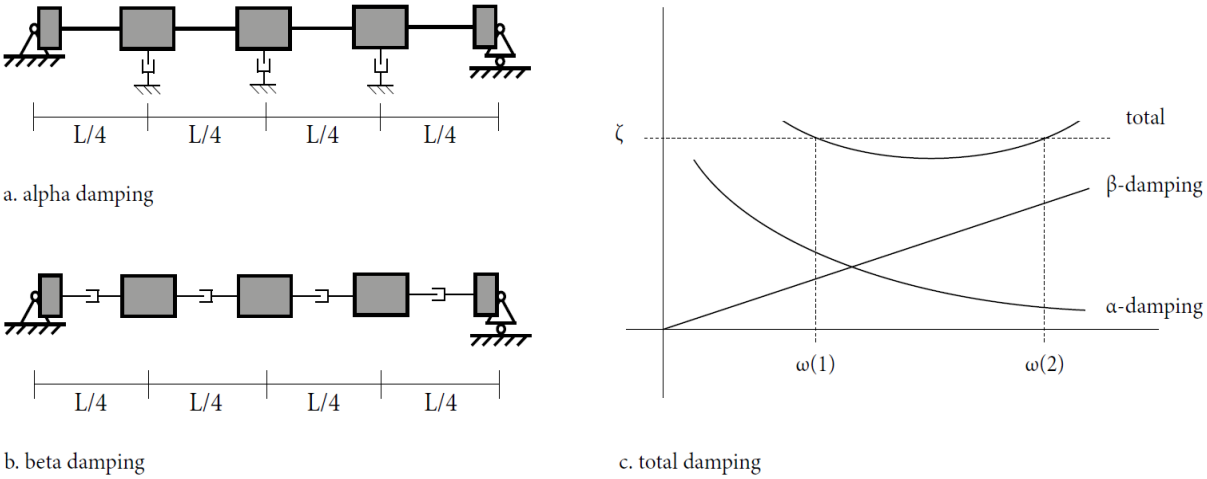

Figure 4.6: Proportional damping

4.3.4 Natural frequencies

The total solution for the three degree of freedom system can now be described in the general second order differential equation (eq. 4.28). In this equation, the force matrix consists of an external force acting on each mass of the system. This force may be any arbitrary force. Motion for the beam can now be described in the form of

$$\frac{\rho Al}{4}\begin{bmatrix}1&0&0\\0&1&0\\0&0&1\end{bmatrix}\begin{bmatrix}\ddot{x}_1(t)\\\ddot{x}_2(t)\\\ddot{x}_2(t)\end{bmatrix}+\begin{bmatrix}\alpha\frac{\rho Al}{4}+\beta\frac{4416}{7}\frac{EI}{l^3} & -\beta\frac{4224}{7}\frac{EI}{l^3} & \beta\frac{1728}{7}\frac{EI}{l^3}\\ -\beta\frac{4224}{7}\frac{EI}{l^3} & \alpha\frac{\rho Al}{4}+\beta\frac{6144}{7}\frac{EI}{l^3} & -\beta\frac{4224}{7}\frac{EI}{l^3}\\ \beta\frac{1728}{7}\frac{EI}{l^3} & -\beta\frac{4224}{7}\frac{EI}{l^3} & \alpha\frac{\rho Al}{4}+\beta\frac{4416}{7}\frac{EI}{l^3}\end{bmatrix}\begin{bmatrix}\dot{x}_1(t)\\\dot{x}_2(t)\\\dot{x}_3(t)\end{bmatrix}+$$

$$\frac{EI}{l^3}\begin{bmatrix}\frac{4416}{7} & -\frac{4224}{7} & \frac{1728}{7}\\ -\frac{4224}{7} & \frac{6144}{7} & -\frac{4224}{7}\\ \frac{1728}{7} & -\frac{4224}{7} & \frac{4416}{7}\end{bmatrix}\begin{bmatrix}x_1(t)\\x_2(t)\\x_3(t)\end{bmatrix}=\begin{bmatrix}F_1(t)\\F_2(t)\\F_3(t)\end{bmatrix} \tag{4.37}$$

The solution that is found can also be described in the undamped case, if the damping coefficients are simply equal to zero. Evaluating the differential equation without any external force acting on the system, an eigenvalue problem can be formulated which approximates the natural frequencies of the exact solution. Solving for arbitrary values of x (i.e. $x_n(t) \neq 0$) renders the first three natural frequencies of the three degree of freedom model in this case. The eigenvalue problem is then equal to

$$\left(\frac{EI}{l^3}\begin{bmatrix}\frac{4416}{7} & -\frac{4224}{7} & \frac{1728}{7}\\ -\frac{4224}{7} & \frac{6144}{7} & -\frac{4224}{7}\\ \frac{1728}{7} & -\frac{4224}{7} & \frac{4416}{7}\end{bmatrix}-\omega_n^2\frac{\rho Al}{4}\begin{bmatrix}1&0&0\\0&1&0\\0&0&1\end{bmatrix}\right)\begin{bmatrix}x_1(t)\\x_2(t)\\x_3(t)\end{bmatrix}=\begin{bmatrix}0\\0\\0\end{bmatrix} \tag{4.38}$$

The natural frequencies that are found by solving the eigenvalue problem can be compared to the natural frequencies found in the exact solution, by recalling that the exact natural frequency can be found by evaluating the eigenvalue problem that was found for the exact solution (eq. 6.14). In the exact case, an infinite number of eigen values is found from

$$\omega^2 = \beta^4\frac{EI}{\rho A} \rightarrow \omega = \frac{n^2\pi^2}{l^2}\sqrt{\frac{EI}{\rho A}} \tag{4.39}$$

As an example, a steel tube (120x60x4) has been evaluated for both the discretized solution, the analytical solution and a finite element model (Table 4.1). It should be noted that the first few natural frequencies are approximated better when the number of lumped masses increases. Although larger Eigen modes are not accurately predicted at all, it can still be concluded that the discretized models performs quit accurate, as these higher natural frequencies also have a negligible effect on the total deformation. The three degree of freedom model can only take into account the first three natural frequencies of the system where mode one and two are predicted fairly accurate. Although this model looks rather inaccurate by only using three degrees of freedom, it should be noted that the first Eigen mode affects the total deformation for roughly 67% , whereas the second respectively third mode shape affect the total deformation for around 17% and 7%. This implies that all other Eigen modes larger than the first three contribute to the total system for only 9%. It seems thus ratified to use a discretized model with three degrees of freedom.

Natural frequency	Analytical solution	1 degree of freedom	2 degrees of freedom	3 degrees of freedom	FE Model	% of total deflection
1^{st}	137.399	136.402	137.253	137.358	140.111	67%
2^{nd}	549.596	–	531.578	545.609	556.546	17%
3^{rd}	1236.592	–	–	1158.446	1181.666	7%
4^{th}	2198.386	–	–	–	–	<9%
5^{th}	3434.977	–	–	–	–	
n^{th}	∞	–	–	–	–	

Table 4.1: Natural frequencies from the discretized model compared to the analytical solution and a finite element model

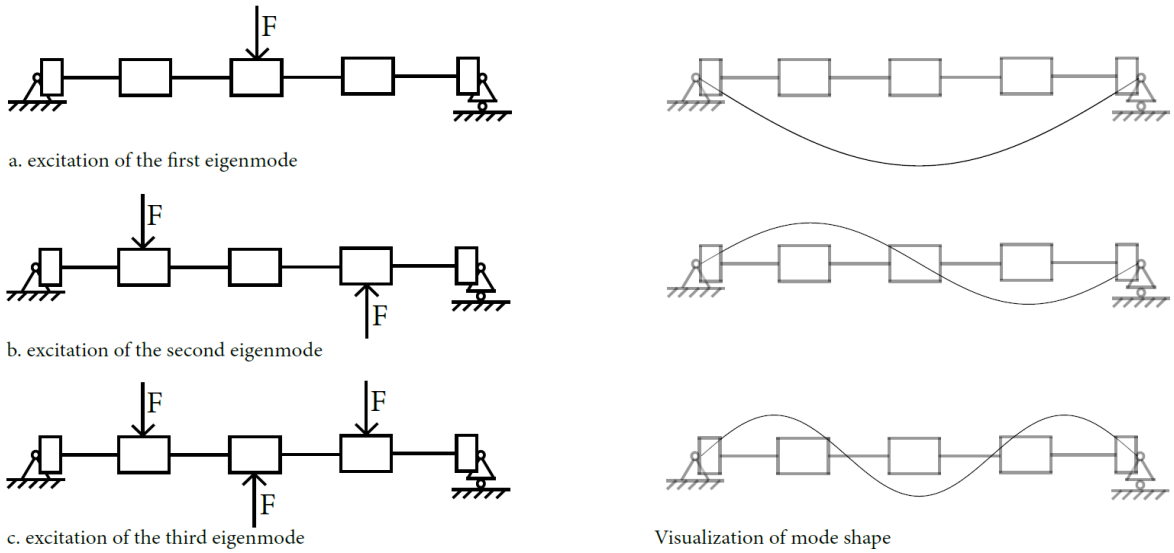

Figure 4.7: Mode shapes

4.4 Numerical approximations

As for now, the continuous system was simplified insofar, that the differential equation is now second order and only has a full derivative in time. Furthermore, the freedom of each mass in the lumped mass model is restricted to only one direction and the limited number of degrees of freedom also results in a limited number of mode shapes, influencing the system. The remaining multiple degree of freedom system theoretically can be solved analytically, albeit in a complex fashion even for elementary systems. Moreover, it is not possible or at least highly complex to solve non-linearity's in the analytic method. A non-linear force, like for instance step loading, could theoretically be approximated by using the so called Fourier Series (Dym, 1972). Unfortunately, this is very complex and time consuming to do in an analytical fashion. As non-linearity's are an important factor in the numerical model, the lumped mass model is approximated numerically. Hence, the main principles that are used in this project regarding numerical approximations are described in this section.

4.4.1 Explicit and implicit methods

There are different strategies when it comes to numerical solving complex differential equations. Common known approximation methods include Euler's methods or the Runge-Kutta algorithm, for instance. The basis, however, of these numerical approximations is always to essentially 'undo' calculus by presenting a small but finite difference instead of the derivative. That means that the procedure produces a set of discrete values that will approximate the actual solution. Creating a very small step, this approximation can become so close the actual solution that it is accepted in general (Zwillinger, 1989). In mathematical terms, this implies that

$$\dot{x}(t) = \frac{dx(t)}{dt} = \lim_{\Delta t \to 0} \frac{x(t_{n+1}) - x(t_n)}{t_{n+1} - t_n} = \lim_{\Delta t \to 0} \frac{x(t_{n+1}) - x(t_n)}{\Delta t} \tag{4.40}$$

Rewriting in terms of the future state of the system renders

$$x(t_{n+1}) = x(t_n) + \dot{x}(t)\Delta t \tag{4.41}$$

Two types of numerical approximation methods include explicit and implicit solving, where the former method calculates the future state $f(\mathbf{x}(t_{n+1}), t_{n+1})$ of the system by evaluating the current state $f(\mathbf{x}(t_n), t_n)$ of the system (eq. 4.41). The explicit fourth order Runge-Kutta algorithm was used to numerically approximate the lumped mass model in this report. The second order differential equation is first rewritten in two differential equations, reducing this set of equations to the first order. This renders a displacement vector and a derivative of the displacement vector, which is equal to the velocity vector. Considering the general mass spring damper equation (eq. 4.28), this can be described as

$$\mathbf{x_1}(t) = \mathbf{x}(t)$$

$$\mathbf{x_2}(t) = \dot{\mathbf{x}}(t) = \mathbf{v}(t) \tag{4.42}$$

Taking the derivative of these two vectors results in

$$\dot{\mathbf{x}}_\mathbf{1}(t) = \dot{\mathbf{x}}(t) = \mathbf{x_2}(t)$$

$$\dot{\mathbf{x}}_\mathbf{2}(t) = \ddot{\mathbf{x}}(t) \tag{4.43}$$

The second order differential equation, describing the dynamic discretized model, can then be rewritten in terms of $\dot{\mathbf{x}}_\mathbf{1}(t)$ and $\dot{\mathbf{x}}_\mathbf{2}(t)$.

$$\dot{\mathbf{x}}_\mathbf{2}(t) = -\mathbf{M}^{-1}\mathbf{K}\,\mathbf{x_1}(t) - \mathbf{M}^{-1}\mathbf{C}\,\mathbf{x_2}(t) + \mathbf{M}^{-1}\mathbf{F}(t) \tag{4.44}$$

Rewriting this in matrix notation, one finds an expression for $\dot{\mathbf{x}}(t) = [\dot{\mathbf{x}}_\mathbf{1}(t) \quad \dot{\mathbf{x}}_\mathbf{2}(t)]^T$, which is equal to

$$\dot{\mathbf{x}}(t) = \begin{bmatrix} \mathbf{x_2}(t) \\ -\mathbf{M}^{-1}\mathbf{K}\,\mathbf{x_1}(t) - \mathbf{M}^{-1}\mathbf{C}\,\mathbf{x_2}(t) + \mathbf{F}(t) \end{bmatrix} = \mathbf{A}\begin{bmatrix}\mathbf{x_1}(t) \\ \mathbf{x_2}(t)\end{bmatrix} + \begin{bmatrix}\mathbf{0} \\ \mathbf{M}^{-1}\mathbf{F}(t)\end{bmatrix}$$

$$\mathbf{A} = \begin{bmatrix} \mathbf{0} & \boldsymbol{I} \\ -\mathbf{M}^{-1}\mathbf{K} & -\mathbf{M}^{-1}\mathbf{C} \end{bmatrix} \tag{4.45}$$

The derived solution for the derivative of the mass spring damper system is now inserted into the fourth order Runge-Kutta algorithm, which states that

$$A_{n,1} = f(\mathbf{x}(t_n), t_n) = \dot{\mathbf{x}}(t_n) = \quad \mathbf{A}\mathbf{x}(t_n) + \mathbf{F}(t)$$

$$A_{n,2} = f\left(\mathbf{x}(t_n) + \tfrac{\Delta t}{2}A_{n,1}, t_n + \tfrac{\Delta t}{2}\right) = A\left(\mathbf{x}(t_n) + \tfrac{\Delta t}{2}A_{n,1}\right)$$

$$A_{n,3} = f\left(\mathbf{x}(t_n) + \tfrac{\Delta t}{2}A_{n,3}, t_n + \tfrac{\Delta t}{2}\right) = A\left(\mathbf{x}(t_n) + \tfrac{\Delta t}{2}A_{n,2}\right)$$

$$A_{n,4} = f\big(\mathbf{x}(t_n) + \Delta t A_{n,3}, t_n + \Delta t\big) = A\big(\mathbf{x}(t_n) + \Delta t A_{n,3}\big)$$

$$\mathbf{x}(t_{n+1}) = \mathbf{x}(t_n) + \tfrac{1}{6}(A_{n,1} + 2A_{n,2} + 2A_{n,3} + A_{n,4})\Delta t \tag{4.46}$$

The main difference between an explicit approximation and an implicit approximation method is that the latter calculates the future state $f(\mathbf{x}(t_{n+1}), t_{n+1})$ of the system by evaluating the future state of the system rather that the current state (eq. 4.47).

$$x(t_{n+1}) = x(t_n) - \dot{x}(t_{n+1})\Delta t \tag{4.47}$$

This type of approximation is more complex and sometimes requires iterations, however guarantees numerical stability. The most basic implicit method is used in this project, known as the first order Euler Backward Scheme. Numerical stability is then guaranteed for any time increment. It is stated that the derivative that was found for the dynamic model holds for all Δt, hence

$$\mathbf{x}(t_{n+1}) = \begin{bmatrix}\mathbf{x_1}(t_n) \\ \mathbf{x_2}(t_n)\end{bmatrix} - \begin{bmatrix}\mathbf{0} & \boldsymbol{I} \\ -\mathbf{M}^{-1}\mathbf{K} & -\mathbf{M}^{-1}\mathbf{C}\end{bmatrix}\begin{bmatrix}\mathbf{x_1}(t_{n+1}) \\ \mathbf{x_2}(t_{n+1})\end{bmatrix} - \begin{bmatrix}\mathbf{0} \\ \mathbf{M}^{-1}\mathbf{F}(t_{n+1})\end{bmatrix} \tag{4.48}$$

This equation can be rewritten in terms of $\mathbf{x}(t_{n+1})$, by stating that the external force acting on the system in the future state is known. This also implies that the force generated by the actuator must have a time delay that is at least as large as the time increment chosen, as otherwise this force cannot be predicted and the implicit method cannot be used without iterating. Rewriting the implicit method renders an approximation to the dynamic model. For a single degree of freedom system one can find that

$$\mathbf{x}(t_n) = \mathbf{x}(t_{n+1}) - \mathbf{A}\mathbf{x}(t_{n+1})\Delta t = (\mathbf{I} - \Delta t\mathbf{A})\mathbf{x}(t_{n+1})\Delta t$$

$$\mathbf{A} = \begin{bmatrix} 0 & 1 \\ -\frac{k}{m} & -\frac{c}{m} \end{bmatrix} \tag{4.49}$$

$$\mathbf{x}(t_{n+1}) = (\mathbf{I} - \Delta t\mathbf{A})^{-1}\mathbf{x}(t_n) \tag{4.50}$$

Solving this equation leads to an expression for $\mathbf{x}(t_{n+1})$, which is equal to

$$\mathbf{x}(t_{n+1}) = \begin{bmatrix} \frac{c\Delta t+m}{k\Delta t^2+c\Delta t+m} & \frac{m\Delta t}{k\Delta t^2+c\Delta t+m} \\ \frac{k\Delta t}{k\Delta t^2+c\Delta t+m} & \frac{m}{k\Delta t^2+c\Delta t+m} \end{bmatrix} \begin{bmatrix} \mathbf{x_1}(t_n) \\ \mathbf{x_2}(t_n) \end{bmatrix} \tag{4.51}$$

It should be noted that for more than one degree of freedom each future state of mass m_i also depends on the future state of all other masses in the system. As a result, n expressions are found with n unknowns and theoretically all expressions can be solved, albeit in a complex manner for more degrees of freedom.

4.4.2 Stability

The main benefit of the implicit method is numerical stability for all Δt in the negative real part of the imaginary plane, resulting from the future state of the system, which is taken into account. In other words, all differential equations having a derivative converging to zero are implicit solved in a stable manner (Figure 4.8b). And indeed, this is true for all damped vibration problems. On the other hand, higher order approximation methods that are more precise will lead to very complex solutions and are better solved explicitly. The main disadvantage in explicit solving is that overshoot may result in unstable behavior in stiff equations (Figure 4.8a). Hence, it is chosen to solve the dynamic model explicitly where possible in this project. If unstable behavior starts to develop, the problem is solved implicitly.

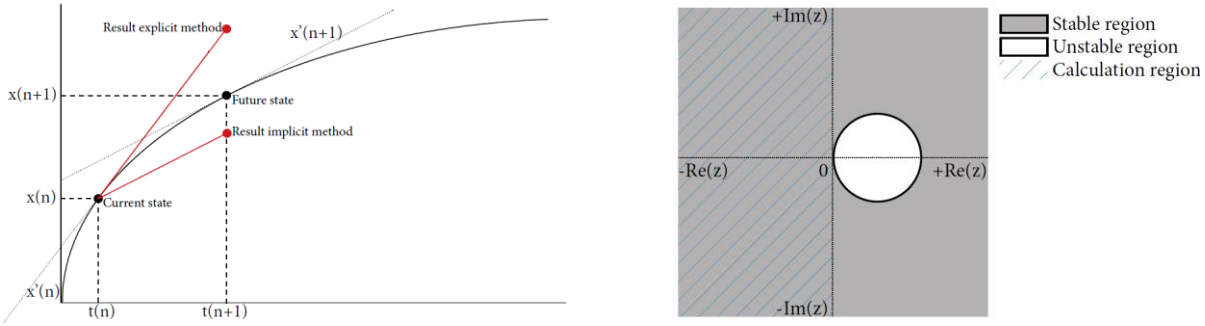

Figure 4.8: Implicit and explicit approximation (a), implicit stable region (b)

The explicit and implicit method are compared for a typical mass spring damper system with its exact solution given for a certain initial velocity and displacement. The explicit method indeed performs much better in small time increments, however starts to develop unstable behavior at a certain increment (Figure 4.10). It must be noted that this transition point is found for smaller time increments if degrees of freedom are extended.

4.5 Discretization of the cable truss

A dynamic model of a simply supported beam can be analyzed numerically by means of a discretized mass spring model with multiple degrees of freedom. As a result, the response to any external force of this beam can be predicted in a numerical approximation. The case study, however, cannot be considered as a beam only, as it includes a cable truss that is placed under the bridge to provide extra stiffness (Figure 4.9).

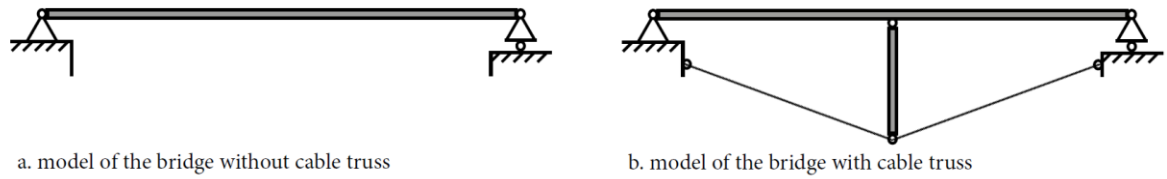

Figure 4.9: Bridge with and without cable truss

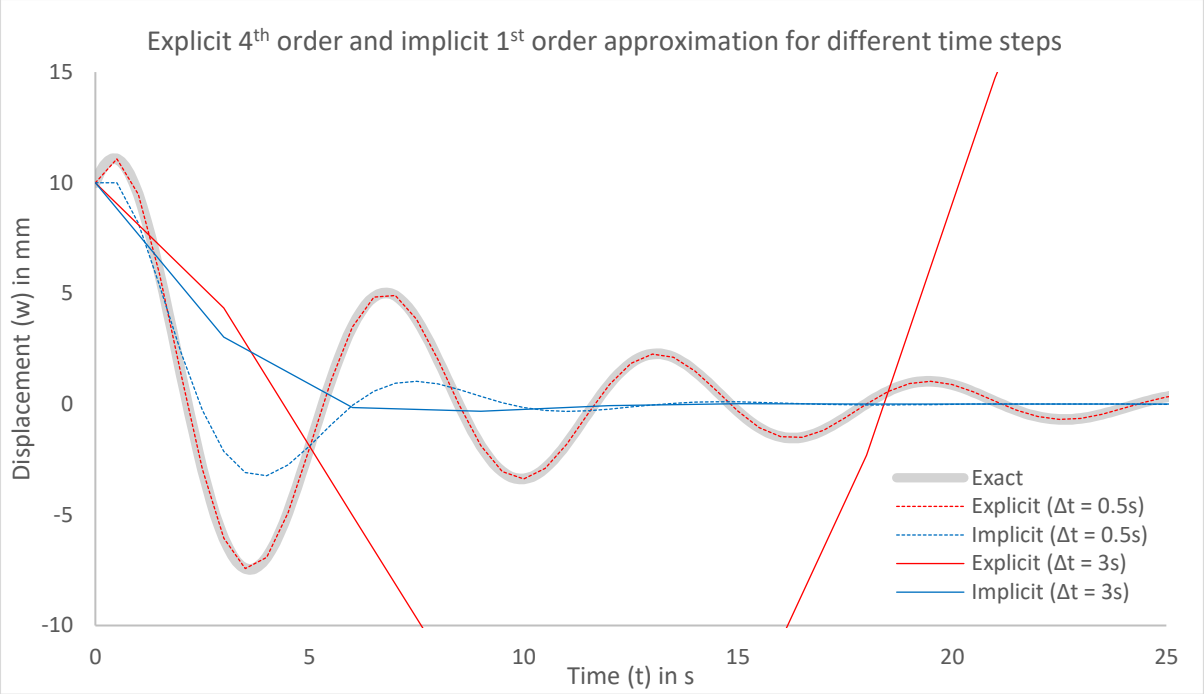

Figure 4.10: Unstable behavior of the explicit approximation

The cable truss is loaded only in tension and in between the wire and the bridge deck, structural elements are added to provide better resistance to vibrations, as will be discussed later in this report. The cable truss is not connected to the bridge directly, but is supported at secondary support locations. In this section, the most important (dynamic) properties of structural steel wire rope are discussed and some steps in the discretization to this part of the bridge are shown.

4.5.1 Stiffness

The steel cable truss is converted into an equivalent spring and damping coefficient to be able to add the truss to the discretized beam model. Steel wire ropes are built from a core, where a number of strands are woven around where the core may be steel or a fiber material. The design tensile strength of a steel wire rope is often much larger than normal structural steelwork. Secondly, the elongation of the wire is non-linear in both the time and the spatial domain. The initial strain of a cable is relatively large for small external forces, whereas the strain decreases when the external force increases. Regarding strain, the strain diagram is different for loading and unloading of the cable and after a number of loading cycles, the stress strain diagram is different again. This also results in a non-linear modulus of elasticity (Feyrer, 2015). Since the cable truss is an important factor in the bridge model, the cable properties of the used wire rope have been determined in the laboratory of the University of Eindhoven. In order to do so, a tensile test was performed and the strain of a test specimen was measured for a number of cycles (Figure 4.11, Figure 4.12). After a number of cycles, the difference in strain converges to a certain σ-ε-diagram, which remains constant for each new load cycle. Using the strain values found from the n^{th} cycle, the modulus of elasticity could be determined as a function of the tensile force in the steel wire, for both loading and unloading (Figure 4.13).

The Young's Modulus found from the experimental is described by a non-linear function with respect to tensile force, which is similar to several literature studies that have been performed. The total force in the steel wires can now be determined by stating that this is an addition of a certain amount of pretension, set by the user, and a force resulting from the external force on the bridge. Since the truss consists here out of four cables, the cable force is equal to

$$F_{wire} = F_p + \frac{1}{4}\frac{F_e}{\sin(\alpha)} \tag{4.52}$$

Figure 4.11: Strain test of the wire rope

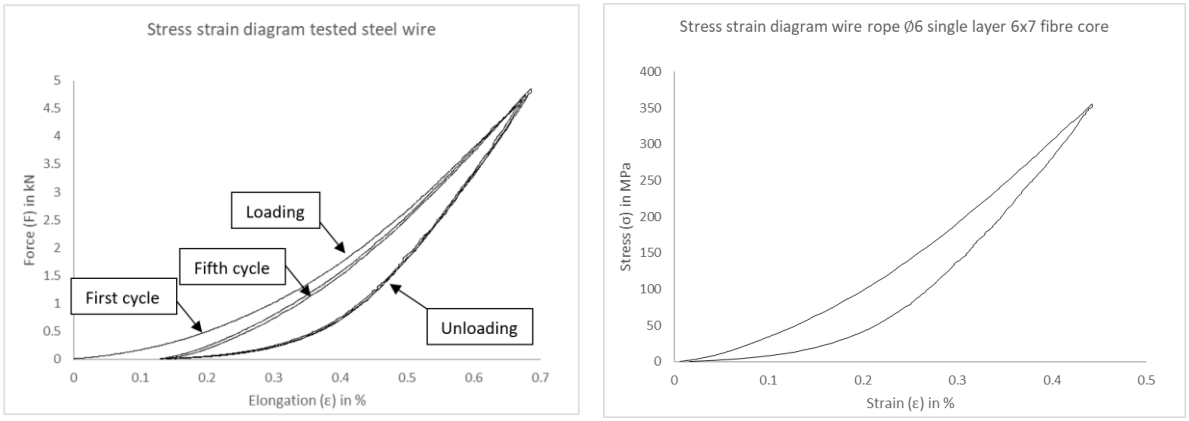

Figure 4.12: Five cycles of loading and unloading (a) and a resulting stress strain diagram after a number of cycles (b)

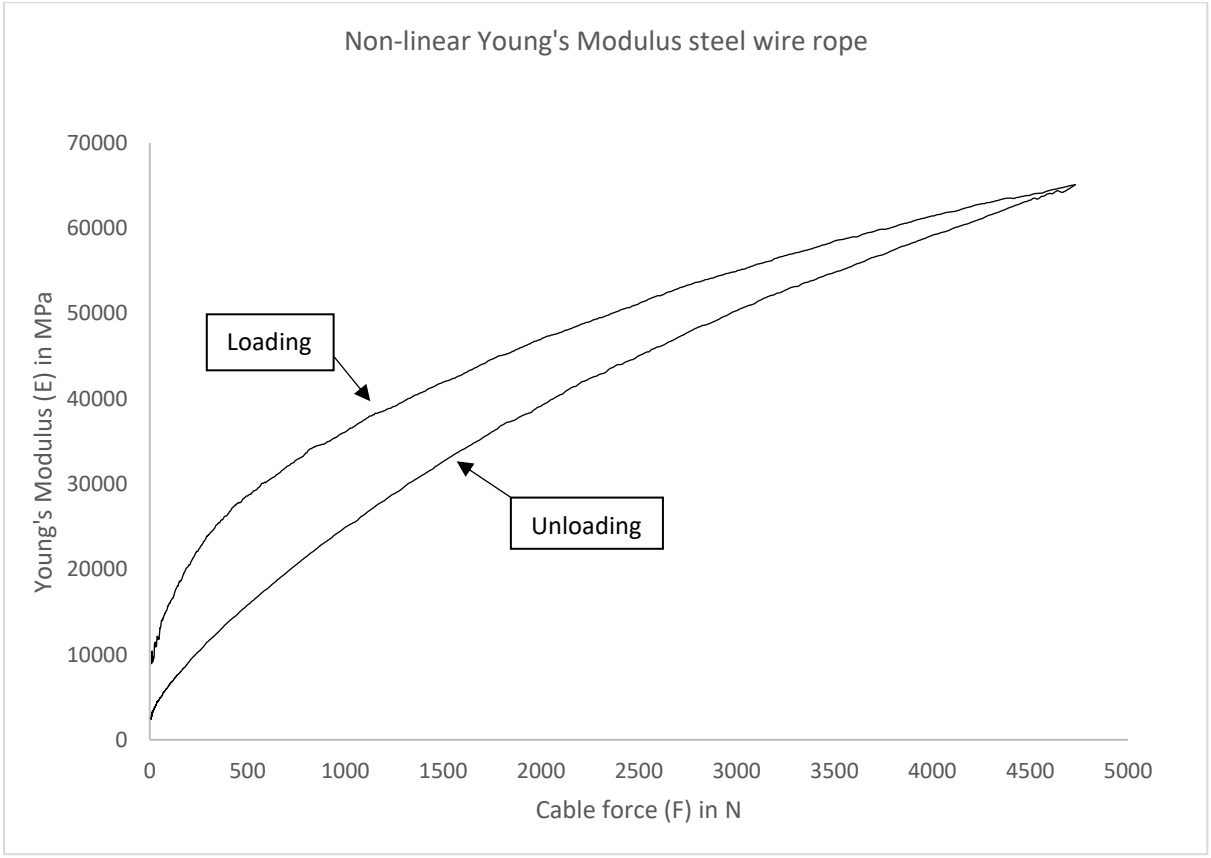

Figure 4.13: Modulus of elasticity for the structural steel wire ropes used in this project (6x7 single layer strand, fibre core)

In this equation, α is the angle between the horizontal x-axis and the cable truss. The advantage of a numerical approximation method compared to an analytical solution is that non-linearity's can be taken into account rather easy, as in each time step, all physical parameters can be updated. In this case, the external force is calculated after every iteration in time and as a result, the stiffness of the cable truss can be determined by using the correct E-modulus at this very time step. The equivalent stiffness is then calculated from the elongation of each wire in vertical direction. As the bridge is supported by four wires in total, this is then equal to

$$k_{wire} = \frac{4\sin(\alpha)EA}{l} \tag{4.53}$$

4.5.2 Damping

A structural steel wire can vibrate in the transverse direction and the longitudinal direction. Although in many applications the transverse direction is of importance (i.e. sound from stringed instruments), it was assumed that in this study the longitudinal direction only has noticeable influence on the system. From several studies (e.g. Feyrer, 2015) it can be shown that damping in longitudinal direction has a certain decay curve, which is similar to damping applied in a mass spring system by means of mathematical convenience rather than actual physical meaning. To that extent, a damping coefficient can be inserted directly into the mass spring model by using an equivalent value for this particular wire (Figure 4.14). As a result, the total discretized solution from (eq. 4.37) can be extended by the values from the cable truss for mass, spring stiffness and damping. The discretized solution is then equal to

$$\begin{bmatrix} \frac{\rho Al}{4} & 0 & 0 \\ 0 & \frac{\rho Al}{4} + m_{wires} & 0 \\ 0 & 0 & \frac{\rho Al}{4} \end{bmatrix} \begin{bmatrix} \ddot{x}_1(t) \\ \ddot{x}_2(t) \\ \ddot{x}_2(t) \end{bmatrix} + \begin{bmatrix} \alpha\frac{\rho Al}{4} + \beta\frac{4416}{7}\frac{EI}{l^3} & -\beta\frac{4224}{7}\frac{EI}{l^3} & \beta\frac{1728}{7}\frac{EI}{l^3} \\ -\beta\frac{4224}{7}\frac{EI}{l^3} & \alpha\frac{\rho Al}{4} + \beta\frac{6144}{7}\frac{EI}{l^3} + c_{wires} & -\beta\frac{4224}{7}\frac{EI}{l^3} \\ \beta\frac{1728}{7}\frac{EI}{l^3} & -\beta\frac{4224}{7}\frac{EI}{l^3} & \alpha\frac{\rho Al}{4} + \beta\frac{4416}{7}\frac{EI}{l^3} \end{bmatrix} \cdot$$
$$\begin{bmatrix} \dot{x}_1(t) \\ \dot{x}_2(t) \\ \dot{x}_3(t) \end{bmatrix} + \begin{bmatrix} \frac{4416}{7}\frac{EI}{l^3} & -\frac{4224}{7}\frac{EI}{l^3} & \frac{1728}{7}\frac{EI}{l^3} \\ -\frac{4224}{7}\frac{EI}{l^3} & \frac{6144}{7}\frac{EI}{l^3} + \frac{4\sin(\alpha)EA}{L} & -\frac{4224}{7}\frac{EI}{l^3} \\ \frac{1728}{7}\frac{EI}{l^3} & -\frac{4224}{7}\frac{EI}{l^3} & \frac{4416}{7}\frac{EI}{l^3} \end{bmatrix} \begin{bmatrix} x_1(t) \\ x_2(t) \\ x_3(t) \end{bmatrix} = \begin{bmatrix} F_1(t) \\ F_2(t) \\ F_3(t) \end{bmatrix} \tag{4.54}$$

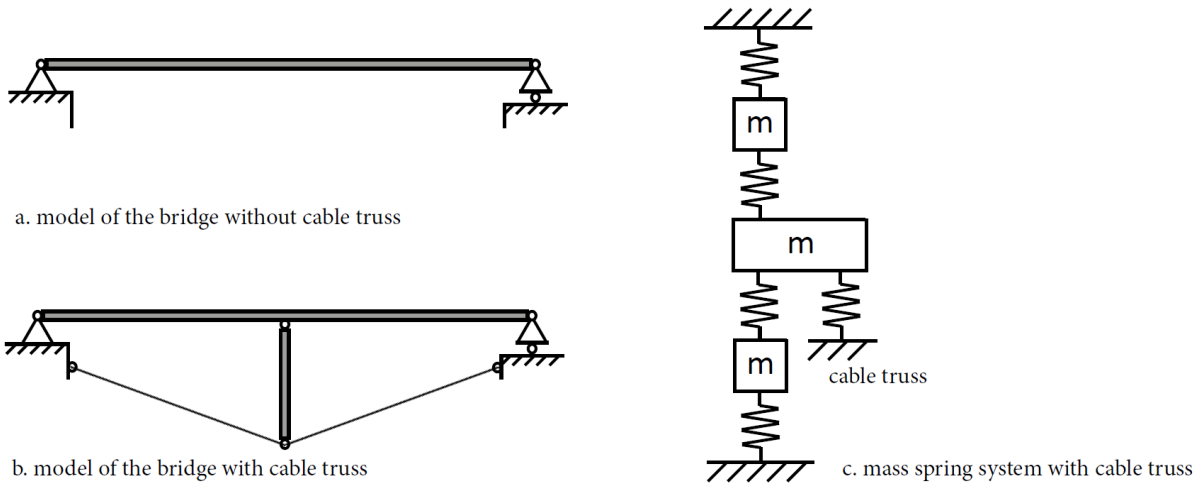

Figure 4.14: Mass spring model of the bridge with cable truss

4.6 Numerical simulation of stabilization methods

The slender bridge design is highly unstable and this will result in a noticeable dynamic response to external loads. In this case, the bridge was designed to be sensitive to vibrations in order to demonstrate the principles of different solution methodologies to stabilization of lightweight structures. As the bridge deck structurally only consists out of two very slender steel tubes, unacceptable deformations and stresses already start to develop for small external loads and as a result, the cable truss was added to the bridge. Hence, the cable truss mainly

contributes to the stiffness of the structure rather than making the bridge more comfortable by reducing vibrations. Regarding the Eurocode, some comfort criteria are described, for instance that vertical mode shapes may not vibrate in a lower frequency than $5\ Hz$, as most of the pedestrians walk around a frequency below this value. Of course, a natural frequency of the structure similar to the walking frequency of a pedestrian is undesirable, as this could cause resonance. Vertical accelerations may not exceed $0.7\ m/s^2$ and horizontally these requirements are even stricter. It should be noted that these requirements are not met by far in the current case study and that additional measurements are necessary. In this case, both a passive damper and a control system were considered. Both systems were implemented in the numerical model in order to examine the influence of each system both separate and as a combination.

4.6.1 Passive system: viscous damping

Viscous damping is actually a form of energy dissipation, similar to all forms of damping. It was already seen that dampers are applied in a number of examples to resist loading configurations that cannot be assumed static, as for instance wind loading on large, relative lightweight stadiums or harmonic loading in area's sensitive to earthquakes (Figure 4.15a). Although dampers are found in many fields of engineering, fluctuating from small to large-scale applications, the principle of each damper is approximately similar. A viscous damper usually consists out of a cylinder, which is filled with a high viscosity fluid, like oil. In this cylinder often two chambers exists, separated by a piston. This piston can then move from the start to the end of the chamber and while this movement occurs, the oil can pass through small openings of the piston (Symans, 1998). As a result, energy is absorbed when the damper deforms and as a result, this system works as an absorber of vibrating systems (Figure 4.15b). Implementing a viscous damper into a mass spring system usually results in negligible damping coefficients for the other elements in this system.

a. damper in a structural application

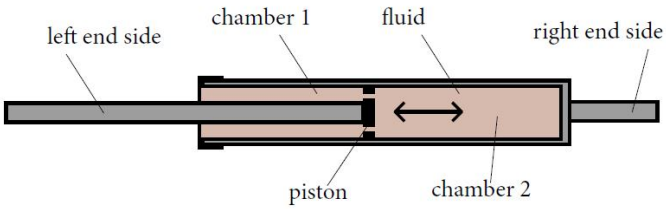

b. schematic model of a damper

Figure 4.15: Viscous damping

The viscous damper is implemented in the numerical model of the bridge exactly in between the cable truss and the bridge deck at mid span. This implies that in between the spring representing the cable truss and the middle mass of the discretized beam an extra degree of freedom is added, consisting out of the damper with a certain damping coefficient and a certain mass. Adding spring stiffness, the damper turns into a shock absorber.

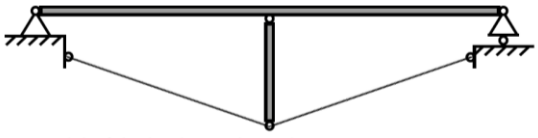

a. model of the bridge without damper

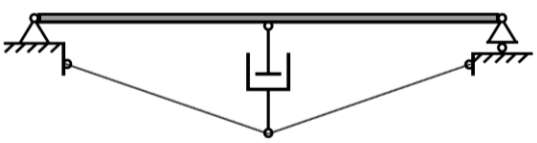

b. model of the bridge with damper

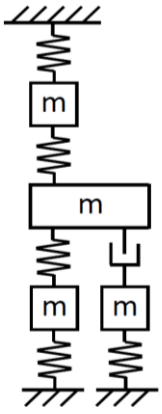

c. damper in the mass spring system

Figure 4.16: Schematic model for a viscous damper

It is now assumed that half of the mass of the damper is included in the center mass of the bridge and that the other half is modeled as the new (fourth degree of freedom) mass, where the total mass is an addition of the damper and the cable truss. Furthermore, it is assumed that the damper must also have a certain spring stiffness, similar to the well-known shock absorbers. This spring stiffness is needed to provide resistance to loads that occur for a relative large period of time. As one could think, a constantly increasing deformation would be the result if no spring stiffness was added in the numerical model, as then no resistance would be present to resist deformation over a longer period of time. The differential equation is extended by the properties of the damper, indicated with $\ldots_d$(Figure 4.16).

$$\begin{bmatrix} \frac{\rho Al}{4} & 0 & 0 & 0 \\ 0 & \frac{\rho Al}{4}+\frac{1}{2}m_d & 0 & 0 \\ 0 & 0 & \frac{\rho Al}{4} & 0 \\ 0 & 0 & 0 & \rho_w Al+\frac{1}{2}m_d \end{bmatrix} \begin{bmatrix} \ddot{x}_1(t) \\ \ddot{x}_2(t) \\ \ddot{x}_3(t) \\ \ddot{x}_4(t) \end{bmatrix} + \begin{bmatrix} \alpha\frac{\rho Al}{4}+\beta\frac{4416}{7}\frac{EI}{l^3} & -\beta\frac{4224}{7}\frac{EI}{l^3} & \beta\frac{1728}{7}\frac{EI}{l^3} & 0 \\ -\beta\frac{4224}{7}\frac{EI}{l^3} & \alpha\frac{\rho Al}{4}+\beta\frac{6144}{7}\frac{EI}{l^3}+c_d & -\beta\frac{4224}{7}\frac{EI}{l^3} & -c_d \\ \beta\frac{1728}{7}\frac{EI}{l^3} & -\beta\frac{4224}{7}\frac{EI}{l^3} & \alpha\frac{\rho Al}{4}+\beta\frac{4416}{7}\frac{EI}{l^3} & 0 \\ 0 & -c_d & 0 & c_{wire}+c_d \end{bmatrix} \cdot$$

$$\begin{bmatrix} \dot{x}_1(t) \\ \dot{x}_2(t) \\ \dot{x}_3(t) \\ \dot{x}_4(t) \end{bmatrix} + \begin{bmatrix} \frac{4416}{7}\frac{EI}{l^3} & -\frac{4224}{7}\frac{EI}{l^3} & \frac{1728}{7}\frac{EI}{l^3} & 0 \\ -\frac{4224}{7}\frac{EI}{l^3} & \frac{6144}{7}\frac{EI}{l^3}+k_d & -\frac{4224}{7}\frac{EI}{l^3} & -k_d \\ \frac{1728}{7}\frac{EI}{l^3} & -\frac{4224}{7}\frac{EI}{l^3} & \frac{4416}{7}\frac{EI}{l^3} & 0 \\ 0 & -k_d & 0 & \frac{sin(\alpha)EA}{L}+k_d \end{bmatrix} \begin{bmatrix} x_1(t) \\ x_2(t) \\ x_3(t) \\ x_4(t) \end{bmatrix} = \begin{bmatrix} F_1(t) \\ F_2(t) \\ F_3(t) \\ F_4(t) \end{bmatrix} \quad (4.55)$$

4.6.2 Active system: a PID controller

In the last few decades, computer technology has evolved tremendously and this development can also be noticed in control engineering. As previously discussed, most of these developments are not found in the built environment. The car and airplane industry are much more developed with regard to control engineering, for instance. Besides viscous damping, a second method has been implemented in this project in the form of an active control system to minimize the response of the lightweight bridge model to external loading. Although much more sophisticated control algorithms exist by now, it should be noted that a very elementary PID-control system was used in this case. Since control engineering is not part of the study structural design at all, it was needed to develop some knowledge to this field of engineering beforehand. As a result, one could think that a more complex control system would require a lot more literature study and in fact, that was not considered the main aim of this project. It should, however, be said that implementing a better algorithm would probably lead to a better response to external loading and that this might be an interesting study in the field of mechanical engineering, for example.

Referring to the literature study, a PID controller consists of three user-defined values, where the proportional gain factor K_P is multiplied by the measured error. The derivative gain factor K_D is then multiplied with the derivative of the error, reducing the amount of overshoot and the integral gain factor K_I is multiplied by the integral of the error, reducing the steady-state error back to zero over time. The total actuator force is then equal to

$$F_A(t) = K_P e(t) + K_I \int e(t)\,dt + K_D \frac{de(t)}{dt} \quad (4.56)$$

The actuator force is implemented into the mass spring system and solved in the Laplace frequency domain, which was already seen for a single degree of freedom mass spring system in the literature study. As a result, the derivative gain factor can be found back in the differential equation as an imaginary damper and the proportional gain factor as an imaginary spring. The actuator force is then found to be equal to

$$F_A(t) = K_P e(t) + \sum K_I \Delta t e(t) - \sum K_I \Delta t x(t) \quad (4.57)$$

In this equation, $x(t)$ is the actual displacement where the actuator force is applied and $e(t)$ is the error at the measurement location. In contrast to the viscous damper, this system should be considered as an active system, resulting in some boundary conditions. First of all, a certain time delay is found in between the moment of actual occurrence of the error and the actuator applied force to this error. Regarding a schematic model of a PID-control system, this error cannot be equal to zero as in practice some time is needed for the measurement device to actually measure the error. Secondly, time delay occurs as a result of the time needed to calculate and activate

the actuator force (Figure 4.17). Furthermore, the actuator can respond at a certain frequency, as a result of its physical boundaries. This implies that a certain minimum threshold in time increment holds. For instance, an actuator responding one hundred times per second ($100\ Hz$) simply cannot respond to a measurement device that can measure the error one thousand times per second ($1\ kHz$). Both phenomenon were implemented in the numerical model to describe a realistic response of the actuator to the measured error. Finally, a control system will not be able to create a force above its physical limit. Hence, a limit force is given to the actuator in the numerical model as well and if the calculated force exceeds this limit, the maximum force is applied.

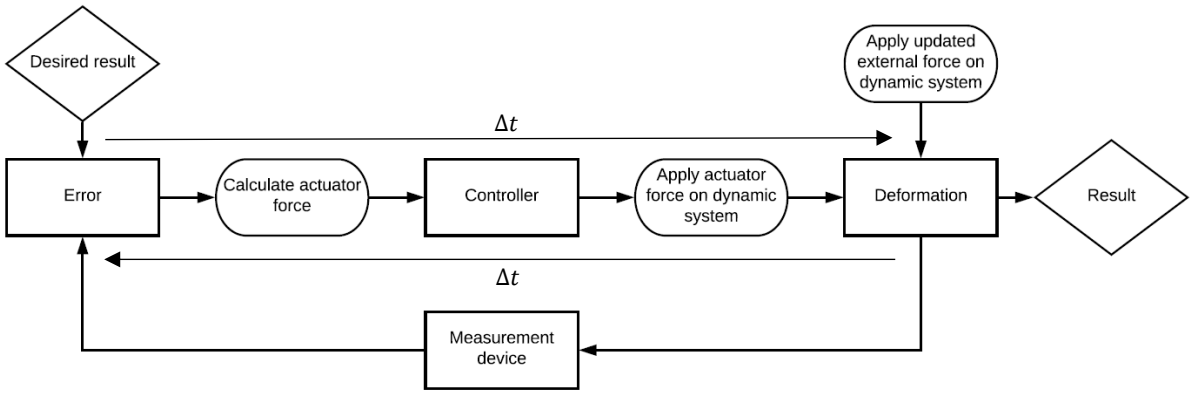

Figure 4.17: Control system: delay time

The actuator was implemented into the discretized bridge model similar to the viscous damper. Again, the four degree of freedom differential equation is found, where the damper values are replaced by the actuator values and where an additional force is added in the force matrix, being equal to the calculated actuator force. This also implies that the damping coefficient from the actuator is equal to the derivative gain value and that the spring stiffness coefficient is equal to the proportional gain factor. Again, the actuator is applied in between the bridge deck and the cable truss, exactly at mid span of the bridge (Figure 4.18).

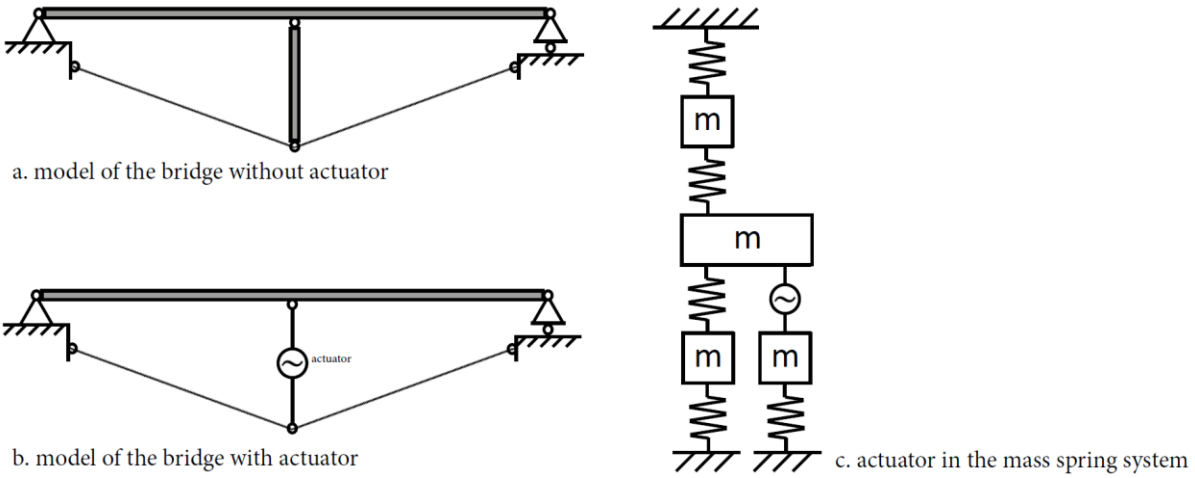

Figure 4.18: Schematic model for the control system

4.7 Software

Discretization of a continuous structure seems to be a proper method to approximate the dynamic response to different external loading situations. Although even the numerically approximated model to the remaining set of differential equations was used, still a huge amount of calculations has to be performed. As a matter of course, this requires the computational power of computer technology. In this project, it has been decided to use the three-dimensional nurbs-modelling package Rhinoceros®, as this software package introduces the possibility of creating self-written scripts with the plugin Grasshopper®. As a result, this allows for an infinite number of

possibilities with regard to parametric design within the field of structural engineering. As Grasshopper has a huge library of standard operations in both drawing tools and mathematical computations, it is rather easy to create a numerical model such as a dynamic response analysis tool. In this project, the plugin Hoopsnake was used in particular as this plugin allows for creating an iteration procedure. As a result, a loop through the discretized time domain can be made. Although a large number of plugins and standard operators is already included, some calculations like the numerical approximation method were made in the programming language c# as custom Grasshopper components. To conclude, this software package includes the ability of both programming initial value problems and visualizing them.

All input parameters that were described in the numerical approximation to a continuous structure are seen in the Grasshopper script as number sliders, making it easy to change input properties and updating the calculation real-time. Before iterating with Hoopsnake, all physical input parameters are converted into their equivalent mass spring damper values. Each iteration goes then through the blue circle, where the Hoopsnake plugin is located. After each iteration the numerical approximation to the next time increment is calculated and these values are stored in lists. Finally, all values are stored into a text file, which is saved in a folder according to the physical properties that were set for this calculation. A number of custom components that were used was also saved into a self-defined library. All components are found in one Grasshopper script (Figure 4.19, Appendix), which visualizes results real-time in the Rhinoceros viewport.

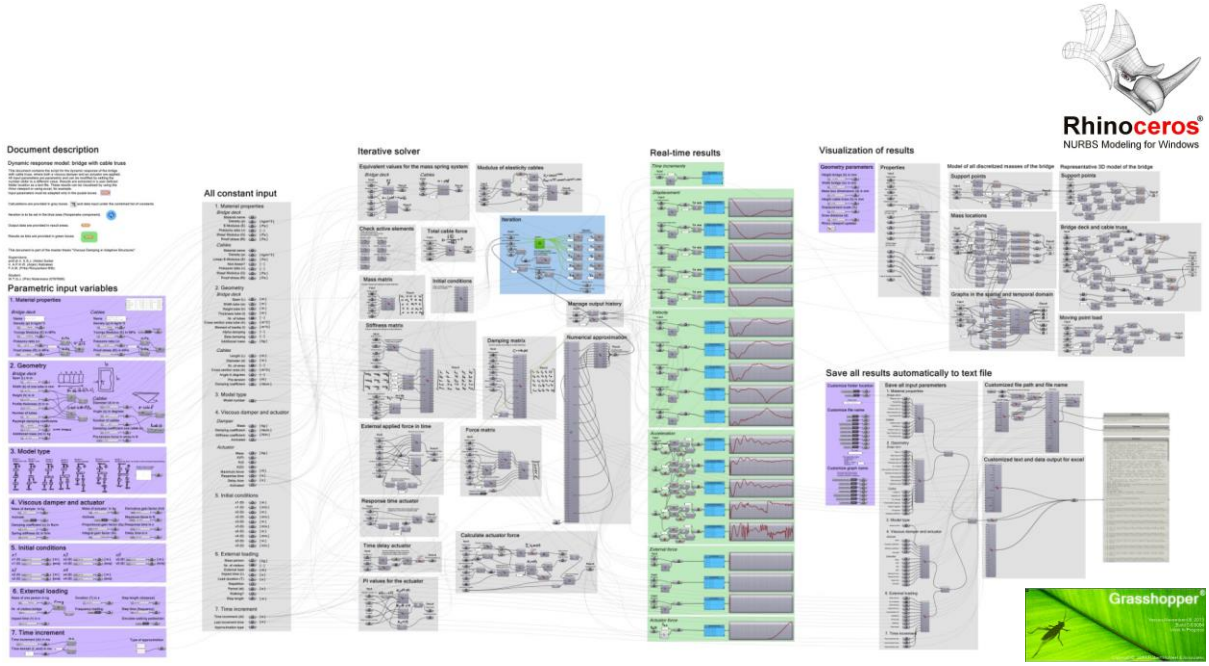

Figure 4.19: Complete visual script in Grasshopper

5 Results from the numerical model

The approach to a numerical simulation for describing the response of a dynamic system has been discussed in the previous chapter from this report. The complex exact solution was approximated by using a discretization in both the spatial and the temporal domain, where the spatial domain simply has been subdivided into a number of predefined locations and where the temporal domain has been divided into a predefined number of time steps. As a result, the response to any external loading configuration can be computed, even if there are non-linearity's in the model. The power of this numerical model thus lies in the approximation to any possible external loading configuration. Comparisons between different models, like for instance using the damper or the actuator, are now made rather easy as there is no need for a physical model. Furthermore, optimized physical input values can be determined, which can then be used in practice without the need for expensive experimental test setups. A number of numerical models and their response behavior is discussed in this part of the report. The main difference in these models is found in using the actuator, using the damper or using both these systems in a combination.

Comparable values to the experimental test setup are used in the numerical approximation for both the bridge deck and the cable truss. To that extent, a realistic comparison to the actual behavior of the physical model in the laboratory is possible. Both the bridge and the steel wires are thus given physical properties for density, Young's modulus and geometry, for instance (Table 5.1, Table 5.2, annex B). It should be noted that only the steel tube profiles are considered for the stiffness of the bridge deck. Some additional stiffness from the wooden walking deck is not considered.

Further, it should be noted that all physical parameters can be adapted to different values, as the numerical model is parametric. This would imply that one could easily examine dynamic behavior for a bridge with a span twice as large, for example. Furthermore, any external loading configuration can be examined in this model, as the external load can theoretically change in each time increment. Loading configurations like walking or running over the actual model of the bridge can thus be simulated by creating multiple impulse loads at the discretized masses of the bridge.

Physical properties bridge deck				
Description	Symbol	Unit	Calculation	Physical value
Density (steel)	ρ	$\left[{}^{kg}/_{m^3}\right]$	–	$7.85E^{+3}$
Young's Modulus	E	$[Pa]$	–	$2.10E^{+11}$
Moment of inertia	I	$[m^4]$	${}^{1}/_{12}\,bh^3$	$8.89E^{-8}$
Span	l	$[m]$	–	$5.00E^{+0}$
Mass (50%)	m	$[kg]$	ρAl	$9.08E^{+1}$
Alpha damping	α	–	–	$5.00E^{-1}$
Beta damping	β	–	–	$2.00E^{-3}$

Table 5.1: Physical properties for the bridge deck

Physical properties cable truss				
Description	Symbol	Unit	Calculation	Physical value
Young's Modulus	E	$[Pa]$	$E = {}^{\sigma}/_{\varepsilon}$	var
Cross section area	A	$[m^2]$	$0.369d^2$	var
Length	l	$[m]$	${}^{1}/_{2}\,l_{bridge}/\cos(\alpha)$	$2.66E^{+0}$
Equivalent mass (50%)	m	$[kg]$	ρAl	var
Stiffness	k	$\left[{}^{N}/_{m}\right]$	$EA\sin(\alpha)/_{l}$	var
Damping coefficient	c	$\left[{}^{Ns}/_{m}\right]$	–	$4.00E^{+1}$

Table 5.2: Physical properties supporting steel wires

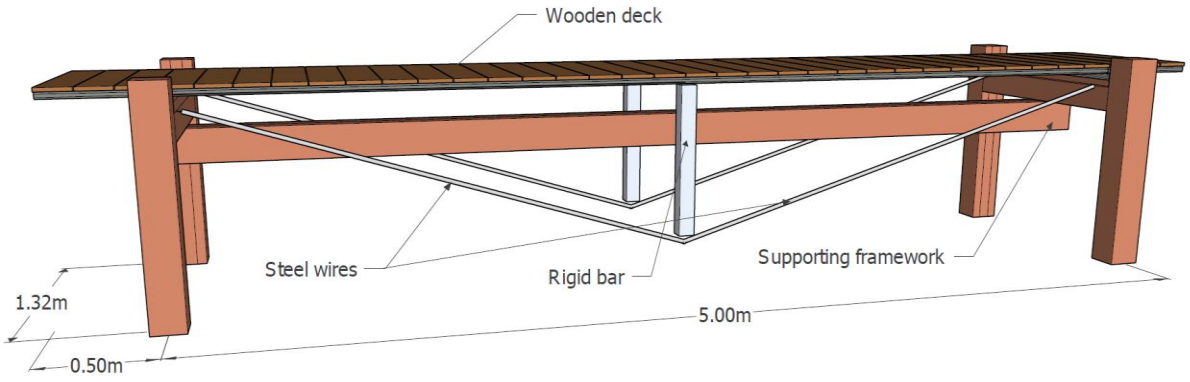

Figure 5.1: Three-dimensional model of the bridge with cable truss

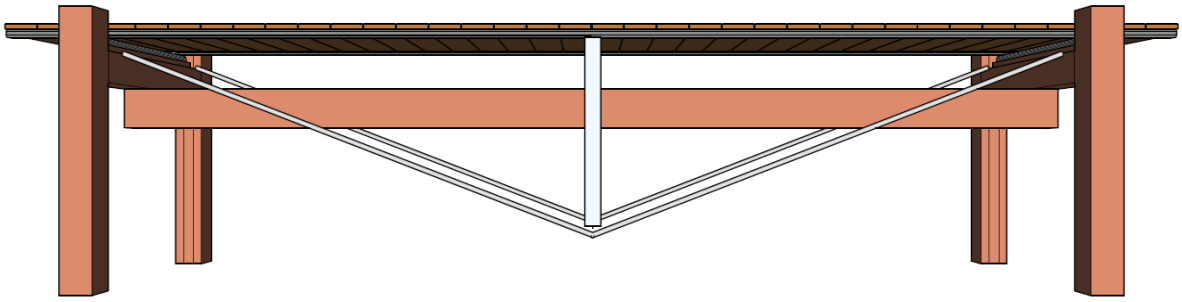

Figure 5.2: Side view of the bridge model

5.1 Loading configurations and design criteria

The case study in this master project consists of a footbridge design, which is loaded when one or more pedestrians are crossing this bridge. To that extent, either walking slowly or running over the bridge could be modelled as a number of impulse loads. Occasionally, it occurs that someone stops while crossing the bridge when one considers enjoying a nice view, for instance. Hence, an external load remaining at the same place for a larger timespan should be included as well in the structural model of the bridge. As a result, two types of (elementary) loading configurations are considered, where the first one is one single impulse load. Secondly, the external load over a longer period of time is considered, which is indicated as a step load in this report. For the impulse in this case, it is assumed that an average person walks with a frequency of $f \approx 2Hz$, resulting in a period of $t \approx 0.5s$ for each step. From this period, it is assumed that the actual force is applied for $0.3s$. In contrast to the impulse load, the step load is assumed to continue from the time of impact towards the end of the numerical simulation. In mathematical terms, the external force $F(t)$ can now be described as

$$F(t) = \begin{cases} 0 & t < t_1 \\ F & t_1 \leq t \leq t_2 \\ 0 & t > t_2 \end{cases} \tag{5.1}$$

$t_2 - t_1 = 0.3s$ for an impulse load

$t_2 - t_1 > 10s$ for a step load (5.2)

For both loading configurations, the force is applied at the center mass of the discretized model for the bridge deck, which is thus equal to a load exactly halfway the bridge span (Figure 5.3). Applying a force on top of the bridge then results in a dynamic response of the bridge model (Figure 5.4, Figure 5.6). The dynamic response shows a decay in amplitude until the vibrations is damped out completely. At this certain time, the steady state error is reached, which is equal to the deformation that is calculated in conventional static structural design.

Obviously, the steady state error is equal to zero for impulse loading, whereas for the step load a deflection remains in time. In order to compare different models from this master study, it is said that the steady state error is negligible if

$$w_{steady-state} < \frac{L}{300} = 17mm \tag{5.3}$$

It should be noted that this steady state error is taken from using an elementary rule of thumb from static structural engineering. Secondly, the maximum measured error in the total time domain may not exceed a certain value. For both impulse and step loading this value is taken into account. As this maximum value only occurs transiently, it is stated that this value may not exceed

$$w_{max} = 1.5w_{steady-state} = 25mm \tag{5.4}$$

Besides the deformation in time, the vibration of the bridge is measured in terms of an acceleration value in time (Figure 5.5). In the Eurocode it is stated that for comfort criteria, vertical accelerations may not exceed

$$a_{max} = 0.7m/s^2 \tag{5.5}$$

As a result, the response of the bridge can be measured in terms of actual physical values. To that extent, different models using the damper and/or the actuator can be compared. It should be noted here that these values are sometimes exceeded, as this particular bridge model is designed extremely lightweight to show dynamic effects. In that case, these values should be minimized as much as possible. In all calculations, downward deflections are taken as negative values, which renders a negative deformation in time in most cases.

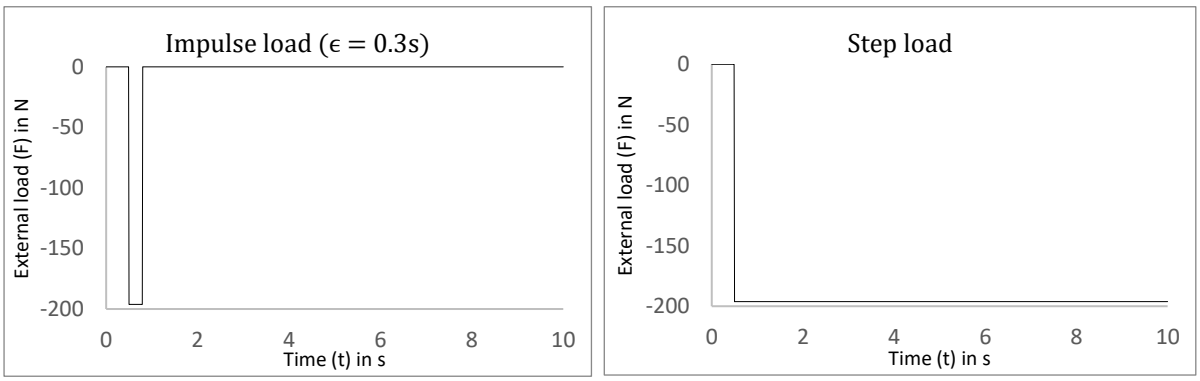

Figure 5.3: Two loading configurations: an impulse load and a step load both applied at $t = 0.5s$ and both equal to 20kg.

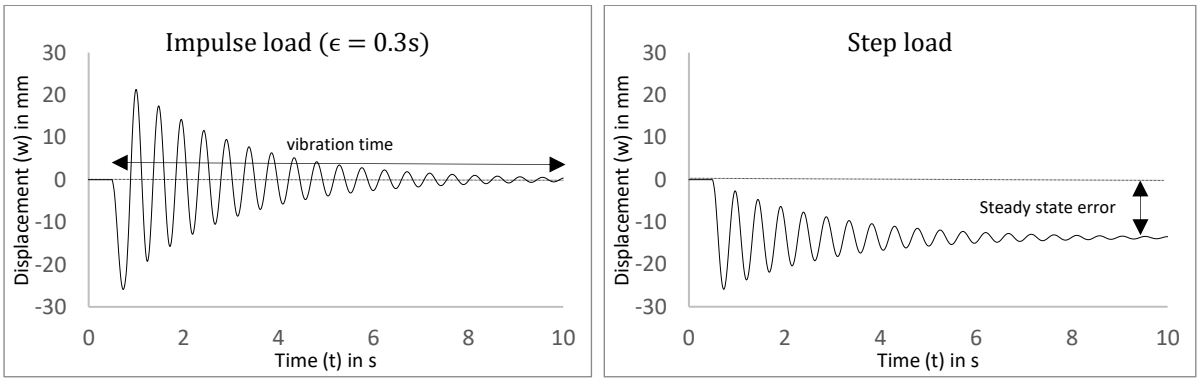

Figure 5.4: Response of the bridge deck only (displacement as a function of time)

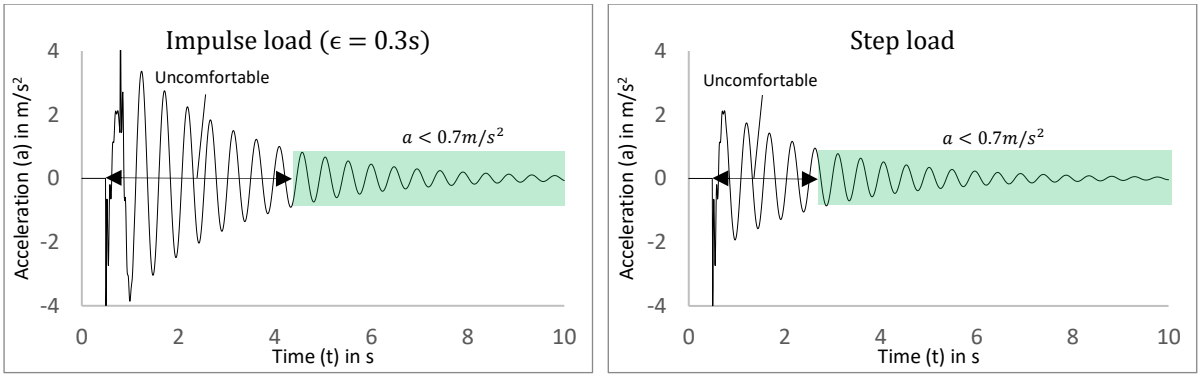

Figure 5.5: Acceleration as a function of time

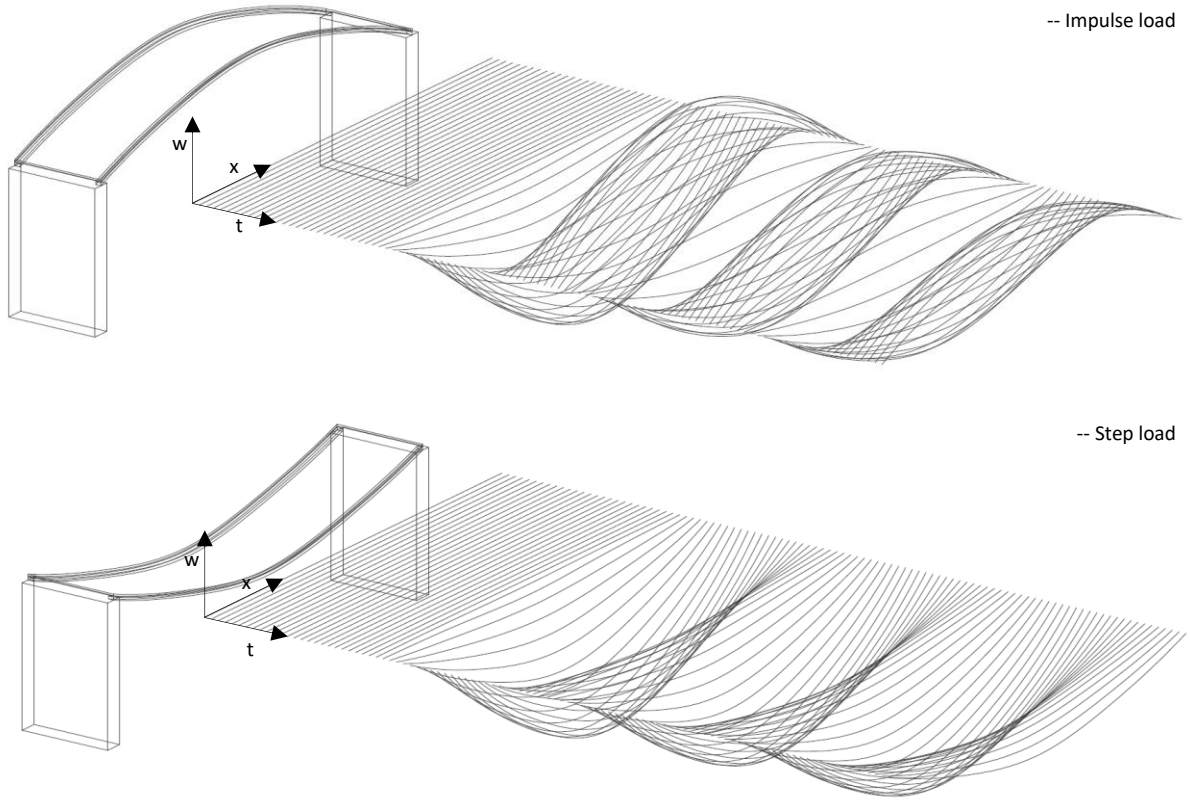

Figure 5.6: Response of the bridge in the spatial and temporal domain (left figure bridge: deformed state at t = 0.2s)

5.2 Additional stiffness from the cable truss

It is seen that the bridge deck already deforms heavily for a very small external load and as a result, the experimental bridge deck was thus stiffened by using a cable truss. As the stiffness of the cable truss depends on the cross section, the Young's Modulus and the angle in between the horizontal line and the cable, all of these values can be adapted in order to increase or decrease the stiffness of the cable truss. The stiffness of the steel wires is considered non-linear according to the stress strain curve measured in the laboratory (Figure 5.7). The difference in loading and unloading is considered as well. For the measured cable in the experimental setup, it was found that

$$E_{loading} \approx 3117.9F^{0.3574}$$

$$E_{unloading} \approx (4 * 10^{-7})F^3 - 0.0044F^2 + 25.075F + 3900 \quad (5.6)$$

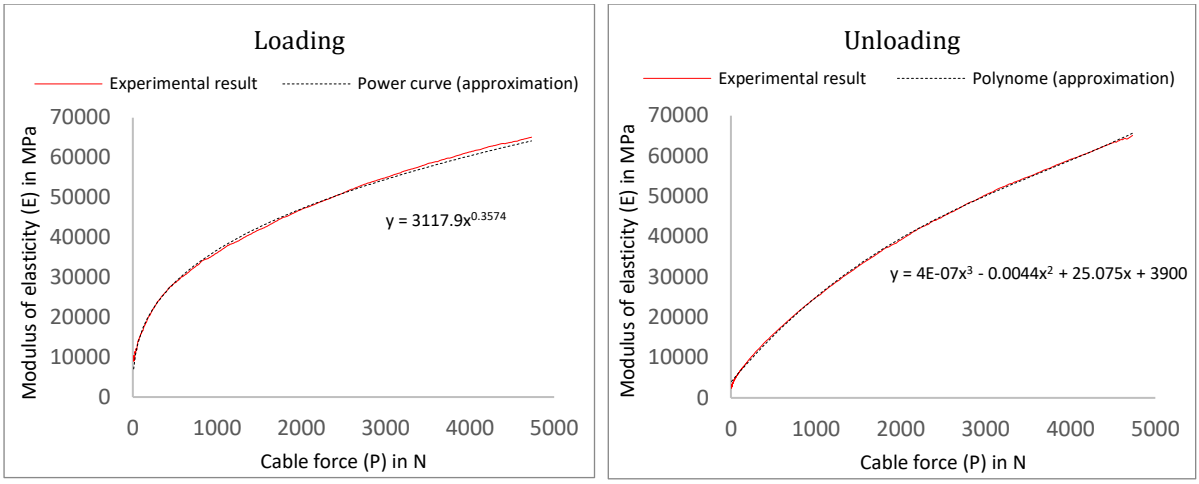

Figure 5.7: Approximate equation for the Young's Modulus of the steel cables

In the comparison of the bridge with and without cable truss, an external load being equal to the mass of one person was applied (i.e. $F = 750N$). It is seen that the cable truss is favorable in terms of both deformation and acceleration. Although the unprestressed cable truss already shows a tremendously improved model, the physical parameters of the cable truss can be modified to improve the response behavior even further. This is seen in different comparisons, where the angle of the cable, the amount of prestress and the diameter are adapted and compared to the standard values (Figure 5.8, Figure 5.11). The deformation compared to the exact same bridge without the cable truss is approximately reduced by a factor five and the steady state error is reached more than four times as fast when using the standard values for the cable truss (Figure 5.9, Figure 5.10).

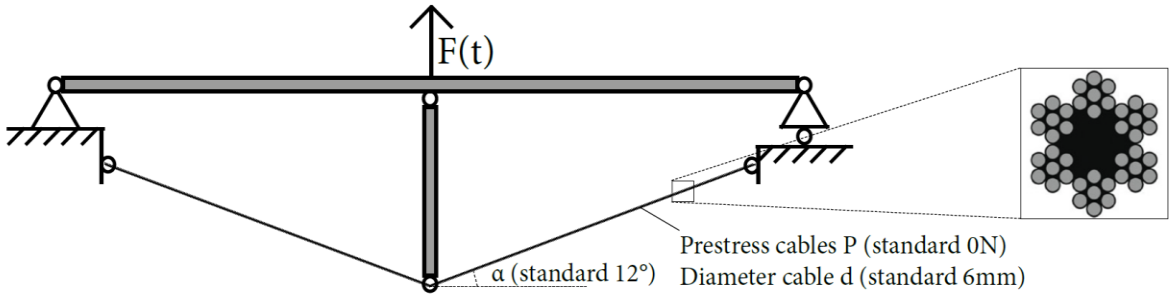

Figure 5.8: Standard values used for the cable truss

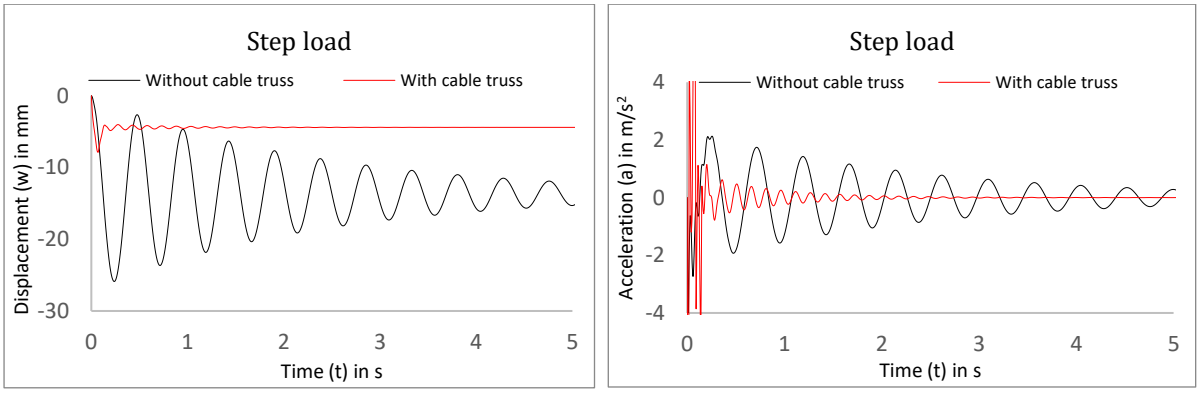

Figure 5.9: Comparison bridge with and without cable truss (standard values)

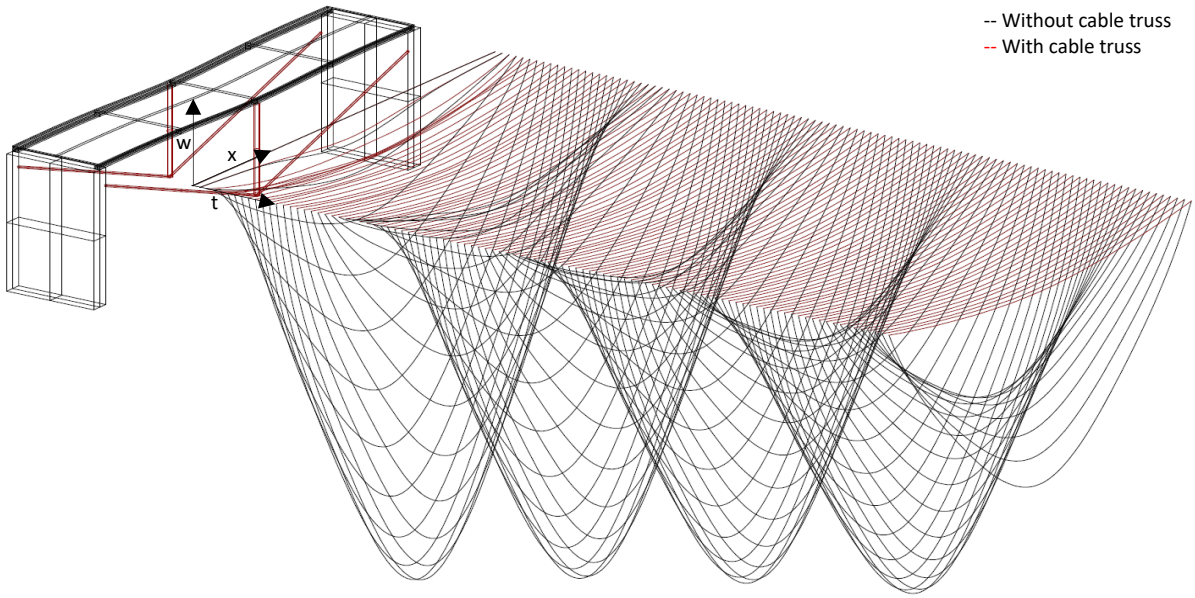

Figure 5.10: Response of the bridge in the spatial and temporal domain (with and without cable truss, standard values)

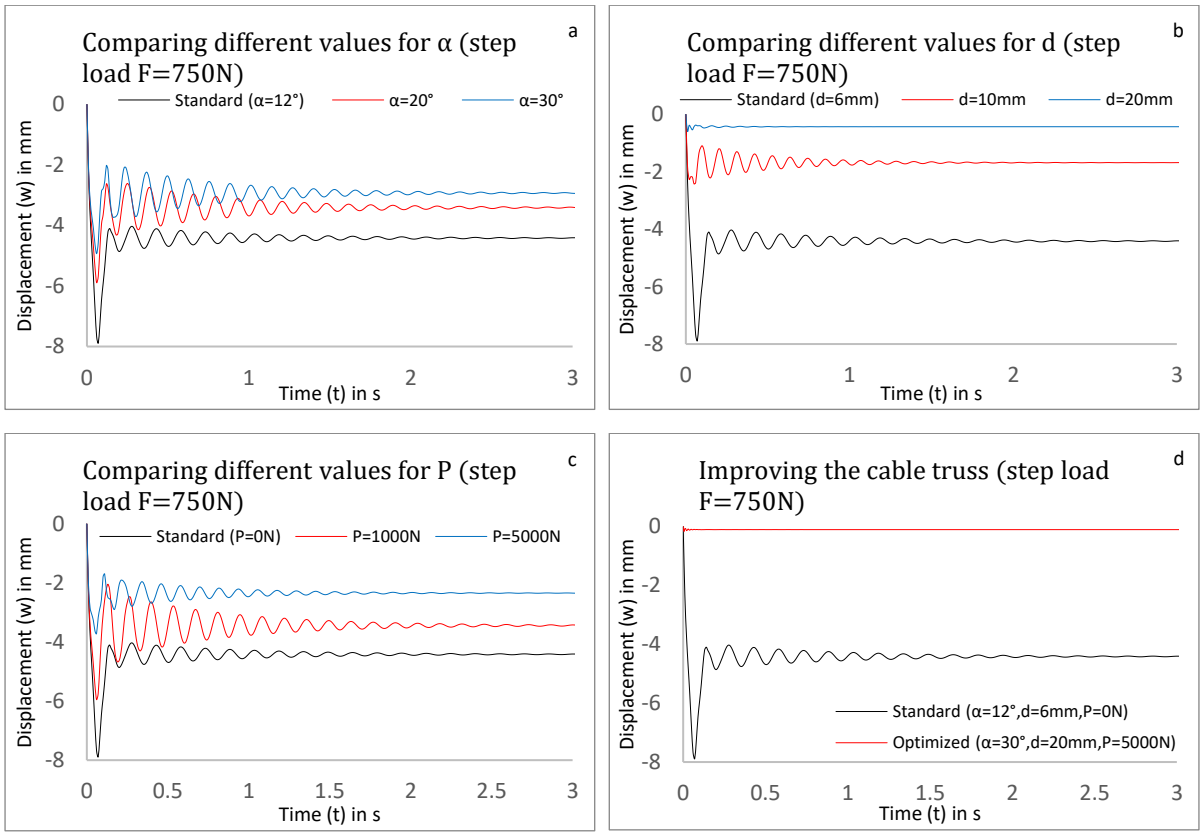

Figure 5.11: Modifying values for angle (α), diameter (d) and prestress (P)

When loading the bridge with a force equivalent to one pedestrian, it is seen that the best improvement in additional stiffness is found when the cable diameter is increased. This is true for both the steady-state and the maximum error (Table 5.3). Recalling eq. (4.53), this can be explained by the fact that the equivalent vertical spring stiffness increases linearly with regard to the cross sectional area, whereas it does not increase linearly with regard to the angle. Furthermore, the stiffness increases linearly regarding the modulus of elasticity, but this value does not increase linearly with regard to the prestress force in the cable. To that extent, one could

conclude that increasing the diameter of the steel cables improves the stiffness of the truss system, without introducing additional forces (prestress) or changing the geometry (angle). When increasing all physical values to their (approximate) practical maximum values, it is seen that the deformation reduces to only two percent of the standard bridge model. Using these 'optimized' parameters, one can see that the bridge starts to vibrate in its third mode shape, indicating that the stiffness of the bridge in between one end and mid span is becoming governing over the stiffness of the total system. Local deformation thus becomes larger at one and three quarter of the bridge, even if the external load is applied at mid span (Figure 5.12). It should be noted that increasing physical parameters seems reasonable in this relative small scale bridge design, but that this might not be possible in a larger scale design. In further models including the damper and the actuator, the standard physical parameters are used for the cable truss, unless indicated otherwise. This also holds for the physical properties of the bridge deck.

Model	Physical values	$w_{steady-state}$	%	w_{max}	%
Standard	$\alpha = 12°, d = 6mm, P = 0N$	$4.41mm$	100	$7.89mm$	100
Larger α	$\alpha = 20°, d = 6mm, P = 0N$	$3.41mm$	77	$4.76mm$	60
Larger α	$\alpha = 30°, d = 6mm, P = 0N$	$2.92mm$	66	$4.21mm$	53
Larger d	$\alpha = 12°, d = 10mm, P = 0N$	$1.68mm$	38	$2.42mm$	31
Larger d	$\alpha = 12°, d = 20mm, P = 0N$	$0.43mm$	9	$0.59mm$	7
Prestress	$\alpha = 12°, d = 6mm, P = 1000N$	$3.71mm$	84	$5.95mm$	75
Prestress	$\alpha = 12°, d = 6mm, P = 5000N$	$2.34mm$	53	$3.44mm$	44
Optimized	$\alpha = 30°, d = 20mm, P = 5000N$	$0.11mm$	2	$0.17mm$	2

Table 5.3: Steady-state and maximum error for modifying the physical parameters

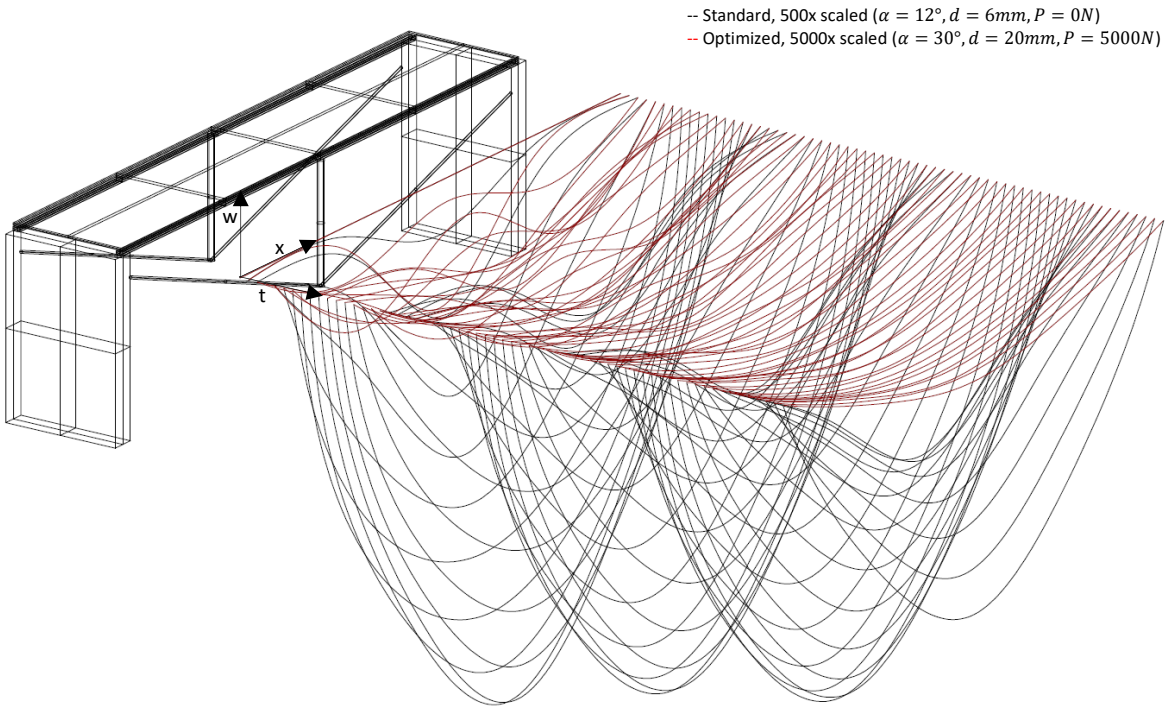

Figure 5.12: Deformation in spatial and temporal domain

5.3 Viscous damping

As a passive improvement to uncomfortable vibrations, a viscous damper was modelled in between the bridge and the cable truss (Figure 5.13). It was assumed in the numerical models that the damper adds a certain mass to the system, which is assumed ten kilograms in this case. Initially, the spring stiffness for the cable truss was calculated using the standard values as described in the previous section. This also includes zero prestress force, leading to a relative low modulus of elasticity for the cables.

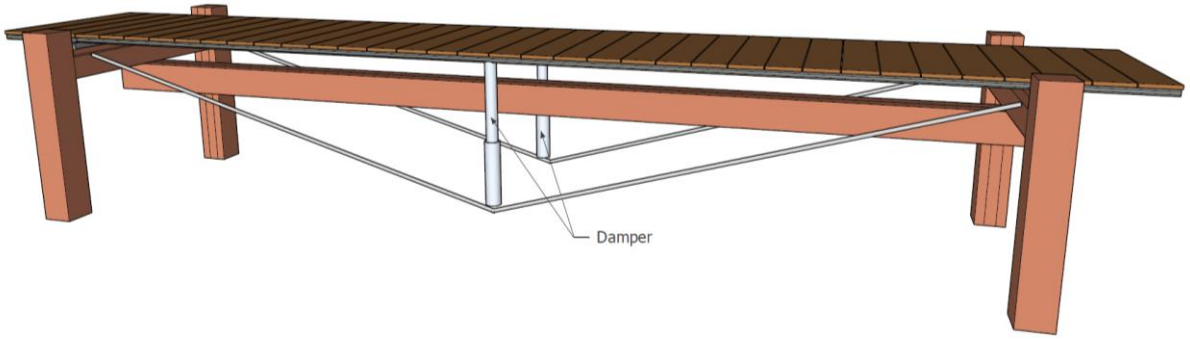

Figure 5.13: Model of the bridge with two dampers, applied at mid-span

5.3.1 Efficiency of the damper

The damping coefficient is varied and is compared to the bridge without damping for impulse loading. As the cable provides a relative low stiffness, it is seen that the complete bridge easily starts to vibrate in a certain frequency, which converges to the vibration of the bridge with a rigid connection to the cable truss when the damping coefficient goes to infinity. As a result, just adding damping will not directly lead to a more comfortable structure. One could say on the one hand that a small amount of damping will result in large deformations, converging to the response of the bridge deck only for zero damping. On the other hand, a large amount of damping will result in a vibration almost equal to that of the bridge with cable truss only, where deformation is reduced but vibrations are damped out after a larger amount of time (Figure 5.14). In the case of using standard values, it could be concluded that a damping coefficient equal to $c \approx 2000 Ns/m$ performs best on comfort criteria, whereas the maximum deflection is exceeded in this case (Table 5.4).

Damping coefficient	Standard values cables ($\alpha = 12°, d = 6mm, P = 0N$)		Improved values cables ($d = 10mm, P = 1000N$)		Spring added ($d = 10mm, P = 1000N$)	
	w_{max}	$t_{die-out}$	w_{max}	$t_{die-out}$	w_{max}	$t_{die-out}$
No cables	$99.7mm$	$\gg 3s$	$99.7mm$	$\gg 3s$	$99.7mm$	$\gg 3s$
$c = 500$	$74.4mm$	$1.8s$	$74.5mm$	$2.2s$	$35.1mm$	$2.3s$
$c = 1000$	$60.1mm$	$1.1s$	$60.3mm$	$1.1s$	$30.1mm$	$1.2s$
$c = 2000$	$44.6mm$	$0.8s$	$44.8mm$	$0.7s$	$24.2mm$	$0.8s$
$c = 5000$	$27.3mm$	$1.3s$	$26.2mm$	$0.4s$	$18.4mm$	$0.6s$
$c = 10000$	$12.2mm$	$1.4s$	$15.9mm$	$0.6s$	$13.0mm$	$0.8s$
$c = 20000$	$10.3mm$	$2.1s$	$4.5mm$	$0.8s$	$4.42mm$	$1.1s$
No damping	$8.3mm$	$> 3s$	$2.1mm$	$> 3s$	$2.1mm$	$> 3s$

Table 5.4: Comparison of the maximum deflection and the time needed to die out the vibration for different values for both the damper and the cable truss

Increasing the equivalent stiffness of the cable truss will lead to a more stiff connection of the mass that is modelled in between the viscous damper and the cable truss. As a result, it is obvious that the amount of damping can now be increased further, and that this transition point from damping to vibration of the total systems occurs for larger amounts of damping (Figure 5.17). In fact, this transition point will never be reached if the cables are assumed infinitely stiff. In the case of the improved values, the point where the vibration is died

out is found for a larger damping coefficient ($c = 5000Ns/m$) and moreover, this point is reached twice as fast (Figure 5.15, Figure 5.16).

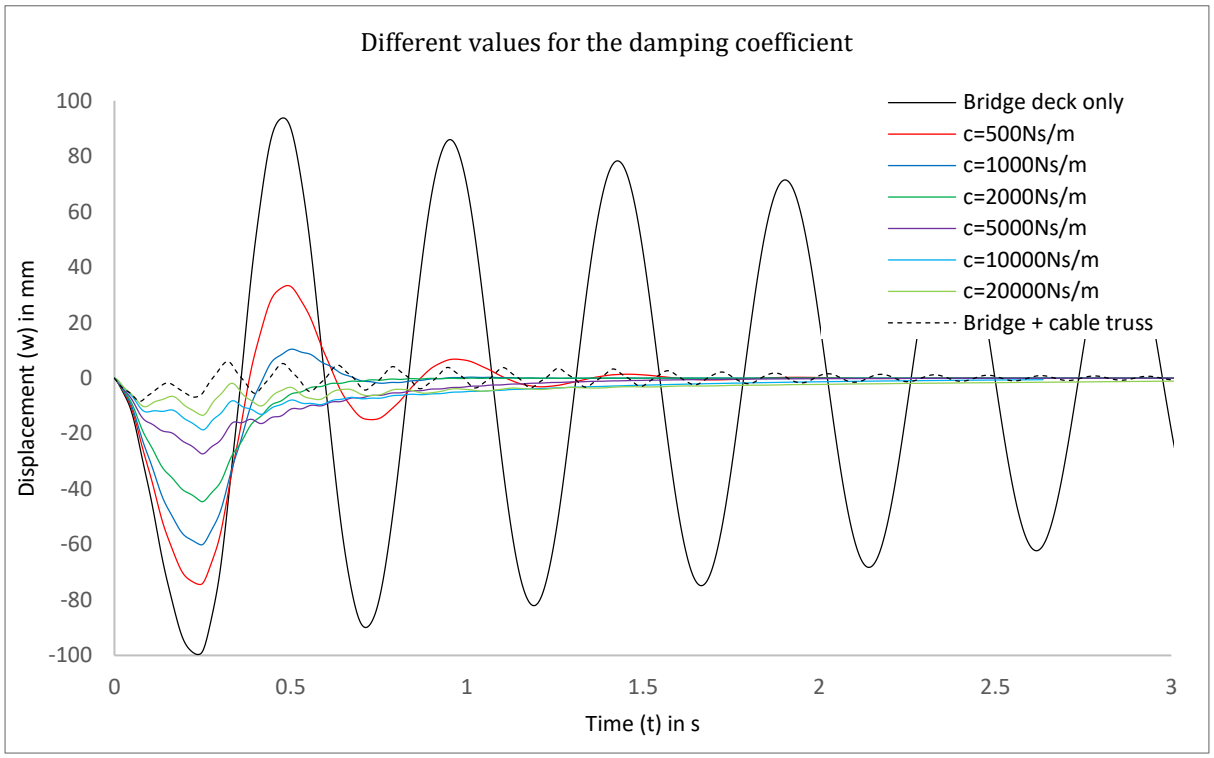

Figure 5.14: Response of the mid-point of the bridge to an impulse load for different damping coefficients

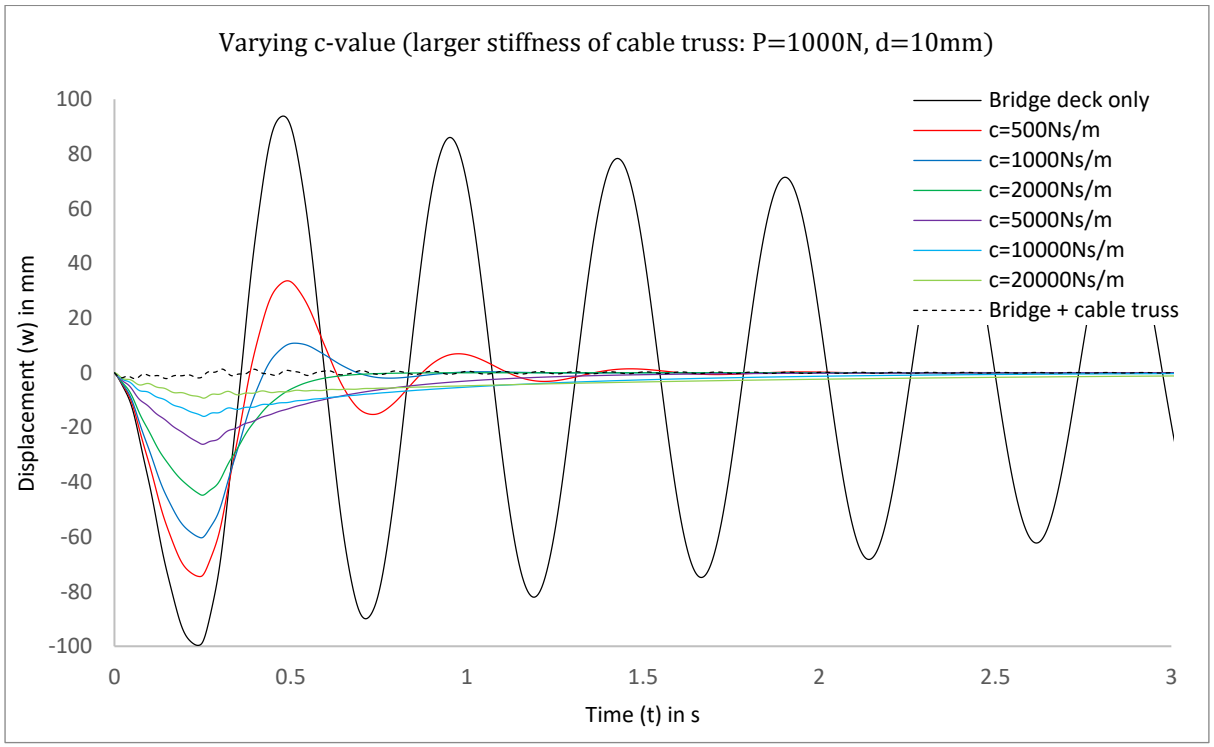

Figure 5.15: Response of the mid-point of the bridge to an impulse load with increased values for the cable truss stiffness

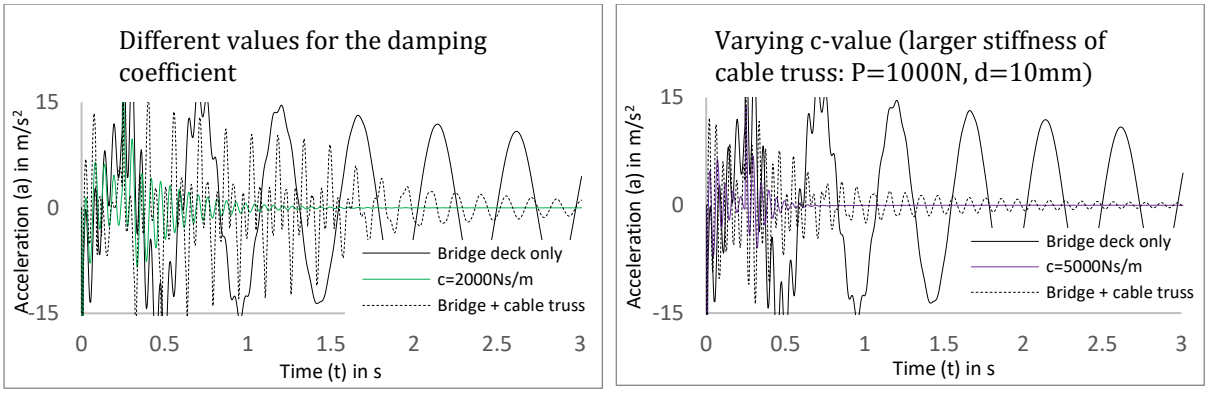

Figure 5.16: The acceleration is reduced much faster in time when using a viscous damper

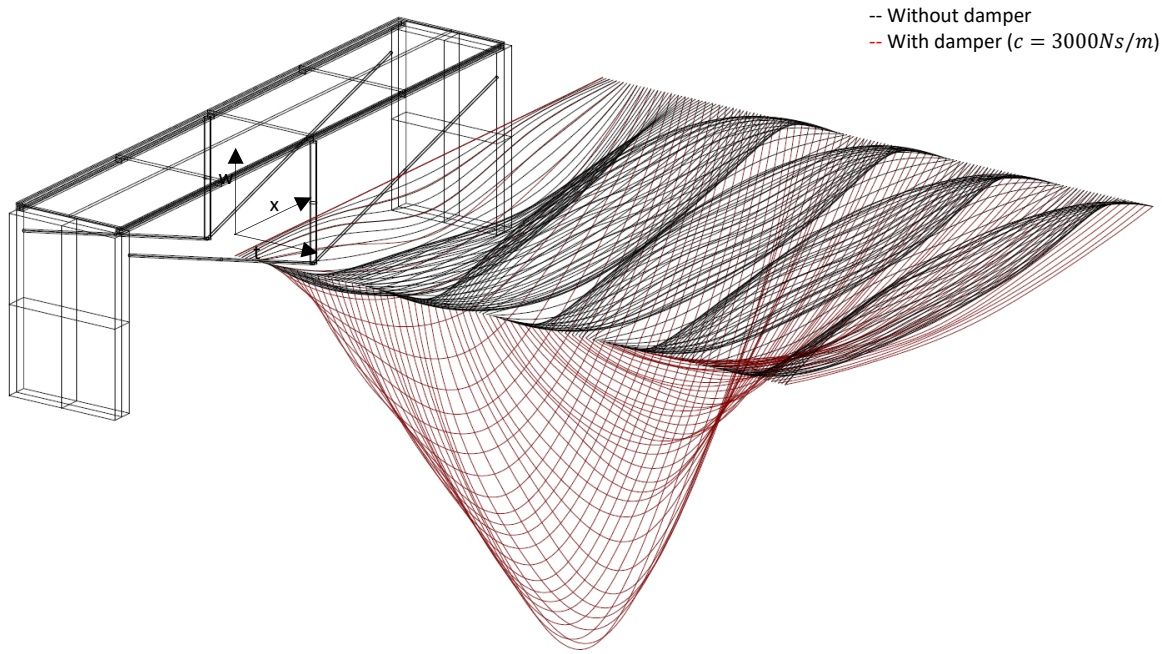

Figure 5.17: Three-dimensional plot of the displacement of the bridge with and without damper

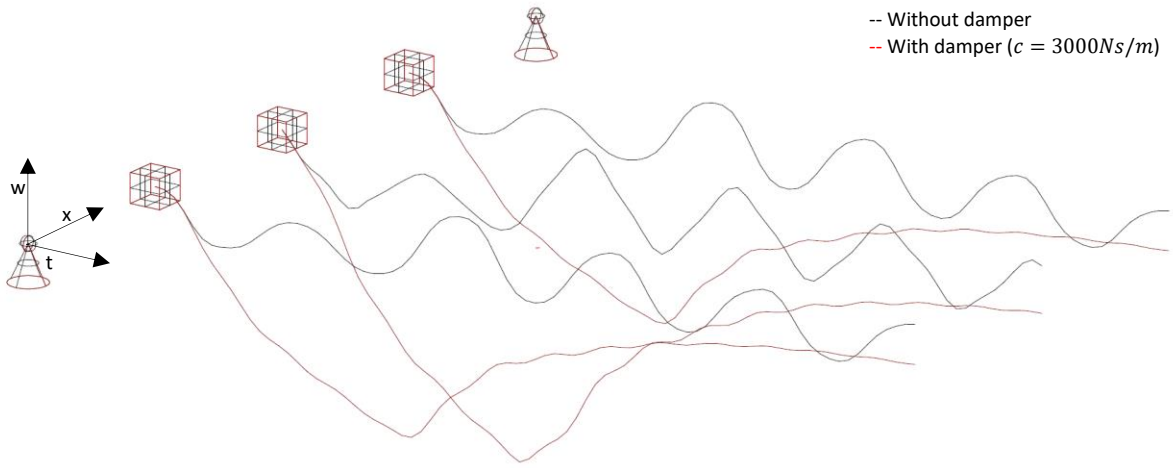

Figure 5.18: Three dimensional plot of the displacement of each individual discretized mass

5.3.2 Steady-state error

For impulse loading, adding more damping reduces the deformation, as the damping coefficient actually delays the response on the external force. As a result, a very small deformation can be obtained even if the impulse load is a relatively large force. Applying a step load on the structure, it can be shown that the deformation theoretically increases to infinity, as an external force now constantly acts on top of the damper, without any reaction force that can resist the ever-increasing deformation. This problem can be solved by adding a physical value for spring stiffness to the damper. In fact, the damper is then transformed into a shock absorber, including both a value for damping and spring stiffness coefficient (Figure 5.19). Again, similar values for the damping coefficient are applied and a spring is added (Table 5.4, Figure 5.20). As a result, it can be seen that the long-term deformation from a step load decreases and that the maximum deformation from an impulse load decreases as well (Figure 5.21, Figure 5.22). It should be noted that the improvement of adding a spring is less noticeable for impulse loading than for step loading. Secondly, adding the spring reduces the deformation and hence, reduces the effectiveness of the damper.

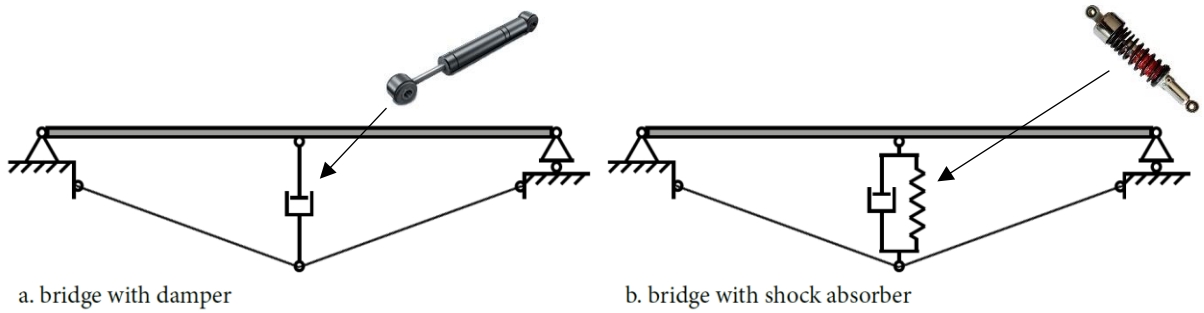

Figure 5.19: Schematic model of a viscous damper and a shock absorber

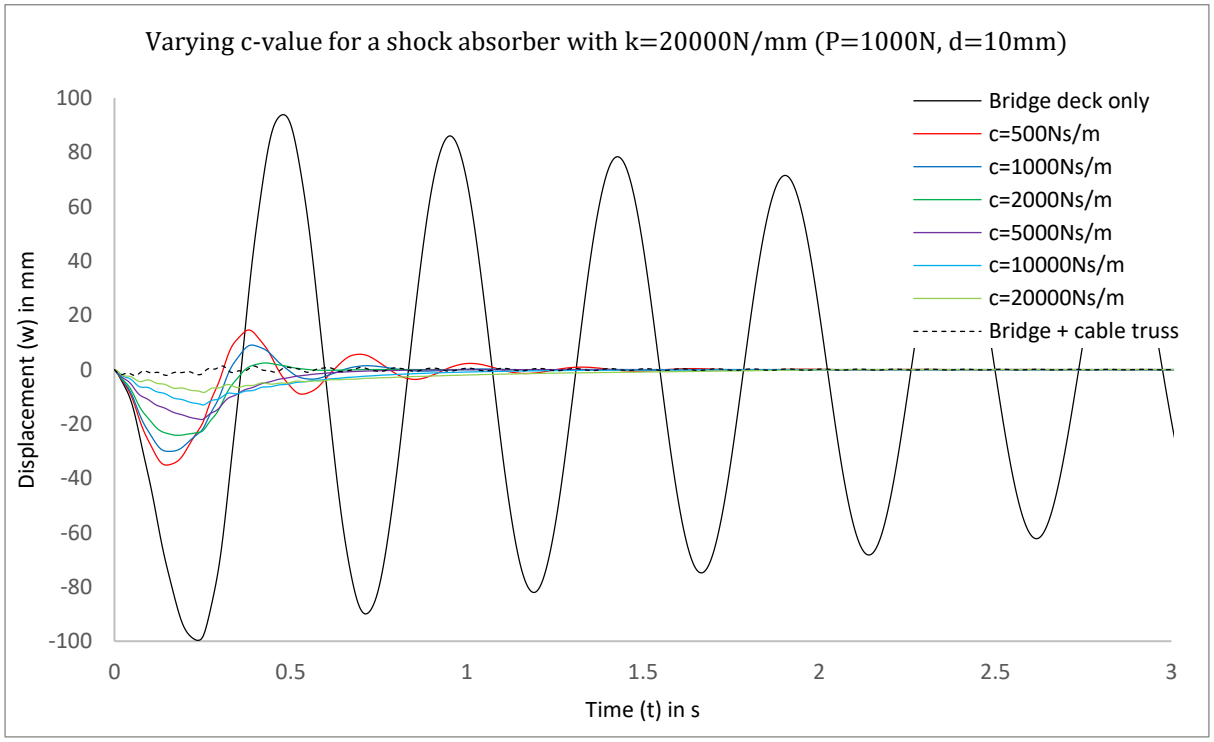

Figure 5.20: Response of the mid-point of the bridge to an impulse load when a 'shock absorber' is applied (k=20000N/mm)

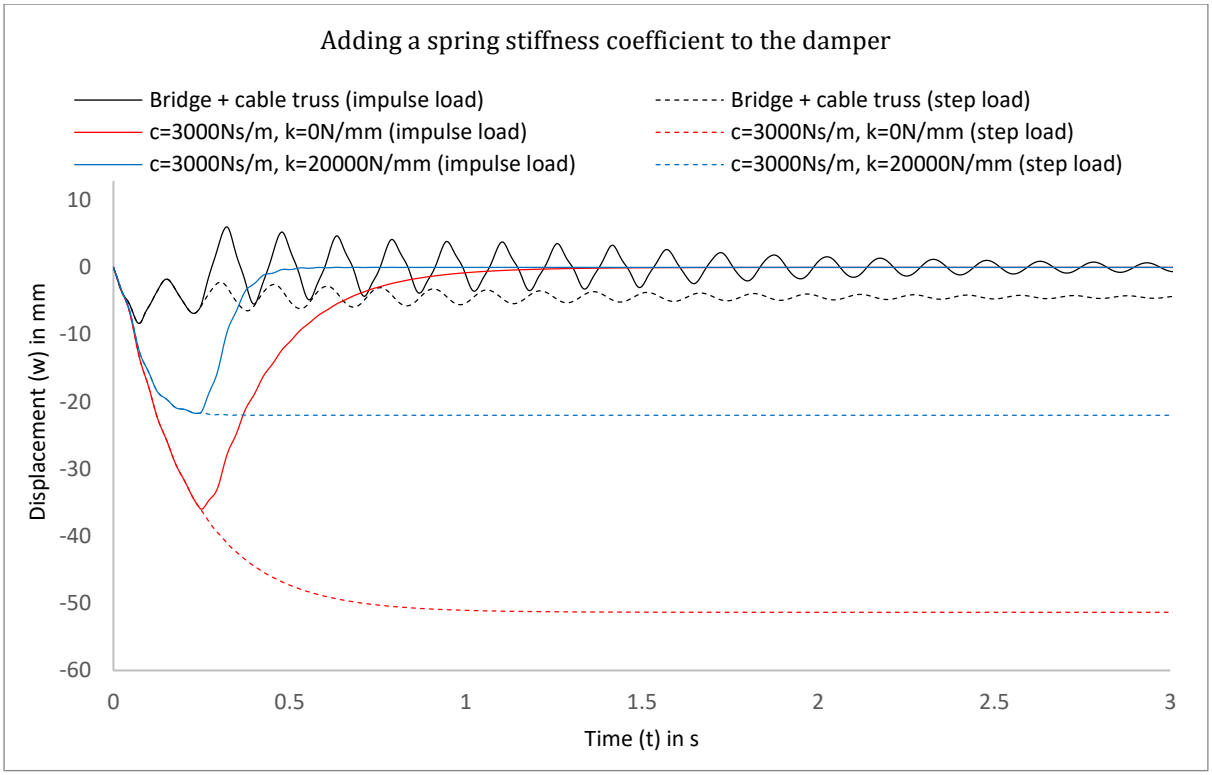

Figure 5.21: Difference in deformation when using a shock absorber for both step and impulse loading

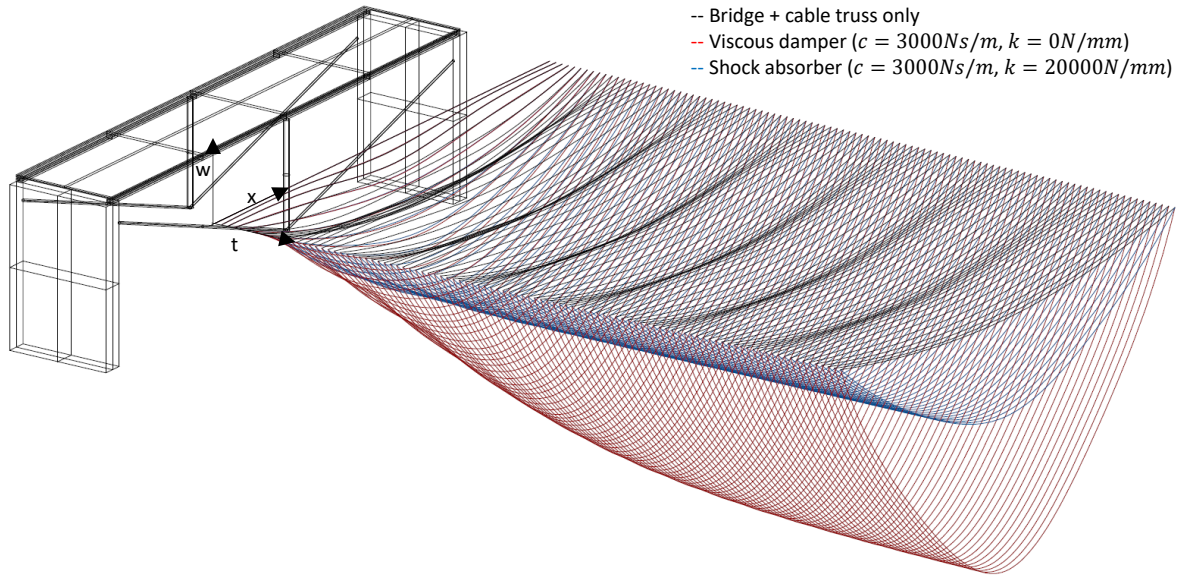

Figure 5.22: Three-dimensional plot of the displacement of the bridge for a step load

5.4 Control system

In contrast to viscous damping, a control system is considered an active system consisting out of a measurement device, a software package and an actual physical actuator. The described PID-algorithm that was described earlier is used to calculate the actuator force on the dynamic system. Besides the three user-defined parameters of the control system, other variables like time delay, response time and a physical limit force have to be taken into account in the control system. Firstly, the response is shown for the bridge model with and without actuator

where the proportional, derivative and integral gain are varied. Here, it should be said that the actuator is not assumed infinitely stiff, sometimes resulting in a larger maximum deformation compared to the bridge without actuator. This phenomenon was also found in the physical model of the bridge that was built in the laboratory. On the other hand, the connection between the cable truss and the bridge deck is considered infinitely stiff when no actuator is included in the model, resulting in zero relative displacement between the cable truss and the bridge deck (Figure 5.23, Figure 5.24). In all models concerning the actuator, it is now assumed that the actuator is active, even if all actuator values are set to zero. The actuator force now must extend its own virtual spring, whereas in practice the actuator can deform 'freely'. In the numerical model, the actual actuator force is thus calculated as

$$F_{act,real} = F_{act,total} - k_{actuator} * (u_{bridge} - u_{cable\ truss}) \tag{7.7}$$

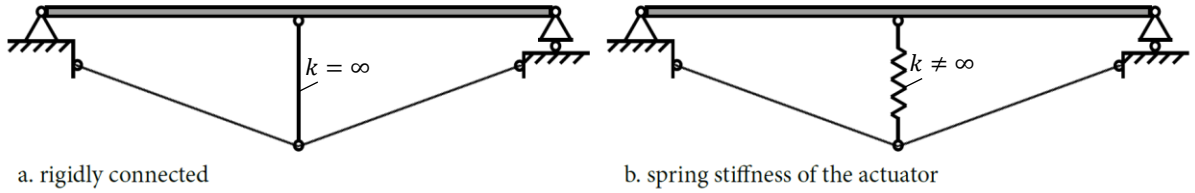

Figure 5.23: Difference in bridge without actuator (a) and with actuator (b)

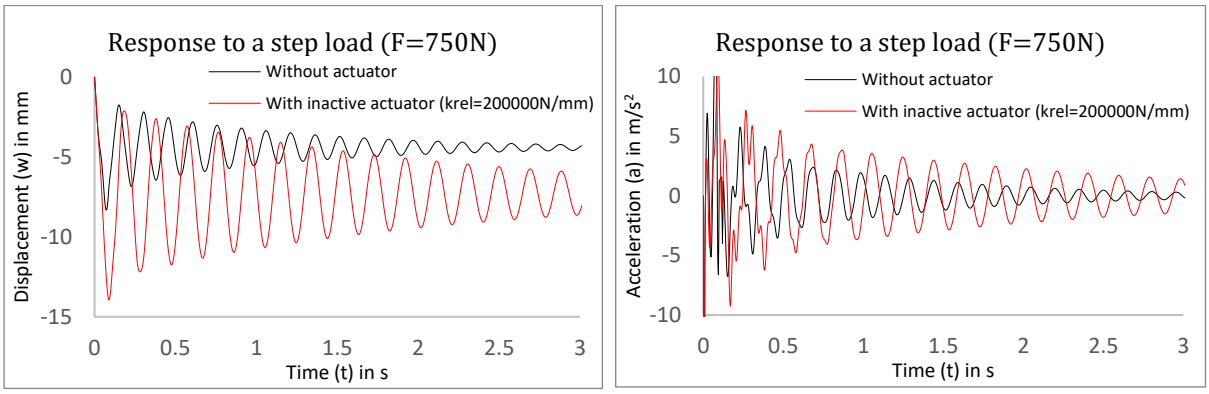

Figure 5.24: Response without actuator (rigid connection) and with inactive actuator (spring connection)

In the literature study, it was already stated that the proportional gain of a PID-controller is in fact an additional spring which is multiplied by the measured error to calculate the force to apply. This can now also be shown in the bridge model with actuator (Figure 5.25). It is seen that increasing the proportional gain value leads to a better reduction of the steady-state error, whereas this also leads to a larger overshoot. In addition, the derivative gain factor is added and this leads to a virtual damper added to the dynamic model, as well as an additional term to the actuator force, leading to a better dynamic response of the actuator (Figure 5.26). It should be noted that it was already found that this derivative gain factor is an uncertain factor in practice. As a result, comfort criteria are met in the numerical model relatively easy simply by increasing the derivative gain factor, whereas this is not the case in the practical application. It should, therefore, be noted that this derivative gain value was taken relatively low compared to the other two values in most of the numerical analyses. Finally, the integral gain value is added and this results in a reduction of the steady-state error, which now converges to zero in time (Figure 5.27). In this case, the steady-state error is an actual error, as a step-load is applied as an external force. If one should model an impulse load, it is obvious that this steady-state error always converges to zero. It should be noted that in all numerical simulations a step load was implemented as external force, regarding the actuator. In this way, the deformation control of the actuator can best be simulated. Besides the user-defined PID-variables, the control system included some other parameters that have been implemented in the numerical model. As was stated already in the previous section, time delay must be included as it is simply impossible to respond on the measured error without losing some time in between the measurement and the

actual force application. To that extent, it can be seen that a larger time delay always results in incorrect actuator forces, which can even result in an increased vibration time compared to the bridge without actuator (Figure 5.28).

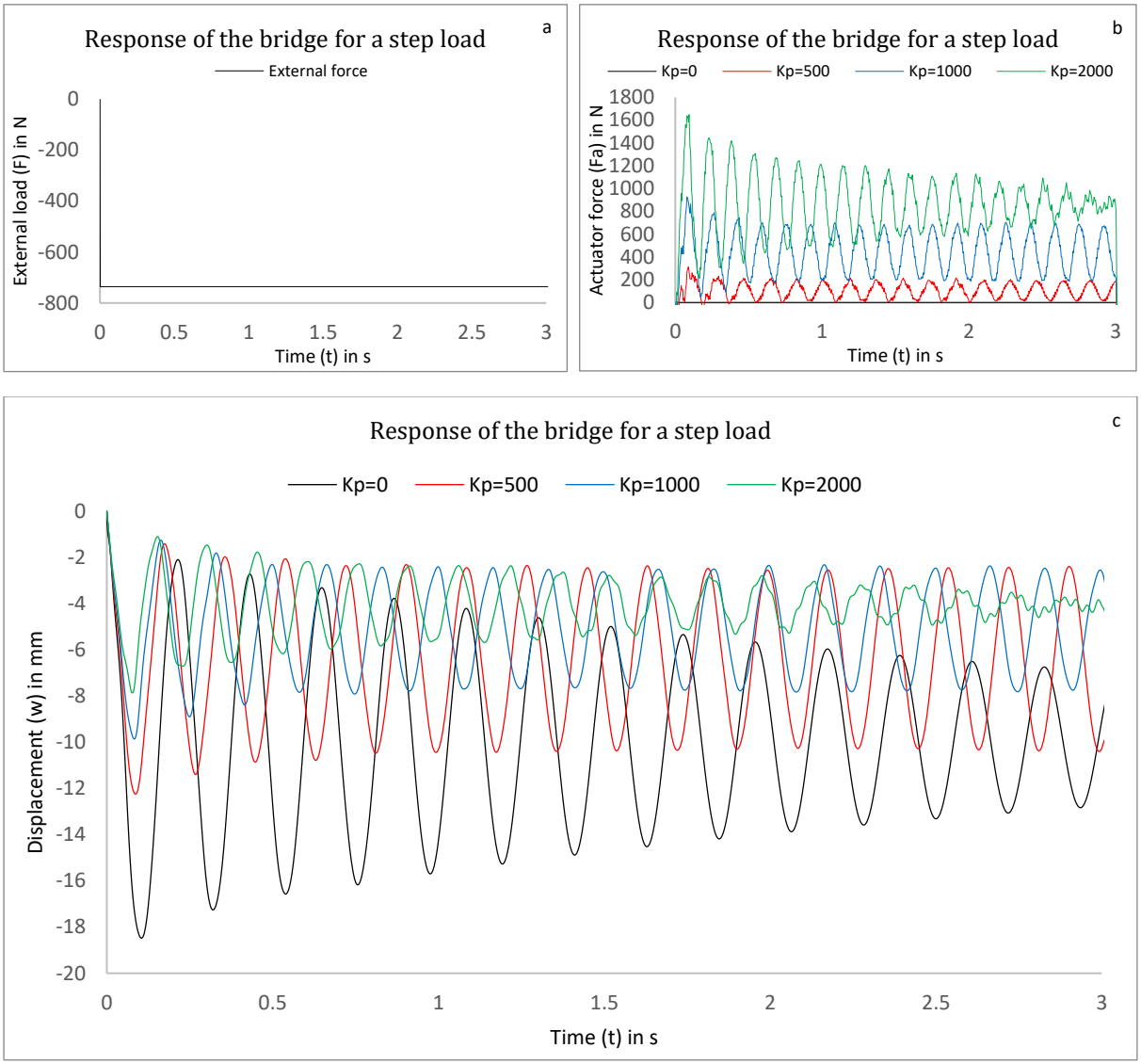

Figure 5.25: Increasing the K_P value: external applied force (a), actuator force (b), displacement (c)

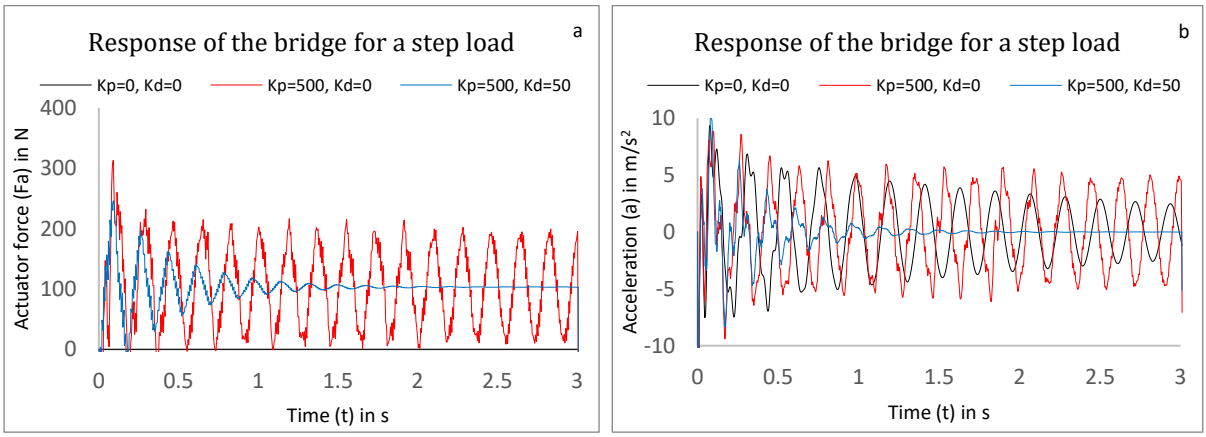

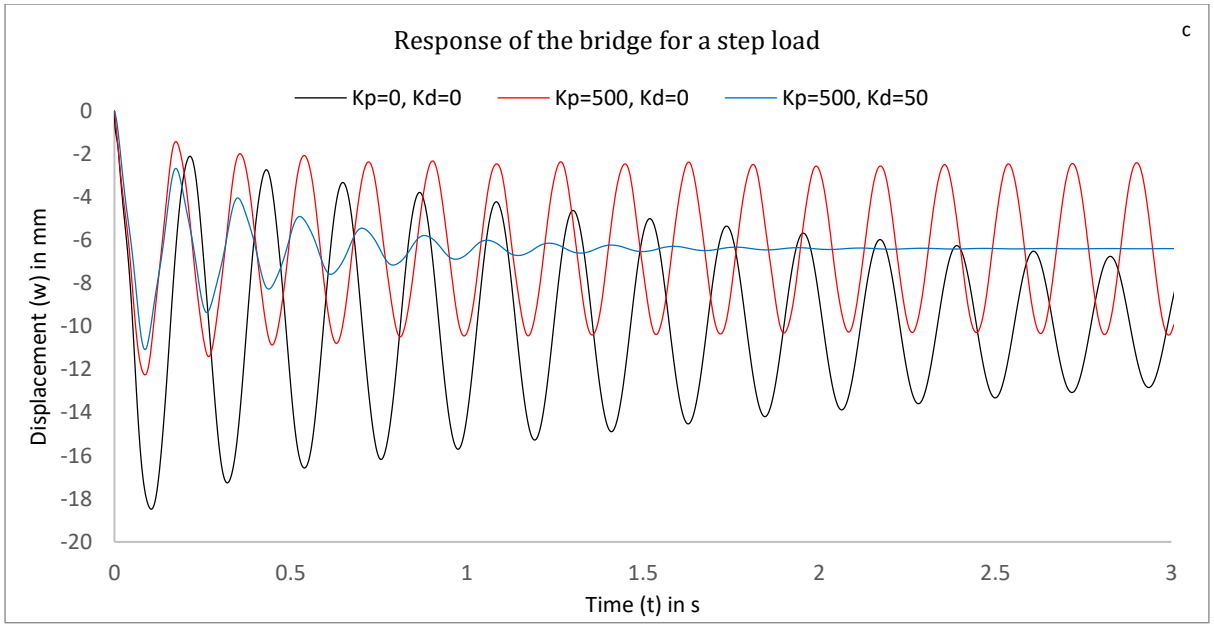

Figure 5.26: Using a K_D value: actuator force (a), acceleration (b), displacement (c)

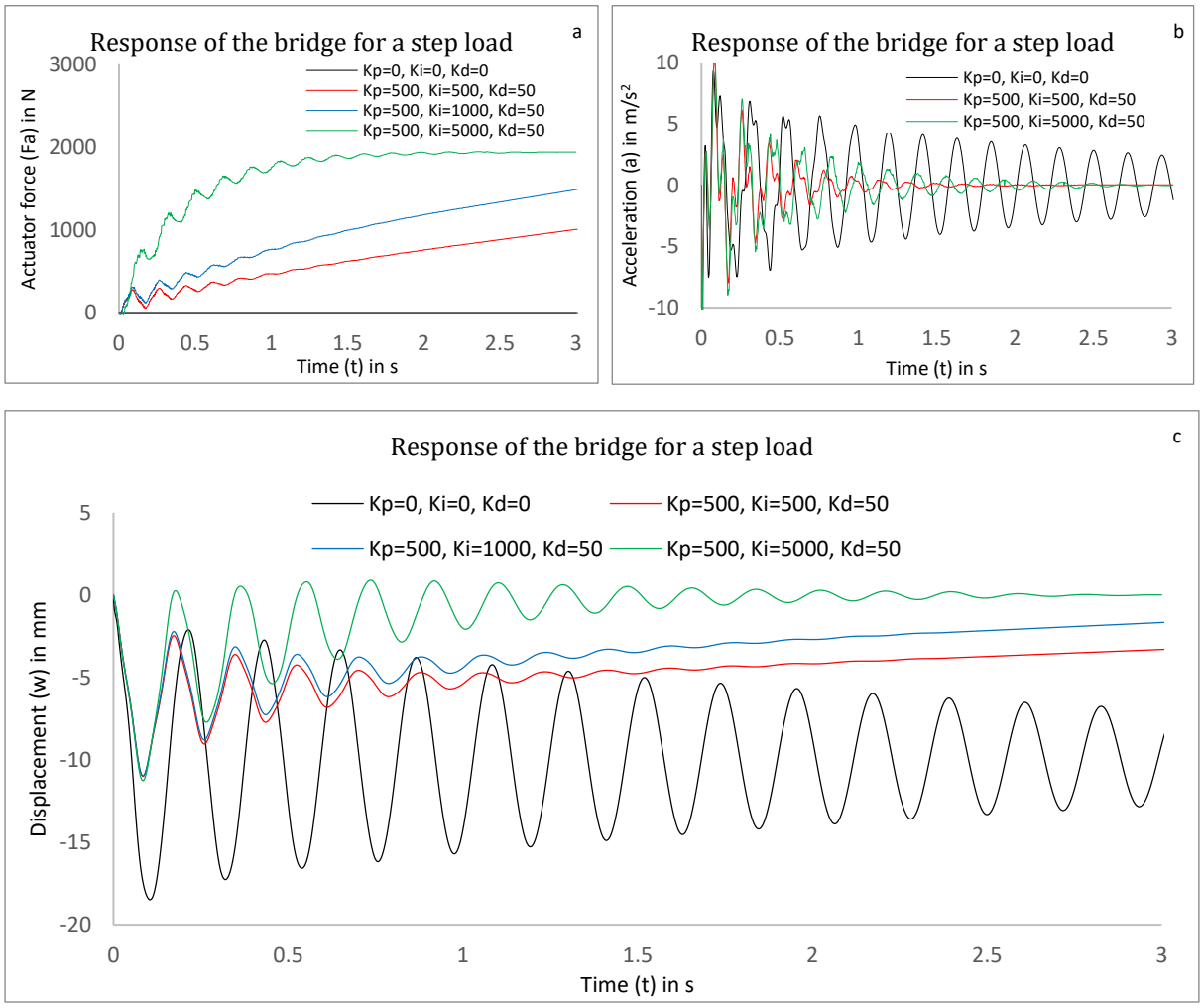

Figure 5.27: Increasing the K_I value: actuator force (a), acceleration (b), displacement (c)

It should be noted here, that the actuator in the practical model responds relative fast and that these extreme conditions will not occur in practical examples. A second limitation in hardware in the actuator was implemented as the maximum response time. This refers to the actual minimum time interval that is required in between two controlled actuator forces. Similar to the delay time, this time interval is quite small in present applications (i.e. $> 20Hz$). Some values were computed and obviously, it is seen that a larger response time leads to worse actuator behaviour, which is seen in the displacement graph of the bridge deck (Figure 5.29).

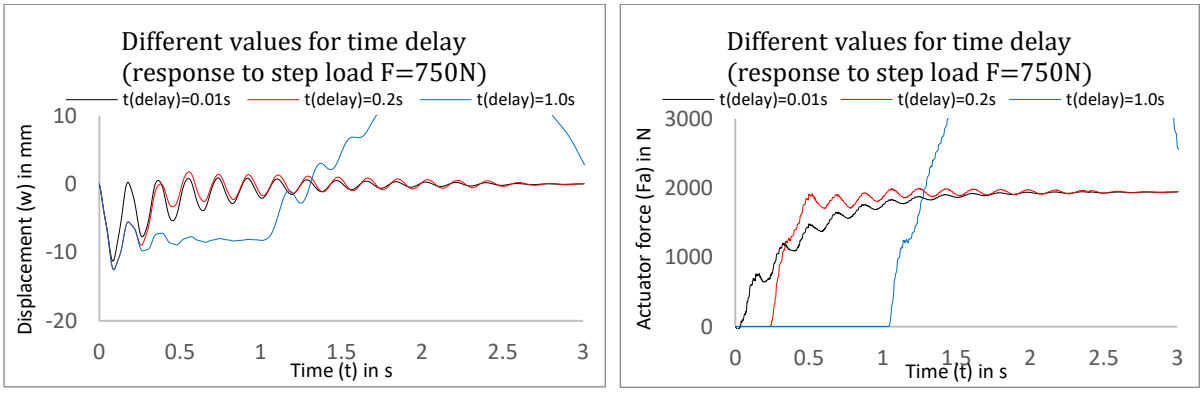

Figure 5.28: Different values for time delay in the PID-controller (K_P=500, K_I=5000, K_D=50)

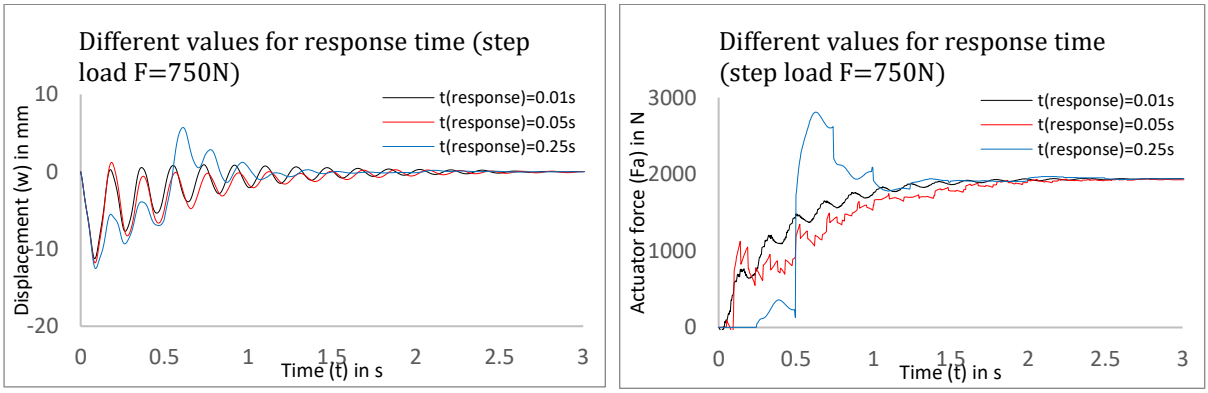

Figure 5.29: Different values for response time of the actuator (K_P=500, K_I=5000, K_D=50)

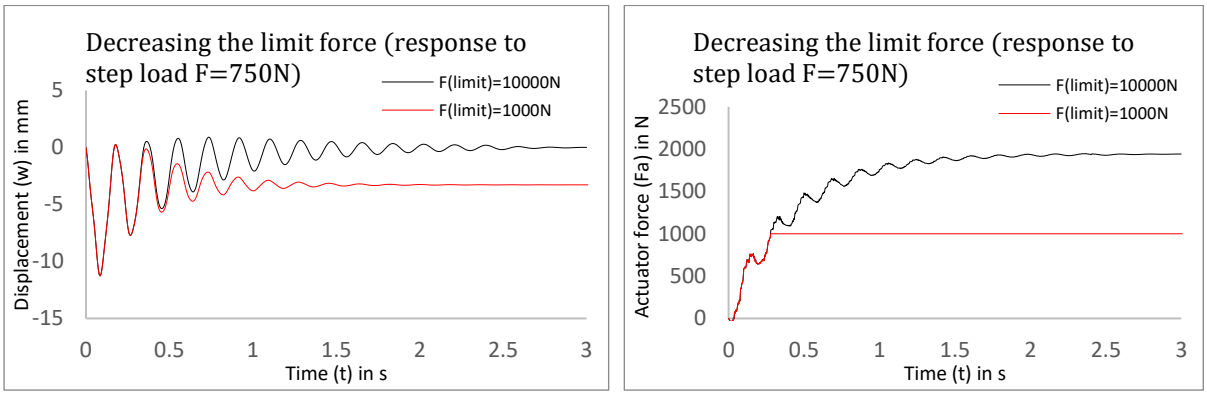

Figure 5.30: Decreasing the limit force of the actuator (K_P=500, K_I=5000, K_D=50)

Finally, a limitation force was given to the actuator, which can be controlled by a variable in the numerical analysis as well. If the computed actuator force exceeds this maximum, the maximum force is simply applied as actuator force to the model. It can be seen that a steady-state error remains if the actuator force is smaller than the external applied force (Figure 5.30).

To conclude, the actuator can perform quite well on deformation control if the described parameters are limited, but vibration control is guaranteed better when using a viscous damper (Figure 5.31). A number of limitations were discussed, which are dependent on the quality of the actuator that is used in a comparable application. It is seen that decreasing these limitation variables can lead to worse results in terms of both displacement and vibration control.

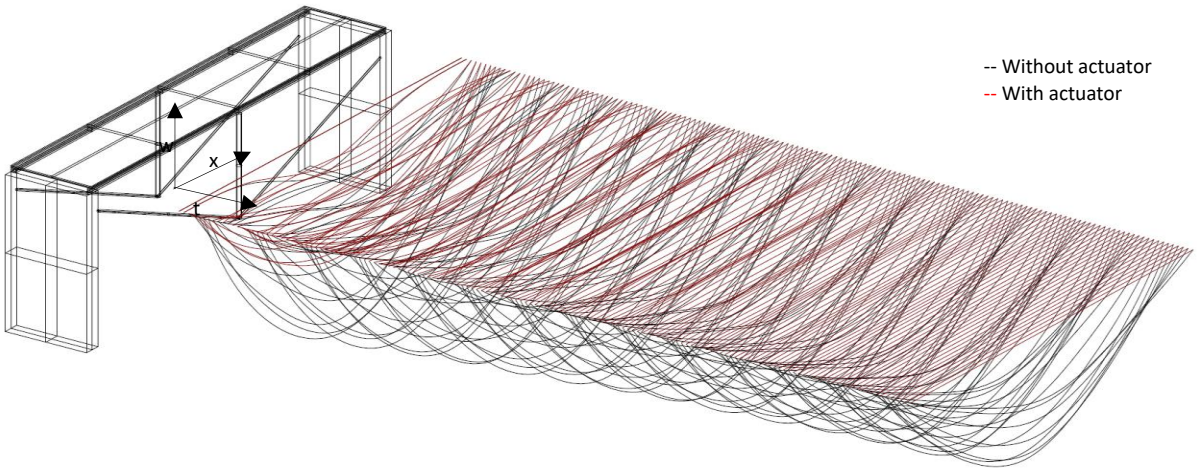

Figure 5.31: Three-dimensional plot of the displacement of the bridge deck in time, with and without actuator (K_P=500, K_I=5000, K_D=50, F_{limit}=10000N, t_{delay}=0.01s, t_{resp}=0.01s)

5.5 Damping in an active system

It can be concluded from the numerical analysis that an actuator can provide deformation control, which means that the steady-state deformation converges to zero in time. On the other hand, it can be seen that vibrations are better controlled or in other words damped out much faster when using the damper. Furthermore, the damper is not sensitive to delay time, power independent and is probably cheaper than an expensive control system. After discussing the advantages and disadvantages of both methods, the main purpose is to combine the viscous damper and the PID-controller. As a result, the combination of both systems should lead to the elimination of the disadvantages of both methods. Two different models were considered, including a model where the damper and actuator are connected in series and a model where a top deck is introduced on top of the bridge. In this model, damping is implemented in between those two bridge decks (Figure 5.32).

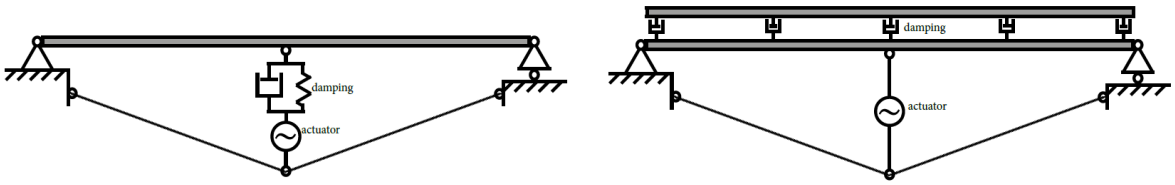

a. model of the bridge with damper and actuator

b. model of the bridge with a damped top deck

Figure 5.32: Damping combined with an actuator: two models

5.5.1 Connection in series

As a first combined model, the damper and actuator are connected in series. As indicated in the figure, the damper is here placed on top of the actuator. This implies that the numerical model has to be extended with an extra degree of freedom, as the damper and actuator are placed in series. Recalling the second order differential equation for a multiple degree of freedom system, the matrices are now equal to

$$\mathbf{M} = \begin{bmatrix} \frac{\rho Al}{4} & 0 & 0 & 0 & 0 \\ 0 & \frac{\rho Al}{4} + \frac{1}{2}m_d & 0 & 0 & 0 \\ 0 & 0 & \frac{\rho Al}{4} & 0 & 0 \\ 0 & 0 & 0 & \frac{1}{2}m_a + \frac{1}{2}m_d & 0 \\ 0 & 0 & 0 & 0 & \frac{1}{2}m_a + \rho_w Al \end{bmatrix} \qquad \mathbf{F} = \begin{bmatrix} 0 \\ F \\ 0 \\ F_A \\ -F_A \end{bmatrix}$$

$$\mathbf{C} = \begin{bmatrix} \alpha m + \beta k & \beta k & \beta k & 0 & 0 \\ \beta k & \alpha m + \beta k & \beta k & -c_d & 0 \\ \beta k & \beta k & \alpha m + \beta k & 0 & 0 \\ 0 & -c_d & 0 & c_d + K_D & -K_D \\ 0 & 0 & 0 & -K_D & \frac{sin(\alpha)EA}{L} + K_D \end{bmatrix}$$

$$\mathbf{K} = \begin{bmatrix} \frac{4416}{7}\frac{EI}{l^3} & -\frac{4224}{7}\frac{EI}{l^3} & \frac{1728}{7}\frac{EI}{l^3} & 0 & 0 \\ -\frac{4224}{7}\frac{EI}{l^3} & \frac{\rho Al}{4} + \frac{1}{2}m_d & -\frac{4224}{7}\frac{EI}{l^3} & -k_d & 0 \\ \frac{1728}{7}\frac{EI}{l^3} & -\frac{4224}{7}\frac{EI}{l^3} & \frac{4416}{7}\frac{EI}{l^3} & 0 & 0 \\ 0 & -k_d & 0 & k_d + k_a + K_P & -(k_a + K_P) \\ 0 & 0 & 0 & -(k_a + K_P) & \frac{sin(\alpha)EA}{L} + k_a + K_P \end{bmatrix} \qquad (5.8)$$

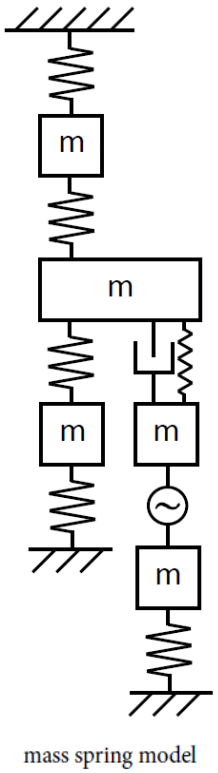

mass spring model

The main benefit of this system is that heavy vibrations are damped out quite fast with the viscous damper, resulting in a steady-state error that is reached without observing one single harmonic vibration. As a result, the actuator starts to respond on the steady-state deformation rather than the vibration of the bridge. This then results in better performance of the actuator, as it was found from the previous model that the actuator performs quite well on deformation control. In the first numerical analysis, an impulse load was applied to the dynamic model, which results in a better dynamic response than the model with the actuator only. It should, however, be noted that using only the damper results in a slightly better dynamic response, as here no steady-state deformation occurs at all. This implies that the actuator thus should not respond at all. On the other hand, it is seen that activating the actuator reduces the maximum error. Furthermore, the actuator is now much less sensitive to fluctuations in its input parameters, as results are shown for relatively extreme values for proportional and integral gain. It is seen that for impulse loading, there is only a small difference in using a shock absorber or a damper (Figure 5.33, Figure 5.34).

Besides impulse loading, a step load was applied to the described dynamic model. Obviously, the steady-state error is not reduced if the viscous damper (without a spring stiffness) is used. It can be seen that adapting the actuator can improve the steady-state error at short-term, but in the end, the maximum deformation is reached, which is equal to the deformation of the bridge deck only. To that extent, it can again be concluded that using the shock absorber performs much better for step loading, as the error now reduces back to zero. It may thus be concluded that the positive effect of the shock absorber outweigh the slightly negative effects on vibration control (Figure 5.35, Figure 5.36).

Finally, it can be obtained that even time delay does only have a minor influence on the behavior of the total system if one decides to use the shock absorber and the actuator in series (Figure 5.37). As a result, using the shock absorber in combination with the actuator results in a good compromise of vibration and deformation control, where the influence of fluctuating parameters is much less noticeable, especially for the actuator.

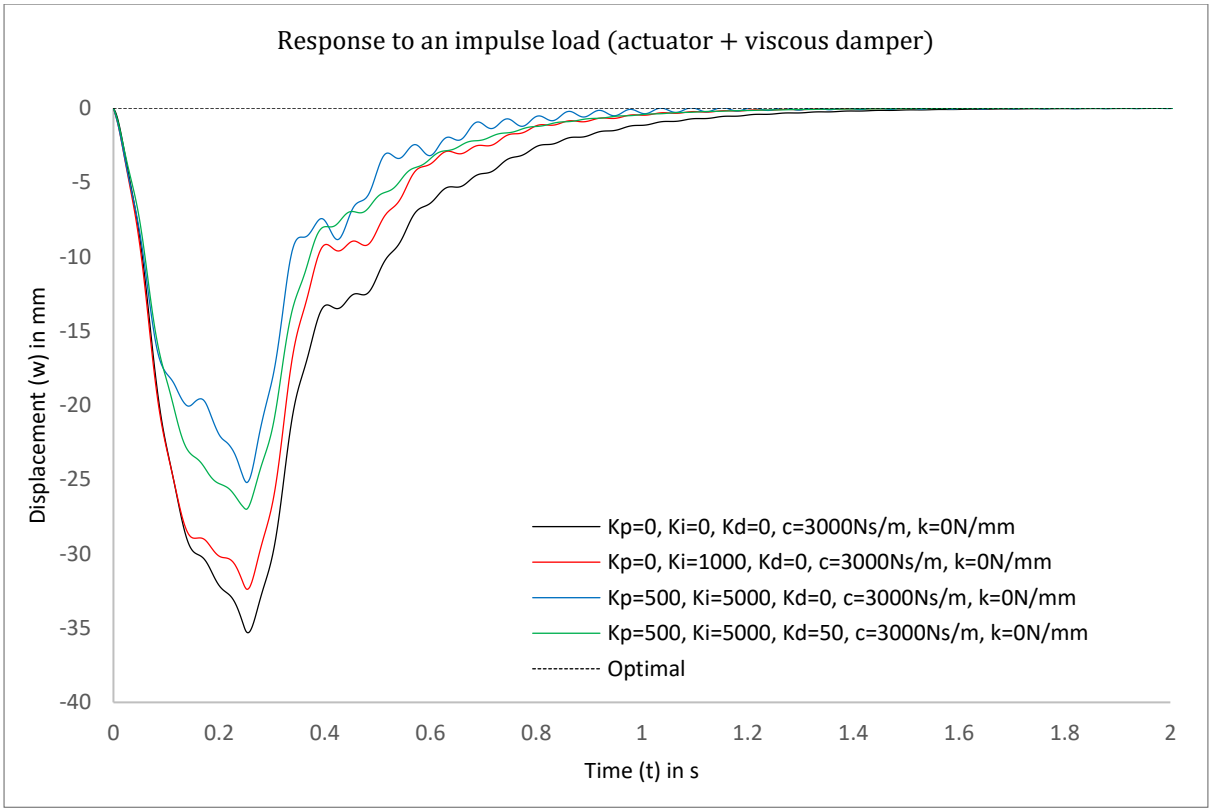

Figure 5.33: Different values for the actuator, when using the actuator in series with a viscous damper

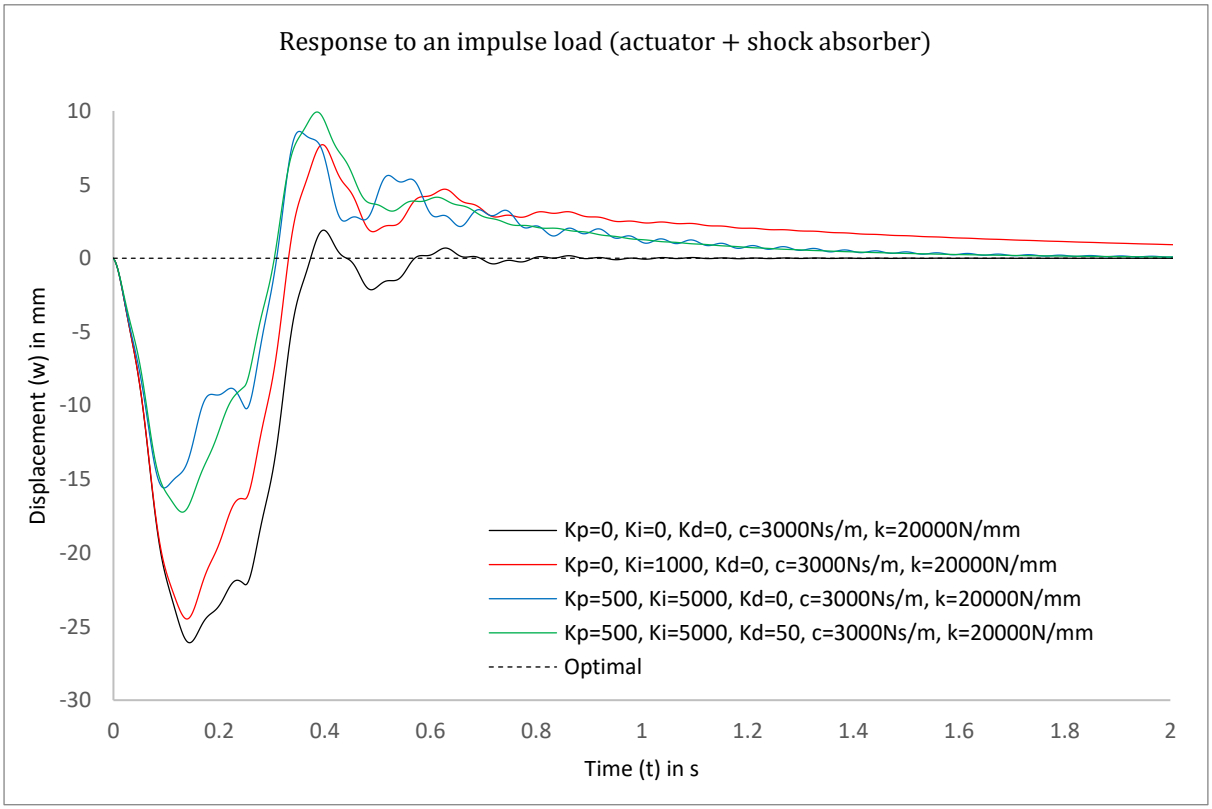

Figure 5.34: Different values for the actuator, when using the actuator in series with a shock absorber

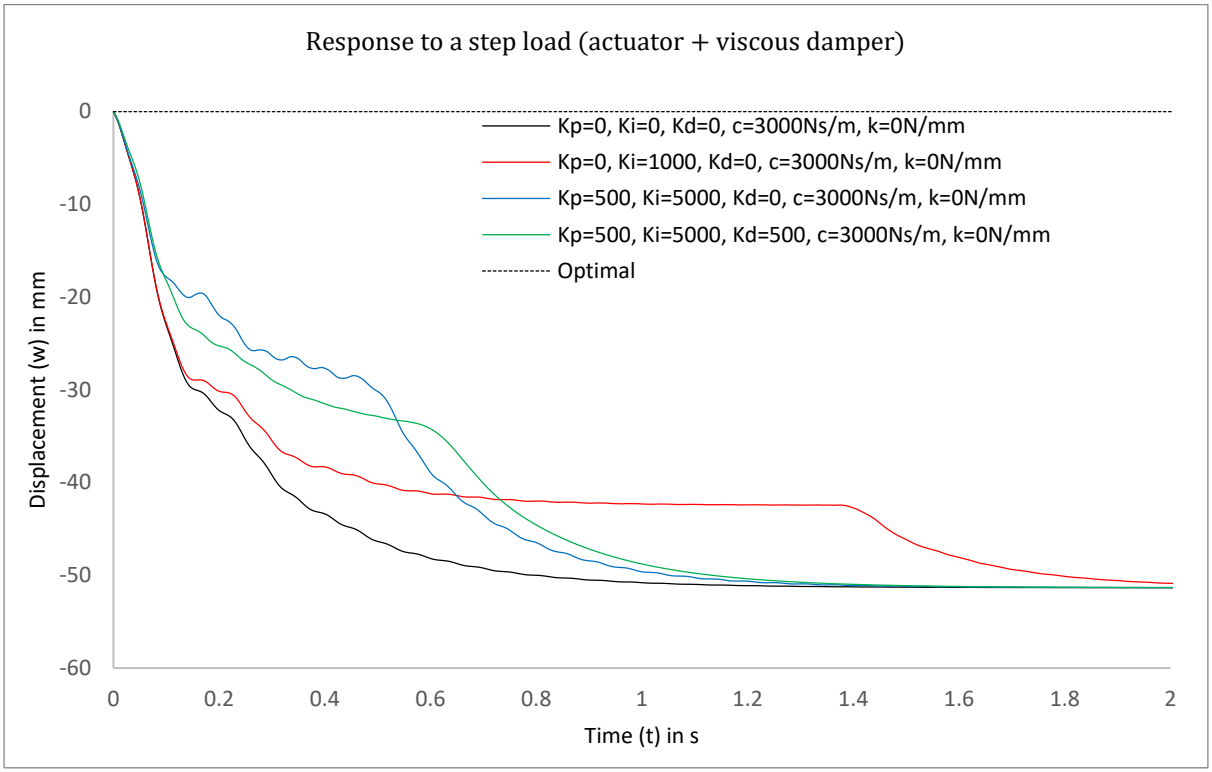

Figure 5.35: Different values for the actuator, when using the actuator in series with a viscous damper

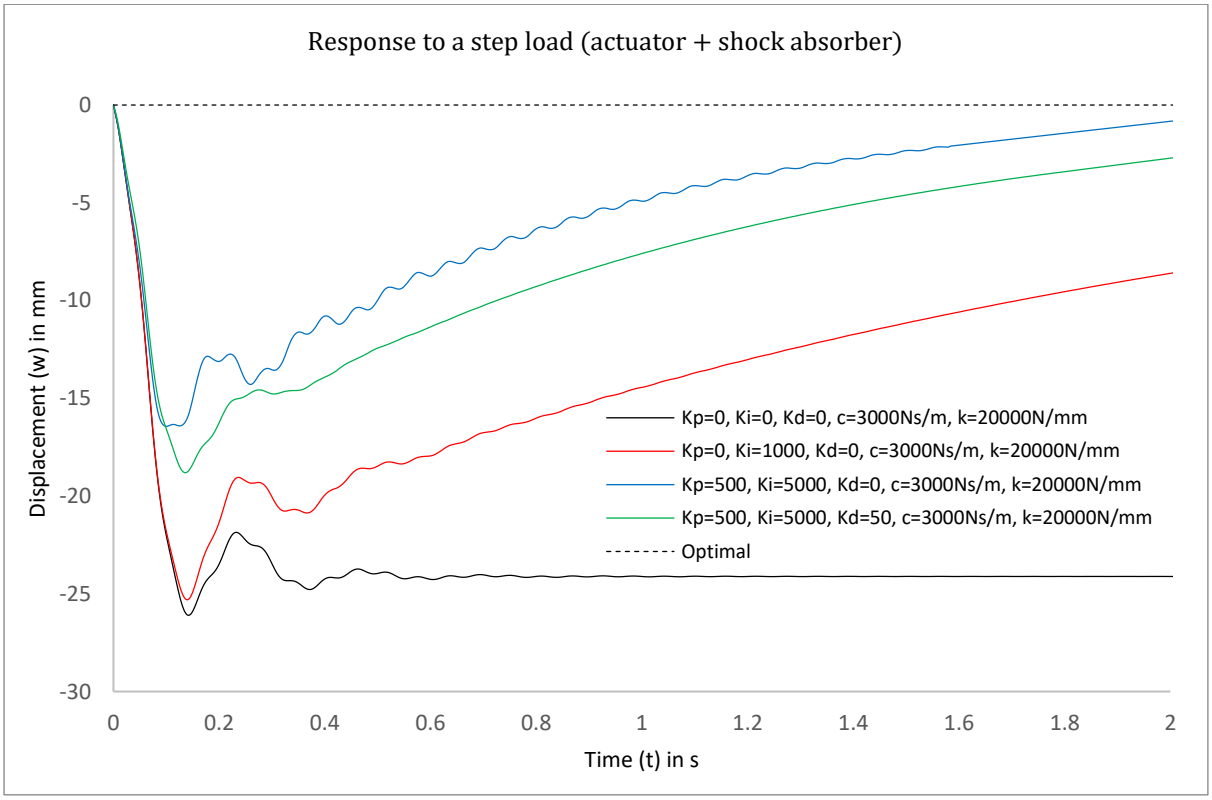

Figure 5.36: Different values for the actuator, when using the actuator in series with a shock absorber

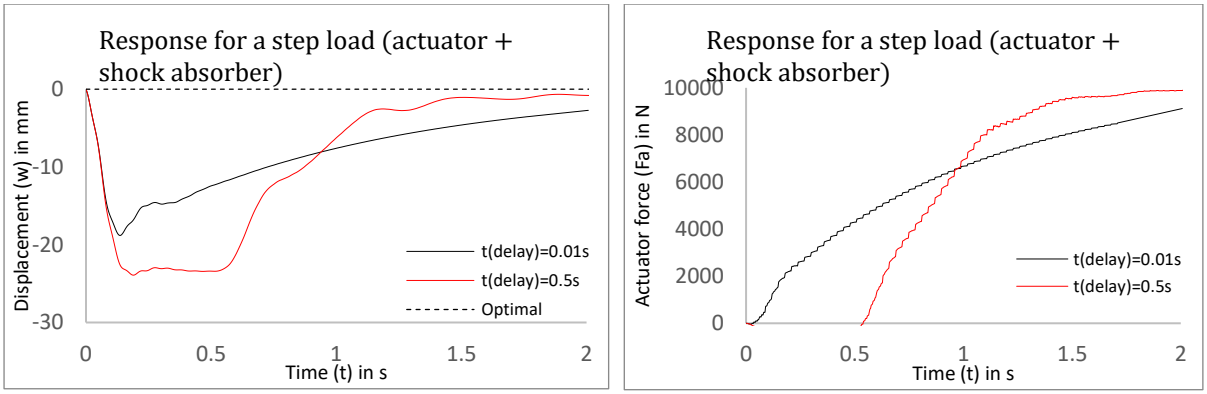

Figure 5.37: Influence of delay time on the behavior of the bridge model

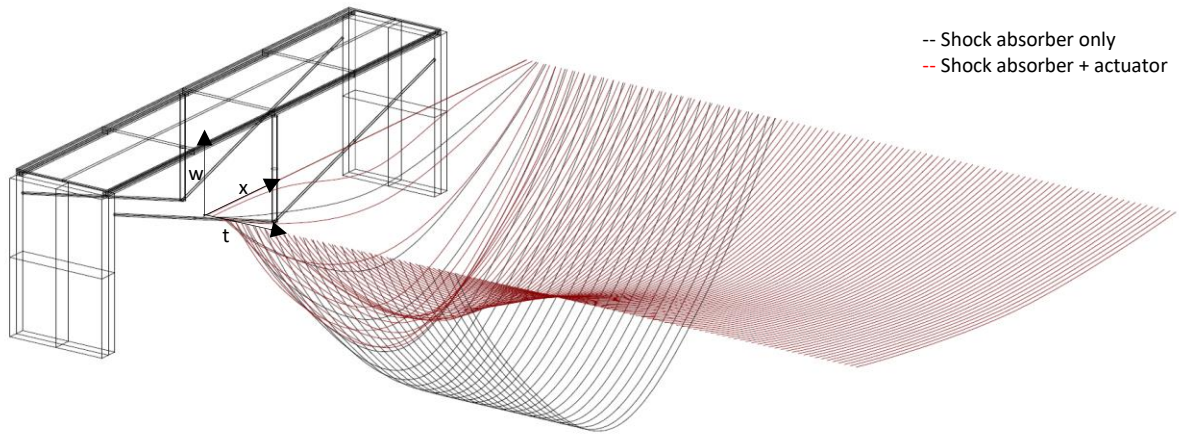

Figure 5.38: Three-dimensional plot of the displacement in time for a step load, with and without actuator (actuator: K_P=500, K_I=5000, K_D=50, F_{limit}=10000N, t_{delay}=0.01s, t_{resp}=0.01s, damper: c=3000Ns/m, k=20000N/mm)

5.5.2 A damped top layer

Another improvement that is investigated into more detail is a bridge deck with a damped top layer. In this model, the bridge deck consists out of two layers and within these layers viscous damping is added. The damped interlayer could for instance be a rubber layer which is loaded into shear when the two layers of the bridge deck start to deform. Because of shear deformation, the bridge deck is damped more than the original model of the bridge. This extra layer of damping was added to the model by simply increasing the β-value for Rayleigh damping. In case of a comparison between both models, the total amount of added Rayleigh damping should be approximately equal to the total amount of viscous damping in the shock absorber. Generally, adding more damping to the bridge deck results in better vibration control, when this model is compared to the bridge with actuator only. The actuator, however, is more sensitive to user-defined input for K_P, K_I and K_D. Furthermore, physical values like time delay have more influence than in the previous model, where the damper and actuator were placed in series. As a positive side effect, it appears that relative large deformations are not found at all in this model. This could be explained by the fact that damping is now much better divided over the total span of the bridge. The viscous damper, which is not present in this case, mainly caused these deformations in previous models. The β-value was multiplied ten times and one hundred times and for both values the displacement and acceleration over time is shown (Figure 5.39). It should be noted here, that a multiplication of one hundred times the default β-coefficient is approximately equal to a viscous damping ratio of $c = 30000Ns/m$ for the shock

absorber, whereas ten times the β-value approximates the used value for the shock absorber in the previous model.

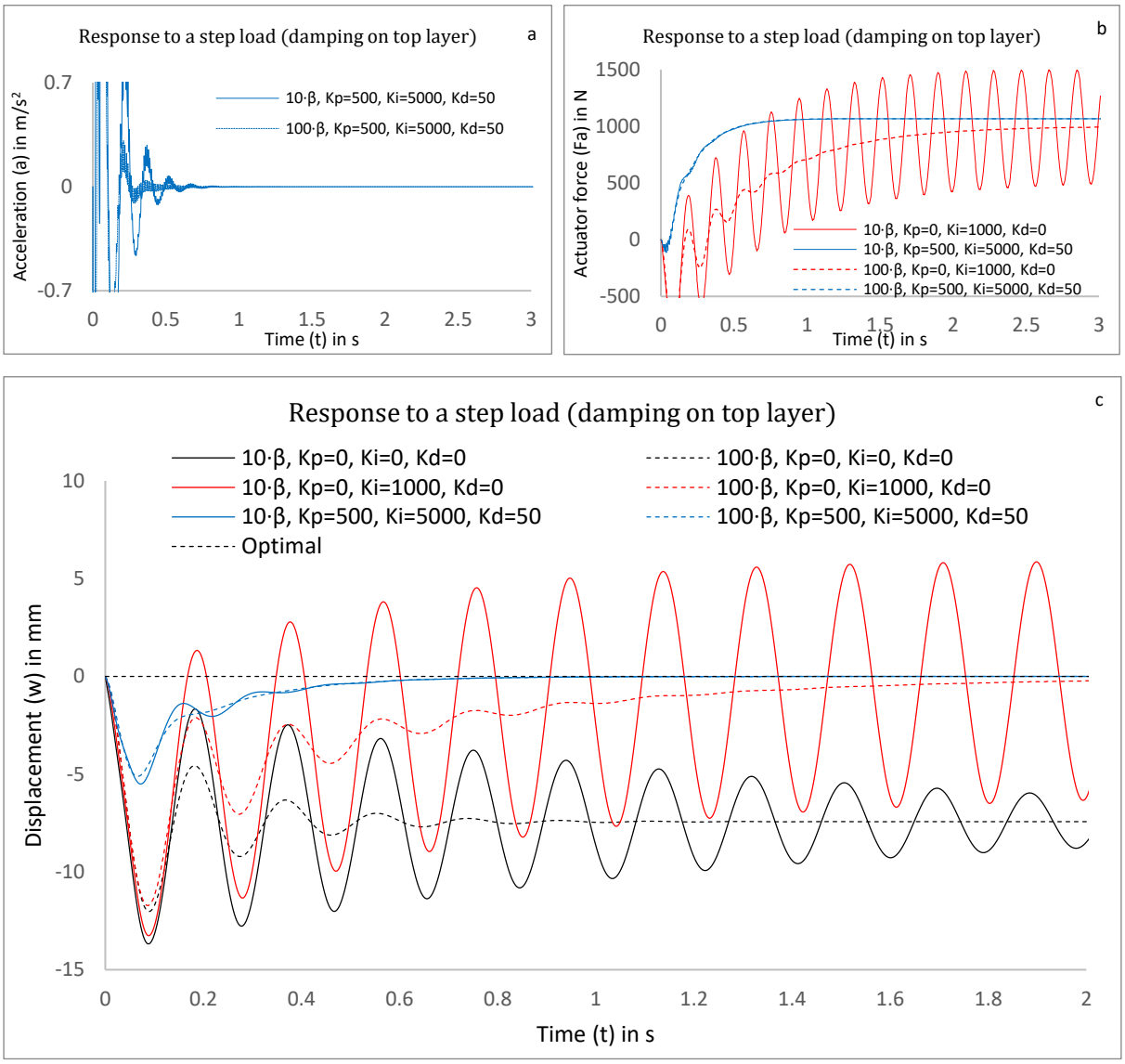

Figure 5.39: Response to a step load: acceleration (a), actuator force (b) and displacement (c)

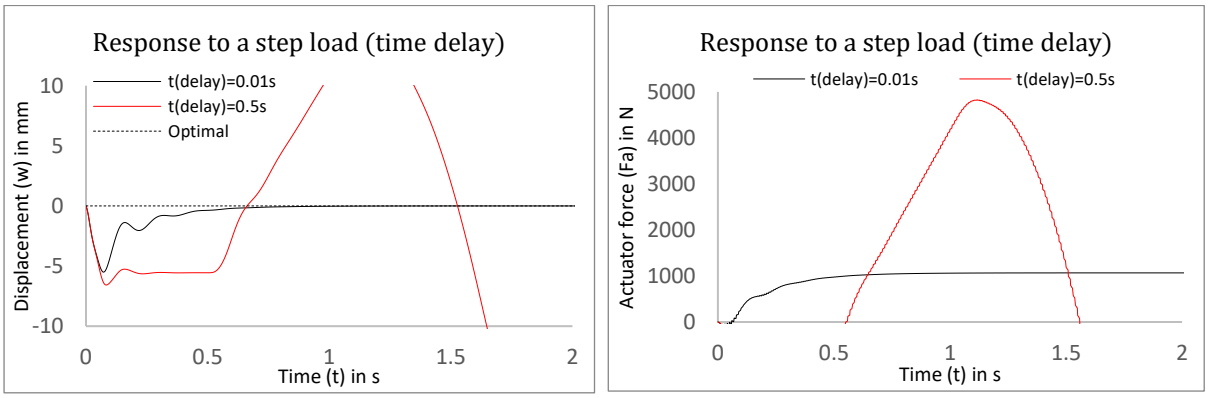

Figure 5.40: Sensitivity to time delay (development of instable behavior) for K_P=500, K_I=5000, K_D=50

5.6 Performance

A number of dynamic models concerning a small-scale pedestrian footbridge has been analyzed by means of a numerical tool for dynamic analysis. Because of many input variables, each model could be examined for different physical properties and the advantages and disadvantages of each model were described. In this section, all models are compared for a few loading configurations, with regard to different design criteria like deformation and vibration control (Figure 5.41). First, the comparison is made for both the impulse and step load and secondly, a realistic load case was simulated that could practically be expected on the case study. In all comparisons, the numerical simulation is still done for one pedestrian with a mass equal to $m = 75kg$. Furthermore, it should be noted that the cable properties were assumed a little better than standard (i.e. $d = 10mm$, $P = 1000N$), as the difference in behaviour between models is seen better when the cables provide a little more stiffness. This diameter was also used in the actual physical model of the bridge for experimental testing.

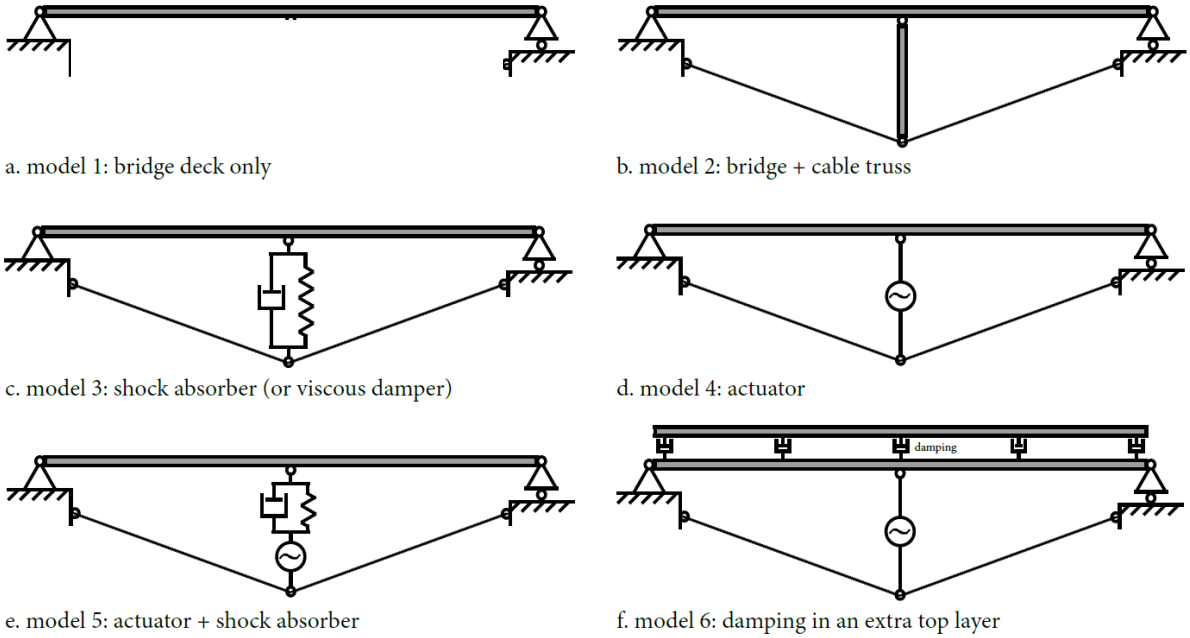

Figure 5.41: All different models for the pedestrian bridge design

5.6.1 Short and long-term loads

As for all models, the dynamic response was simulated for both short and (relatively) long-term loading. As for now, these load cases are considered again for all models including the shock absorber, the actuator or both. It can now be stated that the best result for vibration control is found for the model with only a viscous damper (or a shock absorber), as the time needed to die out completely is smallest for this model. On the other hand, it is seen that this is the only model where a relatively large steady-state error remains and to that extent, this model performs poorly on deformation control. In addition, the steady-state error does not even meet the deflection criteria stated for this bridge design. Combining damping with an actuator seems a better overall solution, as vibrations are damped out faster to the one hand, and the actuator is less sensitive to user-defined input to the other hand. The main difference in these two combined models is that the first one seems to respond a little faster on vibrations, whereas deformations remain smaller in the total time domain for the second one. Furthermore, the viscous damper in model five seems to respond better on poor conditions for the actuator (i.e. large time delay, zero derivative gain and so on), whereas model six is a little more sensitive to these conditions. In general, it may be concluded that both combined models perform well, especially if they are compared to the second model without any stabilization improvements. This may be concluded for both deformation and vibration control.

	Load	w_{max}	$w_{steady-st}$	$t_{die-out}$	$t_{a<0.7m/s^2}$
Model 2	Impulse load	$2.2mm$	$0.0mm$	$> 3s$	$2.3s$
	Step load	$2.2mm$	$1.3mm$	$> 3s$	$1.3s$
Model 3	Impulse load	$21.6mm$	$0.0mm$	$1.2s$	$0.5s$
	Step load	$21.9mm$	$21.9mm$	$0.6s$	$0.2s$
Model 4	Impulse load	$13.0mm$	$0.0mm$	$> 3s$	$0.8s$
	Step load	$13.1mm$	$0.0mm$	$2.5s$	$1.3s$
Model 5	Impulse load	$24.5mm$	$0.0mm$	$2.2s$	$0.9s$
	Step load	$24.5mm$	$0.0mm$	$1.5s$	$0.6s$
Model 6	Impulse load	$11.7mm$	$0.0mm$	$1.8s$	$0.7s$
	Step load	$11.8mm$	$0.0mm$	$1.4s$	$0.7s$

Table 5.5: Comparison for all models (deformation and acceleration)

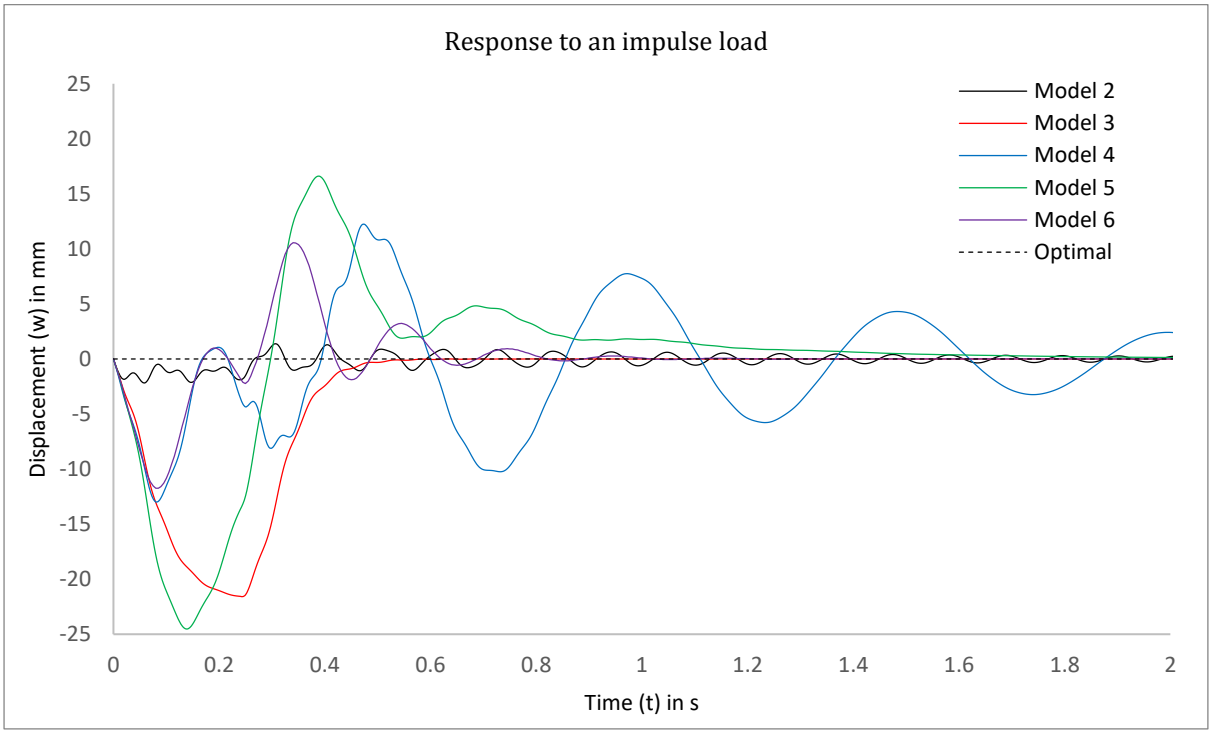

Figure 5.42: Displacement over time for all models (K_P=200, K_I=2000, K_D=1, t_{delay}=0.1s, t_{resp}=0.01s, c_d=3000Ns/m, k_d=20000N/mm, F_{imp}=735N, t_{imp}=0.25s)

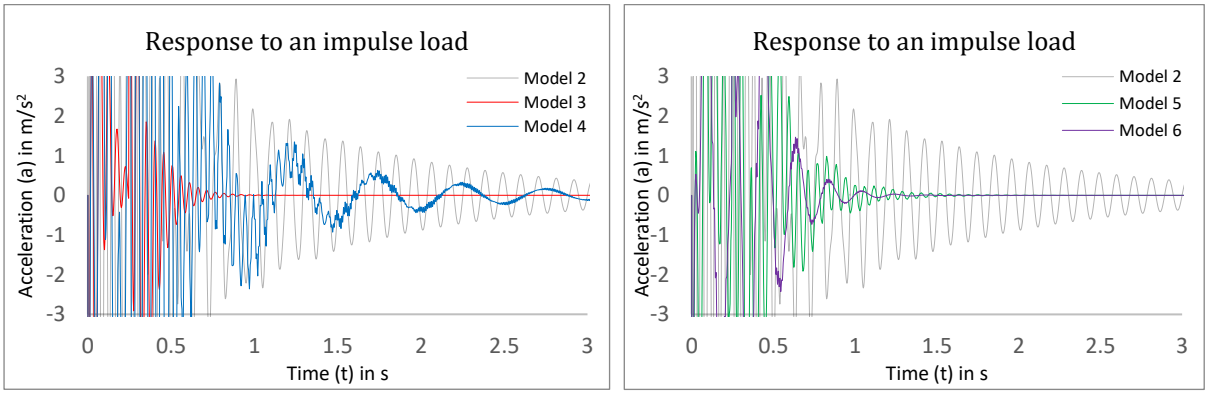

Figure 5.43: Acceleration over time for all models (K_P=200, K_I=2000, K_D=1, t_{delay}=0.1s, t_{resp}=0.01s, c_d=3000Ns/m, k_d=20000N/mm, F_{imp}=735N, t_{imp}=0.25s)

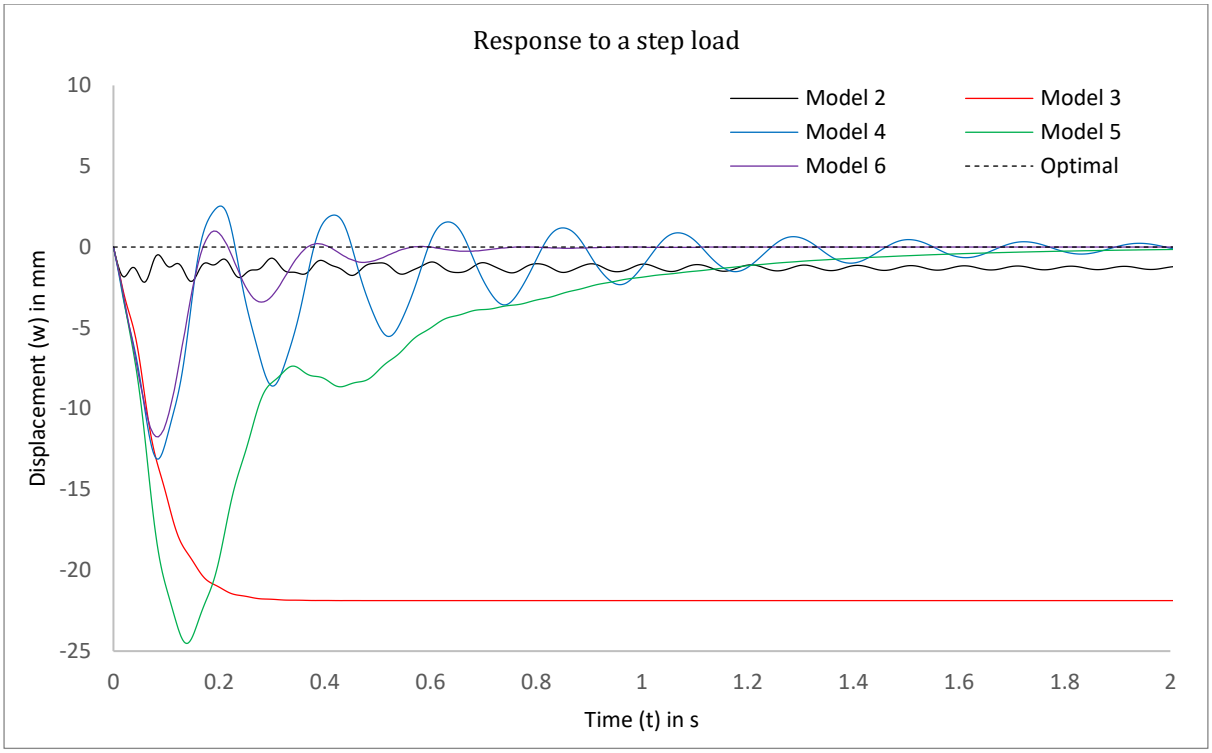

Figure 5.44: Displacement over time for all models (K_P=200, K_I=2000, K_D=1, t_{delay}=0.1s, t_{resp}=0.01s, c_d=3000Ns/m, k_d=20000N/mm, F_{imp}=735N, t_{step}>3s)

5.6.2 Realistic load cases

Considering a structural bridge design, a realistic external load would not consist out of just one impulse load, as pedestrians are assumed to be constantly crossing a bridge, creating multiple impulse loads at different locations along the bridge span. Furthermore, it can be presumed that another typical case for a pedestrian bridge would be standing on the bridge for a while. All these types of loading configurations can be predicted by the numerical model, as the discretization in the time domain allows for non-linear terms for all input parameters, including the external load. Since all models are already compared for the standard loading conditions, only a few are shown for some typically expected load cases. Since the bridge deck is discretized by four elements, some assumptions are made for these load cases as well. Walking over the bridge is considered the first load case. Here, some typical values are assumed for walking frequency and span of each step. The span of each step was here taken equal to one eight of the total bridge span so that these steps correspond to the discretized mass locations. Running over the bridge was simulated as a second load case, where the step span and the frequency were taken twice as large. In mathematical terms, this can be written as

$$f_{walking} = 2Hz \qquad f_{running} = 4Hz$$
$$T_{step,walking} = 0.5s \qquad T_{step,running} = 0.25s$$
$$L_{walking} = 0.625m \qquad L_{running} = 1.250m \tag{5.9}$$

As a third load case, it was said that the pedestrian stops for a while at mid-span, before crossing the bridge in total. The impulse time at mid span is here taken as a larger value. Finally, this results in three typical loading configurations (Figure 5.45). It should be noted here that a step in between two discretized masses was approximated as half the load to the left side and half the load to the right side. As a result of the moving point load in time, each of the three discretized masses concerning the bridge deck is loaded as a function of time. This implies that the first step is set on the first mass for running, whereas the first step is set in between the support point and the first mass for walking and so on. For standing, an extra time interval is added when the

pedestrian is standing on the second mass. For each load case, the external load can now be placed at the right mass for each time interval (Figure 5.46, Table 5.6).

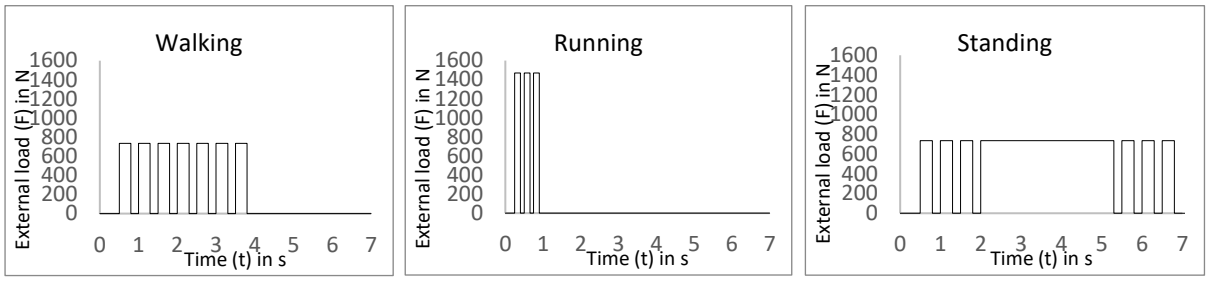

Figure 5.45: Typical load cases

	Step 0	Step 1	Step 2	Step 3	Step 4	Step 5	Step 6	Step 7	Step 8
Case 1: walking	$t = 0$ $F_1 = 0$ $F_2 = 0$ $F_3 = 0$	$t = 0.5$ $F_1 = F/2$ $F_2 = 0$ $F_3 = 0$	$t = 1.0$ $F_1 = F$ $F_2 = 0$ $F_3 = 0$	$t = 1.5$ $F_1 = F/2$ $F_2 = F/2$ $F_3 = 0$	$t = 2.0$ $F_1 = 0$ $F_2 = F$ $F_3 = 0$	$t = 2.5$ $F_1 = 0$ $F_2 = F/2$ $F_3 = F/2$	$t = 3.0$ $F_1 = 0$ $F_2 = 0$ $F_3 = F$	$t = 3.5$ $F_1 = 0$ $F_2 = 0$ $F_3 = F/2$	$t = 4.0$ $F_1 = 0$ $F_2 = 0$ $F_3 = 0$
Case 2: running	$t = 0$ $F_1 = 0$ $F_2 = 0$ $F_3 = 0$	$t = 0.25$ $F_1 = 2F$ $F_2 = 0$ $F_3 = 0$	$t = 0.5$ $F_1 = 0$ $F_2 = 2F$ $F_3 = 0$	$t = 0.75$ $F_1 = 0$ $F_2 = 0$ $F_3 = 2F$	$t = 1.0$ $F_1 = 0$ $F_2 = 0$ $F_3 = 0$	–	–	–	–
Case 3: standing	$t = 0$ $F_1 = 0$ $F_2 = 0$ $F_3 = 0$	$t = 0.5$ $F_1 = F/2$ $F_2 = 0$ $F_3 = 0$	$t = 1.0$ $F_1 = F$ $F_2 = 0$ $F_3 = 0$	$t = 1.5$ $F_1 = F/2$ $F_2 = F/2$ $F_3 = 0$	$t = 2.0$ $F_1 = 0$ $F_2 = F$ $F_3 = 0$	$t = 5.5$ $F_1 = 0$ $F_2 = F/2$ $F_3 = F/2$	$t = 6.0$ $F_1 = 0$ $F_2 = 0$ $F_3 = F$	$t = 6.5$ $F_1 = 0$ $F_2 = 0$ $F_3 = F/2$	$t = 7.0$ $F_1 = 0$ $F_2 = 0$ $F_3 = 0$

Table 5.6: Load on each mass in time for different load cases

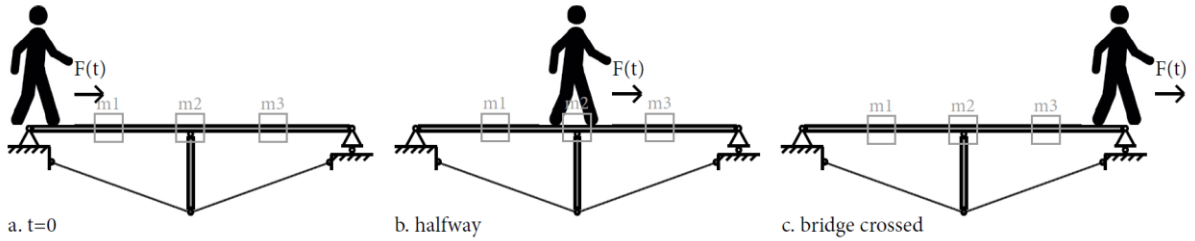

Figure 5.46: Moving point load in time

Again, it can be concluded that adding viscous damping only results in the best dynamic response for running, since the external applied load is most close to impulse loading. The amount of damping may be a little larger for best performance here, compared to other load cases like walking, as the impulse loads resulting from running are more powerful and thus more damping is needed to give a proper response. On the other hand, the model including both the actuator and the damper performs best for standing, as the steady-state error is important in this model as well. In the case of walking, it is seen that the actuator starts to respond on the overall error by simply increasing the actuator force. This results in a slightly positive deformation overall, which in turn results in deformations close to zero when the impulse load is active. It may be stated that this positive deformation can be judged peculiar, as it is against nature that something deforms in the opposite way of the external load direction. It can be seen that after a while, the actuator finds an equilibrium response over time (Figure 5.47, Figure 5.48, Figure 5.49). To conclude, the overall performance seems to be best for the model that combines the actuator with damping, concerning all load cases walking, running and standing. Here, mainly the integral gain value should be evaluated, as this value now seems to deform the bridge too much in positive direction during impulse loading. Reducing this value would lead to slower response to a step-load (in the case of standing).

Figure 5.47: Response to the first load case: walking (K_P=10, K_I=1000, K_D=1, t_{delay}=0.1s, t_{resp}=0.01s, c_d=3000Ns/m, k_d=20000N/mm)

Figure 5.48: Response to the second load case: running (K_P=10, K_I=1000, K_D=1, t_{delay}=0.1s, t_{resp}=0.01s, c_d=3000Ns/m, k_d=20000N/mm)

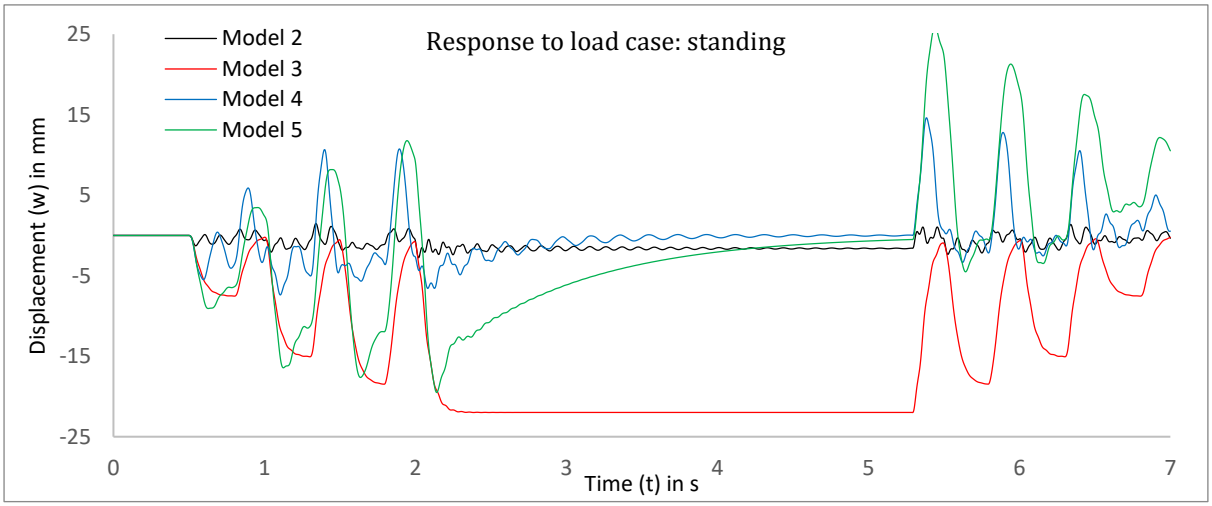

Figure 5.49: Response to the third load case: standing (K_P=10, K_I=1000, K_D=1, t_{delay}=0.1s, t_{resp}=0.01s, c_d=3000Ns/m, k_d=20000N/mm)

5.6.3 Adding more dampers

In all previous models, the center mass of the bridge deck has been used to obtain and compare results and although damping results in a much better response to vibrations for this mass, the discretized masses located on one and three quarter of the bridge span still show uncomfortable vibrations in time. Obviously, the long-term deformation of these masses remains small, as the relative span between the center mass and the support location is only half the span of the total bridge. As a result, one may assume that deformation is controlled adequately using one actuator. On the other hand, the dynamic response may be improved by adding more dampers. In this case, damping was added in between the actuator and the two side masses of the bridge deck. A distinction was made between adding shock absorbers (Figure 5.50) or viscous dampers (Figure 5.51). It should be noted here, that the total amount of damping and spring stiffness was taken equal to the model with one shock absorber. However, these coefficients are now equally divided. For the model with three shock absorbers, this implies that each absorber has both a damping coefficient and a spring stiffness coefficient equal to one third of the standard model. For the other model, only the damping coefficient is divided, resulting in a spring stiffness for the middle absorber equal to the standard value.

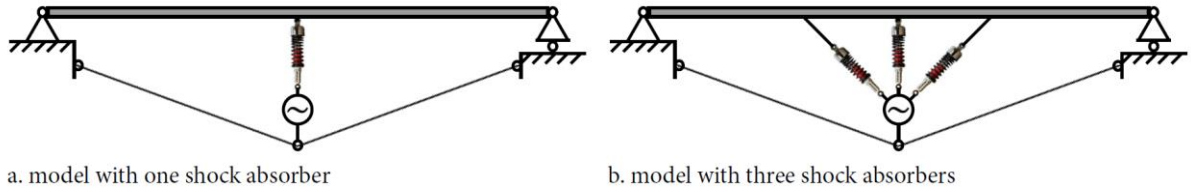

Figure 5.50: Adding more shock absorbers to the bridge

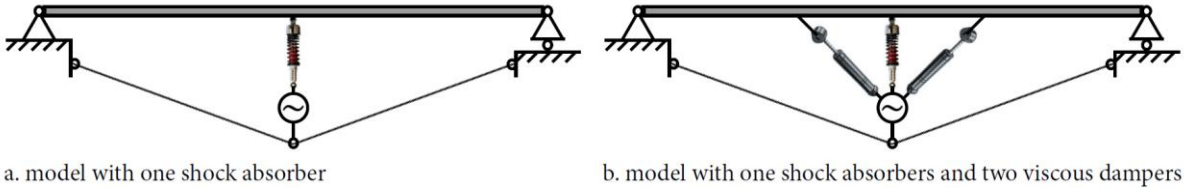

Figure 5.51: Adding viscous dampers to the bridge

Obviously, the model with only one shock absorber performs quite well for the center mass, which in the response graph is indicated as 'Mass 2' (Figure 5.46). On the other hand, the two other discretized masses (Mass 1 and 3) still show vibration issues, which could be considered uncomfortable (Figure 5.52). Furthermore, it can be seen that these vibrations start to increase after a number of impulse loads have taken place. In other words, comfort is only found if a pedestrian is halfway the span, whereas walking at three quarter of the span of the bridge may be judged very uncomfortable. Adding two viscous dampers at each side, it can be concluded that now vibrations are damped out quite fast for each mass, resulting in a better overall comfort criterion (Figure 5.53, Figure 5.54). Furthermore, it was found that the difference in using three shock absorber or two additional viscous dampers does only have a minor difference, where the model with three shock absorbers performs best in terms of comfort criteria.

Clearly, using only damping at center span seems to damp out vibrations so well, that vibrations having a maximum at center span do not occur anymore. Nevertheless, this does not hold for any even frequency, as here always a point of zero deformation is found at exactly center span. Hence, applying damping at center span will never decrease these even vibrations. The second natural frequency is the most important here, because all higher frequencies have much less influence on the total deformation and this frequency is indeed observed in numerical models, and even in the experimental test, one can observe this second frequency whereas the first natural frequency is not observed at all anymore.

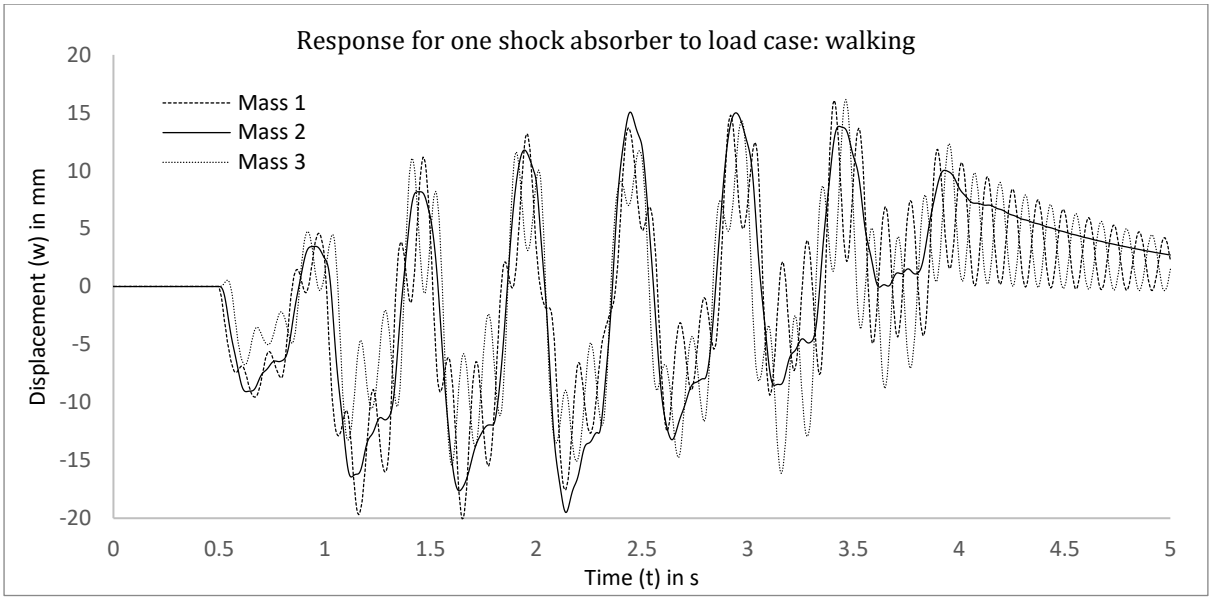

Figure 5.52: Response to load case: walking, for using only one shock absorber at each side (K_P=100, K_I=1000, K_D, t_{delay}=0.01s, t_{resp}=0.01s, c_d=3000Ns/m, k_d=20000N/mm)

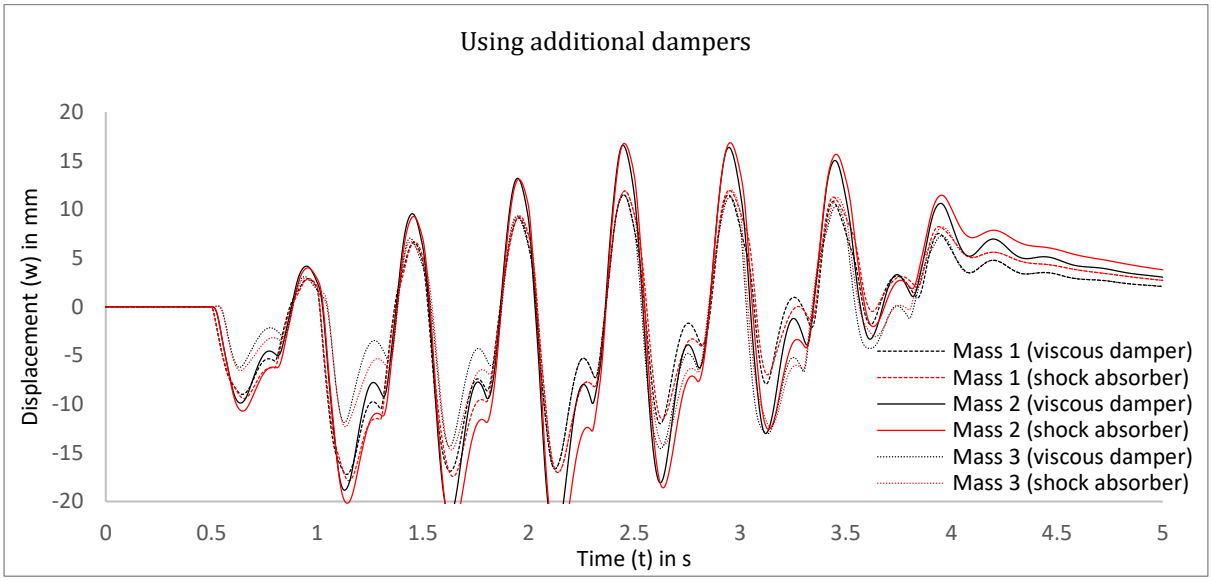

Figure 5.53: Response to load case: walking, for using one shock absorber and two dampers at each side (K_P=100, K_I=1000, K_D=1, t_{delay}=0.01s, t_{resp}=0.01s, c_d=1/3c_{stand}=1000Ns/m, k_d=20000N/mm)

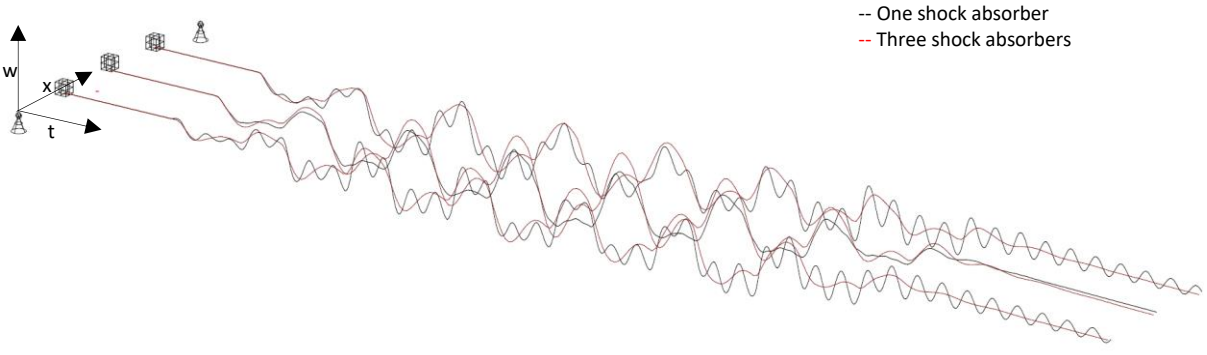

Figure 5.54: Three-dimensional plot of the displacement in time for load case: walking

6 Experimental research

This project contains a number of principles regarding dynamic analysis of structures, where some assumptions and simplifications had to be made in order to create a numerical approximation model for predicting the dynamic response of the pedestrian footbridge design on different external load cases. As a result, one may obtain that results from these numerical models should be verified by means of experimental testing. To that extent, a physical model was tested in the Pieter Van Musschenbroek Laboratory at the University of Eindhoven. In this part of the report, the main principles for the experimental setup are discussed and some results that were obtained during testing are compared to the numerical simulations.

6.1 The footbridge design

As a start for the footbridge design, a steel frame has been built already as seen in the problem description of this report. The steel frame provides the main supporting structure for both the steel bridge deck and the cable truss. A supporting location is provided by two steel columns, connected to a steel beam at a height of approximately one meter at each side. Another steel beam was provided between the supporting steel provisions in the longitudinal direction in order to provide both stability to the frame and to resist additional compression forces resulting from the cable truss. On top, hinged connections are seen, upon which two steel tubes are located, providing the main structure of the bridge deck. The span length of the bridge is equal to five meters (annex B). Finally, a walking deck was provided by means of timber elements in perpendicular direction to the steel tubes. So far, the experimental model of the pedestrian bridge was already built (Figure 6.1). As a result of the relative lightweight design it can be seen that deformation already is significant for only the dead weight of the bridge itself. This was also obtained in the numerical simulations, where the bridge deformed heavily under loading conditions for one pedestrian, for example.

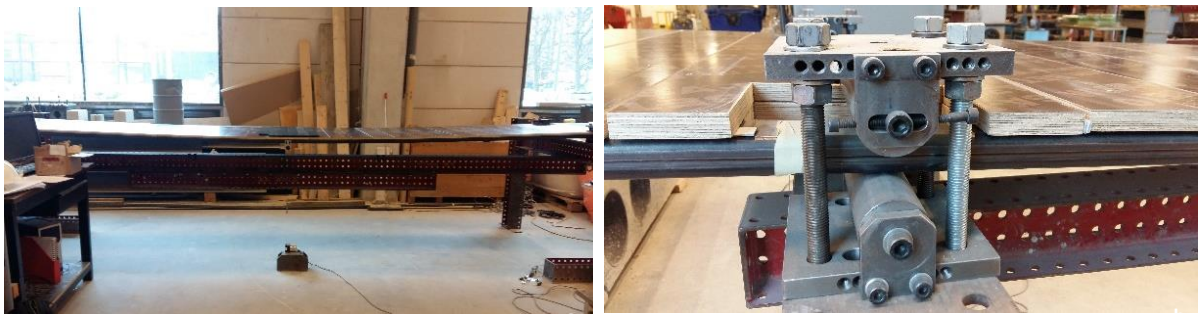

Figure 6.1: Experimental test setup (a) and support detail (b)

Similar to the numerical approach, measurements on the experimental model were started by evaluating the bridge deck only. To do so, two measurement devices have been used, which can measure deformation in time at a speed of one kilohertz. Exactly at mid-span, the deformation of the bridge was measured at the left and right steel tube of the bridge deck. In this way, the averaged center deformation can be compared to the results that were found in numerical analysis and the main principles in using damping or a control system can be compared and verified. Before starting measurements, these devices were calibrated (Figure 6.2, annex C).

As this bridge deck is very limited in strength properties regarding its cross section, only a small external load equal to twenty kilograms was applied exactly at mid-span and exactly in between the two steel tubes. It should be noted here, that for all other experimental tests the cable truss is added to the bridge and that much more load can be applied to the structure in these cases. Nevertheless, the start of this experimental research includes the bridge deck only, similar to the starting point in the numerical simulations. A harmonic motion was obtained by measuring the deformation of the bridge in time, which is a direct result of the step load that was applied on top. Only applying a small mass gave rise to a vibration that took more than twenty seconds to die out completely, resulting from the low Rayleigh Damping coefficient for the steel tubes. This motion was compared to the numerical model by applying a step load with equal mass at the center discretized mass. Comparing the dynamic response, it was found that the numerical model provides a fairly good agreement to the experimental setup (Figure 6.3).

Figure 6.2: Calibration of measurement device

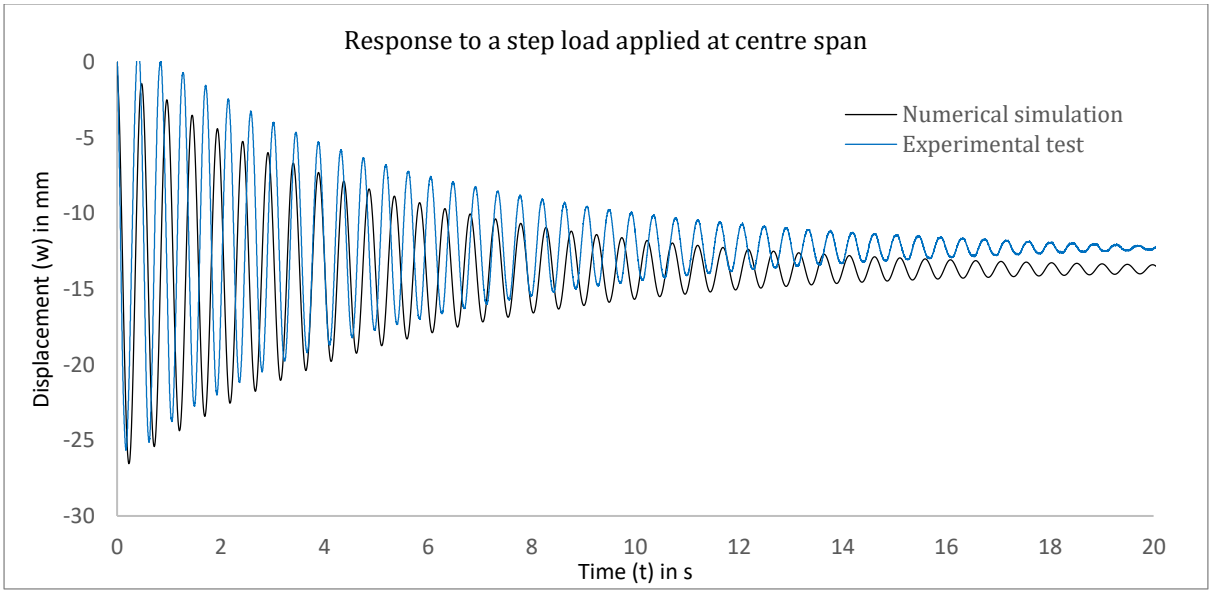

Figure 6.3: Comparison of the experimental model to the numerical simulation for an external load applied at center span

Although the numerical simulation shows a fairly good agreement overall, some remarkable differences are obtained as well. For instance, the steady-state error is larger in the numerical model than in the experimental test. This could be explained by the fact that the bridge is not fully simply supported in practice, as these roller supports can transfer a small moment as well. Furthermore, only the stiffness of the steel beams was taken into account in the numerical analysis, whereas the walking deck is kept in place by wooden spacers, which also provides some additional stiffness to the structure. Regarding dynamics, a small difference in stiffness also accounts for a change in natural frequency, resulting in a slightly smaller or larger period. This also implies a constructive error during time, resulting in large errors at a specific time increment. For instance, the error at 5.95s in the comparison is almost equal to a double amplitude. Although these errors are found when evaluating a comparison locally, it can be concluded that the overall comparison shows a good agreement after all. Eventually general agreement such as die-out time, maximum error and steady-state error are much more important than having an exact agreement at each point in the complete graph.

6.2 The cable truss

The main structure of the pedestrian footbridge comprises both a walking deck and a cable truss, where the latter was already seen in the initial pedestrian footbridge (Figure 3.2). Regarding the numerical results, the cable truss of the initial design was rebuilt using steel wires with a larger diameter (i.e. 10 mm instead of 6 mm). The equivalent stiffness of the cable truss in vertical direction is thus enlarged, so that overdamping of the system will not occur as fast as for the smaller cables. Hence, the effect of viscous damping will become much more visible. Similar to the smaller cables, a tensile test was performed in order to measure the modulus of elasticity. Again, it was assumed that the effect of cable stiffening is to be neglected after five loading cycles and

that a constant stress strain diagram can be used for each loading cycle after the fifth one. It should be noted that the effect of cable stiffening is larger if tensile stress in the cable is larger. If a cable was loaded initially to a certain value for an infinite number of cycles, the effect of cable stiffening is not found at all at each new loading cycle. However, loading this exact same cable to twice that certain value will again lead to cable stiffening in the first few loading cycles. Hence, the modulus of elasticity improves further, even for loads beneath the initial value. After a number of cycles, the stress strain diagram again remains constant. In this case, the pretension from the dead load of the bridge itself was measured and calculated. Furthermore, it was assumed that all measurements are taken with an external load equal to one person. This implies that the total cable force will not exceed $P = 3kN$. Hence, the steel wire was loaded up to this value for five cycles and the resulting stress strain diagram was used for numerical simulations (Figure 6.4). Furthermore, the cable was also loaded in five cycles for different maximum loads (annex D). It can indeed be obtained from these tensile test results that the cable stiffening effect occurs every time the cable loaded up to larger values.

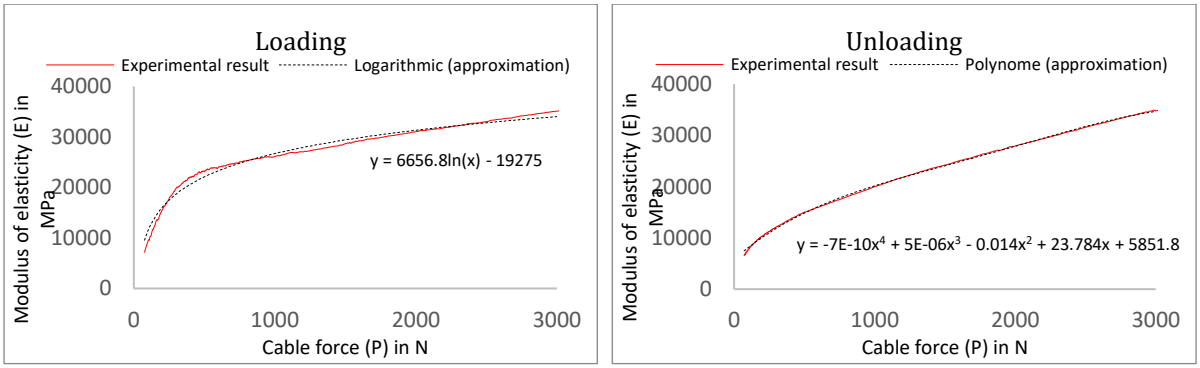

Figure 6.4: Results for loading and unloading for P=3kN (including their approximate functions)

Besides increasing the diameter of the cables, some adaptations were made in the connections too, so that failure is simply not possible in any of these connections (Figure 6.5, Figure 6.6). Furthermore, the pretension in the cables was measured by two additional force gauges, applied at one side of the bridge for each cable truss (Figure 6.7c). The results that were obtained from these force gauges showed good agreement to the hand calculations of the experimental bridge. As already described, the obtained tensile forces in the cables were used for estimating the modulus of elasticity, resulting in an accurate approximation of the stiffness of the cable truss in vertical direction. Using turnbuckles, the pretension in the cables can also be regulated to some extent. Applying zero pretension, an initial deformation of the bridge is found under its own dead load, whereas tightening the cable reduces this initial deformation back to zero (Figure 6.7a, Figure 6.7b). Two actuators are positioned in between the bridge deck and the cable truss, where each actuator is located exactly at half the span of the bridge. Initially, the actuators were inactive in order to measure the deformation (in time) of the bridge where only the cable truss was added. Similar to the numerical simulations, the bridge was evaluated with and without any pretension force in the cable truss. The pretension force that was measured in the experimental model was copied to the numerical simulation in order to compare the practical situation to the numerical analysis.

Figure 6.5: Pedestrian bridge with cable truss ⌀10 steel wires (a) and measurement devices (b)

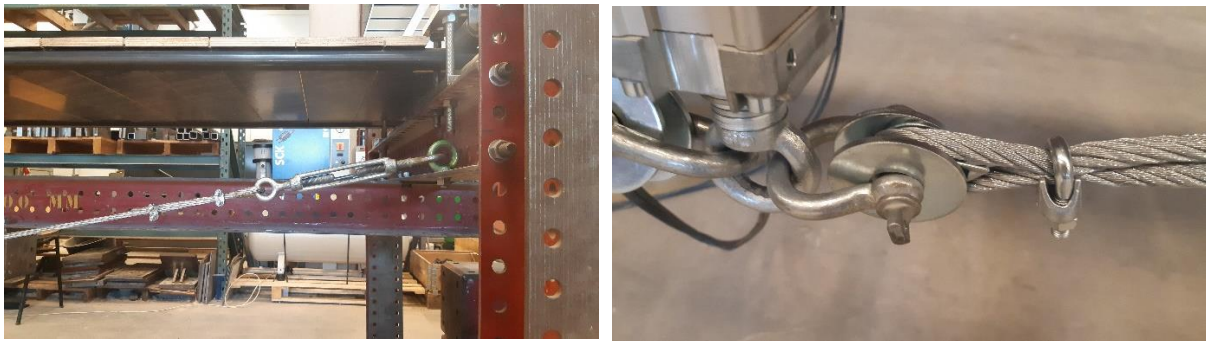

Figure 6.6: Connection details of the cable truss, including turnbuckles to provide user-defined pretension in the cables

Figure 6.7: Bridge without (a) and with pretension in the cables (b) and measuring the cable pretension (c)

A pretension force of $P \approx 1.5kN$ is necessary in each steel wire of the cable truss in order to reduce the deformation of the bridge under its own weight back to zero. This is in accordance with the hand calculations provided in annex B, where it was found that the pretension in the cables must be equal to $P = 1528N$. Furthermore, the additional tensile force in each cable is equal to $P \approx 1.0kN$ for the load from one person, which is also in agreement with calculations by hand. A measurement was taken from one person crossing the bridge halfway (Figure 6.8, Figure 6.9). It can be seen that the cable force is equal to the force of the dead weight only at starting position, whereas the tensile force is equal to the force of the dead weight and the additional pedestrian at the end of the measurement. In between, the additional force of the pedestrian generates more tension in the cable truss, which also implies that the modulus of elasticity improves and that the spring stiffness coefficient in vertical direction enlarges during a certain loading event. It should be noted that the cable force exceeds the force that is calculated in the steady-state error at some points, which is a direct result of (dynamic) impulse loading. Each new impulse load, equal to a new step during walking, is clearly seen in both graphs.

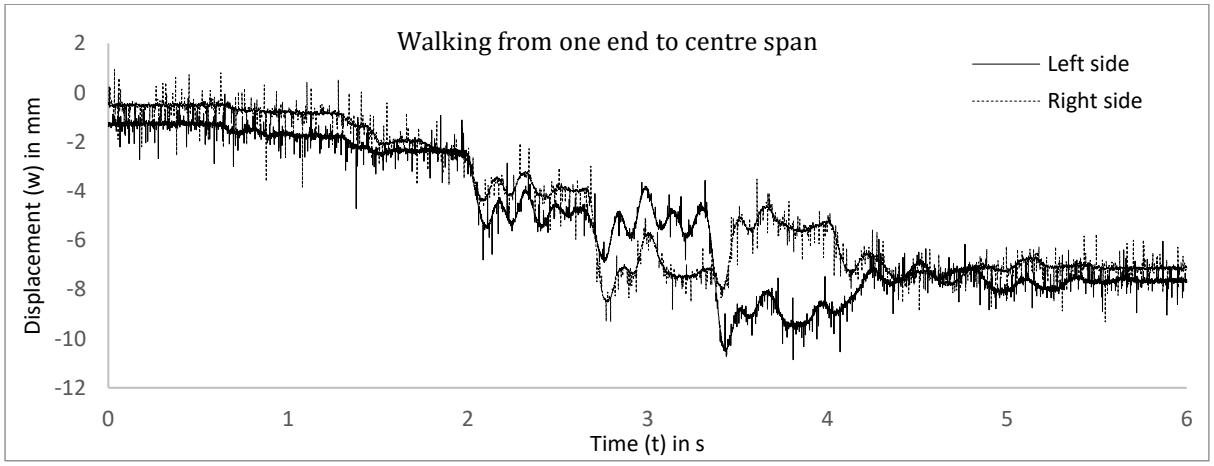

Figure 6.8: Crossing the bridge (deformation in time)

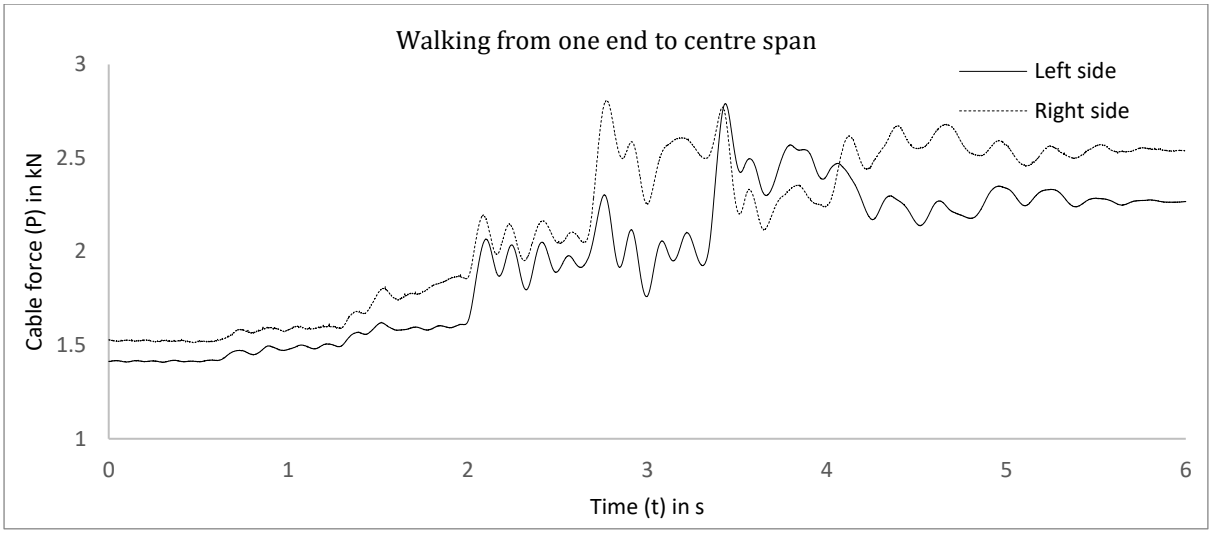

Figure 6.9: Crossing the bridge (cable force as a result of the additional external force)

Many experimental tests are performed by measuring the deformation resulting from one pedestrian. Although each test was visually performed by walking or standing in the middle of the two measurement devices (i.e. exactly in between the left and right steel tube of the bridge deck), is should be noted that small deviations are found when a test is performed multiple times. The difference in left and right measurement device is sometimes different, as external load is not always precisely centered and as a pedestrian is not guaranteed a load that will result in exactly the same graph for two equal tests. Regarding the previous measurement (Figure 6.8, Figure 6.9), it should be noted that an extreme difference in left and right measurement device was obtained here and that it can be stated that this should be taken the upper limit in differences between the two measurement sides. Nevertheless, main differences regarding the principles of using damping or a control system are found in each test that is performed and it should thus be noted, that most of the results in this chapter are compared in this line of thought. Here, the averaged value of the left and right measurement device is then used. Furthermore, a controlled test is performed as a final test to compare all models in the final part of this report.

The amount of pretension that was measured in the force gauges is a direct result of the dead weight of the bridge itself. The amount of pretension, however, can be adapted by tightening or loosening the turnbuckles. From an experimental point of view, the vibration of the bridge can thus also be compared for using zero or a large pretension force. The pretension in the cables was initially measured for the bridge being perfectly horizontal and the displacement over time was compared to the bridge where the cable truss was not pretensioned at all. In this case, the cables were tightened just as much to straighten them, so that in fact a small pretension is needed to lift the dead load of the cable truss itself. This pretension force, however, can be neglected. Furthermore, the zero point for this measurement was taken as the deformation of the bridge under its own dead load, without additional loading. It is now seen that tightening the steel cables indeed results in more stiffness of the total bridge, which is a direct result of the enlarged modulus of elasticity. Besides the steady-state error, the maximum error just after impact time has become smaller as well (Figure 6.10). Furthermore, the frequency becomes larger for the bridge with tightened cables. This can theoretically be explained by the larger spring stiffness in vertical direction for the case with pretension in the cables, as the natural frequency increases with the square root of the spring stiffness coefficient, as the mass remains equal. Both the reduction in deformation and the increased frequency ratio can thus already be obtained by adding a relatively small pretension force in the cable truss. It should be noted that both increasing the diameter of the cables and changing the cable truss angle also increases the stiffness of the bridge, which is similar as found in the numerical simulations.

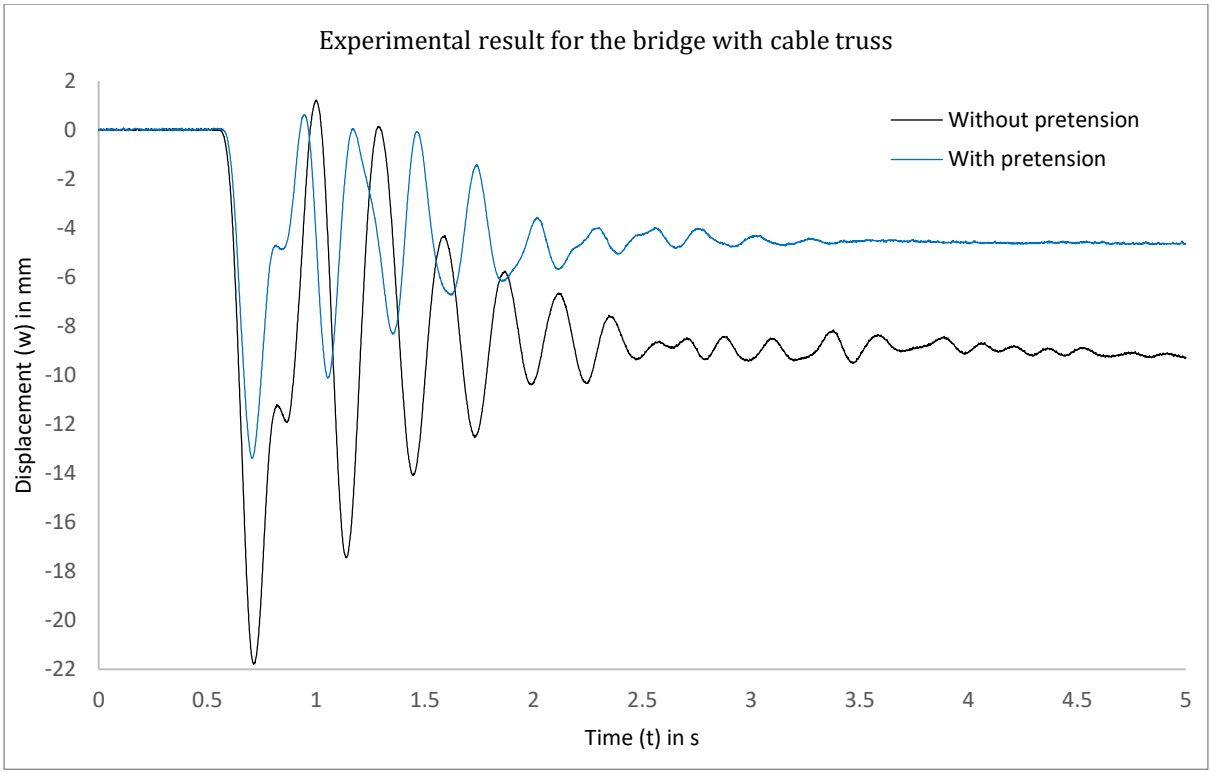

Figure 6.10: Displacement as a function of time for the case without and with pretension in the cables

The initial deformation of the pedestrian bridge under its dead load should always be equal to zero. Besides tightening the cables, this dead load deformation can also be cancelled by activating the actuators. As a result, one may assume that the dead load deformation will always be equal to zero and that the pretension in the cable truss will thus always be equivalent to the value that was found for the pretensioned case. Hence, all further measurements include the pretensioned cable truss, where $P \approx 1.5kN$.

Different load cases were considered, which were taken equal to the numerical simulations. Both running and walking over the bridge were thus considered. Furthermore, walking over the bridge with a stop at center span was considered as well. Measuring the displacement over time, it can be seen that for walking the frequency is indeed around two hertz, which was assumed in the numerical simulations as well. Each impulse is clearly seen in the response graph, and the deformation resulting from this response increases as the pedestrian is half way (Figure 6.11). In the case of running, the impulses are shorter and faster, resulting in a frequency that is approximately half the frequency of walking. Furthermore, it is seen that each impulse is more powerful in the case of running. This results in a larger maximum deflection of the bridge (Figure 6.12). Again, the first and fourth impulse have less influence on the deformation at center span than the second and third impulse, as these are located more close to the center. Finally, walking over the bridge was combined with a stop at mid-span. Clearly, this results in a constant steady-state error, as there is no actuator active to reduce this error back to zero (Figure 6.13). The response before and after the stop at center span is approximately equal to the load case where the pedestrian simply walks over the bridge without stopping in between. It should be noted in these averaged measurements, that a person could walk slowly and gentle over the bridge, whereas walking faster (and creating impulses that are more powerful) would result in a graph that will approach the case of running. Therefore, all load cases are taken into account when different experimental models are compared. In this way, the differences in using damping or a control system can be compared for all these load cases and it can be seen of these improvements actually result in better performance for all load cases and to what extent these improvements are better in specific loading configurations.

Figure 6.11: Walking over the bridge: experimental measurement at center span, averaged value

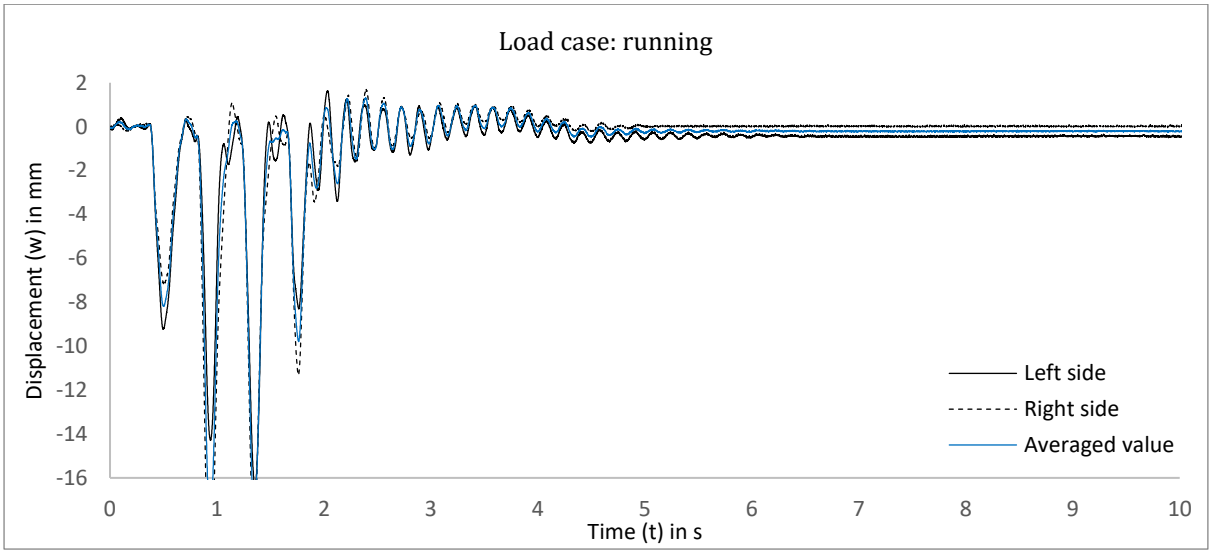

Figure 6.12: Running over the bridge: experimental measurement at center span, averaged value

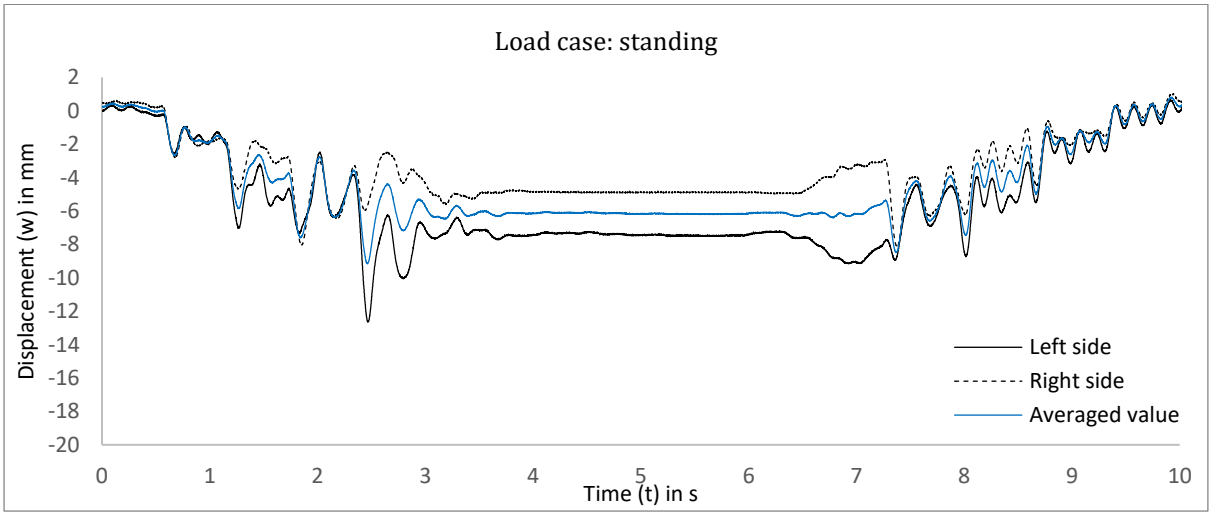

Figure 6.13: Walking over the bridge with a stop at mid-span: experimental measurement at center span, averaged value

Several load cases like walking and running show an overall agreement to the numerical analysis. For instance, the theoretical walking frequency for both running and walking is in agreement with the experimental results. Moreover, a comparison to the numerical and experimental result is shown in one graph (Figure 6.14). Here, it can be seen that the comparison is not as good as for the bridge without cable truss. The total amount of damping of the system seems to be underestimated in the numerical model, as the experimental test shows a more heavily, but still underdamped response to each impulse load. Values for damping of the total system seem thus be larger than theoretical values found in various literature studies for separate structural parts such as the steel wires (Feyrer, 2015). This may be explained by the fact that not all other forms of damping in this structure are taken into account, especially damping through the structure to the ground. Secondly, it can be shown that the maximum deformation from an impulse load is larger in practice than was found in the numerical study. This value is also influenced by the intensity of a footstep in this case, which may vary from one person to another. A certain variation was not modelled in the numerical simulations. Regarding the numerical analysis, it is seen that positive values are found in the displacement analysis. In experimental tests, is appeared that values above zero were measured very rarely. This difference may be explained by the fact that impulse loads were simulated with a time duration shorter than the actual time needed to take one step. This implies that there is a small time of zero force at all locations in between each new step. This results in a steady-state error being equal to zero in these certain time steps, which will create a small upward shift of the vibration. In practice, it seems that the external load of the pedestrian is present at all time and that there is no such time interval where the bridge is unloaded completely. This leads to a response graph that better resembles a constant step load, however, still showing peak displacements resulting from impulses.

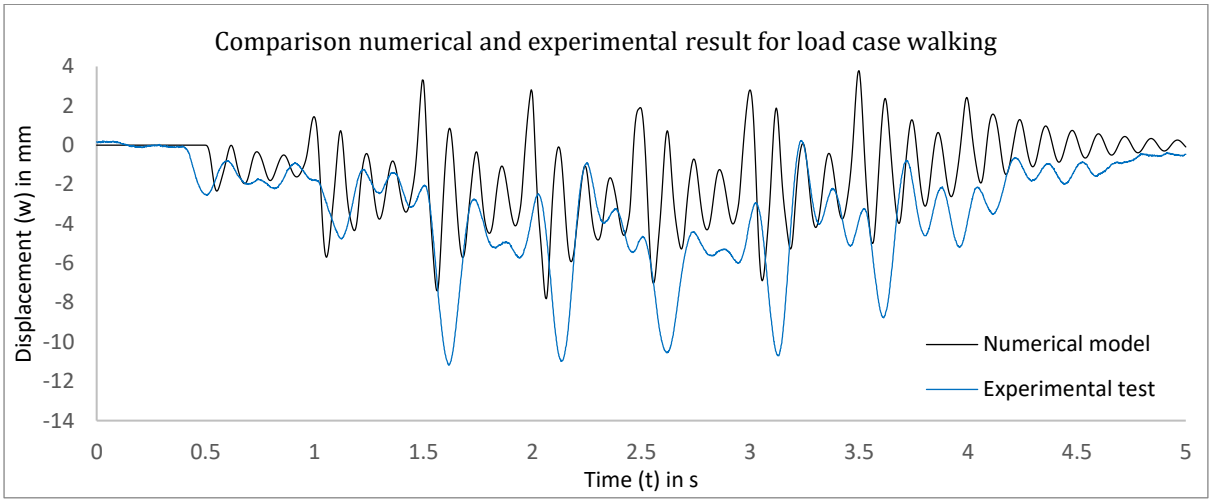

Figure 6.14: Numerical and experimental result for the load case 'walking', with pretensioned cables

6.3 Actuators

The actuators that are used were already seen in the bridge model (Figure 6.5). One actuator is positioned at each side of the bridge, exactly halfway the span of the bridge. Both actuators are based on a small rotational controlled engine, which then induces a linear displacement of the actuator in vertical direction. Each actuator is controlled through a custom-made program in Labview®, which is here called a VI (virtual instrument). Each VI has its own home screen (Figure 6.16), which can be adapted by self-written visual code (Figure 6.15). In this case, an elementary PID control system was modelled to respond on the measured error. The input error is updated real time at a speed of one kilohertz, whereas the program only is executed once in fifty milliseconds. As a result, a prescribed displacement of the actuator is calculated each cycle, resulting in the actuator shifting to that prescribed position. Multiple input parameters such as proportional and integral gain or movement speed can be adapted real-time. It should be noted that one actuator is positioned at each side of the bridge and that each actuator has its own sensor. Hence, measurements relate to the averaged value, whereas each actuator responds on the correct measurement at each side, resulting in a correct actuator force for each side.

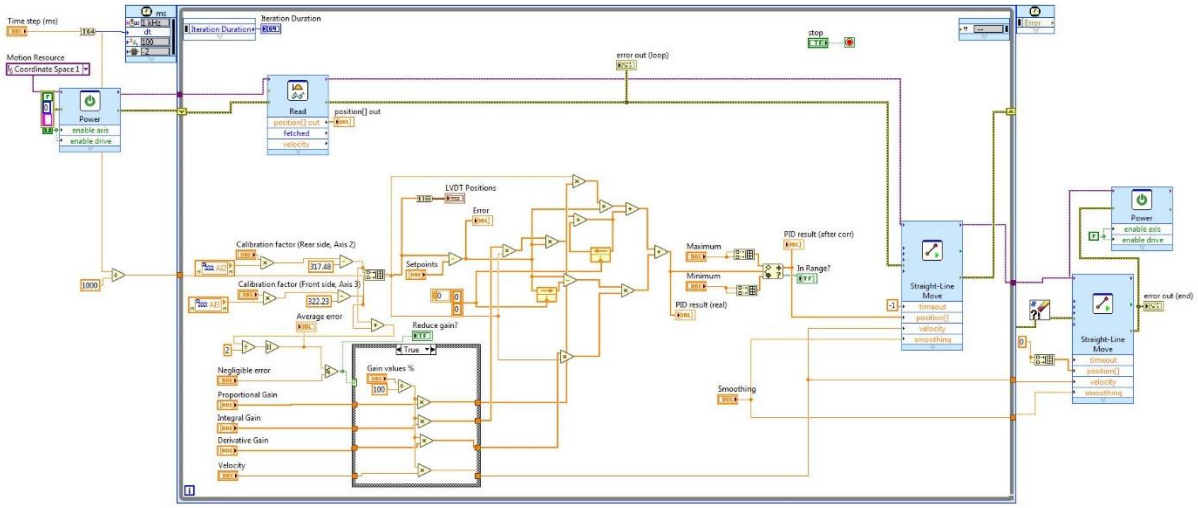

Figure 6.15: Sensor and PID-controller in Labview, visual programming

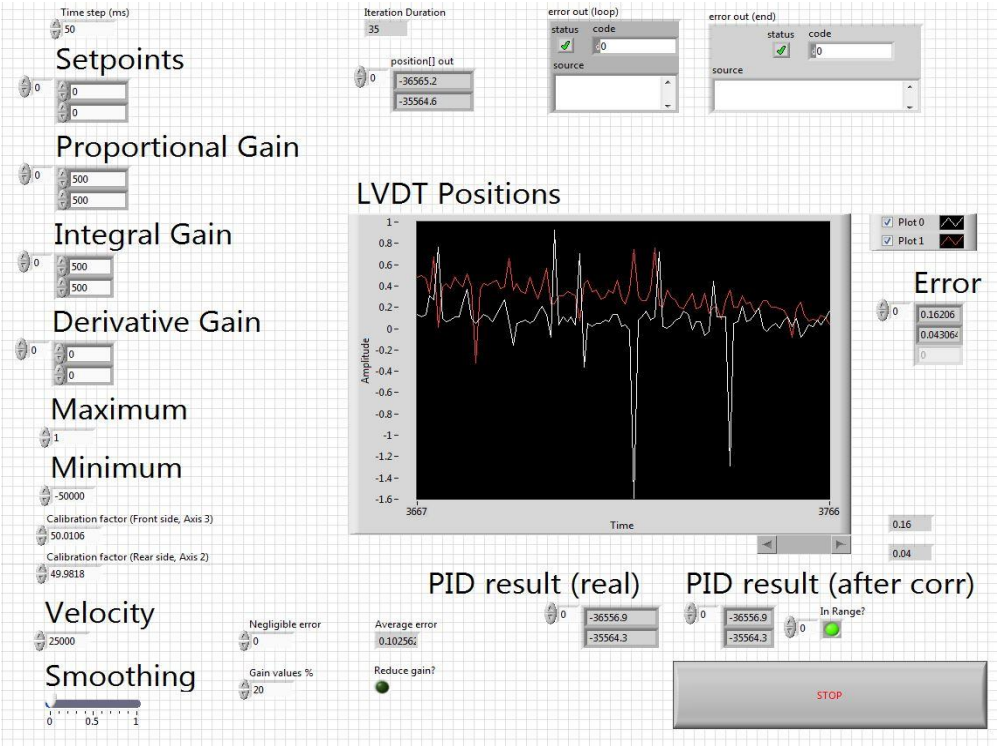

Figure 6.16: Sensor and PID-controller in Labview, running the code

6.3.1 Gain values

Similar to the numerical simulations, a number of parameters determines the behavior of the actuator. For the PID-controller, this includes the three typical parameters proportional, integral and derivative gain, where the proportional gain value is simply multiplied by the measured error, which results in an external force to reduce this error. Comparing different values for proportional gain, one could obtain that the steady-state error reduces for larger values for K_P, whereas an overshoot starts to develop as well (Figure 6.17). Hence, better performance is not guaranteed by simply increasing the proportional gain value. This was also found in numerical analysis. It should be noted here, that activating the actuator results in a slightly smaller coefficient for stiffness of the actuator. This can be seen in the figure for the case where the actuator is not activated, where the maximum error is smaller than for the activated actuator (for $K_P = 500$). Of course, increasing the value for proportional gain again starts to reduce the maximum error. Similar conclusions were drawn from numerical analysis as well.

The problem regarding the steady-state error was solved by adding an integral gain term to the actuator in the numerical simulations and this integral gain term was thus included in the experimental model for the actuator as well, where this value leads to a converging error in time. Obviously, increasing the term for integral gain leads to a faster response to the steady-state error (Figure 6.18).

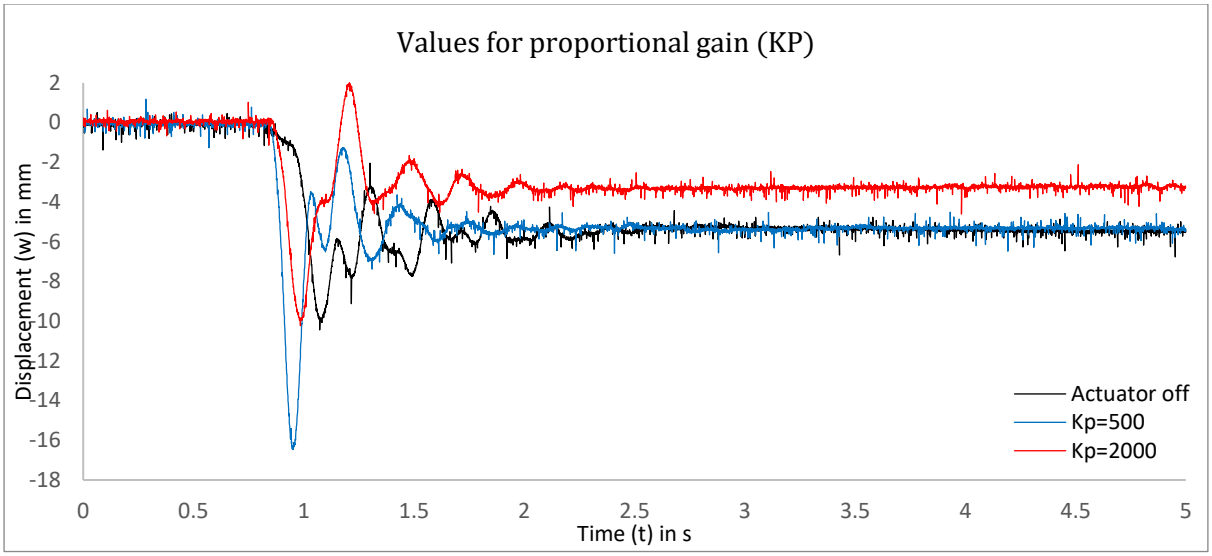

Figure 6.17: Proportional gain values in the PID-controller, experimental results

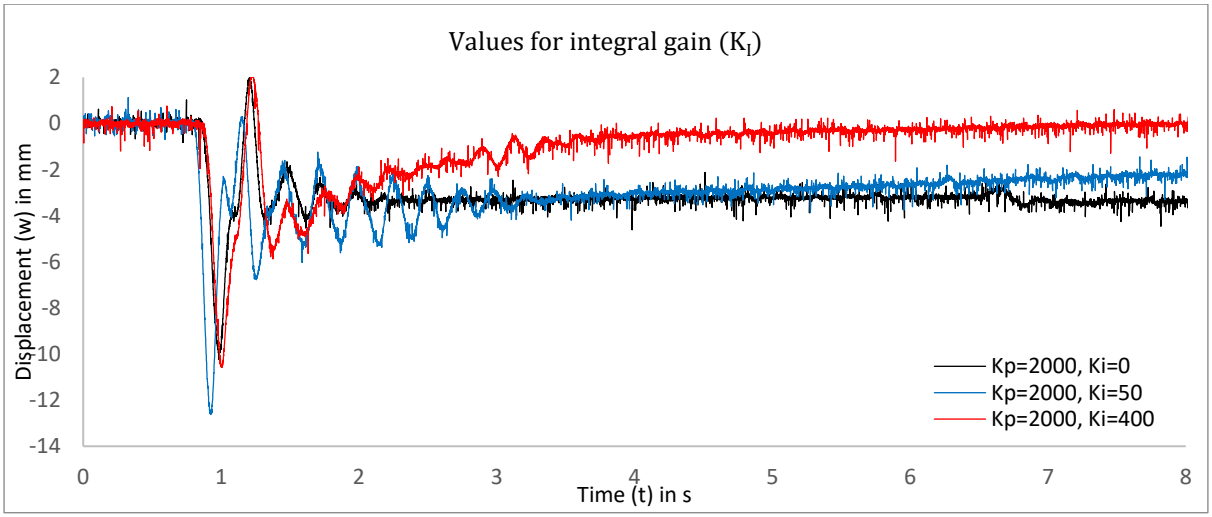

Figure 6.18: Integral gain values in the PID-controller, experimental results

Derivative gain was included in the experimental model by stating that the derivative is equal to the difference in error in between each time step. Hence, the error measured at t_{i-1} was subtracted from the error measured at t_i and then multiplied by the derivative gain value times the time step. Although the derivative gain value was responsible for adding imaginary damping to the actuator in numerical analysis, this phenomenon does not occur at all in the experimental model. Increasing the K_D-value only does have a negligible impact on the total behavior of the actuator. In other words, the PID controller acts more like a PI controller in practice. This is shown by comparing the control system with and without derivative gain, in the case that the actuator goes from its initial position to the given set point (Figure 6.19). This phenomenon also has led to the main problem regarding the actuators: vibration control seems to be very difficult with this elementary control system. Both in numerical analysis and in experimental research it is thus seen that vibrations remain problematic, where it should be noted that a more sophisticated control system might lead to a better response to vibrations.

Besides gain values, the velocity response of the actuator can be adapted. This variable is part of the actuator software and here, the response speed of the actuator is then calculated by using a control algorithm within the software of the actuator itself. Increasing the response velocity of the actuator leads to a faster response, however, it is seen that instable behavior starts to develop if this value is chosen too large, similar to the integral and proportional gain values (Figure 6.20).

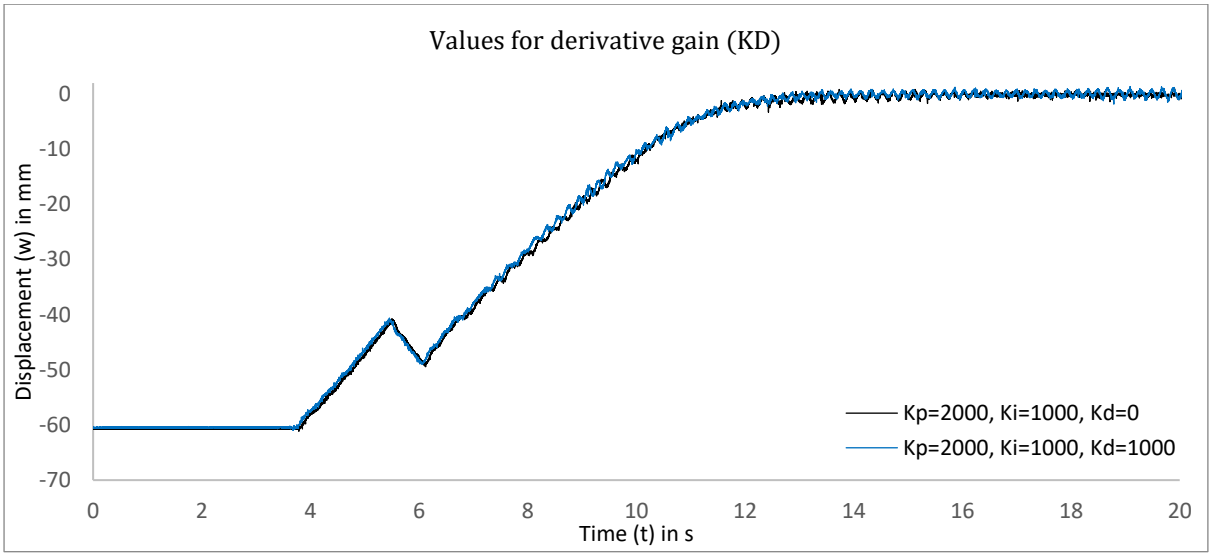

Figure 6.19: Derivative gain values in the PID-controller, experimental results

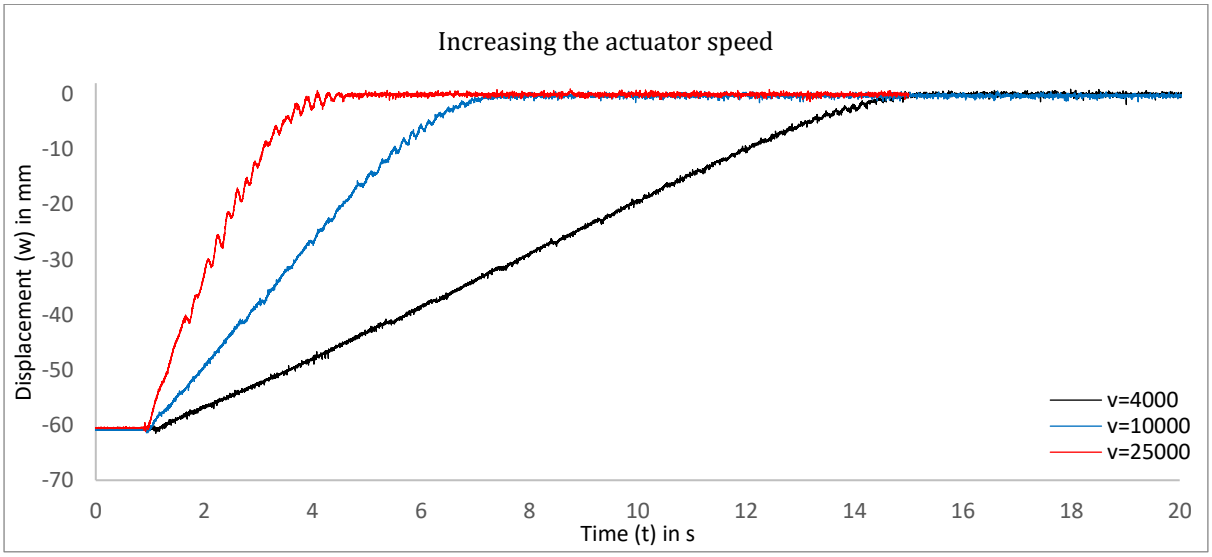

Figure 6.20: Velocity values in the PID-controller (K_P=2000, K_I=1000, K_D=0), experimental results

6.3.2 Instable behavior

In multiple numerical analysis, instable response of the actuator was found for certain gain values. This phenomenon was seen in the experimental model as well. Theoretically, the initial error is always exactly equal to zero, which means that all displacements in the mass spring model will be equal to zero at all time, regardless the chosen gain values. In practice, however, the measured error is never equal to exactly zero, as there is always some kind of noise present. As a result, large gain values will lead to unstable behavior even if the bridge is in its initial position (i.e. no external force is present). This unstable behavior can lead to an ever-increasing error because of the actuator responding to its own generated error (Figure 6.21).

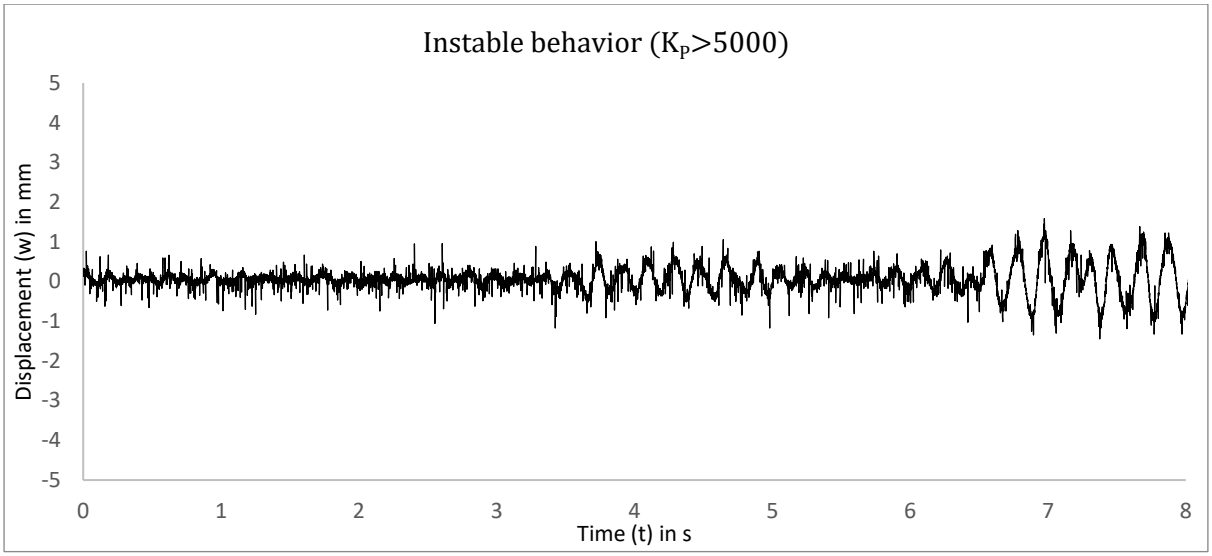

Figure 6.21: Instable behavior of the actuator for large values for K_P and/or K_I

Sudden unstable behavior is undesirable in the case where no external load is present at all. Thus, large gain values may not be used when the measured error only consists out of noise, even if large gain values are necessary to respond fast to external loading. Therefore, an additional case structure was added to the VI, where it was said that gain values are considerably reduced by a certain factor if the error is smaller than a certain value that is found from noise in the measurement, in most cases equal to one millimeter (Figure 6.22). The actuator now only responds much less aggressive to small errors, which implies that the self-exited vibrations without any external load are no longer observed. This does not mean, however, that instable behavior is excluded in case of external loads from a pedestrian for large gain values. In the programmed PID controller, the problem of instability remains if the actuator is prompted for a quick response, as deformations are much larger than a few millimeters. Again, it should be noted that this PID controller is relatively simple and that a more sophisticated algorithm for a control system would probably result in a better response, so that instability might play a smaller role. However, the main research question includes the improvement of vibration control by means of viscous damping, where the elementary PI-system remains and is supported by the viscous damper mainly for vibration control.

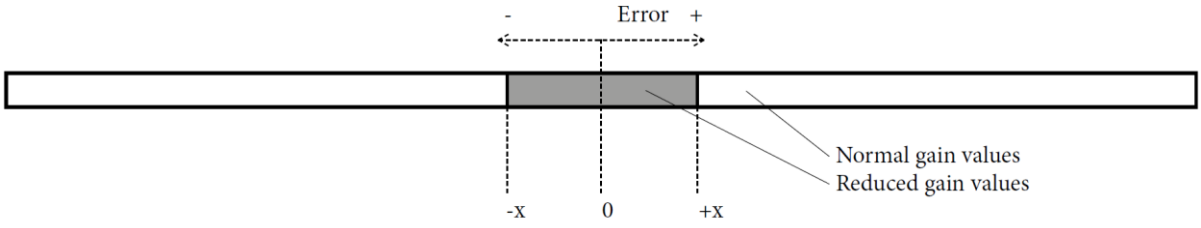

Figure 6.22: Limiting the response to a minimum error

6.3.3 Response to load cases

Due to practical reasons, the pretension in the cable truss (and the force gauges) is released at all time, except for moments when measurement are taken. This implies that the bridge is deformed heavily in its initial position. The actuator starts to decrease this deformed situation when starting a measurement, according to the given gain values. For most measurements, the reference position (i.e. zero error) was taken equal to the height of the two support positions, creating a perfectly straight bridge deck. This reference position, which is also indicated as the set point, can also be adapted to different values, creating a more curved bridge deck (Figure 6.23). Here, a higher set point leads to more pretension in the cable truss, which in turn leads to a larger stiffness coefficient of the truss itself. This can be compared to the measurements that were taken in the bridge with

cable truss only, where tightening the cable truss led to similar cases for the pedestrian bridge design. Using the actuator, however, provides a much faster adaptation of the pretension in the cables. Increasing the set point, it can be seen that the cable truss is much stiffer compared to the bridge deck itself, as the downward deformation of the cable truss is much smaller than the upward deformation of the bridge deck. More stiffness leads then again to less deformation and a larger frequency, which is favorable in terms of comfort criteria. Hence, it may be concluded that besides choosing actuator parameters, there are more adaptable variables in the bridge itself that may have a positive influence in the response to external loading. Nevertheless, a set point equal to zero was maintained for all measurements regarding the typical loading configurations like walking or running over the bridge.

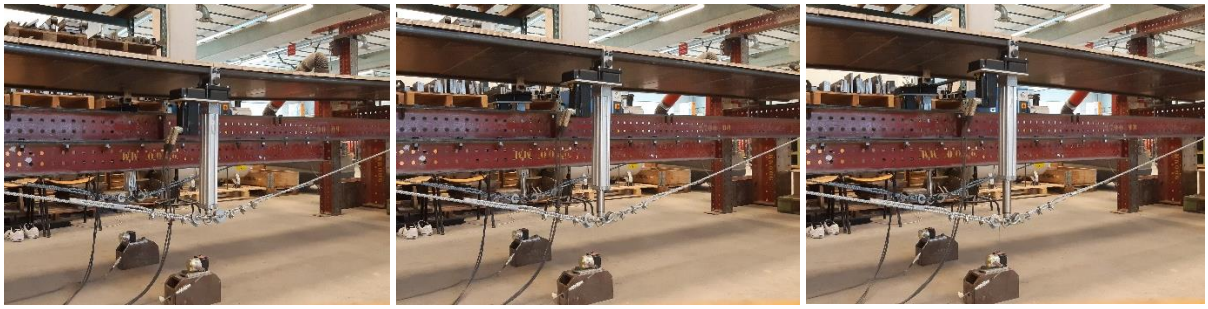

Figure 6.23: Changing the set point in the Labview script to generate different values for stiffness of the cable truss.

The different load cases that are described already in the numerical analysis are also tested for the experimental part in the case of an activated actuator. Clearly, the influence of the actuator is visible for all different load cases. It is seen for all cases that deformation is reduced, especially in the case of standing (Figure 6.24, Figure 6.25 and Figure 6.26). The more the gain values are increased, the smaller the deformation is for all cases. Furthermore, the 'integral windup' is seen for all cases, which means that the deformation of the bridge becomes positive over time, due to the integral term in the PID-controller. Initially, deformation is reduced to approximately zero for the case of walking over the bridge, with and without an intermediate stop. When the pedestrian crosses halfway, the deformation seems to become slightly larger than zero, resulting in a contrary deformation with respect to external loading. This creates the unreal feeling that a support has been added halfway through the span, although it is known that this is not the case. Differences in gain values do not stand out that much here, as the difference in for instance two or five millimeters deflection (resulting from each impulse) is not noticeable for a pedestrian at all. It is mainly the reaction speed of the actuator, which ensures that the deformation remains so small that it is thought that an extra support point is present.

Besides the positive effect on deflection control, it should be noted that vibration control is not reached at all. Moreover, vibrations are sometimes even heavier and need more time to die out. In contrast to a maximum deflection of a few millimeters, a vibration of a few millimeters is clearly noticeable when crossing the bridge. Hence, this vibration causes a rather uncomfortable feeling and is therefore not desired. As a result, one may conclude that the actuator performs fairly well on deflection control. Even so well, that it seems like an extra support point has been added halfway through the span. However, vibrations are not damped out at all and the derivative gain value in the PID control system does have negligible influence on the total behavior of the actuator. Hence, one may conclude that the actuator in fact can be described as a PI-controller rather than a PID-controller.

Figure 6.24: Walking over the bridge: experimental measurement at center span

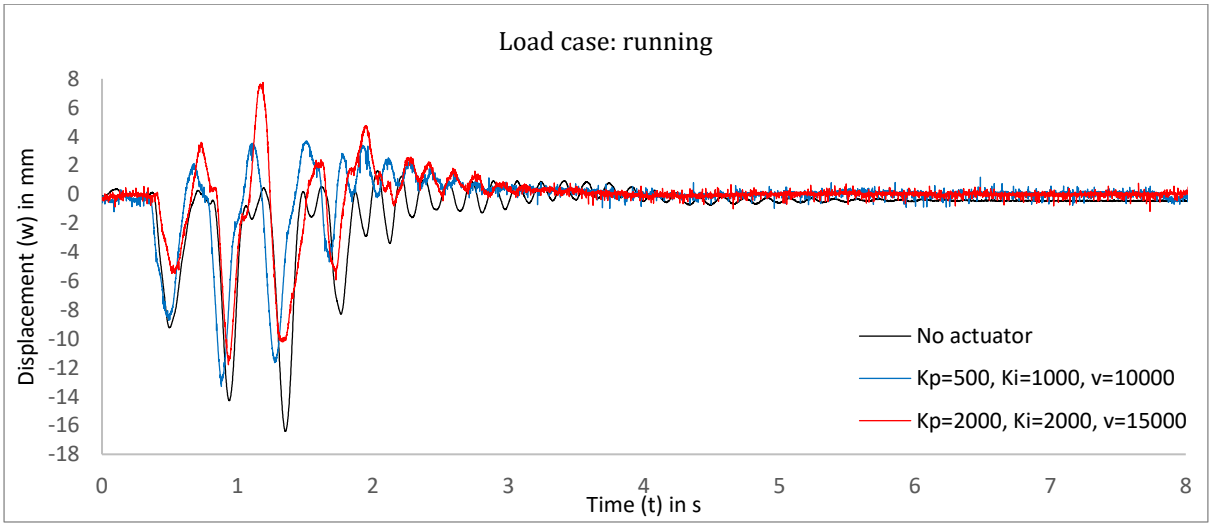

Figure 6.25: Running over the bridge: experimental measurement at center span

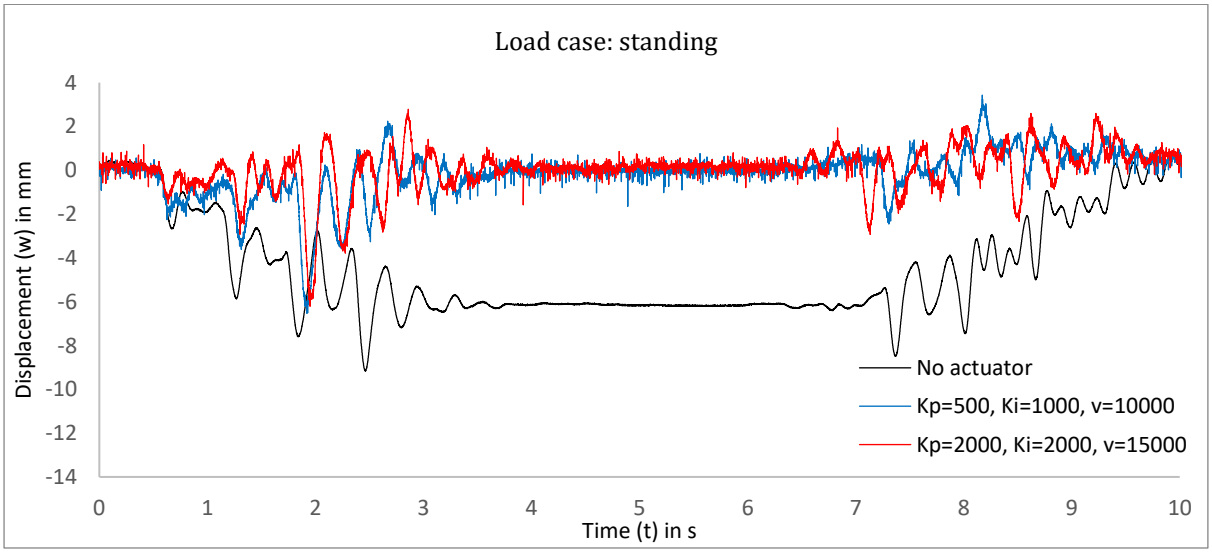

Figure 6.26: Walking over the bridge with a stop at mid-span: experimental measurement at center span

6.4 Viscous damping

It was seen that using actuators results in a fairly good response to external loading, with regard to deformation control. Noticeable vibrations are not damped decently, though. Moreover, vibrations are even amplified if large gain values are used. Instead of using actuators, viscous damping is now applied in the footbridge in the fourth case of the experimental part. Two viscous dampers were ordered at the company 'Intrax Suspension Technology', located in Volkel in The Netherlands. Properties for the dampers were obtained from numerical simulations. An adjustable damping coefficient is included in the viscous damper, where the coefficient can be adjusted from approximately $c \approx 600$ to $1400\ Ns/m$ for each damper. To that extent, the total amount of damping is equal to minimal 1200 and maximal $2800\ Ns/m$. Numerical simulations showed that best performance was obtained when a damping coefficient in between this range was used. Besides the damping coefficient, an additional spring was supplied, which turns the viscous damper into a shock-absorber. The additional springs in the shock absorbers are essential for long-term external loading like for instance dead weight of the structure itself or variable load remaining at one position for a certain time. On the other hand, too many stiffness would lead to a very stiff structural element, allowing very little deflection, which in turn makes the viscous damper very inefficient. Theoretically, the additional spring should thus be as 'weak' as possible, allowing for large deformations, leading to much influence of the damper. However, a certain limit should be taken, limiting the steady-state deformation to a certain value (in this case $k = 20\ N/mm$). The spring now will limit the maximal deformation within proper boundaries, while a noticeable difference is obtained when using the dampers in the experimental setup. The maximum deformation of the bridge resulting from impulse loading is here larger than the steady-state deformation and furthermore, the dampers are compressed a few millimeters already from the dead weight of the bridge deck. Hence, the total stroke of the dampers was taken equal to $l = 100\ mm$, so that the maximum total deformation would never exceed this value. This resulted in two shock absorbers with given properties, using symmetrical damping (i.e. similar damping in the bound and rebound direction) (Figure 6.27). It should be noted that the additional spring is easily removed from the damper, so that one can easily change from a viscous damper to a shock absorber. However, shock absorbers were used for all test cases here. The exact calibration of both dampers is given in annex F, where the damping speed is given for the external applied impulse load.

Both dampers were applied in the experimental model of the bridge, similar to the case with actuators. The total length of the dampers is a little shorter than the total length of the actuators and furthermore, the upper and lower bolt holes are different from the actuators. Two additional provisions were made in order to create a decent connection from the bridge deck to the steel cable truss (Figure 6.29). At the top, an additional aluminum block was added, connecting the primary aluminum provision on the steel tube to the viscous damper. The height of this provision was taken equal to the resulting difference in damper and actuator length. Hereby, the total length from steel tube to cable truss is approximately similar, resulting in a similar angle between the horizontal and the cable truss. This also implies a comparable spring stiffness coefficient for the cable truss in vertical direction for all models including the bridge with cable truss, with and without damper or actuator. Hence, all parameters regarding the bridge model are equal and a reliable comparison can be made for the case with damper, actuator or none.

Two aluminum plates were applied at each side of the bridge, connecting the dampers to the cable truss. The aluminum plates are bolted connected to the dampers and to the cable truss. Furthermore, the two bottom connections are strengthened in horizontal direction (out of plane) by means of a timber element placed on top of the aluminum plates. As a result, instability in the out of plane direction is reduced and sudden failure during testing is prevented. This out of plane instability was not found in the case for the actuators, as the top connection was wider and more close to the steel tubes. Finally, the experimental setup of the bridge now contains the two dampers with their additional provisions (Figure 6.28).

Figure 6.27: Viscous damper (a), spring (b), shock absorber (c) and application in bridge (d)

Figure 6.28: Dampers applied in the experimental model of the footbridge

Figure 6.29: Application of dampers in the bridge model: top detail (a) and bottom detail (b)

6.4.1 Adjustable damping coefficient

The additional spring in the viscous damper was determined by stating that the steady-state deformation should remain within proper limits, whereas as much deflection as possible should be allowed in order to achieve the best possible results from the viscous damper. Hence, the stiffness of the shock absorbers is a fixed value, where it should be noted that the spring is easily replaced by another spring with different properties if necessary. The damping coefficient, however, is a variable value that can be adapted to different values. From numerical simulations, it was assumed that the minimum value should be around the point where the bridge starts to vibrate into its first natural frequency and that the cable truss does not deform at all. This phenomenon can be seen in the experimental test as well (Figure 6.30). The deformation of the bridge in time was measured for an external load (being equal to the load of one person) applied at center span. For the case of moderate damping (i.e. $c \approx 2000\ Ns/m$), the first natural frequency of the bridge deck is found, being equal to approximately two sine waves per second. This frequency was also found in the experimental results for the bridge deck only. Nevertheless, it is now seen that the vibration is damped out after obtaining one sine wave. This implies that that the system may be categorized underdamped, being very close to critical damping. Furthermore, it was obtained that the cable truss showed no vibration at all for the case of minimal damping. It may thus be said that the amount of damping is small enough to ensure that the structure does not start to vibrate as a whole. This was seen in several numerical simulations for larger amounts of damping. Besides using moderate damping (i.e. dampers adjusted exactly in between the minimum and maximum value), the dampers can be adapted to their minimal and maximal values, resulting in a larger or smaller damping ratio. For maximal damping, it was obtained that the cable truss started to vibrate to some extent, proving the numerical symptom of the structure starting to vibrate as a whole for too large amounts of damping. Hence, it may be concluded that the damper performs fairly well in the experimental setup with its predetermined range concerning the damping coefficient.

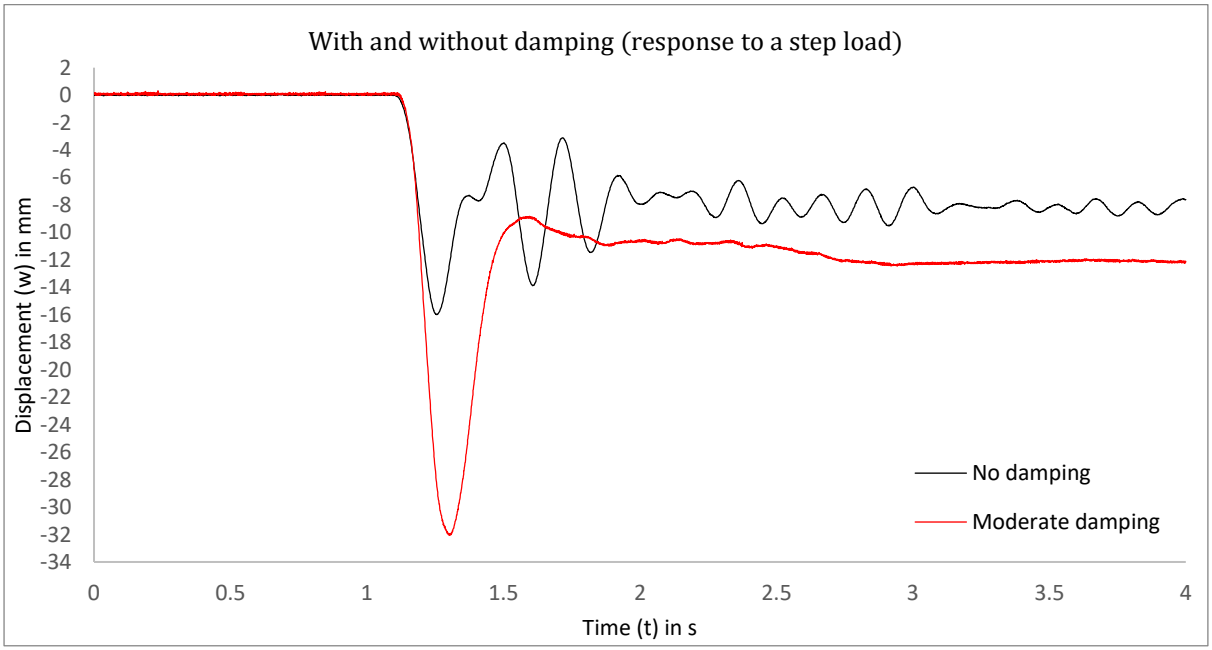

Figure 6.30: Response of the bridge (center span) for different values for the damping coefficient

Although a clear improvement is seen regarding vibration control, it must be noted that an increased deformation remains when using the viscous dampers. Obviously, the additional springs have a negative influence on the stiffness of the bridge model and deformation control is not guaranteed for this particular setup. Although the steady-state deformation remains within the boundary of seventeen millimeters that were given at first, it should be said that this test includes the external load of only one person. Hence, more people crossing the bridge will definitely result in larger deformations, exceeding the limit regarding conventional static design.

6.4.2 Response to load cases

Three different load cases were again considered for the case of viscous damping, where results are compared to the case with a rigid bar, representing the bridge with cable truss without actuator and without damper. For each case, values for damping are taken equal to previously discussed values for minimal, moderate and maximal damping. Clearly, the viscous damper has a large effect on vibration control, as vibrations are damped out for all load cases. For the case of walking it appears that moderate damping performs best. For this particular load case with a frequency of approximately two Hertz, it is seen that the response of the damper is best for a damping coefficient being equal to $c \approx 2000\ Ns/m$. Vibrations are damped out fast, close to critical damping, while the damper is just below the value where the complete bridge starts to vibrate resulting from the system being damped too heavily (Figure 6.31). Vibrations are damped out fairly well, whereas the total deformation is much larger than for the case without damper. Similar results are obtained for the case of standing, where the overall displacement is found to be much larger than when using a viscous damper. The steady-state deformation is more than doubled, compared to the case without damping during the three seconds standing at center span (Figure 6.33). It is thus again seen that the dampers do have a negative effect on deformation control, whereas vibrations are controlled fairly well. Nevertheless, the steady-state deformation remains within the given boundaries regarding the span of the bridge.

In contrast to walking, it seems that maximal damping ($c \approx 2800\ Ns/m$) instead of moderate damping performs best when running over the bridge. A larger damping coefficient delays the response to an impulse more, which is favorable in this case. Impulses resulting from running are quite powerful, yet short-term. Here, the time needed for the damper to fully deform is larger than the total duration of each impulse. This implies that for a larger damping coefficient, the maximum error decreases. This phenomenon is clearly seen in experimental results. First, the maximum deformation increases quite a lot, when comparing the case of minimal damping ($c \approx 1200\ Ns/m$) to the case of no damping. Increasing the damping coefficient further, however, results in a decreasing maximum error, which is best seen for the case of maximal damping (Figure 6.32). Accordingly, best performance is found for maximal damping in the case of running and it might be said that a damping coefficient larger than the maximum physical value would lead to even better results. This is, however, only true for the case of running.

Compared to the bridge with actuator, a clear distinction can be made regarding deformation and vibration control. Vibrations are controlled best using a viscous damper (with additional spring stiffness), whereas one must allow for larger deformations. On the other hand, the control system has proven to control deformations very well, whereas uncomfortable vibrations are found for large gain values. This difference in behavior is thus similar to the results regarding numerical simulations.

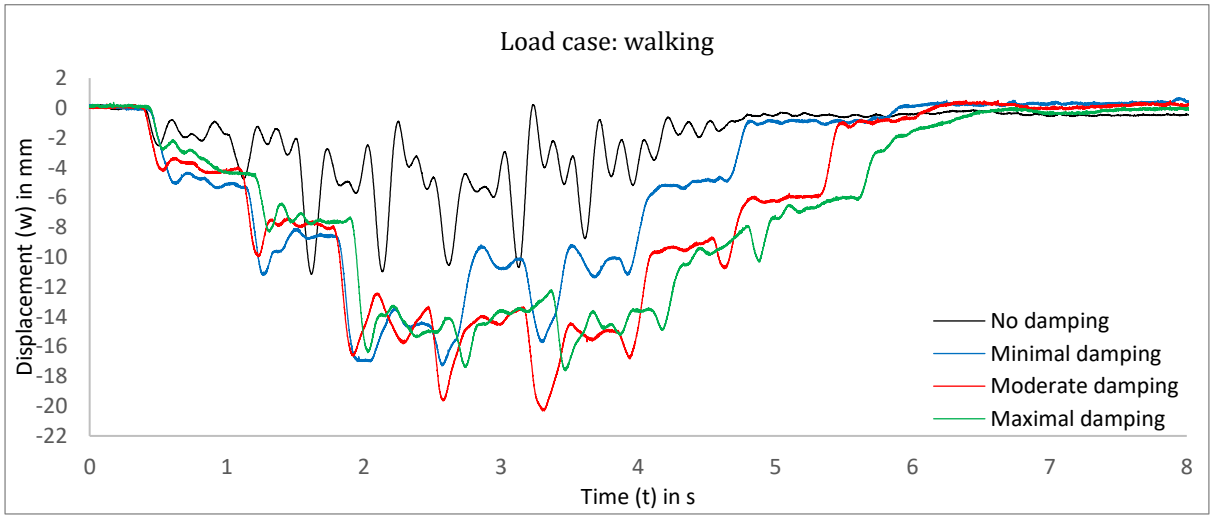

Figure 6.31: Walking over the bridge: experimental measurement at center span

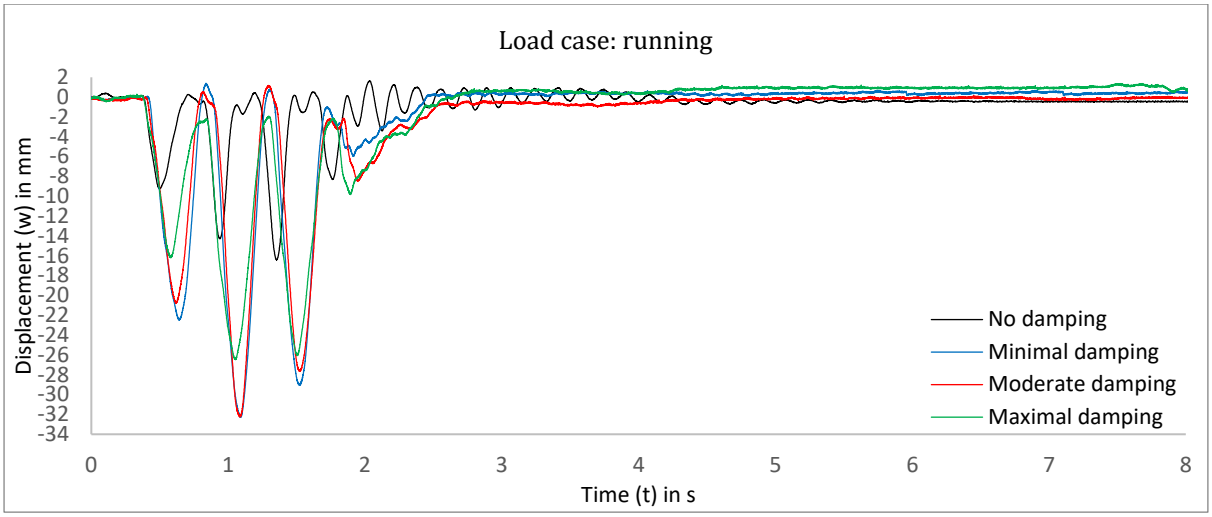

Figure 6.32: Running over the bridge: experimental measurement at center span

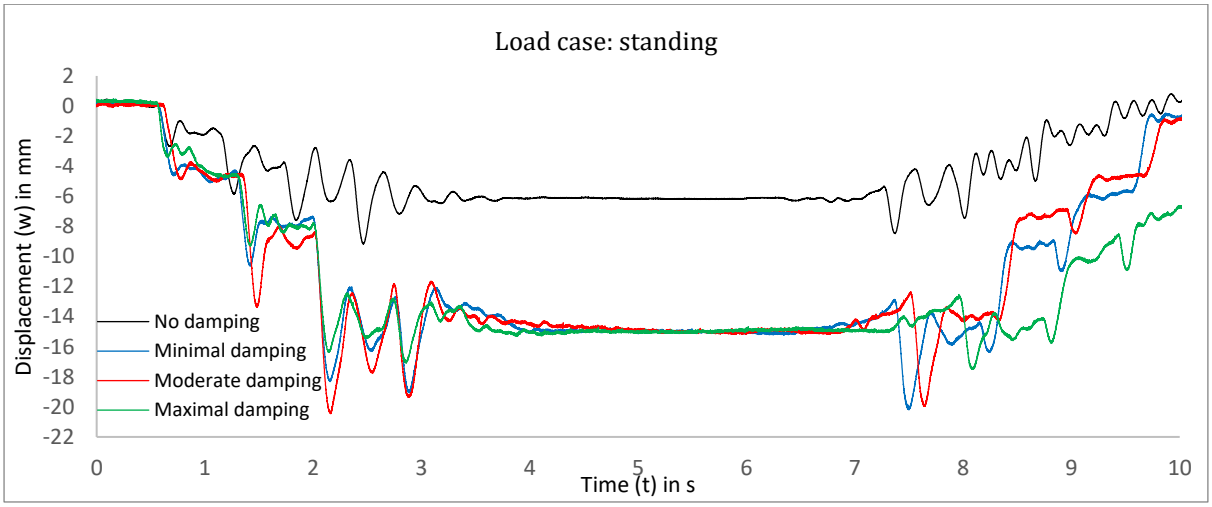

Figure 6.33: Walking over the bridge with a stop at mid-span: experimental measurement at center span

It is seen that the viscous dampers perform quite well in the experimental results, as clearly a reduction in vibrations is obtained from experimental testing. Vibration control is seen in graphs representing displacement versus time and secondly, one can notice the presence of the viscous dampers during a walk over the bridge. The bridge simply cannot possibly be set in vibration, at least, in the first natural frequency and all subsequent odd frequencies of the bridge deck following after the first one. Even jumping on top in the frequency of the bridge does not lead to harmonic motion, as the dampers are slowing down the vibration immediately by dissipating energy. During testing, it was even obtained that the bridge often started to vibrate in its second frequency, while the viscous dampers, located at mid-span, do not have effect on mode shapes that have a dead point halfway the span.

One load case (walking) is shown in a comparison to the initial numerical simulation using the discretized solution in Grasshopper (Figure 6.34). Clearly, the amount of damping seems to agree well. Both in the numerical and experimental result the vibration is damped out after the same amount of time, being approximately half a second. Here, moderate damping (i.e. $c = 2000Ns/m$) is applied in both models. Numerically, the behavior is predicted fairly well, except for some remarkable differences. Firstly, a major movement in upward direction is found in the numerical analysis for each impulse load, whereas in practice this movement is not found at all. Similar to the bridge without damper, this phenomenon is explained by the fact that the total time of one impulse is not equal to the total time that the actual impulse force is applied in the numerical simulations. For each impulse load, it was stated that the total duration of impact is a little smaller and that in between each step

there is a certain time where no force is applied at all. During this time, it is assumed that the pedestrian has no contact with the bridge deck. In practice, it seems that the pedestrian is in contact with the bridge at all time and that this period in between those two impulses is of much less influence, in particular for the case of viscous damping where the dynamic response of the bridge is delayed at all time due to energy dissipation. Furthermore, it must be noted that ideally each impulse duration is equal to half a second in the numerical analysis, whereas in practice these exact moments of impact can differ for each person and even for each unique impulse. Hence, each experimental test gives slightly different results when looking at a specific time interval. Besides the large upward peaks, the experimental results correspond well to the numerical simulations and thus, the principle of viscous damping is found in every result graph. In addition, the viscous dampers are obviously present when walking over the bridge, because the delay time in vibration and the large amount of energy dissipation is noticeable above par.

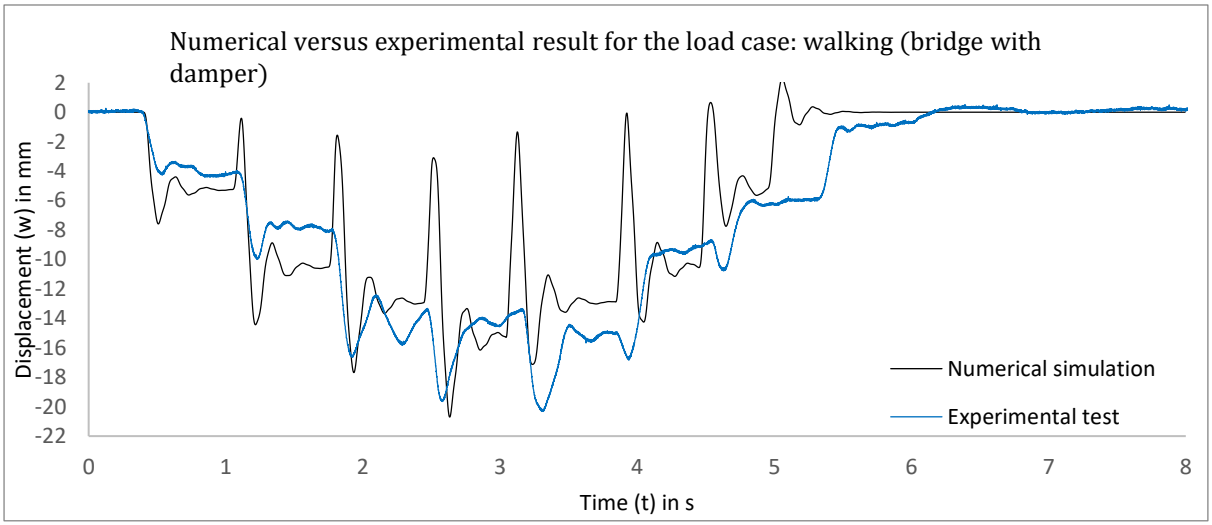

Figure 6.34: Comparison of experimental result with the numerical simulation (k_{damper}=40000 N/mm, c_{damper}=2000 Ns/m)

6.5 Viscous damping in the adaptive footbridge

It has been shown in practical tests that viscous damping can reduce the harmonic motion that was obtained in the bridge where dampers were not applied initially. However, an enlarged deflection was the disadvantageous consequence, especially in the case of staying at mid span for a longer period of time. Where this deflection seems acceptable at first sight, it must be noted that all tests included only one person. In the case of a load consisting of several people, the deflection will increase even further, exceeding the allowable values, especially if the bridge is crossed relatively slowly. It is thus desirable to decrease the deformation that arises over a larger timespan, which is also indicated as the steady-state deformation. Therefore, the last experimental setup comprises the actuator and damper placed in series, where the actuator should be responsible for these long-term deformations.

The total height in between the bridge deck and the cable truss is increased in the final model, as the total height of both the damper and actuator in series is much larger (Figure 6.35). Here, the height of the bridge deck was increased just enough that the angle between the horizontal and the cable truss remains similar to all other tests. To that extent, the stiffness of the cable truss in vertical direction remains similar to all previous tests. An additional aluminum part was provided to connect the actuator and damper rigidly, so that movement is only allowed in vertical direction (Figure 6.36a). As the height of the bridge has increased, stability in out-of-plane direction is not guaranteed as good as for the previous models. Hence, an additional steel support was provided (Figure 6.36b). Two steel plates prevent the actuators from a displacement in out-of-plane direction, whereas vertical movement is allowed as a small gap remains in between each plate and the actuator. In this case, sudden failure due to out-of-plane deflection is prevented. So far, the bridge now comprises the viscous damper and the control system, where the actuators can be regulated using the 'virtual instrument' that was discussed already. Of course, the damping coefficient can also be varied in this model.

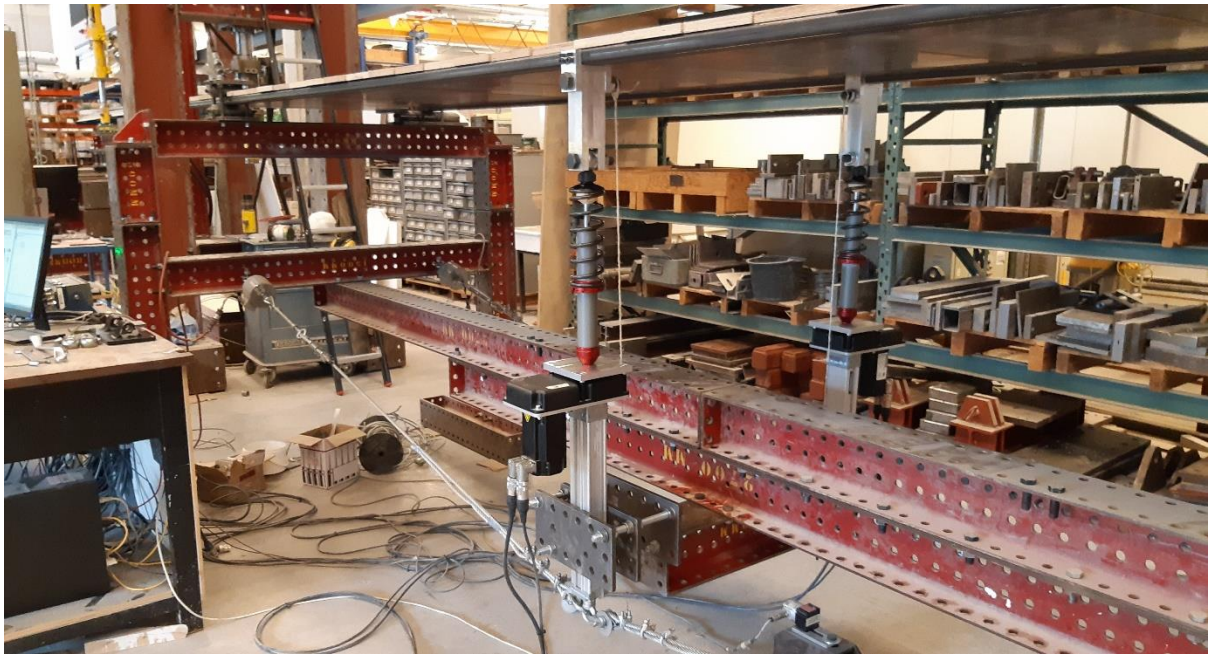

Figure 6.35: Prototype of the footbridge: viscous damper and actuator in series

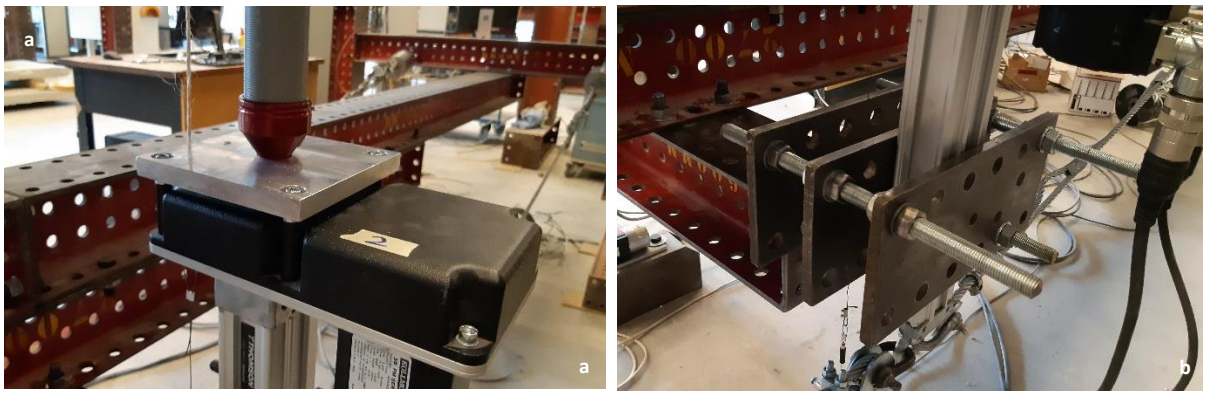

Figure 6.36: Connection between viscous damper and actuator (a) and restraint in out-of-plane direction (b)

6.5.1 Variation of parameters

The final experimental model where damping and active control is combined into one single test setup is tested for several load cases comparable to the previous experimental models. Furthermore, a step load was applied for a wide variation in parameters for both the actuators and the dampers. As all parameters have been described elaborately in the sections regarding solely the actuator or the damper, some important differences are described in the final modal instead of discussing all possible combinations. Accordingly, the model of the damper with actuator is compared to the bridge without damper and without actuator to evaluate improvements. Firstly, it should be noted that the damper obviously reduces vibration issues in the footbridge, as in all cases a continuous harmonic vibrations are hardly noticed. Clearly, the difference is seen in using the minimal and maximal amount of damping (Figure 6.37). Applying more damping, it is seen that the energy dissipation in the viscous damper results in a delayed response, which gives the actuator more time to start responding on the measured error. Accordingly, the maximum deformation is reduced in the case of maximal damping.

Besides an evident improvement in vibration control, one can conclude that the actuator improves control of deformation. Here, it is important to note that gain values should be chosen carefully. Large amounts of proportional or integral gain result in a relatively fast response of the actuator, whereas in practice, this is undesirable. A response of the actuator should be based on the steady-state error rather than the error during

vibration. Hence, a small amount of time is needed for the damper to die-out vibrations in the structure in order to ensure that the actuator does not respond on any vibrations in the structure at all. Increasing gain values can thus lead to additional vibrations from the actuator response. This phenomenon was clearly noticed during experimental testing (Figure 6.38). As a result, one may conclude that it is desirable to choose a decent value for integral gain, as this value is mainly responsible for the error on longer duration, whereas a low value does not directly result in a vibration-sensitive reaction. Hence, proportional gain in the actuator should also remain small, as this factor does not respond in the steady-state error at all. To conclude, the combined model provides a fairly good agreement between vibration and deformation control, where overall results agree with numerical simulations and most importantly, the expected results of this model are indeed obtained. As a proof of concept, it is seen that uncomfortable consequences from a lightweight structure can be (partially) improved using additional systems like dampers and actuators for vibration and deformation control.

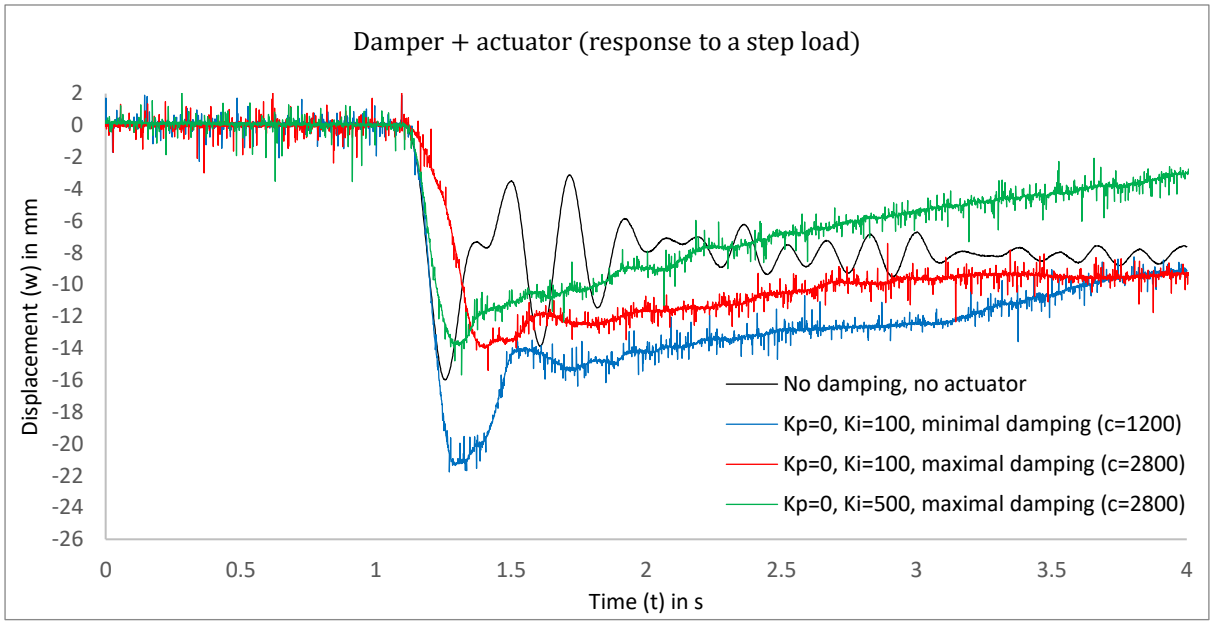

Figure 6.37: Variation in damping coefficient and integral gain value: experimental measurement at center span

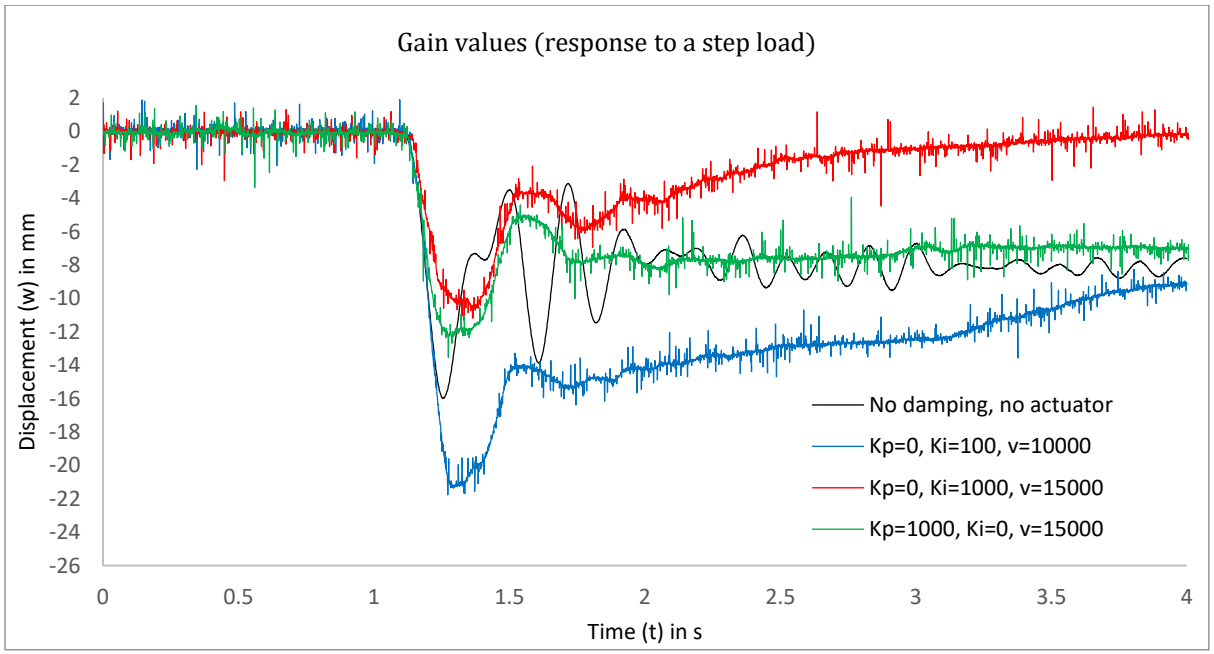

Figure 6.38: Variation in gain values for minimal viscous damping: experimental measurement at center span

6.5.2 Response to load cases

Is has been shown in different models that the integral gain value from the actuator is most responsible for reducing the steady-state error of the adaptive footbridge. As derivative gain did not result in a noticeable difference, this value has not been evaluated in the final model. Furthermore, the proportional gain value has proven its negative side effect to vibration control, as a fast response of the actuator during the vibration time is not desirable. Hence, only the integral was included in the response graphs to different load cases, where it appeared that this value could be optimized to a certain value (Figure 6.39, Figure 6.40). Furthermore, it was already shown that the viscous dampers performed best when moderate damping was set for the case of walking, whereas the maximum amount of damping was needed for the case of running. Using these optimized values, each load case is evaluated for the bridge with the damper and actuator in series. Obviously, the maximum deflection that is obtained remains within the given boundaries that were given as a starting point (i.e. $w_{max} < 25mm$ & $w_{steady-state} < 17mm$). This is now true for all different load cases, whereas vibrations are hardly noticed. Hence, the improvement in both deflection and vibration control is also seen for different load cases as given below.

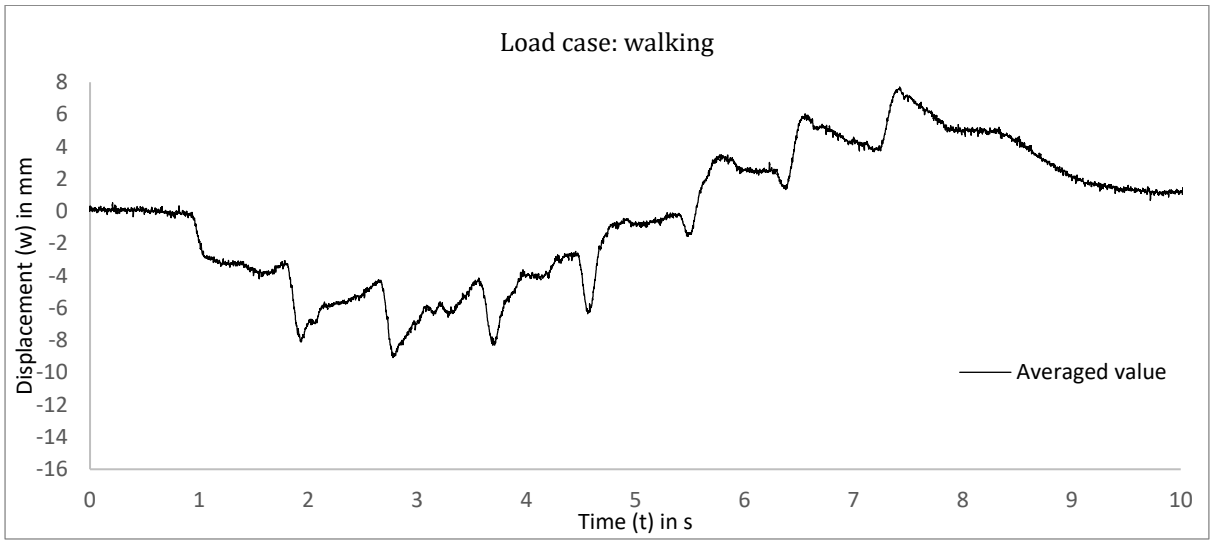

Figure 6.39: Walking over the bridge: experimental measurement at center span, averaged value (K_P=0, K_I=1000, v=10000, moderate damping c_d=2000)

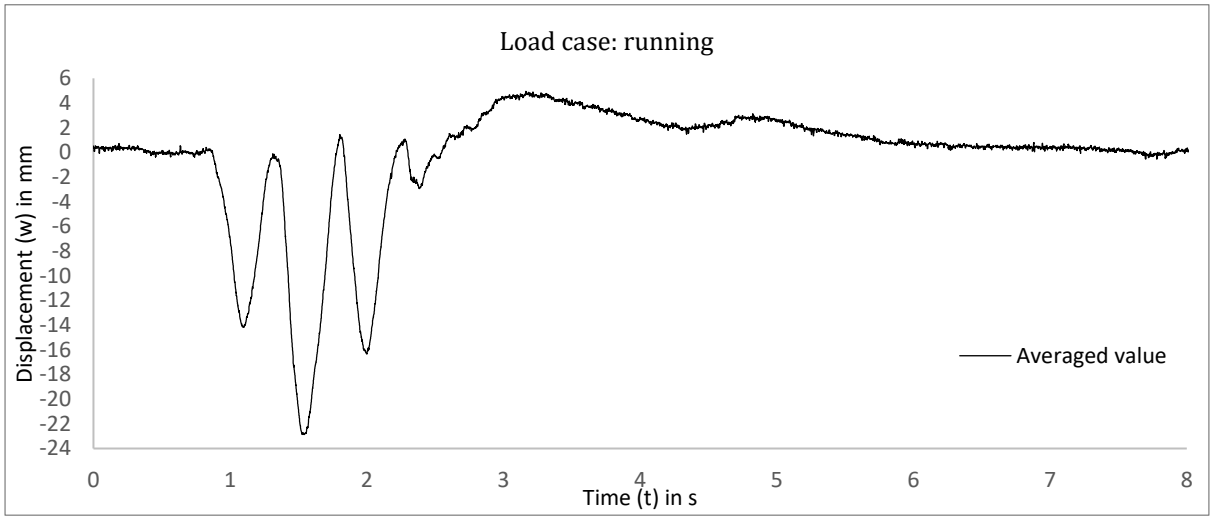

Figure 6.40: Running over the bridge: experimental measurement at center span, averaged value (K_P=0, K_I=1000, v=10000, maximal damping c_d=2800)

In the case of standing, both a dynamic displacement due to walking and a steady-state displacement due to a stop at mid-span are included. Hence, both reducing deformation and reducing vibrations are important in this case. A comparison for all models was thus made for this case, where a clear distinction is seen in using the actuators or the dampers. Once again, it must be noted that all tests include walking over the bridge, which obviously results in ten different graphs if the exact same test is performed ten times. In other words, loads are not controlled perfectly as these tests include a pedestrian as an external loading configuration. This said, the overall differences in between all models become clear once again: vibrations that were found in the original bridge design are neatly damped out using passive damping, whereas deflection can be controlled very well with the PID controller. The connection in series provides a compromise between deflection and vibration control, leading to a deflection within the limits at all time, whereas vibrations are reduced as much as possible (Figure 6.41).

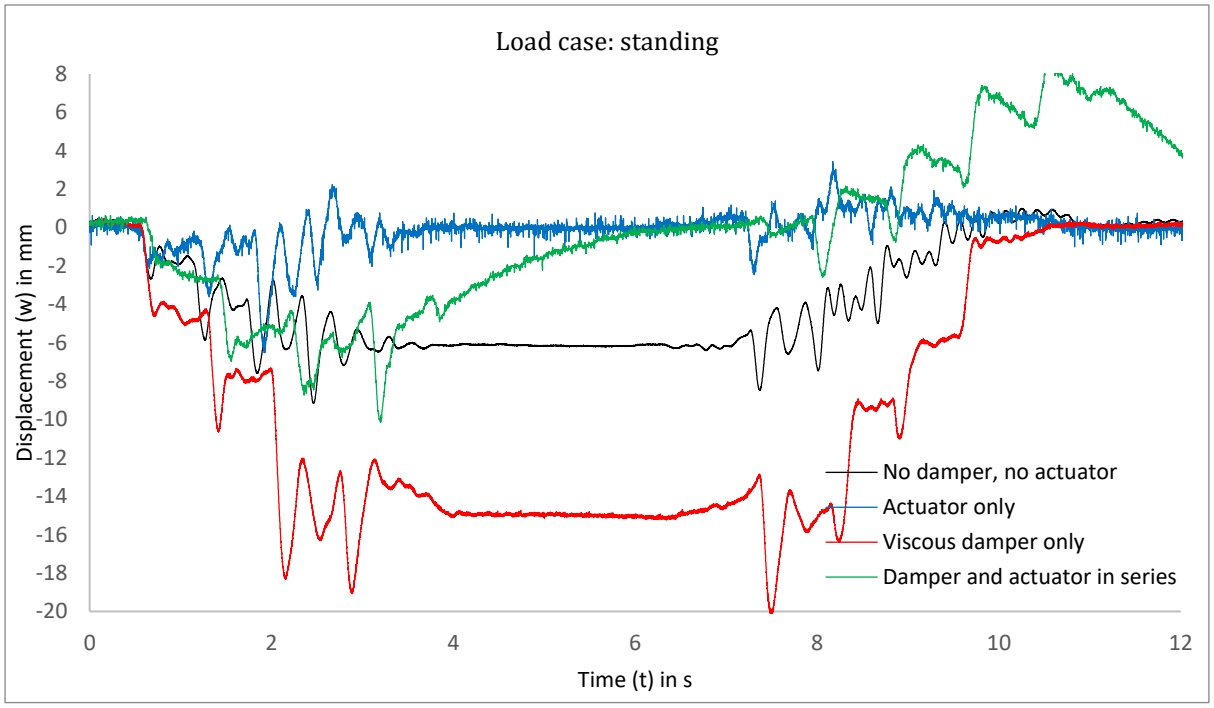

Figure 6.41: Comparison of all models for the case of standing

7 Conclusions

This master thesis on viscous damping in adaptive structures may be considered quite a distinct project in the field of structural engineering. Apart from the use of dynamic analysis instead of conventional static simulations, adaptive structures are quite unique in this field of engineering as well. The vast majority of this project is based on the case study of the footbridge, a lightweight design being very sensitive to both vibrations and large deformations. Two principles were investigated and applied on the case study, where viscous dampers were considered in the first case and an active PID control system in the second case. As a result, a number of conclusions can be drawn from the numerical approach and the experimental setup.

7.1 Experimental testing

The influence of the additional dampers and actuators in the various models has been extensively discussed for both the numerical and experimental approach. Although numerical simulations can be fully controlled (i.e. running a numerical simulation for a number of times will give the exact same result every time), this is not guaranteed in experimental testing. Test results are often influenced by a number of factors such as noise in the measurement device or sudden settlements in the cable truss connections, for example. Moreover, a pedestrian will never walk with exactly the same frequency and step size, let alone that every footstep is placed exactly in the middle of the left and right measurement device. Although results between different models in the previous chapter showed agreement in general with regard to vibration and deformation control, these tests were mainly based on the external load of a person, which thus cannot be controlled as much as in a numerical simulation. Therefore, one final test setup was made to correctly compare the response of all experimental models for one external impact load as controlled as possible (Figure 7.1). A certain mass ($m = 50.30\ kg$) was released above the bridge exactly at the center, where the height was controlled for each test as well (Figure 7.2). A release mechanism was used to ensure that the mass would be released in exactly the same way each time. The impact test was performed at least three times for each set of variables, regarding the damper and the actuator. It should be noted that the difference in measured response between two equal tests is minimal and that this test thus may be considered controlled (annex G). To clarify the difference between all four models, it was decided to use the same parameters in all tests. Hence, values for the PID control system are similar in the response graph, just like the damping coefficient. Furthermore, the averaged value between the left and right measurement device is shown in the result graphs, so that these results can be compared to the one-dimensional numerical analysis.

Figure 7.1: Test setup for the controlled impact test at center span

Figure 7.2: Release mechanism (a) and controlled height of 150mm (b)

Clearly, the influence of the damper is noticeable, regarding the comparison between all four models (Figure 7.3). Although the displacement peak is seen for each model, it is seen that the vibration dies out within one harmonic motion using the damper. This harmonic motion is seen much longer when viscous damping is not used at all. Using the viscous damper, an increase in deformation is obtained, whereas the actuator reduces this deformation back to zero in the combined model. Once again, it can be stated that the PID control system has a positive influence on deformation control, whereas viscous damping helps decreasing vibrations by means of energy dissipation. The combined model shows a compromise between deflection and vibration control, where the steady state error is equal to zero and a harmonic motion is hardly found at all. Nevertheless, one relatively large peak in deformation is still obtained just after impact, as deformation is required for the damper to dissipate energy.

	w_{max}	$w_{steady-state}$	$t_{die-out,5\%}$	$t_{a<0.7m/s^2}$ (EC1)
No actuator, no damper	21.3 mm	5.4 mm	2.7 s	2.3 s
Actuator only	20.0 mm	0 mm	2.0 s	1.7 s
Damper only	30.7 mm	10.5 mm	0.5 s	0.5 s
Damper and actuator in series	29.6 mm	0 mm	0.6 s	0.6 s

Table 7.1: Comparison between deformation and die-out time for all different models. Time is measured from the start of impact at t=1s.

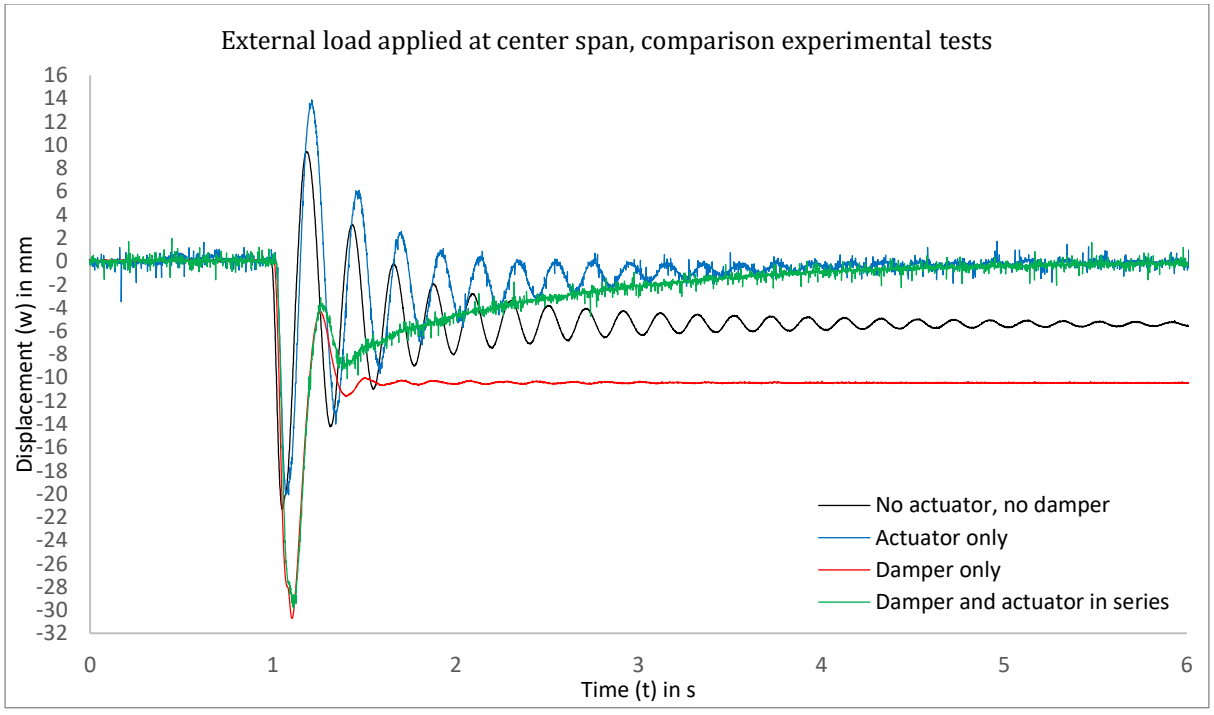

Figure 7.3: Response of all models for the controlled impact test (K_P=0, K_I=500, K_D=0, v=15000, c_{damper}=1200)

7.2 Numerical simulations versus experimental testing

Regarding the approach to the numerical analysis, one can conclude that a lot of approximations and assumptions were needed in order to keep the numerical analysis tool relatively simple. The response to any loading configuration can be computed with this tool, as discretization in the spatial and temporal domain allows for non-linear terms in the calculation. Besides, the numerical approach to analytical solutions simplifies calculus. In this case, it would not even have been possible to solve the response of the footbridge if an analytical approach was used. To conclude, this one-dimensional numerical tool can only be used to approximate the complex reality and although this leads to comparable conclusions in general, local differences are not excluded when comparing reality to computer simulations. Nevertheless, the final impact test that was performed in the experimental setup was also simulated with the numerical tool in Rhinoceros and Grasshopper.

In contrast to all other simulations, the mass is now released from a certain height with regard to the bridge deck. This implies that the external force is not only a long-term load applied on the deck, which can simply be calculated by using Newton's second law. To that extent, the impact of the generated pulse is included to create the correct external load in numerical analysis. First, the time from release to impact time is calculated, where the height between the mass and the bridge deck is similar for each impact test. This renders

$$v = \sqrt{2sg} \tag{7.1}$$

Now, the pulse can be calculated. This is equal to the mass times its velocity at impact time. In mathematical terms

$$p = mv \tag{7.2}$$

Referring to several experimental tests, the time needed for this impulse can be found by the time that is needed to reach the maximum displacement. This is approximately equal to fifty milliseconds. In the first test (bridge only), the maximum displacement was found at $t = 1.046s$, whereas the moment of impact was found at $t = 0.993s$. Now, the impulse force can be calculated by

$$F = \frac{p}{t} \tag{7.3}$$

This implies that the following loading conditions now hold for a simulation of the impact test (annex B). These conditions were applied in the numerical analysis tool.

$$F = \begin{cases} 0 & t \leq 1 \\ 3.5F & 1 < t \leq 1.05 \\ F & t > 1.05 \end{cases} \tag{7.4}$$

Some experimental tests were compared already for several load cases like walking and running over the bridge. These comparisons, however, showed differences in behavior for different practical reasons. As already said, walking cannot be considered a controlled loading configuration, as frequency and most important, step intensity, will be different for every walk along the span. Including the intensity of the mass by calculating the impact load and duration, a comparison to the numerical is much more trustworthy. As a result, a final comparison is shown for each model, according to the footbridge variables that were used in the experimental test for the impact load. General agreement between the numerical prediction model and experimental results is again found, except for local differences over time (Figure 7.4 up to Figure 7.7). The actuator response seems to differ slightly in experimental testing, which can be explained by the fact that the actuators also depend on other software than given in the program in Labview. Furthermore, it is seen that the exact amount of damping can differ in reality. As already stated in the literature study, damping is a quite complex phenomenon, making it very difficult to imply this correctly in mathematical models. An approximate mathematical convenience was used in the form of some damping coefficients, having no physical meaning at all. Having said this, it may be concluded that the numerical analysis tool provides a fairly good prediction to reality. Using viscous damping can indeed lead to better performance with regard to vibration control and the active PID control is very beneficial for regulating the deflection of a slender structure during loading events. This was predicted by a numerical analysis tool and is eventually also validated by means of experimental testing.

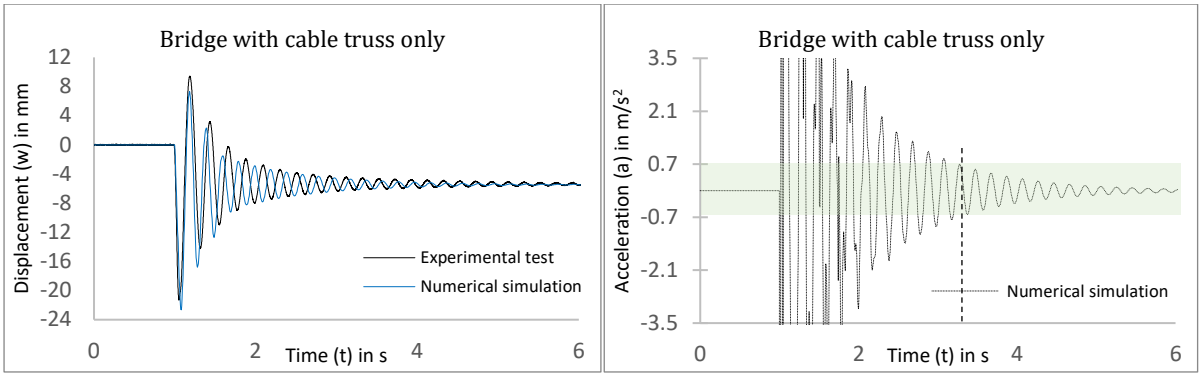

Figure 7.4: Experimental impact test compared to the numerical simulation, bridge with cable truss only

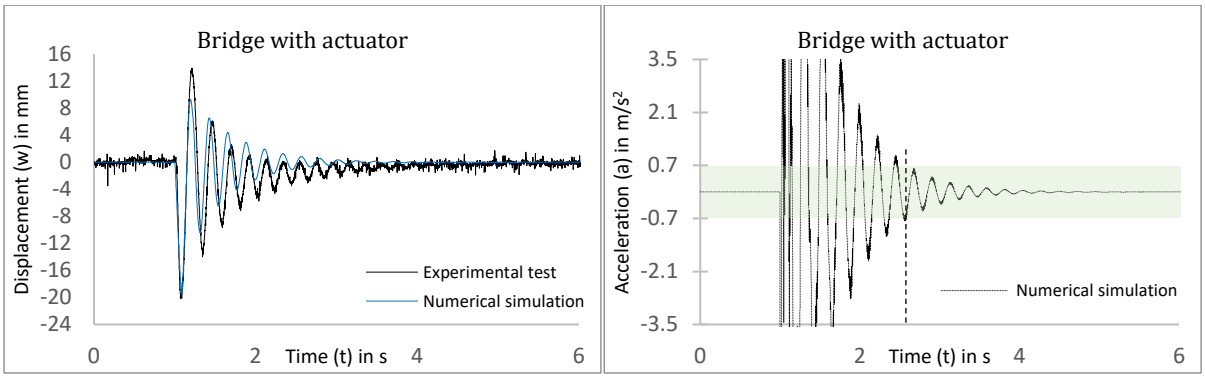

Figure 7.5: Experimental impact test compared to the numerical simulation, bridge with actuator

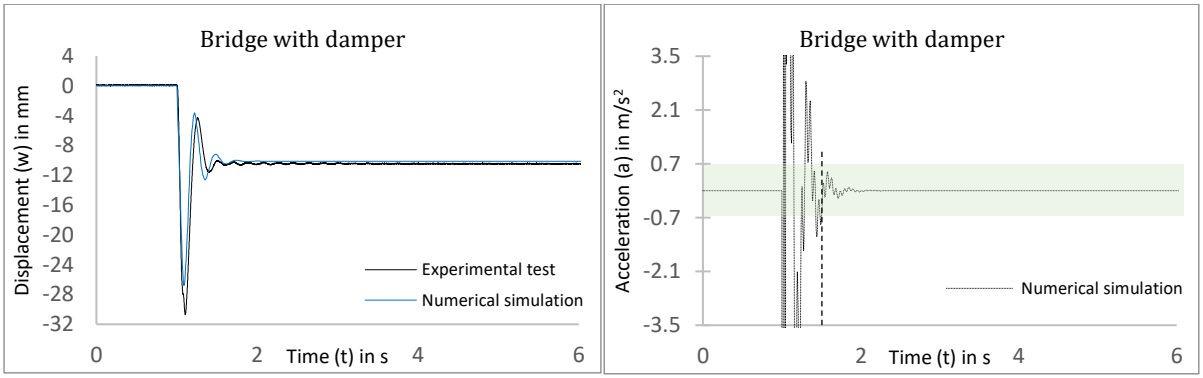

Figure 7.6: Experimental impact test compared to the numerical simulation, bridge with damper

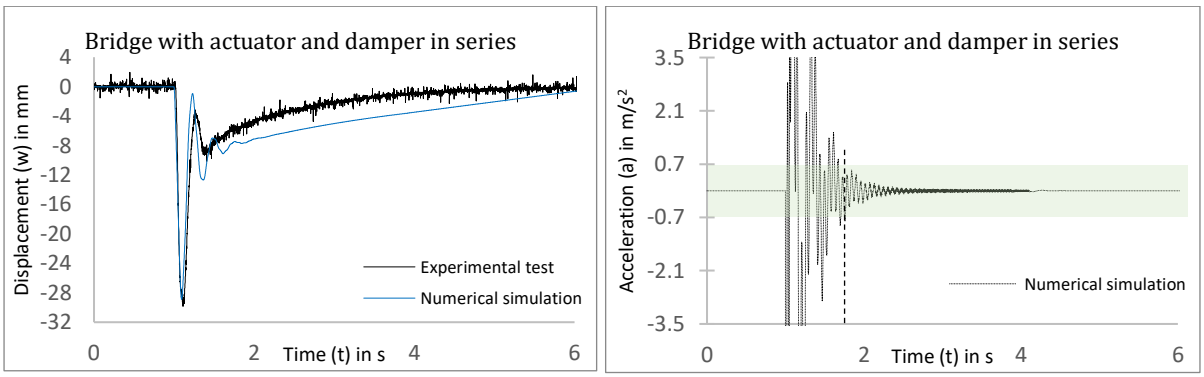

Figure 7.7: Experimental impact test compared to the numerical simulation, bridge with damper and actuator in series

7.3 Recommendations

As a start for this master thesis, a comprehensive literature study was performed to gather some basic insights in the entirely unknown field of dynamics within structural applications. A relatively large amount of time was needed to understand the basic principles of one-dimensional dynamics, as static calculations still predominate the structural part of the built environment nowadays. Furthermore, it was needed to gain insight in common knowledge on elementary control theory, which in this case was based on a PID-control system. On top of that, additional mathematical knowledge was required to discretize complex analytical solutions to dynamic problems in both the spatial and temporal domain. Given this list of additional topics, it may be concluded that mainly the basic principles are implemented in this master study and that investigating each topic into more detail presumably will yield better performance in both the numerical and experimental part of this project. Having said this, it is demonstrated that dynamic behavior can be predicted for structural applications to a certain extent, even if these elementary principles are applied in a one-dimensional approach. General principles are then seen in experimental testing as well, in spite of all these assumptions and simplifications to reality. Perhaps, the results that were obtained may be considered promising for further research into this topic. A few interesting possibilities are delineated here.

- The numerical analysis tool is based on a one-dimensional discretized mass spring system with multiple degrees of freedom. Although this one-dimensional model provides fairly good information on vertical displacement in time, it would be very interesting to increase the design space to two or even three degrees of freedom. Additional configurations could then be included in the dynamic analysis tool, like for instance the response on lateral wind loading or torsional vibrations resulting from asymmetric loading.
- Discretization of both the spatial and temporal domain was needed in order to 'undo' the complexity of analytical algebra. A small introduction was given into explicit and implicit approximation methods, which both have their advantage and disadvantage. Many algorithms are superior to those elementary approximation methods and implementing a more sophisticated approximation would presumably reduce instability problems without decreasing its accuracy.
- It was already seen that damping is nothing but energy dissipation and that each material has some form of damping, albeit negligible in some cases. Although every structural part of the footbridge can be given a decent value for energy dissipation, these values are all based on mathematical convenience rather than physical meaning. This resulted in large deviations between numerical modelling and experimental testing, with regard to damping properties of the footbridge structure. Therefore, viscous damping is an interesting topic to investigate in more detail, especially within the built environment where it has proven its value to vibration-controlled structures.
- Two physical shock absorbers were ordered for experimental testing. It was chosen to maintain values for both energy dissipation and stiffness as variable as possible, so that these dampers can be used in other applications in future experiments as well. Given the development towards more lightweight structures in future, it can be recommended to include damping in more structural applications next to this footbridge. Obviously, this also holds for the actuators.
- This project may be categorized quantitative research, especially with regard to the conclusions that were drawn from the impact test to compare numerical to experimental results. Obviously, dynamic behavior is improved regarding the maximum value for acceleration in the Eurocode. As the combined model comprises a compromise between deflection and vibration control, it may be interesting to add a qualitative part to this research. To that extent, parameters for both the dampers and the actuators could be optimized to the pedestrians needs. Given the physical prototype, it should not be that difficult to have such a study take place.

8 References

Mah, D., et al (2011). House construction CO_2 footprint quantification: a BIM approach. *Construction Innovation*, v11 n2, 161–178.

Dallard, P., et al (2001). The London Millennium Footbridge. *The Structural Engineer*, Volume 79/No.22, Pg. 17.

Billah, K., & Scanlan, R. H. (1990). Resonance, Tacoma Narrows Bridge failure and undergraduate physics textbooks. *American Association of Physics Teachers*.

Walibi Holland heeft oplossing voor trillen van achtbaan Lost Gravity. *Looopings (2016)*.

Dorf, R. C., & Bishop, R. H. (2011). *Modern control systems* (twelfth ed.). Pearson.

Ogata, K. (1970). *Modern control engineering* (fifth ed.). Pearson.

Senatore, G., & Duffour, P., & Winslow P., & Wise C. (2015). Adaptive Truss Prototype to save material. *I-structE Research Award Final Report*.

Rooyackers, F. (2017). Dynamic Control of Adaptive Structures*. Graduation reports University of Eindhoven unit structural design.*

Taylor, D. P. (2006). Damper retrofit of the London Millennium Footbridge – A case study in biodynamic design. *Taylor Devices, Inc*.

Taylor, D.P. (1999). Buildings: Design for Damping. *Taylor Devices, Inc*.

Inman, D. J. (2001). *Engineering vibrations* (third edition ed.). Pearson.

Nicholson, J.W., & Simmonds, J.G. (1977). Timoshenko Beam Theory Is Not Always More Accurate Than Elementary Beam Theory. *Journal of Applied Mechanics*, v44 n2

Cabada, A., et al (2004). Green's function and comparison principles for first order periodic differential equations with piecewise constant arguments. *Journal of Mathematical Analysis and Applications*, v291 p609-697.

Bachmann, H., et al. (1995). *Vibration Problems in Structures*. Birkhauser Verlag.

Dym, H., & McKean, H.P. (1972). *Fourier Series and Integrals*. New York: Academic Press.

Zwillinger, D. (1989), *Handbook of differential equations*. Boston: Academic Press*.*

Feyrer, K. (2015), *Wire Ropes: Tension, Endurance, Reliability* (second ed.). Springer.

Symans, M.D. & Constantinou, M.C. (1998). Passive Fluid Viscous Damping Systems for Seismic Energy Dissipation. *Journal of Earthquake Technology*, 35(4), p 185-206.

Annex A List of figures

Annex B Calculations on experimental test setup

The bridge model with its exact dimensions is used as input for the comparison to the numerical approximation model in Grasshopper. The bridge is simply supported and consists of two steel tubes. Wooden elements of 160mm width are located on top of the steel tubes and provide only a walking deck for the pedestrian.

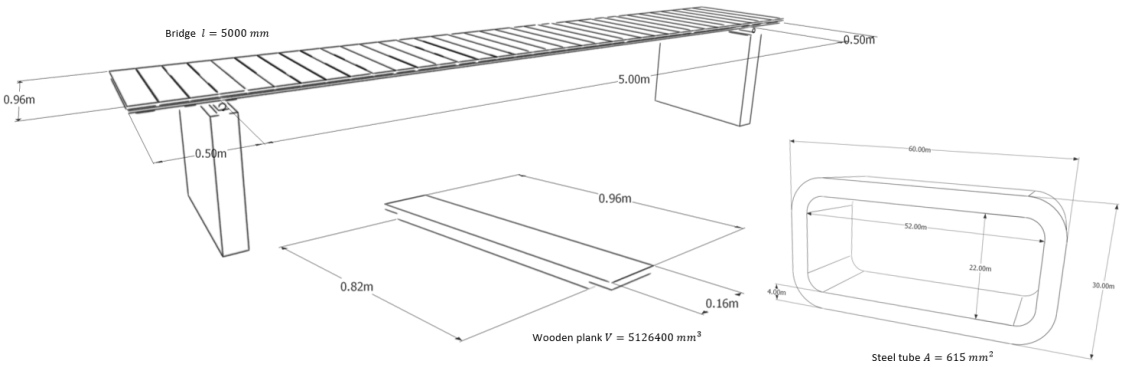

The dead load of the bridge is calculated as

$$q_{DL} = q_{steel} + q_{wood}$$

$$q_{DL} = \left(2 * 615\ mm^2 * 5000\ mm * 7850 \frac{kg}{m^3}\right) + (30 * 3kg)$$

$$q_{DL} = 48.2775 + 90 = 138\ kg$$

$$q_{DL} = 138\ kg * \frac{9.81}{5000} = 0.271\ N/mm$$

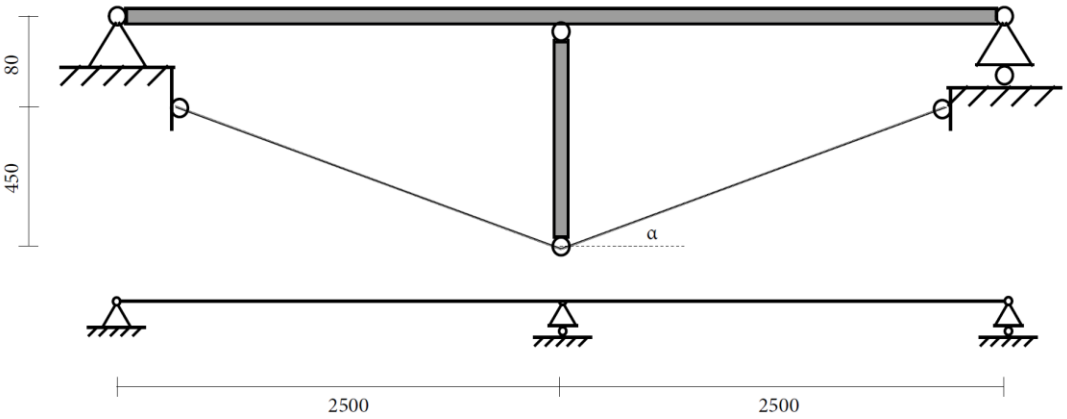

For dead load, the truss model can be considered a beam on three supports. Hence, the vertical reaction in the centre and end supports are equal to

$$F_{v,end} = \frac{3}{8}ql = \frac{3}{8} * 0.271 * 2500 = 254N$$

$$F_{v,centre} = \frac{10}{8}ql = \frac{10}{8} * 0.271 * 2500 = 847N$$

The moment of inertia of the two steel beams is equal to

$$I = 2 * \frac{bh^3}{12} = 2 * \frac{60*30^3 - 52*22^3}{12} = 177717\ mm^4$$

The Young's Modulus of the steel is equal to

$$E_{steel} = 2.1 * 10^5 \frac{N}{mm^2}$$

The bridge without steel cable truss must resist bending moment due to dead load of both the steel and the timber walking deck. It can then be concluded that only 158kg extra weight could be allowed on the bridge. The deformation of the bridge itself due to its own weight can be calculated as

$$\delta = \frac{5}{384} * \frac{qL^4}{EI} = \frac{5}{384} * \frac{0.271*5000^4}{2.1*10^5*177717} = 59.1\ mm$$

The maximum allowable bending moment in the center of the bridge is equal to

$$M_{Rd} = \sigma * \frac{I}{z} = 235 * \frac{177717}{15} = 2784233\ Nmm$$

The bending moment in the center of the bridge due to dead load is equal to

$$M_{Ed} = \frac{qL^2}{8} = \frac{0.271*5000^2}{8} = 846875\ Nmm$$

The maximum allowable force in the center of the bridge may thus not exceed

$$F_{max} = \frac{4(M_{Rd} - M_{Ed,DL})}{L} = \frac{4*(2784233-846875)}{5000} = 1550N = 158kg$$

Taking into account the cable truss, the dead load in the center of the bridge can be much higher. However, the steel tubes still have to span 2.5m. The deformation of the bridge itself due to its own weight can now be calculated as

$$\delta = \frac{5}{384} * \frac{qL^4}{EI} = \frac{5}{384} * \frac{0.271*2500^4}{2.1*10^5*177717} = 3.7mm$$

The maximum allowable bending moment in the center of the bridge is equal to

$$M_{Rd} = \sigma * \frac{I}{z} = 235 * \frac{177717}{15} = 2784233\ Nmm$$

The bending moment in the center of the bridge due to dead load is equal to

$$M_{Ed} = \frac{qL^2}{8} = \frac{0.271*2500^2}{8} = 211719\ Nmm$$

The maximum allowable force in the center of the bridge may thus not exceed

$$F_{max} = \frac{4(M_{Rd} - M_{Ed,DL})}{L} = \frac{4*(2784233-211719)}{2500} = 4116N = 420kg$$

The exact angle of the cable truss is equal to

$$\alpha = \tan^{-1}\left(\frac{450}{2500}\right) = 10{,}2°$$

From here, the exact pretension in the cable can be calculated when the dead load of the bridge is lifted upwards to zero initial deflection. The load of the actuators was taken into account as well.

$$F_v = \frac{847N}{4} + \frac{12*9.81}{2} = 271N \rightarrow F_{pretension,cable} = \frac{271N}{\sin(\alpha)} = 1528N$$

For each extra pedestrian at mid-span, the extra cable force is equal to

$$F_v = \frac{75kg*9.81}{4} = 184N \rightarrow F_{cable} = \frac{184N}{\sin(\alpha)} = 1039N$$

The pulse on the bridge is calculated using the following relations between distance (s), mass (m), velocity (v) and time (t).

$$s = \frac{1}{2}gt^2 \rightarrow t = \sqrt{\frac{2s}{g}} \qquad v = gt = \sqrt{2sg} = \sqrt{2 * 0.15 * 9.81} = 1.7155\frac{m}{s}$$

$$p = mv = 50.30 * 1.7155 = 86.29Ns \qquad F_{eq} = \frac{p}{t} = \frac{86.29}{0.05} = 1726N \text{ applied for } 0.05s \text{ after impact}$$

Annex C Calibration of measurement device

Calibration of channel ADC00

Calibration Channel: ADC-00	
Name:	*PVMlab*
Date:	*vrijdag 1 juni 2018*
Time:	*9:30:29*
Calibration Factor	***49.98179***
R-Squared	*1*

Reading [Volt]	*Physical Value*
1.877	0.000
2.007	6.625
2.260	19.386
2.526	32.559
3.086	60.394
3.750	93.707
4.056	109.105

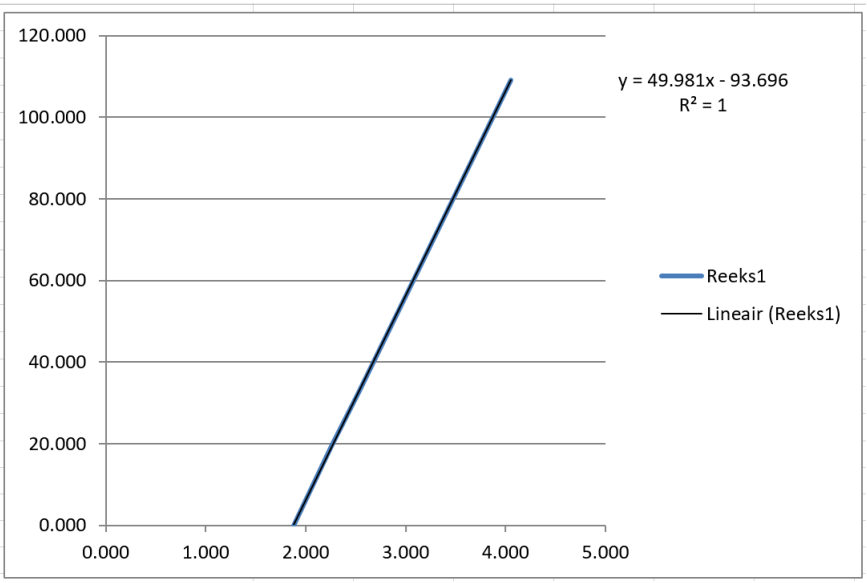

Calibration of channel ADC01

Calibration Channel: ADC-01	
Name:	*PVMlab*
Date:	*vrijdag 1 juni 2018*
Time:	*9:39:15*
Calibration Factor	***50.01064***
R-Squared	*1*

Reading [Volt]	*Physical Value*
1.893	0.000
2.174	14.154
2.564	33.785
2.925	51.909
3.234	67.414
3.567	83.843
4.039	107.316

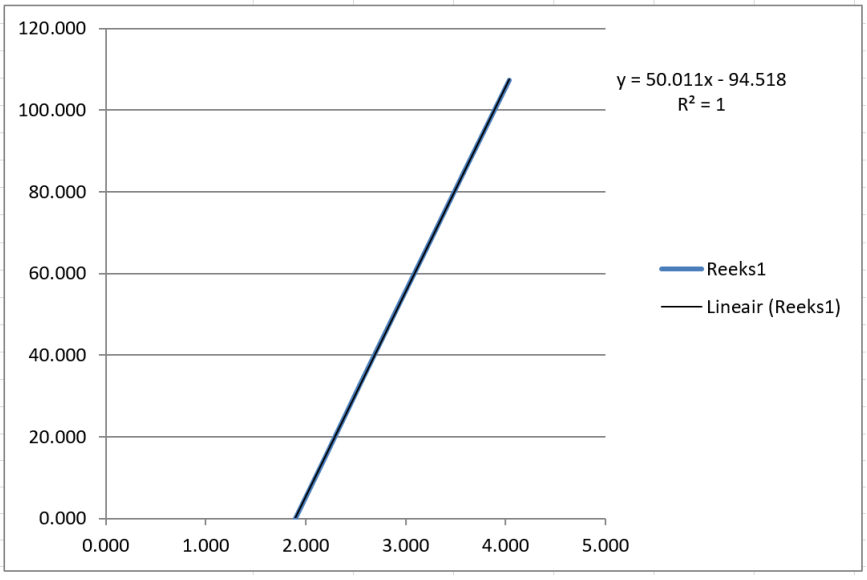

Annex D Tensile test results steel wire rope Ø-10mm

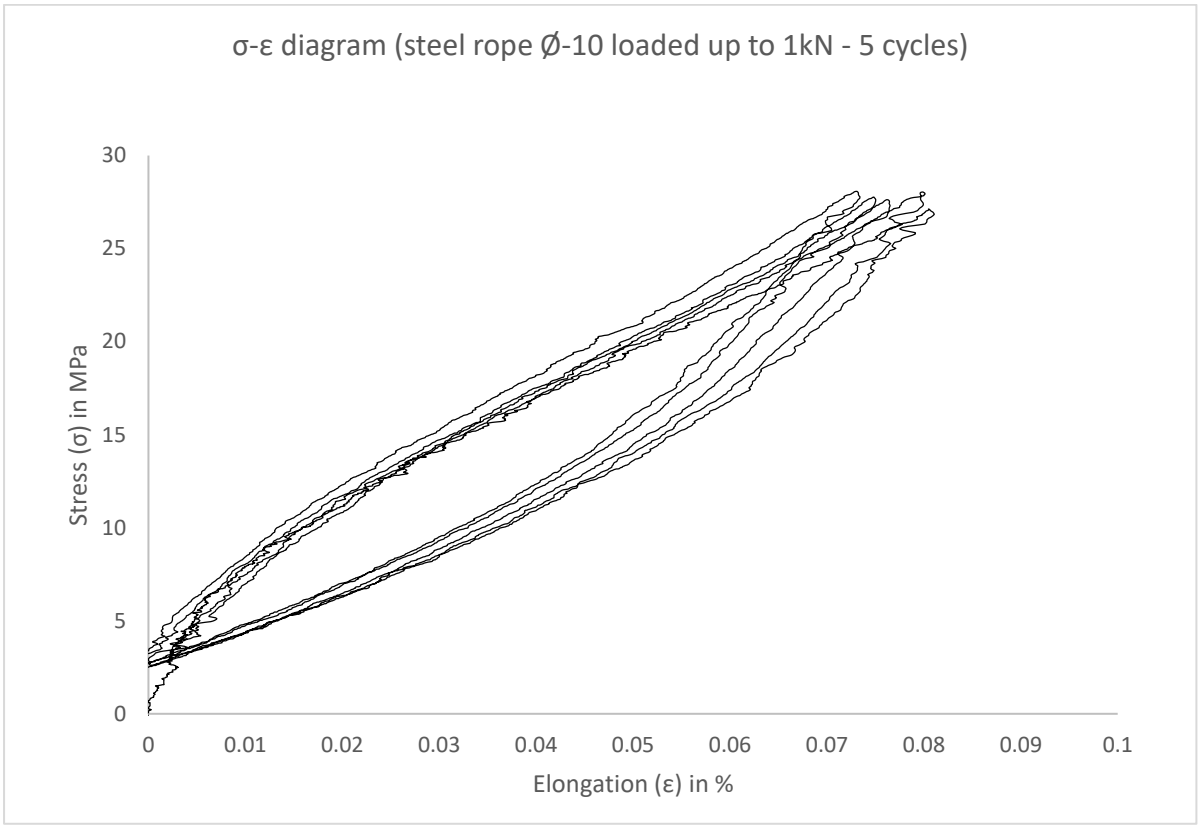

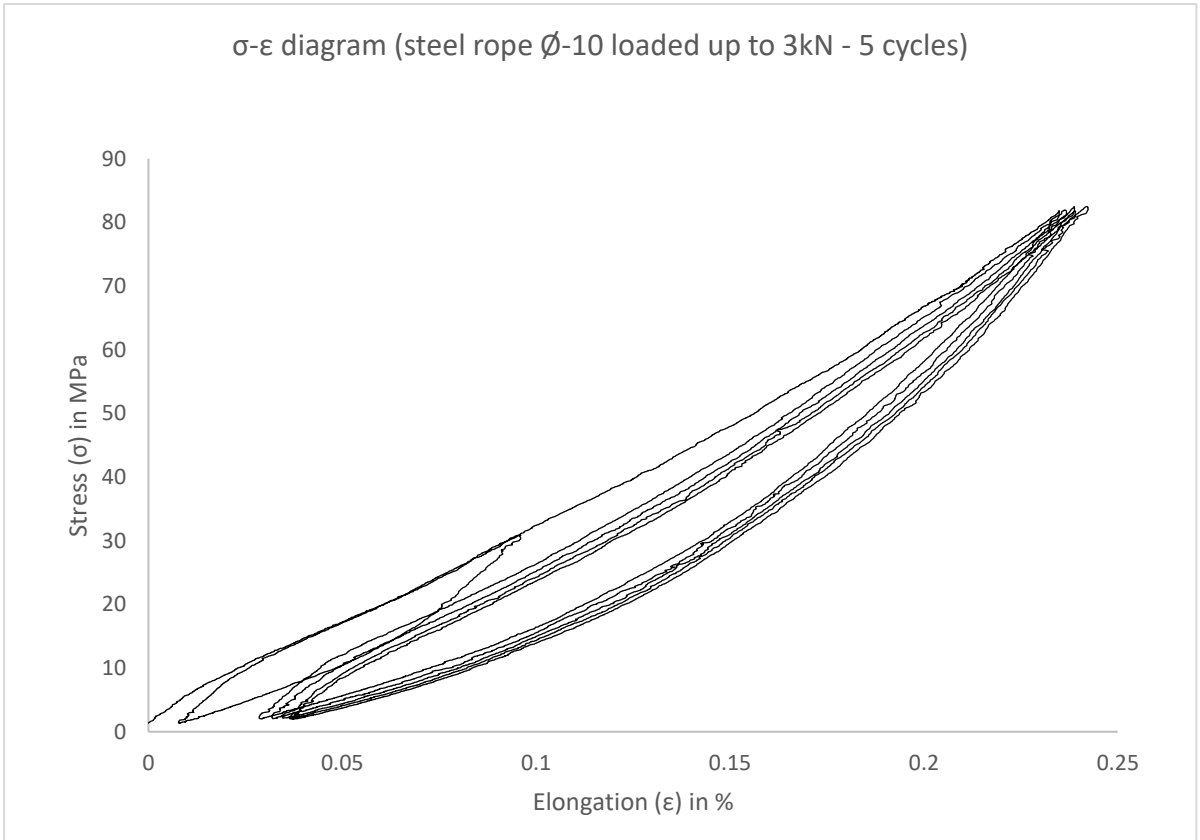

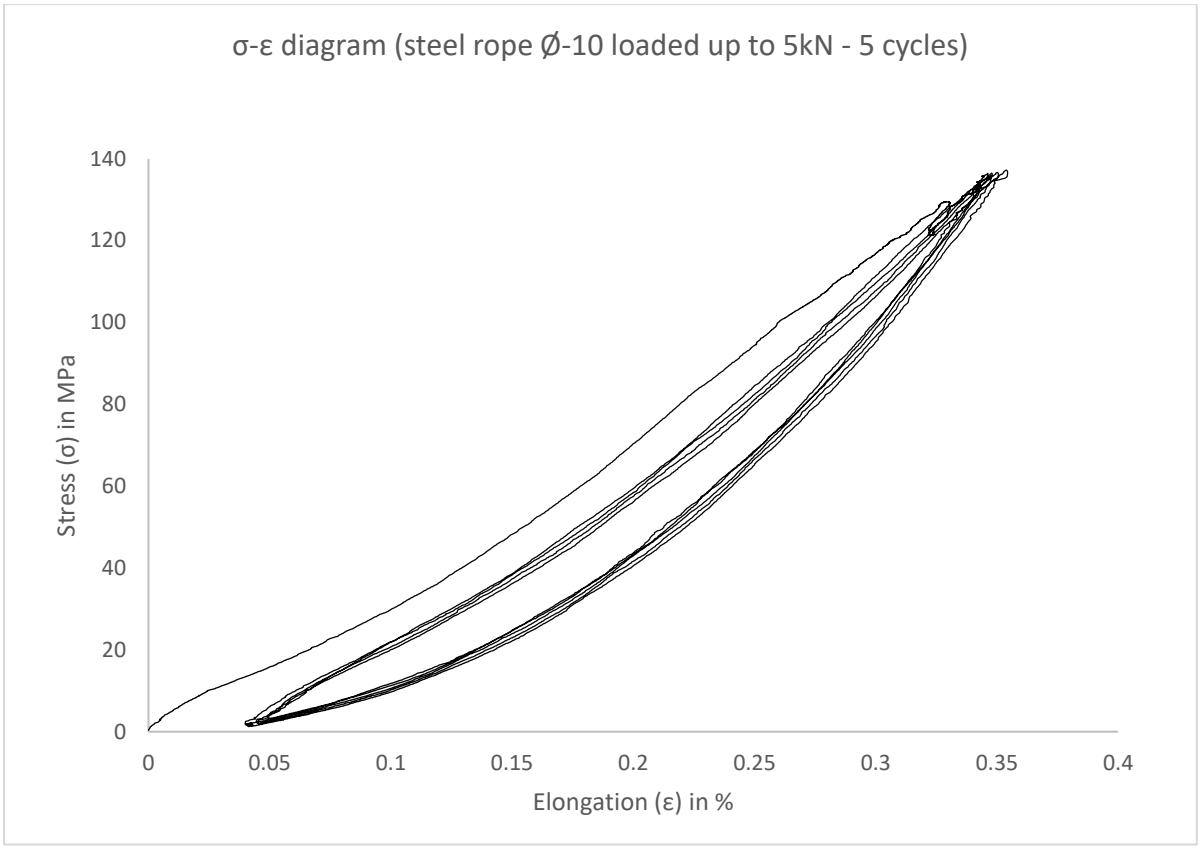
σ-ε diagram (steel rope Ø-10 loaded up to 5kN - 5 cycles)
Stress (σ) in MPa
140
120
100
80
60
40
20
0
0
0.05
0.1
0.15
0.2
0.25
0.3
0.35
0.4
Elongation (ε) in %

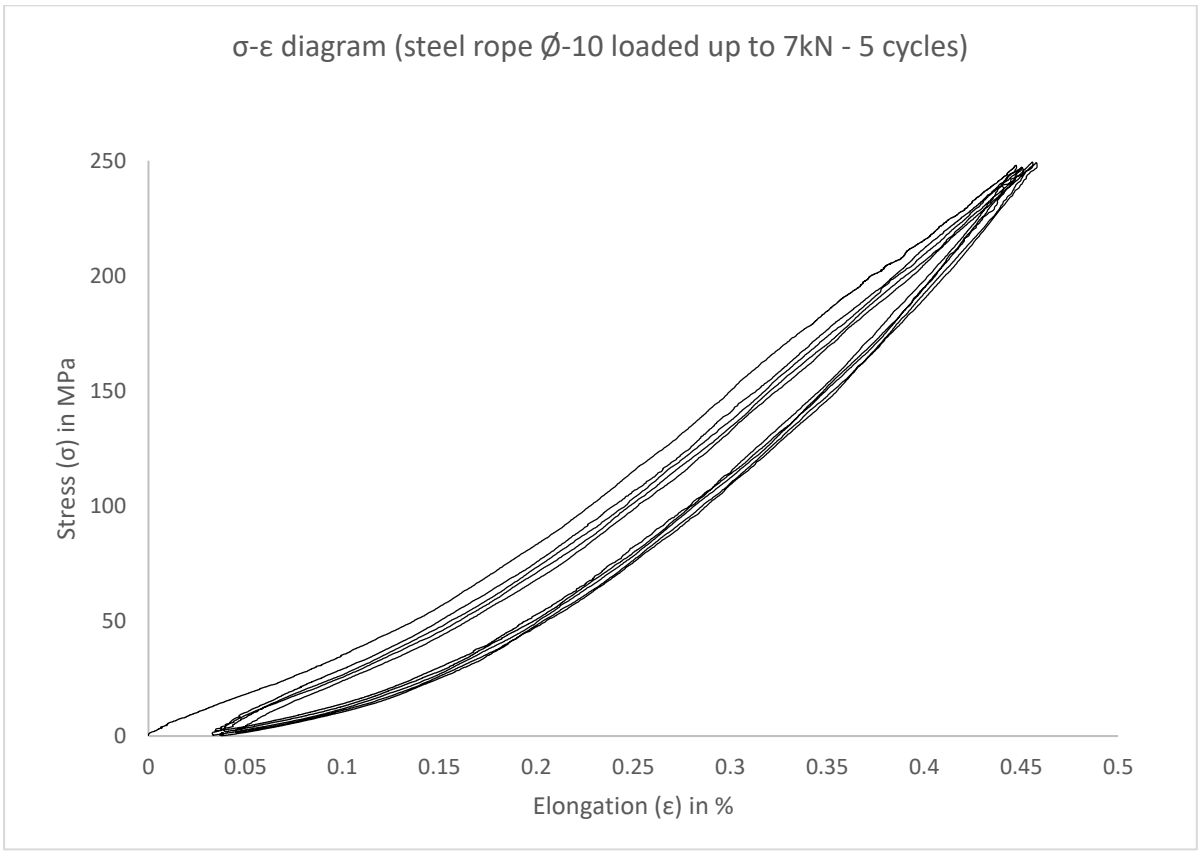
σ-ε diagram (steel rope Ø-10 loaded up to 7kN - 5 cycles)
Stress (σ) in MPa
250
200
150
100
50
0
0
0.05
0.1
0.15
0.2
0.25
0.3
0.35
0.4
0.45
0.5
Elongation (ε) in %

Annex E Example of an output file

All input data
1: Material properties bridge deck - Material = Steel S235 - Density = 7850kg/m3 - E-modulus = 210000000000Pa - Poissons ratio = 0.3 - Shear modulus = 80769230770Pa - Proof stress = 235000000Pa
1: Material properties cable truss - Material = FeP1000 6x7 1-layer fibre core - Density = 7850kg/m3 - Poissons ratio = 0.3 - Shear modulus = 4846153847Pa - Proof stress = 500000000Pa
2: Geometry properties bridge deck - Span = 5m - Height tube = 0.03m - Width tube = 0.06m - Tube thickness = 0.004m - Nr of tubes = 2 - Cross section area = 0.001312m^2 - Moment of inertia = 1.77717333333333E-07m^4 - Alpha damping = 0.3 - Beta damping = 0.0005 - Additional mass deck = 115kg
2: Geometry properties cable truss - Length = 2.555851487162 58m - Diameter = 0.01m - Total wires = 4 - Cross section = 0.0001476m - Angle = 12 - Pretension = 1000N - Damping coefficient = 40Ns/m
3: Actuator properties - Mass = 16kg - Kp = 50000 - Ki = 500000 - Kd = 5000 - Limit force = 10000N - Response time = 0.01s - Delay time = 0.01s - Activated? True - Virtual spring stiffness = 100000N/mm
4: Damper properties - Mass = 12kg - Damping coefficient = 3000Ns/m - Stiffness coefficient = 20000N/mm - Activated? True - Model type = 6
5: External loading properties - Mass person = 75kg - Nr. of visitors = 1 - External load = -735.75N - Impact time = 0s - Load duration = 10s - Repetition? False - Period time = 0.5s - Walking? False - Step length = 0.625m
6: Time step properties - Time increment = 0.003s - Last increment = 2.007s - Approximation type = explicit
Name graph title:
m(eq)=42kg, k(eq)=188352N/m, c(eq)=107Ns/m, model=6, pretension=1000N, damper: c=3000Ns/m, k=20000N/m
Name series:
Wire rope (m1)
Intermediate (m2)
Bridge (m3): Kp=50000, Ki=500000, Kd=5000

t	F1	F2	F3	u1(t)	u2(t)	u3(t)	u4(t)	u5(t)	v1(t)	v2(t)	v3(t)	v4(t)
	v5(t)	a1(t)	a2(t)	a3(t)	a4(t)	a5(t)	F(Act)	E(c)				
0	-735.75	-735.75	-735.75	0	0	0	0	0	0	0	0	0
	0	0	0	0	0	0	0	46177.771854				
0.003	0	-735.75	0	-0.005009	-0.278271	-0.005009	-0.070798	-0.02509	-0.003032	-0.08639	-0.003032	-0.032361
	-0.011644	-1.010549	-28.796531	-1.010549	-10.786926	-3.881426	-0.49831	46177.771854				
0.006	0	-735.75	0	-0.021995	-0.58564	-0.021995	-0.191408	-0.082423	-0.008919	-0.116845	-0.008919	-0.051218
	-0.025351	-1.962585	-10.151831	-1.962585	-6.285686	-4.56904	-4.570763	46177.771854				
0.009	0	-735.75	0	-0.062668	-0.97207	-0.062668	-0.367422	-0.17928	-0.018903	-0.139267	-0.018903	-0.067728
	-0.037777	-3.3277	-7.474124	-3.3277	-5.503302	-4.141895	-10.89853	46177.771854				
0.012	0	-735.75	0	-0.139764	-1.414189	-0.139764	-0.587376	-0.306626	-0.033193	-0.154136	-0.033193	-0.079455
	-0.045571	-4.763438	-4.956216	-4.763438	-3.909148	-2.598128	-18.814152	46177.771854				
0.015	0	-735.75	0	-0.265857	-1.890363	-0.265857	-0.834178	-0.447832	-0.051472	-0.162162	-0.051472	-0.085003
	-0.047093	-6.093117	-2.675268	-6.093117	-1.849107	-0.507238	-28.074995	46177.771854				
0.018	0	-735.75	0	-0.451827	-2.38146	-0.451827	-1.084936	-0.58615	-0.072944	-0.164139	-0.072944	-0.08398
	-0.042926	-7.157145	-0.658905	-7.157145	0.340871	1.389079	-24.721028	46177.771854				
0.021	0	-735.75	0	-0.705553	-2.871503	-0.705553	-1.325368	-0.702848	-0.096421	-0.1618	-0.096421	-0.077393
	-0.033387	-7.825699	0.779411	-7.825699	2.195735	3.179725	-35.965036	46177.771854				
0.024	0	-735.75	0	-1.030927	-3.350028	-1.030927	-1.540638	-0.785288	-0.120457	-0.156815	-0.120457	-0.066909
	-0.02076	-8.012067	1.661697	-8.012067	3.494712	4.208888	-48.338442	46177.771854				
0.027	0	-735.75	0	-1.427302	-3.811511	-1.427302	-1.707716	-0.837714	-0.143494	-0.150058	-0.143494	-0.054033
	-0.009987	-7.679029	2.252534	-7.679029	4.291928	3.591054	-4.825564	46177.771854				
0.03	0	-735.75	0	-1.889366	-4.253968	-1.889366	-1.836468	-0.858545	-0.16401	-0.144452	-0.16401	-0.04141
	-0.000138	-6.83868	1.868408	-6.83868	4.207487	3.283074	2.612823	46177.771854				
0.033	0	-735.75	0	-2.407502	-4.683528	-2.407502	-1.935148	-0.850236	-0.180684	-0.141959	-0.180684	-0.031153
	0.00779	-5.557878	0.831118	-5.557878	3.418978	2.642618	-8.179189	46177.771854				
0.036	0	-735.75	0	-2.968624	-5.110901	-2.968624	-1.993419	-0.834243	-0.192538	-0.142383	-0.192538	-0.023895
	0.009018	-3.951421	-0.14122	-3.951421	2.419499	0.409424	53.987553	46177.771854				
0.039	0	-735.75	0	-3.557331	-5.546704	-3.557331	-2.044549	-0.814511	-0.199022	-0.14806	-0.199022	-0.021295
	0.007985	-2.161427	-1.892535	-2.161427	0.866462	-0.344502	46.56119	46177.771854				
0.042	0	-735.75	0	-4.157289	-6.006702	-4.157289	-2.100132	-0.799977	-0.200071	-0.158739	-0.200071	-0.023397
	0.004097	-0.349738	-3.559642	-0.349738	-0.700597	-1.29612	39.474983	46177.771854				
0.045	0	-735.75	0	-4.752719	-6.504495	-4.752719	-2.154657	-0.811386	-0.196109	-0.172395	-0.196109	-0.028891
	-0.005324	1.320719	-4.551928	1.320719	-1.831103	-3.140187	101.586503	46177.771854				
0.048	0	-735.75	0	-5.329747	-7.047993	-5.329747	-2.2383	-0.847559	-0.187971	-0.189391	-0.187971	-0.037469
	-0.014451	2.712801	-5.665445	2.712801	-2.859469	-3.04219	97.274938	46177.771854				
0.051	0	-735.75	0	-5.877509	-7.644681	-5.877509	-2.355455	-0.907843	-0.176812	-0.20784	-0.176812	-0.047573
	-0.022697	3.719459	-6.149621	3.719459	-3.367875	-2.748655	92.527932	46177.771854				
0.054	0	-735.75	0	-6.388953	-8.295608	-6.388953	-2.490432	-1.000037	-0.163987	-0.224591	-0.163987	-0.056848
	-0.03201	4.275216	-5.583493	4.275216	-3.091714	-3.10438	151.477618	46177.771854				
0.057	0	-735.75	0	-6.861157	-8.99351	-6.861157	-2.658423	-1.110691	-0.150875	-0.239267	-0.150875	-0.064466
	-0.037001	4.370695	-4.892224	4.370695	-2.539357	-1.66385	147.199342	46177.771854				
0.06	0	-735.75	0	-7.295205	-9.729057	-7.295205	-2.83354	-1.238756	-0.138741	-0.248876	-0.138741	-0.068269
	-0.040434	4.044726	-3.202871	4.044726	-1.267644	-1.144351	206.510549	46177.771854				
0.063	0	-735.75	0	-7.695629	-10.485194	-7.695629	-3.003754	-1.377135	-0.128596	-0.252322	-0.128596	-0.067193
	-0.04108	3.381383	-1.148678	3.381383	0.358578	-0.215066	276.869792	46177.771854				
0.066	0	-735.75	0	-8.069475	-11.242908	-8.069475	-3.175351	-1.501801	-0.121098	-0.250491	-0.121098	-0.061593
	-0.034765	2.499365	0.610344	2.499365	1.866836	2.104751	273.686429	46177.771854				
0.069	0	-735.75	0	-8.425182	-11.985868	-8.425182	-3.330992	-1.596689	-0.11652	-0.242946	-0.11652	-0.051615
	-0.023697	1.526246	2.514913	1.526246	3.325986	3.689483	268.993297	46177.771854				
0.072	0	-735.75	0	-8.771439	-12.696825	-8.771439	-3.431873	-1.668307	-0.114743	-0.228322	-0.114743	-0.037004
	-0.014195	0.59223	4.874826	0.59223	4.870303	3.167156	360.193841	46177.771854				
0.075	0	-735.75	0	-9.115984	-13.357088	-9.115984	-3.496123	-1.70119	-0.115269	-0.209984	-0.115269	-0.020123
	-0.001355	-0.175272	6.11263	-0.175272	5.626735	4.280072	357.267432	46177.771854				
0.078	0	-735.75	0	-9.464595	-13.957561	-9.464595	-3.515277	-1.690965	-0.117309	-0.189144	-0.117309	-0.002356
	0.012116	-0.679997	6.946486	-0.679997	5.92233	4.490372	354.13078	46177.771854				
0.081	0	-735.75	0	-9.820414	-14.492486	-9.820414	-3.458529	-1.659095	-0.119904	-0.165403	-0.119904	0.015999
	0.019297	-0.865051	7.913836	-0.865051	6.118568	2.393758	463.662816	46177.771854				
0.084	0	-735.75	0	-10.183553	-14.957027	-10.183553	-3.361585	-1.599842	-0.122019	-0.143173	-0.122019	0.03223
	0.026694	-0.705012	7.409947	-0.705012	5.410175	2.465699	466.150536	46177.771854				
0.087	0	-735.75	0	-10.551081	-15.357979	-10.551081	-3.228394	-1.517332	-0.122688	-0.12369	-0.122688	0.045305
	0.032324	-0.223036	6.494533	-0.223036	4.358463	1.876519	469.919676	46177.771854				
0.09	0	-735.75	0	-10.917454	-15.703789	-10.917454	-3.007241	-1.460147	-0.121129	-0.103782	-0.121129	0.057193
	0.024969	0.519769	6.636004	0.519769	3.96268	-2.451765	714.267633	46177.771854				
0.093	0	-735.75	0	-11.275062	-15.996951	-11.275062	-2.778838	-1.409668	-0.116774	-0.089891	-0.116774	0.064944
	0.021373	1.451465	4.63001	1.451465	2.583611	-1.19843	730.664472	46177.771854				
0.096	0	-735.75	0	-11.615045	-16.255469	-11.615045	-2.547495	-1.360957	-0.109374	-0.081477	-0.109374	0.069009
	0.019404	2.466713	2.804751	2.466713	1.355001	-0.656365	748.456818	46177.771854				
0.099	0	-735.75	0	-11.928379	-16.49449	-11.928379	-2.298957	-1.327108	-0.099056	-0.076306	-0.099056	0.070594
	0.014151	3.439238	1.723839	3.439238	0.528314	-1.751176	846.717082	46177.771854				
0.102	0	-735.75	0	-12.206904	-16.723356	-12.206904	-2.063021	-1.301034	-0.086266	-0.07526	-0.086266	0.069226
	0.010486	4.263516	0.348736	4.263516	-0.455854	-1.221656	868.185947	46177.771854				
0.105	0	-735.75	0	-12.444202	-16.952673	-12.444202	-1.843195	-1.281352	-0.071709	-0.076888	-0.071709	0.065643
	0.007418	4.852368	-0.542819	4.852368	-1.194482	-1.022726	889.172148	46177.771854				
0.108	0	-735.75	0	-12.636283	-17.188176	-12.636283	-1.629154	-1.276944	-0.056276	-0.078823	-0.056276	0.061222
	0.002346	5.144224	-0.645089	5.144224	-1.473725	-1.690403	961.182786	46177.771854				
0.111	0	-735.75	0	-12.781949	-17.429424	-12.781949	-1.437257	-1.281785	-0.040925	-0.080958	-0.040925	0.056259
	-0.000955	5.117108	-0.711536	5.117108	-1.654176	-1.100379	982.146039	46177.771854				
0.114	0	-735.75	0	-12.882853	-17.675176	-12.882853	-1.265043	-1.29195	-0.026582	-0.081948	-0.026582	0.051715
	-0.002665	4.781081	-0.330054	4.781081	-1.514845	-0.570217	1001.81975	46177.771854				
0.117	0	-735.75	0	-12.943276	-17.920267	-12.943276	-1.099249	-1.309584	-0.014055	-0.080118	-0.014055	0.048772
	-0.004358	4.175453	0.609894	4.175453	-0.981074	-0.564215	1056.377946	46177.771854				
0.12	0	-735.75	0	-12.969622	-18.154478	-12.969622	-0.902457	-1.354555	-0.00393	-0.072721	-0.00393	0.049601
	-0.010487	3.375166	2.465795	3.375166	0.276406	-2.042903	1244.247503	46177.771854				
0.123	0	-735.75	0	-12.96958	-18.362394	-12.96958	-0.716343	-1.399523	0.003514	-0.063491	0.003514	0.052799
	-0.009268	2.481233	3.076646	2.481233	1.06601	0.406396	1268.423814	46177.771854				
0.126	0	-735.75	0	-12.951256	-18.537971	-12.951256	-0.518819	-1.433891	0.008278	-0.051355	0.008278	0.059053
	-0.004381	1.588098	4.045419	1.588098	2.084605	1.628793	1326.835352	46177.771854				
0.129	0	-735.75	0	-12.922379	-18.673193	-12.922379	-0.309245	-1.442936	0.010608	-0.03725	0.010608	0.067441
	0.004393	0.776534	4.701676	0.776534	2.795993	2.924741	1350.024605	46177.771854				
0.132	0	-735.75	0	-12.88961	-18.763058	-12.88961	-0.079217	-1.420187	0.010962	-0.021646	0.010962	0.076986
	0.014565	0.117973	5.201186	0.117973	3.181692	3.390762	1371.886452	46177.771854				
0.135	0	-735.75	0	-12.857986	-18.804258	-12.857986	0.184187	-1.371724	0.009957	-0.004783	0.009957	0.086852
	0.022529	-0.334833	5.621013	-0.334833	3.288653	2.654641	1428.867076	46177.771854				
0.138	0	-735.75	0	-12.830525	-18.795166	-12.830525	0.469667	-1.298275	0.008306	0.011352	0.008306	0.095399
	0.029359	-0.550289	5.378344	-0.550289	2.849301	2.276579	1450.361176	46177.771854				
0.141	0	-735.75	0	-12.80808	-18.73972	-12.80808	0.773683	-1.206088	0.006725	0.025713	0.006725	0.101644
	0.033788	-0.527038	4.78713	-0.527038	2.081499	1.4765	1471.564305	46177.771854				
0.144	0	-735.75	0	-12.789468	-18.64464	-12.789468	1.095916	-1.108384	0.005845	0.037813	0.005845	0.105151
	0.03408	-0.293499	4.033294	-0.293499	1.168901	0.097104	1518.683044	46177.771854				
0.147	0	-735.75	0	-12.771818	-18.518182	-12.771818	1.419877	-1.011774	0.006147	0.046329	0.006147	0.10527
	0.032014	0.100696	2.838471	0.100696	0.039711	-0.688487	1541.135813	46177.771854				
0.15	0	-735.75	0	-12.751103	-18.370435	-12.751103	1.783773	-0.955214	0.007929	0.054273	0.007929	0.104312
	0.019932	0.594006	2.648197	0.594006	-0.319133	-4.027447	1751.913566	46177.771854				
0.153	0	-735.75	0	-12.72265	-18.205075	-12.72265	2.125877	-0.922863	0.011308	0.057299	0.011308	0.1008
	0.011645	1.126273	1.00862	1.126273	-1.170864	-2.762396	1788.745744	46177.771854				
0.156	0	-735.75	0	-12.681755	-18.035928	-12.681755	2.443535	-0.905699	0.016184	0.056291	0.016184	0.095667
	0.006497	1.625364	-0.336046	1.625364	-1.710896	-1.715898	1819.721094	46177.771854				
0.159	0	-735.75	0	-12.624379	-17.87367	-12.624379	2.73667	-0.897512	0.022223	0.052442	0.022223	0.089558
	0.003416	2.013096	-1.282852	2.013096	-2.036249	-1.027145	1849.770517	46177.771854				
0.162	0	-735.75	0	-12.547753	-17.725335	-12.547753	3.002098	-0.89216	0.028923	0.046714	0.028923	0.082761
	0.002128	2.233142	-1.909601	2.233142	-2.265805	-0.429102	1864.416101	46177.771854				
0.165	0	-735.75	0	-12.450781	-17.594872	-12.450781	3.244526	-0.889286	0.035685	0.040552	0.035685	0.075803
	0.001085	2.254002	-2.054012	2.254002	-2.319412	-0.347699	1890.423642	46177.771854				
0.168	0	-735.75	0	-12.334199	-17.482244	-12.334199	3.464745	-0.888733	0.041897	0.034864	0.041897	0.069033
	0.000158	2.070861	-1.895876	2.070861	-2.256524	-0.309155	1914.379093	46177.771854				
0.171	0	-735.75	0	-12.20051	-17.385123	-12.20051	3.658359	-0.886228	0.047005	0.029939	0.047005	0.062546
	0.00044	1.702631	-1.641738	1.702631	-2.16227	0.094022	1912.232996	46177.771854				
0.174	0	-735.75	0	-12.05373	-17.300214	-12.05373	3.834974	-0.883971	0.050562	0.026843	0.050562	0.056949
	0.00039	1.185628	-1.031853	1.185628	-1.865807	-0.016555	1931.343927	46177.771854				
0.177	0	-735.75	0	-11.898994	-17.22168	-11.898994	3.997214	-0.882144	0.052277	0.025746	0.052277	0.052471
	0.000437	0.571559	-0.365637	0.571559	-1.492694	0.015462	1948.779633	46177.771854				

0.18	0	-735.75	0	-11.742028	-17.142485	-11.742028	4.186998	-0.905564	0.052057	0.029283	0.052057	0.051114
	-0.00546	-0.073163	1.179038	-0.073163	-0.452273	-1.965368	2118.716867	46177.771854				
0.183	0	-735.75	0	-11.588478	-17.050668	-11.588478	4.363405	-0.933534	0.050039	0.033474	0.050039	0.051338
	-0.006005	-0.672679	1.396996	-0.672679	0.074675	-0.181677	2140.037346	46177.771854				
0.186	0	-735.75	0	-11.443304	-16.944491	-11.443304	4.535439	-0.953758	0.046533	0.038369	0.046533	0.053301
	-0.002699	-1.168729	1.631409	-1.168729	0.654155	1.101941	2160.475026	46177.771854				
0.189	0	-735.75	0	-11.310373	-16.822424	-11.310373	4.706606	-0.955816	0.041949	0.043504	0.041949	0.056361
	0.003369	-1.527833	1.711809	-1.527833	1.020201	2.022426	2164.967807	46177.771854				
0.192	0	-735.75	0	-11.192216	-16.684351	-11.192216	4.885553	-0.938276	0.036765	0.048803	0.036765	0.059859
	0.009504	-1.728136	1.766363	-1.728136	1.165796	2.045042	2182.290363	46177.771854				
0.195	0	-735.75	0	-11.089886	-16.530778	-11.089886	5.07292	-0.903155	0.03148	0.053633	0.03148	0.062848
	0.014498	-1.761514	1.609922	-1.761514	0.996412	1.664788	2198.43104	46177.771854				
0.198	0	-735.75	0	-11.002954	-16.364253	-11.002954	5.263301	-0.853305	0.026572	0.057107	0.026572	0.064367
	0.018069	-1.636008	1.158067	-1.636008	0.506385	1.19045	2201.178473	46177.771854				
0.201	0	-735.75	0	-10.929668	-16.189658	-10.929668	5.455769	-0.796878	0.02244	0.058939	0.02244	0.063974
	0.018953	-1.377588	0.610771	-1.377588	-0.130942	0.294401	2215.231444	46177.771854				
0.204	0	-735.75	0	-10.867249	-16.01264	-10.867249	5.643968	-0.741759	0.019363	0.05868	0.019363	0.061377
	0.017305	-1.025664	-0.086537	-1.025664	-0.865841	-0.549086	2228.835659	46177.771854				
0.207	0	-735.75	0	-10.812288	-15.839958	-10.812288	5.816631	-0.691789	0.017476	0.05581	0.017476	0.056407
	0.01437	-0.628851	-0.956471	-0.628851	-1.656505	-0.978513	2223.827835	46177.771854				
0.21	0	-735.75	0	-10.761206	-15.67807	-10.761206	6.014433	-0.682028	0.01677	0.053743	0.01677	0.051569
	0.002658	-0.235229	-0.689085	-0.235229	-1.612768	-3.904048	2401.404865	46177.771854				
0.213	0	-735.75	0	-10.7106	-15.525898	-10.7106	6.184075	-0.696213	0.017133	0.048764	0.017133	0.045695
	-0.004938	0.120952	-1.659653	0.120952	-1.957979	-2.531867	2420.208969	46177.771854				
0.216	0	-735.75	0	-10.657563	-15.391195	-10.657563	6.321816	-0.720407	0.018339	0.041466	0.018339	0.039502
	-0.00805	0.401982	-2.432559	0.401982	-2.064397	-1.037477	2413.857049	46177.771854				
0.219	0	-735.75	0	-10.600068	-15.27932	-10.600068	6.438322	-0.749581	0.020041	0.033491	0.020041	0.033813
	-0.009282	0.567103	-2.658426	0.567103	-1.896263	-0.410472	2430.050486	46177.771854				
0.222	0	-735.75	0	-10.53723	-15.191089	-10.53723	6.536598	-0.779437	0.021834	0.025697	0.021834	0.02886
	-0.009208	0.597806	-2.598166	0.597806	-1.650837	0.024618	2444.618515	46177.771854				
0.225	0	-735.75	0	-10.469372	-15.125118	-10.469372	6.613394	-0.802811	0.023323	0.018326	0.023323	0.024465
	-0.007232	0.496296	-2.457024	0.496296	-1.465193	0.65865	2431.852275	46177.771854				
0.228	0	-735.75	0	-10.397949	-15.079135	-10.397949	6.67932	-0.821075	0.02416	0.01248	0.02416	0.020945
	-0.005537	0.279124	-1.948573	0.279124	-1.173142	0.565116	2441.86932	46177.771854				
0.231	0	-735.75	0	-10.325326	-15.048207	-10.325326	6.736601	-0.834929	0.02409	0.008344	0.02409	0.018259
	-0.004098	-0.023257	-1.37862	-0.023257	-0.895582	0.479588	2450.28832	46177.771854				
0.234	0	-735.75	0	-10.25446	-15.027284	-10.25446	6.782492	-0.841566	0.022976	0.005564	0.022976	0.016148
	-0.001983	-0.37161	-0.926613	-0.37161	-0.703634	0.704878	2437.464251	46177.771854				
0.237	0	-735.75	0	-10.188544	-15.012287	-10.188544	6.825032	-0.843664	0.020797	0.004456	0.020797	0.014778
	-0.00052	-0.726219	-0.369244	-0.726219	-0.456434	0.487638	2442.717082	46177.771854				
0.24	0	-735.75	0	-10.130646	-14.997628	-10.130646	6.90353	-0.867846	0.017667	0.007306	0.017667	0.015831
	-0.005722	-1.043335	0.949962	-1.043335	0.350748	-1.733726	2598.432072	46177.771854				
0.243	0	-735.75	0	-10.083258	-14.973694	-10.083258	6.972814	-0.894464	0.013842	0.009846	0.013842	0.017511
	-0.006055	-1.275136	0.846641	-1.275136	0.559967	-0.111114	2598.690723	46177.771854				
0.246	0	-735.75	0	-10.047971	-14.941613	-10.047971	7.04199	-0.914877	0.009654	0.012324	0.009654	0.020047
	-0.003605	-1.395802	0.825924	-1.395802	0.845414	0.816601	2608.281005	46177.771854				
0.249	0	-735.75	0	-10.025362	-14.901951	-10.025362	7.115288	-0.923708	0.005445	0.014601	0.005445	0.023059
	0.000247	-1.403177	0.758959	-1.403177	1.004022	1.283894	2617.239875	46177.771854				
0.252	0	-735.75	0	-10.015002	-14.855802	-10.015002	7.19388	-0.918727	0.001539	0.016382	0.001539	0.025917
	0.004383	-1.302	0.5936	-1.302	0.952578	1.378832	2622.110452	46177.771854				
0.255	0	-735.75	0	-10.015541	-14.805137	-10.015541	7.278423	-0.901846	-0.00178	0.017459	-0.00178	0.028045
	0.00759	-1.106166	0.359142	-1.106166	0.709402	1.06901	2629.471418	46177.771854				
0.258	0	-735.75	0	-10.024872	-14.752559	-10.024872	7.366497	-0.877044	-0.004294	0.017547	-0.004294	0.028948
	0.009292	-0.838008	0.029237	-0.838008	0.301225	0.567399	2636.237722	46177.771854				
0.261	0	-735.75	0	-10.040364	-14.701432	-10.040364	7.453435	-0.848783	-0.005874	0.016375	-0.005874	0.028306
	0.009439	-0.526813	-0.390459	-0.526813	-0.214234	0.048816	2639.031231	46177.771854				
0.264	0	-735.75	0	-10.059149	-14.655674	-10.059149	7.535884	-0.822582	-0.006494	0.013952	-0.006494	0.026115
	0.007906	-0.206516	-0.807745	-0.206516	-0.730086	-0.511019	2644.898916	46177.771854				
0.267	0	-735.75	0	-10.078435	-14.618987	-10.078435	7.609493	-0.802946	-0.006229	0.010344	-0.006229	0.02256
	0.005103	0.088407	-1.202757	0.088407	-1.18518	-0.934327	2650.523686	46177.771854				
0.27	0	-735.75	0	-10.095793	-14.593672	-10.095793	7.706113	-0.816537	-0.005234	0.008242	-0.005234	0.019697
	-0.004272	0.331722	-0.700786	0.331722	-0.95422	-3.124799	2797.148619	46177.771854				
0.273	0	-735.75	0	-10.109303	-14.576201	-10.109303	7.78251	-0.847186	-0.003697	0.004582	-0.003697	0.016576
	-0.009421	0.512319	-1.219982	0.512319	-1.040501	-1.716494	2808.169728	46177.771854				
0.276	0	-735.75	0	-10.117662	-14.570263	-10.117662	7.842889	-0.884902	-0.001843	0.00024	-0.001843	0.013994
	-0.011161	0.617746	-1.447098	0.617746	-0.860455	-0.580054	2818.87432	46177.771854				
0.279	0	-735.75	0	-10.120319	-14.576963	-10.120319	7.890041	-0.920635	5.9E-05	-0.004126	5.9E-05	0.012207
	-0.010137	0.634256	-1.455351	0.634256	-0.595926	0.34153	2821.210569	46177.771854				
0.282	0	-735.75	0	-10.117526	-14.595483	-10.117526	7.930533	-0.950039	0.001748	-0.007726	0.001748	0.011333
	-0.007821	0.562925	-1.200142	0.562925	-0.291313	0.771866	2829.499047	46177.771854				
0.285	0	-735.75	0	-10.110273	-14.623003	-10.110273	7.96781	-0.970754	0.003002	-0.010194	0.003002	0.011229
	-0.004946	0.417901	-0.822779	0.417901	-0.034489	0.95852	2836.488804	46177.771854				
0.288	0	-735.75	0	-10.100109	-14.655934	-10.100109	8.003489	-0.981541	0.003669	-0.011451	0.003669	0.011647
	-0.001887	0.222488	-0.418952	0.222488	0.139104	1.019582	2838.31431	46177.771854				
0.291	0	-735.75	0	-10.08892	-14.69066	-10.08892	8.040506	-0.983571	0.003681	-0.011443	0.003681	0.012413
	0.000717	0.003933	0.002637	0.003933	0.255487	0.868009	2842.960841	46177.771854				
0.294	0	-735.75	0	-10.078671	-14.723678	-10.078671	8.079757	-0.978539	0.003051	-0.010376	0.003051	0.013325
	0.002717	-0.210025	0.355864	-0.210025	0.303944	0.666632	2846.865606	46177.771854				
0.297	0	-735.75	0	-10.071172	-14.752247	-10.071172	8.121773	-0.968527	0.001868	-0.008534	0.001868	0.014228
	0.004046	-0.394497	0.613828	-0.394497	0.301045	0.442883	2851.251568	46177.771854				
0.3	0	-735.75	0	-10.067871	-14.773593	-10.067871	8.202711	-0.97976	0.000291	-0.003739	0.000291	0.016728
	-0.001243	-0.525428	1.598542	-0.525428	0.833208	-1.762773	3000.68198	46177.771854				
0.303	0	-735.75	0	-10.069597	-14.780932	-10.069597	8.279586	-0.995771	-0.001441	0.00012	-0.001441	0.019232
	-0.00251	-0.577483	1.28635	-0.577483	0.834642	-0.422375	3009.899122	46177.771854				
0.306	0	-735.75	0	-10.076428	-14.777184	-10.076428	8.357844	-1.008821	-0.003074	0.00326	-0.003074	0.021999
	-0.001276	-0.544466	1.046679	-0.544466	0.922424	0.411076	3023.946513	46177.771854				
0.309	0	-735.75	0	-10.087736	-14.76466	-10.087736	8.439018	-1.013331	-0.004395	0.005643	-0.004395	0.024769
	0.001452	-0.440152	0.794234	-0.440152	0.923442	0.909605	3033.077381	46177.771854				
0.312	0	-735.75	0	-10.102322	-14.745748	-10.102322	8.52438	-1.007451	-0.005239	0.007293	-0.005239	0.027155
	0.004462	-0.281213	0.549965	-0.281213	0.795239	1.003063	3041.645712	46177.771854				
0.315	0	-735.75	0	-10.118584	-14.722759	-10.118584	8.614402	-0.992985	-0.0055	0.008258	-0.0055	0.028796
	0.006674	-0.08712	0.321792	-0.08712	0.540989	0.737546	3053.740633	46177.771854				
0.318	0	-735.75	0	-10.134695	-14.697922	-10.134695	8.705815	-0.972522	-0.005137	0.008404	-0.005137	0.029347
	0.007857	0.12103	0.048513	0.12103	0.183537	0.394108	3061.296156	46177.771854				
0.321	0	-735.75	0	-10.148802	-14.673755	-10.148802	8.79577	-0.949821	-0.004174	0.007738	-0.004174	0.028685
	0.007798	0.321042	-0.222023	0.321042	-0.220651	-0.019436	3068.39124	46177.771854				
0.324	0	-735.75	0	-10.159223	-14.652651	-10.159223	8.88099	-0.928637	-0.0027	0.00632	-0.0027	0.026862
	0.006609	0.491246	-0.472625	0.491246	-0.6077	-0.39655	3074.669961	46177.771854				
0.327	0	-735.75	0	-10.164633	-14.636693	-10.164633	8.95872	-0.912176	-0.000861	0.004303	-0.000861	0.024101
	0.004561	0.612948	-0.67221	0.612948	-0.920329	-0.682593	3081.073569	46177.771854				
0.33	0	-735.75	0	-10.164203	-14.626394	-10.164203	9.063687	-0.927111	0.001171	0.004471	0.001171	0.022496
	-0.004023	0.677455	0.056026	0.677455	-0.535033	-2.861099	3234.428075	46177.771854				
0.333	0	-735.75	0	-10.157578	-14.616401	-10.157578	9.151213	-0.955367	0.003245	0.003465	0.003245	0.020901
	-0.007916	0.691343	-0.335374	0.691343	-0.531635	-1.297838	3243.08133	46177.771854				
0.336	0	-735.75	0	-10.144845	-14.60943	-10.144845	9.227444	-0.986778	0.005216	0.002104	0.005216	0.020027
	-0.00838	0.657053	-0.453659	0.657053	-0.291312	-0.154732	3254.659591	46177.771854				
0.339	0	-735.75	0	-10.126544	-14.605847	-10.126544	9.297389	-1.01376	0.006932	0.00098	0.006932	0.020048
	-0.006532	0.571991	-0.37481	0.571991	0.00695	0.615992	3265.423733	46177.771854				
0.342	0	-735.75	0	-10.103642	-14.604476	-10.103642	9.364497	-1.031183	0.008265	0.000431	0.008265	0.0208
	-0.003311	0.444339	-0.182895	0.444339	0.250888	1.073598	3272.055003	46177.771854				
0.345	0	-735.75	0	-10.077424	-14.60334	-10.077424	9.432674	-1.037543	0.009133	0.000711	0.009133	0.022036
	0.000167	0.289273	0.093237	0.289273	0.411755	1.159395	3280.50807	46177.771854				
0.348	0	-735.75	0	-10.04934	-14.60001	-10.04934	9.503532	-1.033347	0.00951	0.001795	0.00951	0.023422
	0.003273	0.125632	0.361303	0.125632	0.462049	1.035473	3287.961731	46177.771854				
0.351	0	-735.75	0	-10.020829	-14.592349	-10.020829	9.577166	-1.020298	0.009427	0.003488	0.009427	0.024647
	0.005684	-0.02764	0.564553	-0.02764	0.408311	0.803661	3293.264865	46177.771854				
0.354	0	-735.75	0	-9.993163	-14.578919	-9.993163	9.653477	-1.001229	0.008963	0.005564	0.008963	0.0255
	0.007141	-0.154771	0.69179	-0.154771	0.284487	0.485622	3299.323344	46177.771854				
0.357	0	-735.75	0	-9.967325	-14.559035	-9.967325	9.731277	-0.979073	0.008228	0.007721	0.008228	0.025839
	0.007667	-0.244896	0.719099	-0.244896	0.129997	0.175312	3305.047531	46177.771854				
0.36	0	-735.75	0	-9.943933	-14.53912	-9.943933	9.845526	-0.980874	0.007364	0.01222	0.007364	0.027345
	0.001358	-0.287996	1.499626	-0.287996	0.502126	-2.102881	3456.340796	46177.771854				
0.363	0	-735.75	0	-9.923103	-14.492437	-9.923103	9.952274	-0.990756	0.00655	0.015297	0.00655	0.028544
	-0.001057	-0.271269	1.025773	-0.271269	0.399636	-0.805036	3467.945843	46177.771854				
0.366	0	-735.75	0	-9.904419	-14.444794	-9.904419	10.055033	-1.000352	0.005955	0.017241	0.005955	0.029779
	-0.000762	-0.198299	0.648061	-0.198299	0.4116	0.098322	3479.60884	46177.771854				
0.369	0	-735.75	0	-9.887046	-14.392231	-9.887046	10.15612	-1.004222	0.005688	0.018284	0.005688	0.030977
	0.001076	-0.089169	0.347602	-0.089169	0.399415	0.612679	3489.623274	46177.771854				
0.372	0	-735.75	0	-9.869911	-14.337297	-9.869911	10.257164	-1.000393	0.005801	0.018643	0.005801	0.031902
	0.003305	0.037692	0.119638	0.037692	0.308103	0.742995	3500.118999	46177.771854				
0.375	0	-735.75	0	-9.851856	-14.281952	-9.851856	10.358006	-0.98939	0.006298	0.018439	0.006298	0.032268
	0.005147	0.165712	-0.067926	0.165712	0.122137	0.613879	3509.840477	46177.771854				
0.378	0	-735.75	0	-9.831778	-14.227852	-9.831778	10.456284	-0.972719	0.007138	0.017678	0.007138	0.031819
	0.006325	0.280092	-0.253752	0.280092	-0.149566	0.392646	3514.5003	46177.771854				
0.381	0	-735.75	0	-9.80876	-14.176567	-9.80876	10.551306	-0.953938	0.008242	0.016533	0.008242	0.030526
	0.006379	0.367825	-0.381804	0.367825	-0.431246	0.01797	3522.66104	46177.771854				
0.384	0	-735.75	0	-9.782172	-14.129174	-9.782172	10.640804	-0.936346	0.009498	0.015071	0.009498	0.028446
	0.005451	0.418831	-0.487291	0.418831	-0.693271	-0.309227	3530.285134	46177.771854				
0.387	0	-735.75	0	-9.751745	-14.08655	-9.751745	10.720879	-0.921217	0.010778	0.013255	0.010778	0.025678
	0.004172	0.42643	-0.605299	0.42643	-0.922592	-0.426241	3529.718773	46177.771854				
0.39	0	-735.75	0	-9.717616	-14.048526	-9.717616	10.828266	-0.934905	0.011954	0.013897	0.011954	0.024281
	-0.003557	0.39219	0.214027	0.39219	-0.465613	-2.576494	3679.032806	46177.771854				

0.393	0	-735.75	0	-9.680217	-14.009039	-9.680217	10.920787	-0.960629	0.012948	0.013666	0.012948	0.023087
	-0.006972	0.331156	-0.076992	0.331156	-0.398141	-1.138115	3691.140346	46177.771854				
0.396	0	-735.75	0	-9.640177	-13.97021	-9.640177	11.001603	-0.987016	0.013704	0.012997	0.013704	0.022562
	-0.006732	0.252162	-0.22305	0.252162	-0.174838	0.079743	3694.928347	46177.771854				
0.399	0	-735.75	0	-9.598292	-13.93278	-9.598292	11.077955	-1.007779	0.014169	0.012529	0.014169	0.022875
	-0.004553	0.15491	-0.155855	0.15491	0.104289	0.726432	3705.648655	46177.771854				
0.402	0	-735.75	0	-9.555495	-13.895869	-9.555495	11.153455	-1.019222	0.014308	0.012504	0.014308	0.023803
	-0.001445	0.046434	-0.008373	0.046434	0.309342	1.036054	3715.36018	46177.771854				
0.405	0	-735.75	0	-9.512773	-13.858142	-9.512773	11.22878	-1.019176	0.014122	0.012873	0.014122	0.024933
	0.002023	-0.061966	0.122939	-0.061966	0.376625	1.155923	3717.652396	46177.771854				
0.408	0	-735.75	0	-9.471056	-13.818503	-9.471056	11.306713	-1.009364	0.013646	0.013707	0.013646	0.025982
	0.004791	-0.15885	0.277872	-0.15885	0.349693	0.92254	3725.180305	46177.771854				
0.411	0	-735.75	0	-9.431127	-13.775867	-9.431127	11.386781	-0.99248	0.012943	0.014801	0.012943	0.026647
	0.006571	-0.234284	0.36489	-0.234284	0.221647	0.593654	3731.992415	46177.771854				
0.414	0	-735.75	0	-9.393542	-13.729871	-9.393542	11.466231	-0.970725	0.012098	0.015811	0.012098	0.026668
	0.007544	-0.281726	0.336518	-0.281726	0.006853	0.324161	3732.523427	46177.771854				
0.417	0	-735.75	0	-9.358594	-13.68108	-9.358594	11.544984	-0.947881	0.011199	0.01664	0.011199	0.026025
	0.007396	-0.299727	0.27624	-0.299727	-0.214314	-0.04943	3738.292953	46177.771854				
0.42	0	-735.75	0	-9.326316	-13.629417	-9.326316	11.655677	-0.950096	0.01034	0.019501	0.01034	0.026382
	0.000648	-0.286287	0.953829	-0.286287	0.119148	-2.249196	3882.465347	46177.771854				
0.423	0	-735.75	0	-9.296411	-13.570499	-9.296411	11.754764	-0.961372	0.009636	0.020808	0.009636	0.026359
	-0.002134	-0.234576	0.435728	-0.234576	-0.007703	-0.927243	3888.042185	46177.771854				
0.426	0	-735.75	0	-9.268257	-13.508685	-9.268257	11.847251	-0.974184	0.009182	0.021079	0.009182	0.026437
	-0.002384	-0.151413	0.090388	-0.151413	0.025888	-0.083453	3899.078522	46177.771854				
0.429	0	-735.75	0	-9.241038	-13.446781	-9.241038	11.935745	-0.983411	0.009013	0.020644	0.009013	0.026637
	-0.001134	-0.056264	-0.145211	-0.056264	0.066671	0.416794	3909.608429	46177.771854				
0.432	0	-735.75	0	-9.213903	-13.386683	-9.213903	12.020147	-0.985432	0.009121	0.01964	0.009121	0.026712
	0.000983	0.035858	-0.334476	0.035858	0.025213	0.705659	3912.509373	46177.771854				
0.435	0	-735.75	0	-9.186083	-13.329823	-9.186083	12.102985	-0.980872	0.00946	0.018416	0.00946	0.026519
	0.00277	0.113257	-0.408029	0.113257	-0.06451	0.595459	3921.151655	46177.771854				
0.438	0	-735.75	0	-9.156977	-13.276755	-9.156977	12.183628	-0.971545	0.009964	0.017065	0.009964	0.025869
	0.003855	0.16801	-0.450383	0.16801	-0.216498	0.361599	3928.979461	46177.771854				
0.441	0	-735.75	0	-9.126214	-13.227859	-9.126214	12.258726	-0.958477	0.01055	0.015492	0.01055	0.024585
	0.004481	0.195295	-0.524527	0.195295	-0.428184	0.208944	3927.491357	46177.771854				
0.444	0	-735.75	0	-9.093685	-13.183668	-9.093685	12.329428	-0.945173	0.011126	0.013945	0.011126	0.02279
	0.004116	0.19208	-0.515508	0.19208	-0.598346	-0.121934	3933.694259	46177.771854				
0.447	0	-735.75	0	-9.059557	-13.144073	-9.059557	12.394264	-0.934155	0.011601	0.012442	0.011601	0.020595
	0.003057	0.158242	-0.500973	0.158242	-0.731554	-0.352786	3939.434152	46177.771854				
0.45	0	-735.75	0	-9.024258	-13.108049	-9.024258	12.483409	-0.947763	0.011904	0.013187	0.011904	0.019678
	-0.003492	0.100895	0.248341	0.100895	-0.30567	-2.183143	4069.171146	46177.771854				
0.453	0	-735.75	0	-8.98834	-13.070094	-8.98834	12.560432	-0.971111	0.012014	0.013217	0.012014	0.018991
	-0.006209	0.036575	0.009972	0.036575	-0.228876	-0.905615	4079.44635	46177.771854				
0.456	0	-735.75	0	-8.952373	-13.031973	-8.952373	12.629989	-0.995358	0.011936	0.012969	0.011936	0.018978
	-0.006021	-0.025918	-0.082536	-0.025918	-0.004412	0.062789	4089.483542	46177.771854				
0.459	0	-735.75	0	-8.916916	-12.994237	-8.916916	12.694497	-1.013004	0.011674	0.012646	0.011674	0.019572
	-0.00367	-0.087332	-0.107935	-0.087332	0.19786	0.783551	4091.556081	46177.771854				
0.462	0	-735.75	0	-8.882507	-12.956857	-8.882507	12.759274	-1.021484	0.01124	0.012606	0.01124	0.020618
	-0.00068	-0.144642	-0.013385	-0.144642	0.348607	0.996676	4099.771606	46177.771854				
0.465	0	-735.75	0	-8.849623	-12.918998	-8.849623	12.825911	-1.020376	0.010663	0.012864	0.010663	0.021765
	0.002197	-0.192294	0.086324	-0.192294	0.382521	0.958904	4107.09727	46177.771854				
0.468	0	-735.75	0	-8.818628	-12.879967	-8.818628	12.893286	-1.010111	0.009989	0.013229	0.009989	0.022617
	0.004682	-0.224549	0.121375	-0.224549	0.284004	0.828382	4107.971423	46177.771854				
0.471	0	-735.75	0	-8.789729	-12.83965	-8.789729	12.962304	-0.993872	0.009275	0.013676	0.009275	0.022981
	0.006095	-0.23821	0.148965	-0.23821	0.121433	0.471226	4113.682445	46177.771854				
0.474	0	-735.75	0	-8.762963	-12.798101	-8.762963	13.031316	-0.974957	0.008576	0.01401	0.008576	0.022704
	0.006436	-0.232798	0.111351	-0.232798	-0.092584	0.113663	4118.960339	46177.771854				
0.477	0	-735.75	0	-8.738203	-12.755965	-8.738203	13.096958	-0.955447	0.007944	0.013963	0.007944	0.021688
	0.006102	-0.21085	-0.015537	-0.21085	-0.338566	-0.111658	4118.308151	46177.771854				
0.48	0	-735.75	0	-8.715194	-12.713639	-8.715194	13.191351	-0.960041	0.007422	0.015816	0.007422	0.021609
	-0.000416	-0.173794	0.617609	-0.173794	-0.026188	-2.172501	4252.111386	46177.771854				
0.483	0	-735.75	0	-8.693508	-12.666888	-8.693508	13.275233	-0.974697	0.007072	0.016379	0.007072	0.021285
	-0.003434	-0.116764	0.187663	-0.116764	-0.108041	-1.005889	4262.010094	46177.771854				
0.486	0	-735.75	0	-8.672552	-12.619302	-8.672552	13.350407	-0.990594	0.006937	0.015961	0.006937	0.021084
	-0.003614	-0.045138	-0.139404	-0.045138	-0.067233	-0.060225	4266.003427	46177.771854				
0.489	0	-735.75	0	-8.651681	-12.573392	-8.651681	13.421484	-1.003046	0.007011	0.015072	0.007011	0.021132
	-0.002361	0.0247	-0.296068	0.0247	0.015996	0.417853	4275.11065	46177.771854				
0.492	0	-735.75	0	-8.630317	-12.530268	-8.630317	13.490312	-1.009579	0.007257	0.01398	0.007257	0.021283
	-0.000511	0.081979	-0.364205	0.081979	0.050397	0.616727	4283.463521	46177.771854				
0.495	0	-735.75	0	-8.608025	-12.490384	-8.608025	13.556186	-1.008729	0.007619	0.012746	0.007619	0.021261
	0.001552	0.120678	-0.411401	0.120678	-0.00717	0.687571	4284.699097	46177.771854				
0.498	0	-735.75	0	-8.584554	-12.453997	-8.584554	13.620945	-1.002336	0.008032	0.011614	0.008032	0.020958
	0.00296	0.137687	-0.377079	0.137687	-0.101101	0.469233	4291.201507	46177.771854				
0.501	0	-735.75	0	-8.55985	-12.420785	-8.55985	13.683769	-0.992699	0.00843	0.0106	0.00843	0.020259
	0.003587	0.132743	-0.338019	0.132743	-0.232919	0.209207	4297.038096	46177.771854				
0.504	0	-735.75	0	-8.53405	-12.390477	-8.53405	13.741826	-0.980989	0.008753	0.009567	0.008753	0.019072
	0.003789	0.107503	-0.344513	0.107503	-0.395882	0.067063	4295.34439	46177.771854				
0.507	0	-735.75	0	-8.507465	-12.363096	-8.507465	13.796129	-0.970011	0.008945	0.008663	0.008945	0.017542
	0.003241	0.064142	-0.301168	0.064142	-0.509976	-0.182558	4299.979058	46177.771854				
0.51	0	-735.75	0	-8.480549	-12.337451	-8.480549	13.876985	-0.982419	0.008976	0.010036	0.008976	0.017277
	-0.002928	0.010347	0.457654	0.010347	-0.088196	-2.056239	4429.215432	46177.771854				
0.513	0	-735.75	0	-8.453765	-12.308096	-8.453765	13.946113	-1.002623	0.008863	0.010539	0.008863	0.01709
	-0.005141	-0.037709	0.167655	-0.037709	-0.062241	-0.737623	4432.572091	46177.771854				
0.516	0	-735.75	0	-8.427487	-12.277282	-8.427487	14.009572	-1.022917	0.008642	0.0107	0.008642	0.017441
	-0.004776	-0.073539	0.053582	-0.073539	0.11679	0.121559	4441.505265	46177.771854				
0.519	0	-735.75	0	-8.401999	-12.245779	-8.401999	14.070974	-1.037865	0.00834	0.01079	0.00834	0.018311
	-0.002823	-0.100836	0.030186	-0.100836	0.290252	0.651132	4449.880625	46177.771854				
0.522	0	-735.75	0	-8.377508	-12.213695	-8.377508	14.131738	-1.043891	0.007981	0.010882	0.007981	0.01942
	-1.1E-05	-0.119592	0.030555	-0.119592	0.369426	0.937058	4452.970482	46177.771854				
0.525	0	-735.75	0	-8.354142	-12.180982	-8.354142	14.194474	-1.041075	0.007595	0.011118	0.007595	0.020504
	0.002588	-0.12865	0.07861	-0.12865	0.36132	0.866531	4459.649483	46177.771854				
0.528	0	-735.75	0	-8.331934	-12.147342	-8.331934	14.259107	-1.031	0.007215	0.011426	0.007215	0.021263
	0.004513	-0.126711	0.102721	-0.126711	0.25318	0.641628	4465.641487	46177.771854				
0.531	0	-735.75	0	-8.310814	-12.11279	-8.310814	14.323558	-1.015489	0.006874	0.011611	0.006874	0.021438
	0.005721	-0.113648	0.06174	-0.113648	0.058144	0.402544	4466.806616	46177.771854				
0.534	0	-735.75	0	-8.290623	-12.077861	-8.290623	14.387504	-0.997907	0.006599	0.01165	0.006599	0.020973
	0.005888	-0.09173	0.012768	-0.09173	-0.154978	0.055885	4471.700664	46177.771854				
0.537	0	-735.75	0	-8.271139	-12.043183	-8.271139	14.449029	-0.981146	0.006404	0.011426	0.006404	0.01987
	0.005197	-0.064952	-0.074602	-0.064952	-0.367591	-0.230396	4476.337096	46177.771854				
0.54	0	-735.75	0	-8.252113	-12.008862	-8.252113	14.535677	-0.986976	0.006301	0.012918	0.006301	0.019629
	-0.00093	-0.034395	0.497551	-0.034395	-0.080363	-2.04239	4597.808228	46177.771854				
0.543	0	-735.75	0	-8.233225	-11.971008	-8.233225	14.612128	-1.002261	0.006317	0.01329	0.006317	0.019224
	-0.003738	0.005235	0.123716	0.005235	-0.134966	-0.936014	4607.056085	46177.771854				
0.546	0	-735.75	0	-8.214084	-11.932642	-8.214084	14.681646	-1.019521	0.006468	0.012951	0.006468	0.019077
	-0.004071	0.050656	-0.113029	0.050656	-0.049074	-0.110843	4616.229741	46177.771854				
0.549	0	-735.75	0	-8.194301	-11.895556	-8.194301	14.745894	-1.032678	0.006737	0.012169	0.006737	0.019194
	-0.002631	0.089655	-0.260365	0.089655	0.039113	0.48001	4619.751451	46177.771854				
0.552	0	-735.75	0	-8.173586	-11.860736	-8.173586	14.808526	-1.039546	0.007082	0.011335	0.007082	0.019499
	-0.000633	0.114938	-0.278158	0.114938	0.10171	0.665855	4627.491844	46177.771854				
0.555	0	-735.75	0	-8.151784	-11.828164	-8.151784	14.870552	-1.03975	0.007454	0.01059	0.007454	0.019777
	0.001302	0.123812	-0.248189	0.123812	0.092662	0.645128	4634.441927	46177.771854				
0.558	0	-735.75	0	-8.128887	-11.797554	-8.128887	14.930764	-1.033449	0.007804	0.009898	0.007804	0.019775
	0.002998	0.11676	-0.230948	0.11676	-0.000885	0.565258	4635.322295	46177.771854				
0.561	0	-735.75	0	-8.105025	-11.768726	-8.105025	14.990199	-1.023153	0.00809	0.009379	0.00809	0.019423
	0.003884	0.095486	-0.173014	0.095486	-0.117036	0.295223	4640.71335	46177.771854				
0.564	0	-735.75	0	-8.080443	-11.74125	-8.080443	15.047802	-1.011302	0.008279	0.008975	0.008279	0.018672
	0.004004	0.062741	-0.134445	0.062741	-0.250366	0.0399	4645.627299	46177.771854				
0.567	0	-735.75	0	-8.055477	-11.714917	-8.055477	15.101089	-0.999065	0.008343	0.008528	0.008343	0.017494
	0.003754	0.021608	-0.149193	0.021608	-0.392945	-0.08306	4644.688876	46177.771854				
0.57	0	-735.75	0	-8.030519	-11.689086	-8.030519	15.180383	-1.008397	0.008279	0.010184	0.008279	0.017455
	-0.001937	-0.02148	0.551995	-0.02148	-0.01269	-1.897155	4767.075556	46177.771854				
0.573	0	-735.75	0	-8.005909	-11.658762	-8.005909	15.250584	-1.025825	0.00812	0.011031	0.00812	0.017471
	-0.004238	-0.052921	0.28258	-0.052921	0.005193	-0.766985	4775.938088	46177.771854				
0.576	0	-735.75	0	-7.98185	-11.626151	-7.98185	15.314321	-1.042922	0.007916	0.011333	0.007916	0.017849
	-0.003842	-0.068135	0.100469	-0.068135	0.126143	0.132134	4780.100518	46177.771854				
0.579	0	-735.75	0	-7.958434	-11.592603	-7.958434	15.376226	-1.055007	0.007696	0.011466	0.007696	0.018635
	-0.002047	-0.073345	0.044573	-0.073345	0.261886	0.598236	4788.183913	46177.771854				
0.582	0	-735.75	0	-7.935673	-11.558484	-7.935673	15.438426	-1.059693	0.007482	0.011579	0.007482	0.019612
	0.000295	-0.071406	0.037681	-0.071406	0.325578	0.780765	4795.582864	46177.771854				
0.585	0	-735.75	0	-7.913522	-11.523868	-7.913522	15.500888	-1.056064	0.007292	0.011648	0.007292	0.020455
	0.002679	-0.063239	0.022889	-0.063239	0.281153	0.794458	4798.289526	46177.771854				
0.588	0	-735.75	0	-7.891882	-11.488926	-7.891882	15.564655	-1.045931	0.007143	0.011738	0.007143	0.020956
	0.00437	-0.04979	0.029805	-0.04979	0.166754	0.563836	4804.172798	46177.771854				
0.591	0	-735.75	0	-7.870615	-11.453744	-7.870615	15.628657	-1.031799	0.007045	0.011761	0.007045	0.020933
	0.005191	-0.032413	0.007743	-0.032413	-0.007593	0.273699	4809.536252	46177.771854				
0.594	0	-735.75	0	-7.849553	-11.418712	-7.849553	15.690157	-1.015554	0.007005	0.011541	0.007005	0.020261
	0.005361	-0.013436	-0.073307	-0.013436	-0.223886	0.056532	4809.699028	46177.771854				

Annex F Specification of dampers in experimental setup

Damping velocity versus external applied force is given in the graph. Here, the pink graph indicates minimal damping and the blue graph indicates maximal damping. Damping can be adapted within these values.

SPA UK

Dyno shock

User

CO LOGO

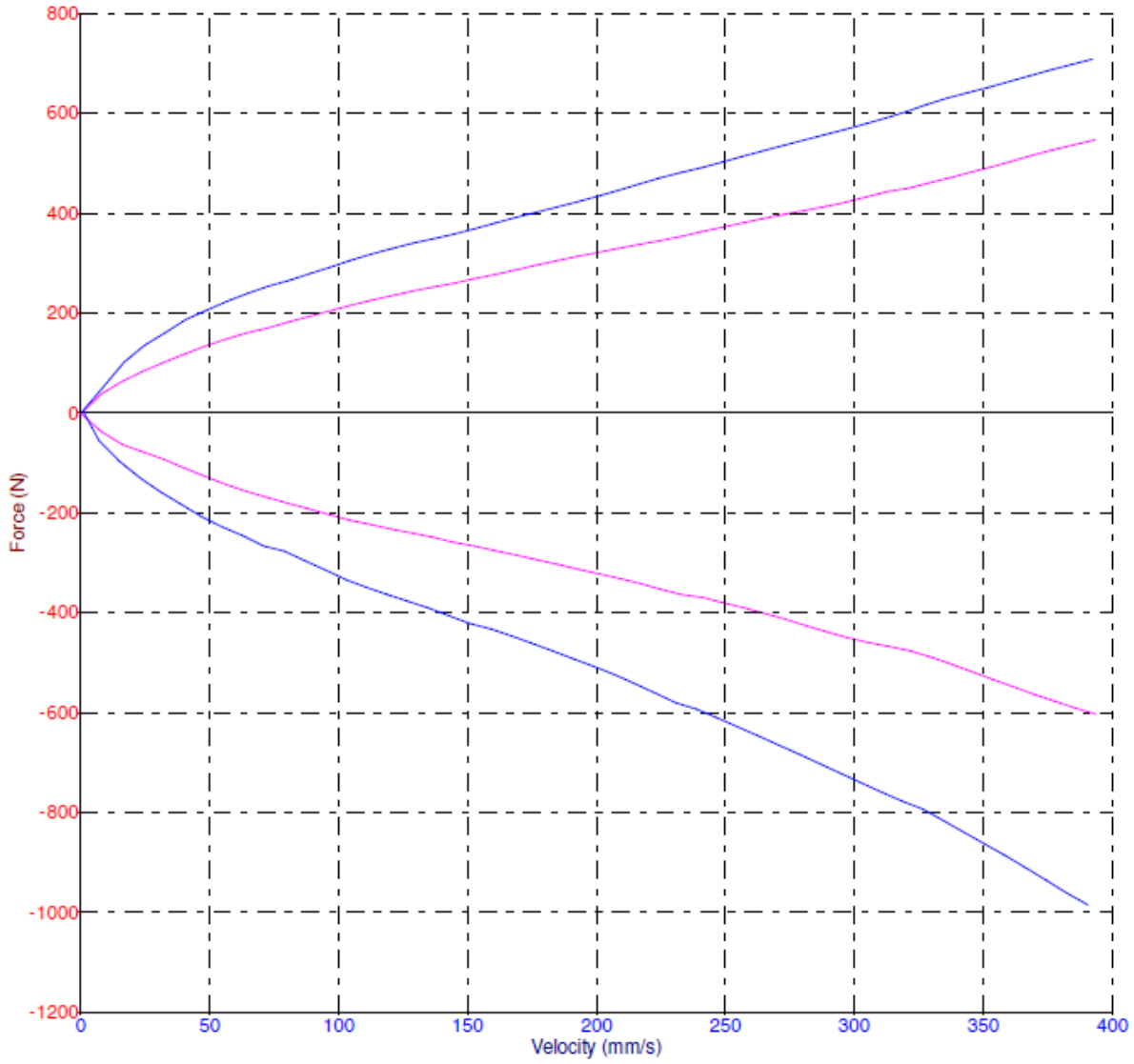

Annex G Test results from controlled experimental testing

Part 1: bridge with cable truss only, no actuator and no damper applied.

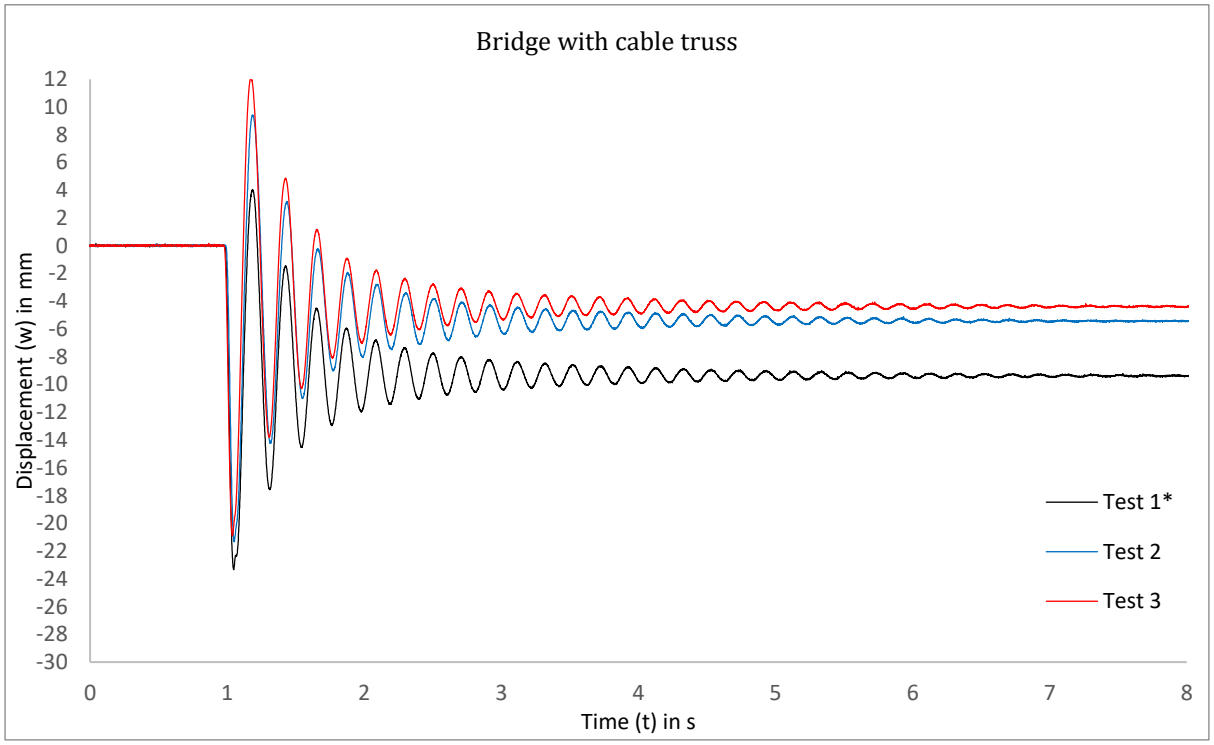

**settlement of connection between cable and steel main structure, larger permanent deformation*

Part 2: bridge with actuator (K_P=0, K_I=500, K_D=0, v=15000), no damper applied.

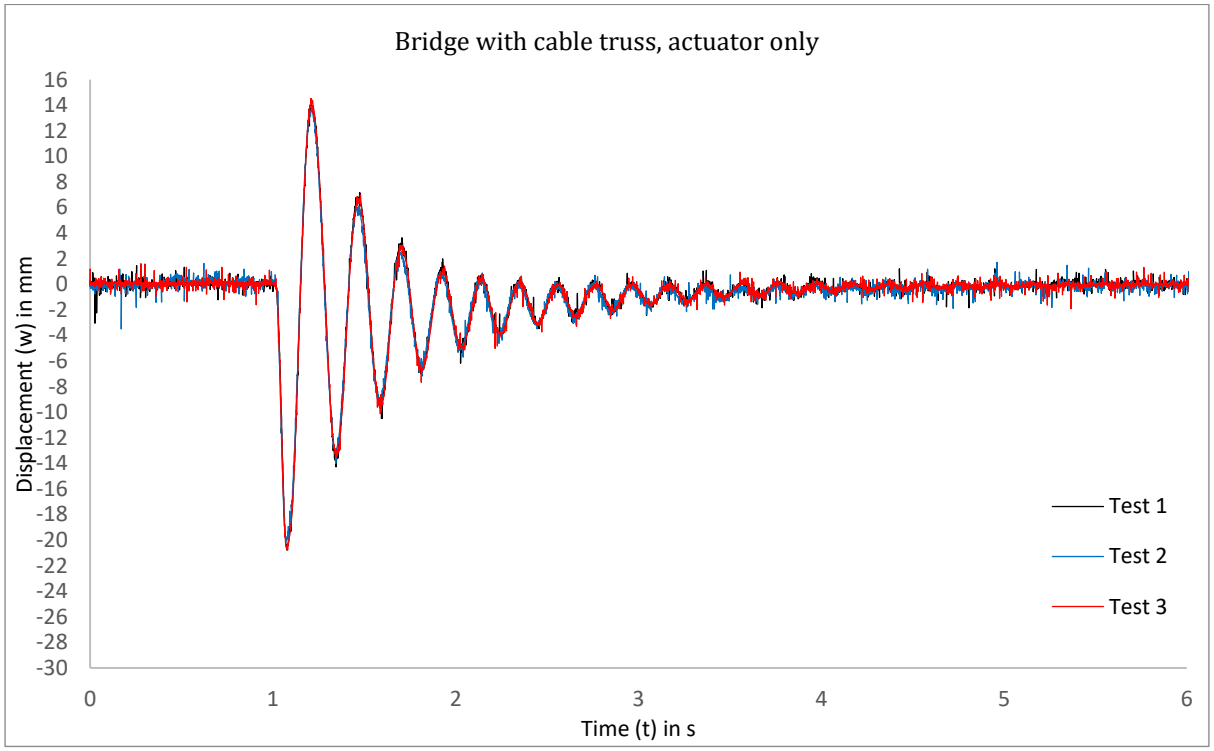

Part 3: bridge with damper (c=1200), no actuator applied.

Part 4: bridge with actuator (K_P=0, K_I=500, K_D=0, v=15000) and damper (c=1200) in series.